NEOTECTONIQUE DE L'ARC VOLCANIQUE QUATERNAIRE DES ANDES DU SUD DU CHILI ENTRE 37° ET 42° S

Luis Enrique Lara Pulgar

UNIVERSITE TOULOUSE III – PAUL SABATIER
UFR SVT

THESE

Pour obtenir le grade de

DOCTEUR DE L'UNIVERSITE TOULOUSE III

Discipline : Sciences de la Vie et de la Terre

Présentée et soutenue

par

Luis Enrique LARA PULGAR

le 7 novembre 2006

Titre :

NEOTECTONIQUE DE L'ARC VOLCANIQUE QUATERNAIRE DES ANDES DU SUD DU CHILI ENTRE 37° ET 42° S

Directeur de thèse

Alain LAVENU

Jury

Mr. Joseph Martinod	Prof. UPS	Toulouse	Président
Mr. Alain Demant	Prof. UC	Marseille	Rapporteur
Mr. Damien Dhont	Prof. UPPA	Pau	Rapporteur
Mr. Gérard Hérail	D.R. IRD	Toulouse	Examinateur
Mr. Alain Lavenu	D.R. IRD	Toulouse	Directeur

Pour Amanda et Emília,
mes petites filles et mon inspiration majeure

Tables des Matières

Résumé

Les Andes du Sud au Chili se développent sur la marge active du continent Sud Américain, entre la plaque de Nazca et la plaque de l'Amérique du Sud et sont le résultat global de la convergence oblique durant le Cénozoïque. L'arc volcanique quaternaire, représenté par la Zone Volcanique Sud (ZVS: 33º-46ºS) présente une architecture qui peut être mise en rapport avec la déformation crustale développée dans cette marge convergente. Les provinces méridionales de la ZVS, situées entre 37ºS et le Point Triple du Chili (46ºS), coexistent avec la Zone de Faille Liquiñe-Ofqui (ZFLO), une structure d'intra-arc de longue vie. En particulier, l'arc volcanique dans le segment 37º-42° est formé par une série de chaînes volcaniques transversales et des groupes de cônes monogéniques situés sur la ZFLO dont l'évolution est le résultat de l'interaction entre les processus magmatiques et la néotectonique de l'arc volcanique.

L'étude de la néotectonique entre 37º-42ºS, avec l'analyse des caractéristiques principales du volcanisme dans cette région, permettent d'établir qu'une telle interaction est complexe au-delà de la relation spatiale évidente entre des volcans et des failles. D'abord, elle souligne l'influence de la croûte continentale fracturée qui est sous-jacente à l'arc volcanique. Tant la configuration préalable de l'arc que les anisotropies du substratum exercent un fort contrôle sur l'ascension, la mise en place et l'évolution des magmas quaternaires comme on peut le signaler, par exemple, dans le cas du Complexe Volcanique Puyehue-Cordón Caulle.

Le régime de déformation quaternaire, caractérisé par une transpression générale dextre avec une contrainte horizontale maximale (σ_1=σ_{Hmax}) NE-SW, contrôlerait spécialement la distribution et l'évolution des chaînes transversales holocènes ainsi que les cônes de flanc dans les stratovolcans. Ce régime de contraintes régionales, en tout cas, dévie localement en s'adaptant aux structures du substratum. De même, des tenseurs de compression existent dans quelques secteurs et expliqueraient le soulèvement relatif de surfaces qui sont signalées dans la morphologie de la cordillère. Ces mouvements verticaux dans la ZFLO s'associeraient aussi avec des épisodes discrets de volcanisme qui permettent l'ascension de magmas primitifs directement depuis la source asthénosphérique.

Cependant, des tenseurs de transpression comme de compression maintiennent un σ_1=σ_{Hmax} constant de direction NE-SW, ce qui justifie l'influence de la tectonique dans le transport de magma à travers la croûte comme étant une caractéristique d'échelle régionale.

De même, bien que moins récurrent, le déclenchement à distance d'éruptions volcaniques en raison de grands séismes dans la zone de subduction est un facteur additionnel qui explique certains épisodes et il est superposé au régime de déformation corticale à l'intérieur de l'arc volcanique.

Finalement, l'étude à l'échelle régionale des régimes de déformation crustale et le volcanisme associé permettent de comprendre comment se forme l'architecture complexe d'un arc volcanique, dont l'évolution spatiale et temporelle est contrôlée par une multiplicité de facteurs mais qui présente d'importantes régularités des transferts de masse à travers la croûte.

Abstract

The Southern Andes in Chile occur along the active margin between Nazca and South American plates and they are a global result of the oblique convergence since the Cenozoic. Quaternary volcanic arc, there represented by the Southern Andean Volcanic Zone (SVZ: 33°-46ºS) shows an architecture that can be related with the crustal deformation along the convergent margin. The southern provinces of the SVZ between 37ºS and the Chile Triple Junction (46ºS), occur next to the Liquiñe-Ofqui Fault Zone (LOFZ), a long-lived intra-arc system. Specifically, the arc segment between 37°-42°S is formed by several oblique volcanic chains and clusters of monogenetic cones located atop of the LOFZ, which are a result of the interaction between magmatic and tectonic processes in the arc.

Neotectonic study of the volcanic arc between 37°-42°S, together with the analysis of the main features of volcanism in the region, allow to establish a rather complex interaction, beside the close spatial relationship between volcanoes and faults. First of all, the influence of the prefractured continental crust that underlies the arc should be remarked. The previous arc geometry and the basement anisotropy exert a strong control on the magma ascent, as can be observed on the Puyehue-Cordón Caulle Volcanic Complex case-study.

Quaternary stress regime, characterised by a dextral transpression with a NE-SW-striking maximum horizontal stress (σ_1=σ_{Hmax}), controls specially the distribution and magmatic evolution of the Holocene oblique chains and the flank cones of stratovolcanoes as well. This regional stress regime locally deviates according to basement structure. In addition, compressive stress tensors can partially explain the relative uplift that can be observed on the first order morphology of the Andean orogen. These vertical displacements can be related to discrete volcanic events that would pump primitive magmas directly from the asthenospheric source.

However, both transpressional and compressive tensors have a constant NE-SW- striking σ_1 (σ_{Hmax}), which support the regional influence of crustal tectonics on magma ascent and volcanism.

With minor frequency, remote seismic triggering by large subduction earthquakes is an additional factor that could explain some volcanic episodes and superposes to the ongoing crustal stress regime along the arc.

Lastly, the regional-scale study of the stress regimes and the volcanic features of arc segments allow understanding how the complex arc architecture is configured and how the mass transfer occurs through the crust.

Resumen

Los Andes del Sur en Chile se desarrollan en el margen activo entre la placa de Nazca y la placa de Sudamérica y son resultado global de su convergencia oblicua en el Cenozoico. El arco volcánico Cuaternario, representado por la Zona Volcánica Sur (ZVS: 33-46ºS) presenta una arquitectura que puede relacionarse con la deformación cortical desarrollada en este margen convergente. Las provincias meridionales de la ZVS, situadas entre los 37ºS y el Punto Triple de Chile (46ºS), coexisten con la Zona de Falla Liquiñe-Ofqui (ZFLO), una estructura de intraarco de larga vida. En particular, el arco volcánico en el segmento 37º-42°S está formado por una serie de cadenas volcánicas transversales y grupos de conos monogénicos situados sobre la ZFLO cuya evolución es resultado de la interacción entre los procesos magmáticos y la tectónica del arco.

El estudio de la neotectónica del arco volcánico entre 37º-42ºS, junto al análisis de las características principales del volcanismo en la región, permiten establecer que tal interacción es compleja más allá de la evidente relación espacial entre volcanes y fallas. En primer lugar, destaca la influencia de la delgada corteza continental prefracturada que subyace al arco volcánico. Tanto la configuración previa del arco como las anisotropías del basamento ejercen un fuerte control sobre el ascenso y evolución magmática como puede advertirse, por ejemplo, en el caso del Complejo Volcánico Puyehue-Cordón Caulle.

El régimen de deformación cuaternario, caracterizado por una transpresión general dextral con esfuerzo horizontal máximo (σ_1=σ_{Hmax}) NE-SW, controlaría especialmente la distribución y evolución de las cadenas transversales holocenas así como los conos de flanco en los estratovolcanes. Este régimen de esfuerzo regional, en todo caso, se desvía localmente ajustándose a las estructuras del basamento. Asimismo, tensores de compresión existen en algunos sectores y explicarían el alzamiento relativo que se advierte en la morfología del orógeno. Estos movimientos verticales en la ZFLO se asociarían también con episodios discretos de volcanismo que succionarían magmas primitivos directamente desde la fuente astenosférica.

No obstante, tanto los tensores de transpresión como de compresión mantienen un σ_1 (σ_{Hmax}) constante de dirección NE-SW, lo que justifica la influencia de la tectónica en el transporte de magma a través de la corteza como un rasgo de escala regional.

Asimismo, aunque menos recurrente, el gatilleo a distancia de erupciones volcánicas a causa de grandes sismos en la zona de subducción es un factor adicional que explica ciertos episodios y se superpone al régimen de deformación cortical al interior del arco volcánico.

Finalmente, el estudio a escala regional de los regímenes de deformación cortical y el volcanismo asociado permiten comprender como se configura la compleja arquitectura de un arco volcánico, cuya evolución espacial y temporal está controlada por una multiplicidad de factores pero que presenta regularidades importantes en la transferencia de masa a través de la corteza.

Remerciements

La recherche développée dans cette thèse est le produit d'une longue réflexion qui a pris beaucoup de temps à trouver les conditions favorables pour sa réalisation. Elle est aussi le résultat d'un effort d'équipe même si, pour diverses circonstances, son développement principal se produisait plutôt en solitaire. Des discussions fondamentales avec José Cembrano et Alain Lavenu ont illuminé le cadre conceptuel et ont produit les publications principales. De nombreuses conversations avec Hugo Moreno, Alejandro Sanhueza, Andrés Pavez, Andrés Folguera, Carolina Rodríguez, Hugo Corbella et Charles Stern ont permis d'intégrer leurs expérience et perspective aux problèmes d'intérêt commun. José Darrozes et Frédéric Christophoul ont gentiment collaboré pendant mes séjours dans le Laboratoire des Mécanismes et Transferts en Géologie de l'Université Paul Sabatier (Toulouse).

Cette recherche a été développée en parallèle avec mon travail régulier comme géologue dans le Service National Géologie et Mines (Sernageomin) du Chili et elle fait partie d'un programme de collaboration entre Sernageomin et l'IRD (Institut de Recherche pour le Développement). Bien que je n'aie pas disposé de temps exclusivement consacré à ce travail, j'ai reçu, dans ce Service, compréhension et soutien à des moments critiques et c'est pourquoi je considère cette thèse comme une contribution scientifique aux programmes réguliers de mon institution.

En faisant un compte rapide, je puis affirmer que cette recherche est le résultat fondamentalement d'un effort soutenu et des circonstances spéciales auxquelles ont contribué les personnes que je mentionne. Strictement, il existait l'importante probabilité de ne pas arriver à ce point et je conçois, par conséquent, une fierté légitime de la réalisation atteinte mais aussi une conscience profonde des difficultés qu'il faut dépasser dans des conditions défavorables.

Il ne faudrait pas non plus oublier ceux qui ont compliqué le succès de cette tâche. En suivant une ancienne légende des indiens de l'Amazonie, je ne mentionnerai pas ces noms pour ne pas invoquer les mauvais esprits. Ils ignorent probablement que, sans se proposer, ils ont été aussi un stimulant parce qu'une plus grande difficulté, requiert plus de conviction et de compromis.

Sans aucun doute, Alain Lavenu, mon directeur de thèse, a facilité avec sa préoccupation et sa générosité le développement de cette recherche. Son humilité et sa sagesse ont été une inspiration jusqu'à aujourd'hui. Nos conversations à propos de la géologie, du vin, de l'Histoire et de la Politique ont indubitablement été la meilleure scène pour avancer dans ce projet et permettre de connaître un être humain de façon complète; je me réjouis de cette expérience autant que du résultat scientifique. Je le remercie spécialement aussi pour son hospitalité en me recevant à Pau dans sa famille.

Parmi mes collègues et amis chiliens je dois de sincères remerciements à Hugo Moreno, qui a partagé généreusement son expérience lors d'innombrables occasions et continue à le faire dans nos projets institutionnels. José Cembrano a été un stimulant intellectuel et humain bien au-delà des problèmes scientifiques sur lesquels nous avons pensé pendant environ dix années.

Alain Lavenu a aimablement corrigé le texte en français et, avec Nicole Guerrero, ils ont résolu diligemment aussi les affaires administratives que j'aurais pu difficilement résoudre à distance.

Je remercie sincèrement les rapporteurs Damien Dhont et Alain Demant pour leur intérêt dans ma recherche et leurs observations précises. De même, les examinateurs Joseph Martinod et Gérard Hérail ont cordialement pris part à la soutenance et ont contribué à une discussion stimulante.

Ma reconnaissance va aussi à Claude Robin et au projet ECOS-Sud C01U03 qui a financé un de mes séjours à Clermont-Ferrand et à Toulouse. Dans d'autres occasions mes visites m'ont permis de suivre les stimulants symposiums de Géodynamique Andine et je remercie Gérard Hérail (IRD) pour leur financement. Conicyt-IRD, par un projet d'échange 2006, a financé mon dernier séjour dans lequel je présente mes résultats finaux. Le travail en cours, qui en découle et poursuit les sujets développés dans cette thèse, se développe au moyen du projet Fondecyt 1060185 (2006-2008).

Finalement, et probablement le plus important, mes petites filles, Amanda et Emilia, ont été l'inspiration principale de cette aventure. Je me rappelle la nostalgie que j'avais d'elles les jours passés dans la Résidence Jean Rieux ou dans les hôtels modestes proches de la faculté. Renate Wall les a affectueusement veillées pendant mes séjours en France et durant les nombreux congrès et les missions que j'ai effectués.

Je consacre cette thèse à mes filles, Amanda et Emilia, qui chaque jour me surprennent et m'enseignent beaucoup plus que je le fais pour elles.

La Reina (Santiago), août 2006

Chapitre 1. Introduction

1.1 Avant-propos

Il est peu habituel dans les recherches de sciences naturelles ou de sciences exactes d'inclure un préambule qui fixe le cadre conceptuel ou philosophique dans lequel on développe une thèse et ses conclusions. À son tour, la méthode scientifique, appliquée de manière simplement formelle et stricte, peut ne pas rendre compte de la diversité des options qui apparaissent pendant le développement de la recherche. Considérant ceci, on a voulu établir un point central : les résultats présentés ici ne permettent pas d'établir un modèle simple de cause à effet, unidirectionnel, entre le volcanisme et la tectonique dans les Andes du Sud, comme une explication à chacune des observations ou des hypothèses de travail. Par contre, les données montrent objectivement qu'une constellation de facteurs, opérant selon un processus naturel, ne les expliquent que partiellement. Précisément cette diversité de facteurs est celle que l'on a voulu souligner en construisant un modèle à variables multiples qui rende compte aussi de la difficulté à appréhender la vérité scientifique dans sa totalité. En paraphrasant Wittgenstein (Wittgenstein, 1958 ; 1969), la vérité - et par extension la vérité scientifique - peut difficilement être atteinte et une contribution scientifique pourrait se limiter, alors, à la description organisée des faits et les nombreuses explications possibles. Ceci pourrait ne pas être surprenant dans d'autres disciplines, mais dans les Sciences de la Terre, en général, il est suspect d'observer la proposition de modèles très simplifiés qui rejettent certaines options selon un critère plutôt esthétique ou, plus grave encore, en écartant des solutions parce qu'elles vont simplement à l'encontre des données. Par conséquent, on a choisi ici de rejeter la tentation d'établir une vérité verticale et on préfère faire valoir le paradoxe philosophique qui admet plusieurs explications pour un même fait et une multiplicité de facteurs qui influencent les phénomènes étudiés. Alors, dans cette thèse on discutera plusieurs des conditions ou des facteurs et on développera en profondeur l'argumentation au point d'affaiblir les bases

centrales de cette recherche ou forcer au maximum la valeur des données. On espère au moins contribuer modestement à situer de manière correcte le problème en l'état des connaissances actuelles en énonçant toutes les explications possibles. De même, les faiblesses du schéma proposé ou les questions encore en suspens pourront être résolues avec facilité en établissant ainsi un point de départ pour de futures recherches.

1.2 Problème scientifique et hypothèse de recherche

Le problème scientifique abordé dans cette étude est la relation entre le volcanisme et la néotectonique de l'arc volcanique dans un segment des Andes du Sud. L'objectif général est de comprendre la nature de cette relation et des facteurs qui la conditionne. Le problème posé s'inscrit dans un problème plus vaste qui est la relation entre le magmatisme et la tectonique dans les marges convergentes. Même si les conditions physiques dans lesquelles le passage et la mise en place de magmas se produisent dans les différents niveaux de la croûte continentale, certaines relations générales paraissent être répétées bien qu'avec une expression concrète différente. Pour ceci, la dernière étude de ces cas requiert des approximations méthodologiques différentes.

L'hypothèse centrale de ce travail est :

- ***Il existe une relation causale entre le volcanisme et la néotectonique de l'arc volcanique. Le volcanisme -ses caractéristiques pétrogénétiques, la distribution, la morphologie des centres volcaniques et le style éruptif- est un indicateur du régime tectonique régnant pendant sa construction.***

Plus spécifiquement, cette relation causale se manifeste de la manière suivante :

- ***Il existe un contrôle structural strict de la présence du volcanisme quaternaire. Les centres volcaniques sont exclusivement situés sur***

d'anciennes structures du socle ou sur de nouvelles structures formées par la déformation quaternaire.

- ***Il existe un contrôle direct de la cinématique des structures et du régime de déformation crustale sur les caractéristiques pétrogénétiques des magmas acquises dans la région source. Spécifiquement, les magmas primitifs extraits directement du manteau seraient évacués le long de la Zone de Faille Liquiñe-Ofqui (ZFLO) tandis que les chaînes transversales permettraient l'éruption tant de magmas primitifs comme ceux de variétés plus évoluées.***

- ***Il existe un contrôle direct de la cinématique des structures et du régime de déformation crustale sur les caractéristiques pétrogénétiques des magmas acquises pendant le processus de différenciation dans le transit vers la surface ou dans les chambres magmatiques superficielles. Spécifiquement, les domaines compressifs favoriseraient une plus grande résidence crustale et une plus grande différenciation magmatique tandis que les domaines extensifs favoriseraient l'évacuation de magmas moins différenciés.***

- ***Il existe un contrôle direct de la cinématique des structures et du régime de déformation crustale sur les mécanismes éruptifs des centres volcaniques.***

- ***Les mécanismes qui activent le volcanisme sont divers et opèrent à différentes échelles spatiales et temporelles. Le résultat observable est une combinaison locale des conditions générales.***

- ***Le régime de contraintes locales, comme la déviation du champ régional, explique les caractéristiques du volcanisme à l'échelle des centres volcaniques.***

1.3 Secteur d'étude

Comme secteur d'étude, pour prouver les hypothèses de travail, on a choisi le segment d'arc volcanique situé entre 38°S et 42°S (Fig.1-1). Ce

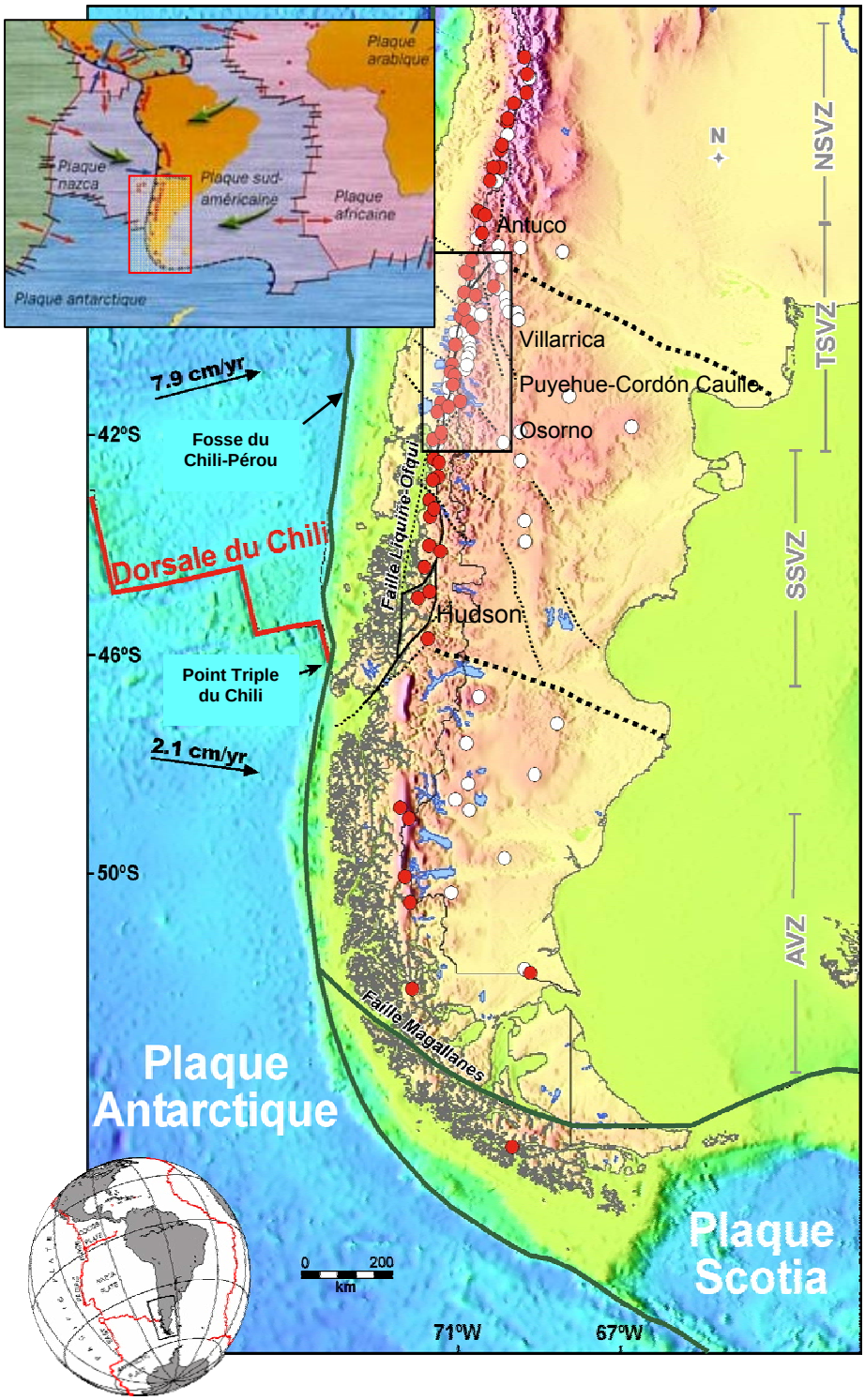

Fig. 1-1. Carte avec le secteur d'étude (encadré). En blanc les volcans du Pliocène-Pléistocène ; en rouge les volcans actifs du Quaternaire d'après Corbella et Lara (sous-presse) et Stern *et al*. (sous presse). Les différentes provinces magmatiques (NSVZ, TSVZ, SSVZ, AVZ) sont montrées d'après López-Escobar *et al*. (1995a). Vitesses de subduction d'apres DeMets *et al*.. 1994.

segment coïncide avec la partie septentrionale de la Zone de Faille Liquiñe-Ofqui (ZFLO) où celle-ci consiste en un ensemble de failles de direction ~NS et NNE d'où se détachent des branches obliques vers l'est. Le secteur d'étude se caractérise par un arc volcanique formé par un front net situé environ à 200 km de la fosse Chili-Pérou et où on trouve d'importants chaînons volcaniques transverses de directions NW et NE. Tant dans ces derniers que le long de la ZFLO, il existe différents types de structures volcaniques (calderas, stratovolcans, systèmes de fissures, cônes pyroclastiques et maars) qui couvrent tout le spectre de composition depuis les basaltes jusqu'aux rhyolites. De même, ce segment d'arc volcanique est implanté dans une croûte continentale mince qui ne dépasse pas 40 km d'épaisseur et dont l'épaisseur élastique variant entre 45 et 70 km (Tassara et Yánez, 2003) garantit son comportement éminemment fragile malgré le gradient thermique important attendu dans un arc volcanique.

1.4 Cadre conceptuel et mise en place des magmas

Depuis le début du 20^{éme} siècle, beaucoup de chercheurs ont élaboré des théories sur les mécanismes de montée des magmas à travers la croûte et les conditions de leur mise en place (plutonisme) ou son évacuation à la surface (volcanisme). En général, les théories considèrent les différents régimes rhéologiques existants dans la croûte inférieure et supérieure. Comme résultat, et spécialement en abordant les processus anciens, les observations géologiques seront de nature différente alors que les fondements de base restent les mêmes. En peu de mots, la fabrique magmatique des plutons et les indicateurs cinématiques de la déformation ductile qui y sont observés sont significativement différents des éléments observés dans l'étude de dykes ou bien des centres volcaniques actuels, dont le niveau d'érosion est très faible et dissimule les systèmes d'épanchement. Dans quelques cas, les grands batholites peuvent efficacement être formés par des systèmes de dykes (Petford *et al*., 1993) et, par conséquent, le transit du magma à travers des intrusions planaires (dykes verticaux et horizontaux) correspond au cadre conceptuel pour comprendre ce processus.

La géométrie des intrusions magmatiques dépend des propriétés mécaniques du magma (viscosité), ainsi que de l'encaissant (élasticité, plasticité) et c'est le contraste de rhéologie entre le magma et son encaissement qui contrôle le mode de mise en place des magmas (Rubin, 1993). Un faible contraste de résistance mécanique favorise la mise en place de plutons, alors qu'un fort contraste favorise la mise en place de dykes par fracturation hydraulique.

Il est généralement considéré que la plupart des intrusions planaires se mettent en place par fracturation hydraulique (Hubbert et Willis, 1957). Les premiers travaux traitant de la mécanique de la fracturation datent de la fin du 19ème siècle et du début du 20^{éme} siècle (Inglis, 1913; Grifith, 1921; Grifith, 1924).

Le magma, en particulier le magma basaltique généré dans le manteau supérieur et qui reste le produit dominant dans les systèmes de subduction avec une croûte continentale relativement mince, se propage par flottabilité ou différence de densité entre le magma et son encaissant. La remontée des magmas se fait par une combinaison des fractures de tension et de cisaillement d'après Hill (1977) et Shaw (1980). La flottabilité est le principal facteur de la remontée des magmas depuis la source mantellique. Par exemple, sous le volcan Kilauea (Fig.1-2), la sismicité a permis de mettre en évidence la présence d'un conduit vertical sous l'édifice volcanique, depuis une profondeur de 34 km environ jusqu'à une chambre magmatique située entre 6 et 2 km de profondeur (Ryan, 1988). A des profondeurs plus superficielles, les roches qui constituent un édifice volcanique sont moins denses que les magmas basaltiques et la flottabilité s'annule. A ce niveau de flottabilité nulle, les magmas se propagent horizontalement. Le niveau de stagnation ou de flottabilité nulle correspondra géologiquement à la formation de chambres magmatiques dans la croûte. Comme on peut le montrer, le niveau nul dépend de la distribution de la pression lithostatique et par conséquent sa situation pourra varier en favorisant soit la coalescence des canaux soit leur individualisation et une sortie directe vers la surface (Takada, 1994). Pour continuer son cheminement depuis le niveau neutre, le magma basaltique devra être surpressurisé, par exemple, au moyen du processus de

différenciation magmatique qui produira une portion différenciée riche en volatils qui pourra continuer son transit vers la surface.

Toutefois, la proximité d'une surface libre affecte aussi la propagation des dykes. La plupart des calculs théoriques correspondent à la propagation dans un milieu infini. Lorsqu'un dyke se met en place dans un milieu semi infini avec une surface libre, le champ de contraintes induit par l'intrusion est modifié et la surface libre est déformée. Le champ de contraintes induit par une chambre magmatique sphérique sous pression est radial et serait à l'origine de la mise en place des 'cone-sheets' et des dykes annulaires (Anderson, 1936; Chadwick et Dietrich, 1995).

Aussi, le régime de contraintes régional influence l'orientation des intrusions magmatiques, une idée évoquée la première fois par Stevens (1911). Il stipulait déjà que les intrusions planaires étaient perpendiculaires à la contrainte minimale, car l'énergie à fournir pour ouvrir une fracture dans cette direction est minimale. Hubbert et Willis (1957) démontrent que pour un tenseur de contraintes extensif, les fractures hydrauliques sont verticales et perpendiculaires à la direction d'extension $\sigma 3$. Dans un régime décrochant, les dykes sont également parallèles à la direction de raccourcissement. Par contre, si le champ de contraintes est purement compressif, $\sigma 3$ est vertical et les fractures horizontales (sills).

Dans une marge continentale de type 'long-lived', l'ouverture de fractures préexistantes peut être importante. La cohésion de ces plans de faille est faible ou nulle et la pression nécessaire pour permettre au magma de s'y propager doit uniquement s'opposer à la contrainte normale au plan et elle est inférieure à la pression nécessaire au magma pour initier une fracture nouvelle (Sibson, 1987; Sibson, 2003). Dans un régime compressif la pression magmatique nécessaire pour créer un dyke est plus importante que dans un régime extensif (Sibson, 2003).

L'analyse de la géométrie des essaims de dykes parallèles peut être un outil pour déterminer l'orientation des paléocontraintes régionales lors de la mise en place de l'essaim (Muller et Pollard, 1977; Nakamura, 1977; Féraud *et al.*, 1987; Hoek et Seitz, 1995). A grande échelle, ces paléocontraintes sont symptomatiques du contexte géodynamique. Dans les volcans polygéniques soumis à une contrainte différentielle, les essaims présentent une géométrie

mixte avec une composante radiale et une composante parallèle (Fig. 1-6). Dans la plupart des cas, l'essaim est alimenté par un centre à proximité duquel les dykes sont principalement radiaux. En s'éloignant du centre, les dykes bifurquent et tendent à se paralléliser dans la direction principale de σ_{Hmax} (Mullet et Pollard, 1977; Nakamura, 1977).

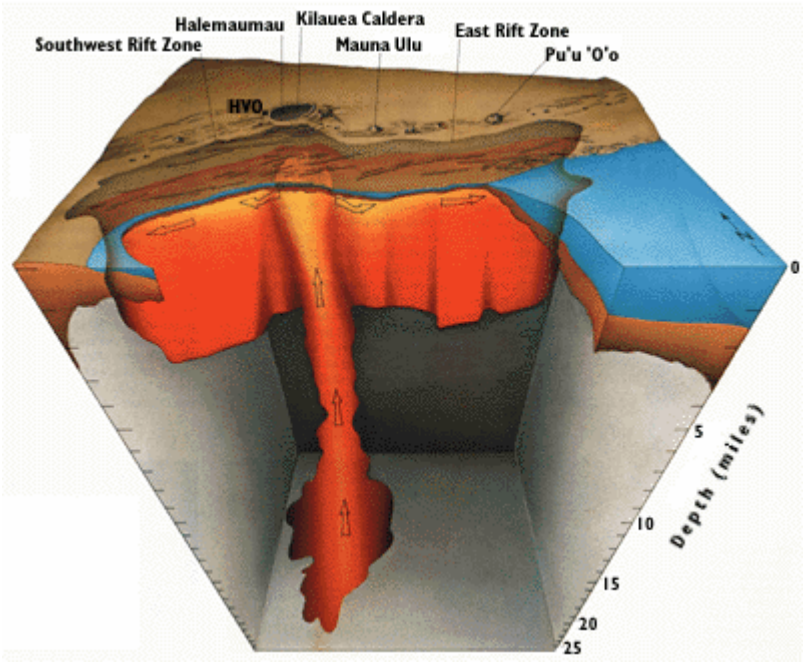

Fig. 1-2. Conduit vertical et chambre magmatique sous le volcan Kilauea d'après Ryan (1988). Le magma se met en place comme les dykes et filons contrôlés par le champ de contrainte régional.

D'autre part, l'injection des dykes dans la croûte peu modifier le champ de contraintes et induire la rotation du tenseur. Si plusieurs dykes se mettent en place à courte distance, ils peuvent interagir et se regrouper pour former un conduit principal. D'après Takada (1994), c'est la cause du volcanisme polygénique. Ainsi, dans un champ de contraintes avec un faible déviateur, les dykes interagissent et sont coalescents et dans un champ avec un fort déviateur, les dykes restent individuels et s'expriment en surface par des volcans monogéniques.

1.5 Cadre géodynamique des Andes du Chili

Les Andes du Chili et la Zone Volcanique Méridionale entre 33º et 46ºS (ZVS ou SVZ en anglais) au Chili centre sud, résultent de la subduction de la

plaque océanique Nazca sous la plaque continentale de l'Amérique du Sud. L'extrémité nord de la ZVS coïncide avec l'impact de la crête de la Dorsale Juan Fernández (DJF) dans la Fosse du Chili-Pérou, où s'observe un changement drastique de l'angle de subduction de la plaque de Nazca au-dessous de l'Amérique du Sud. La frontière méridionale des Andes du Sud est l'intersection

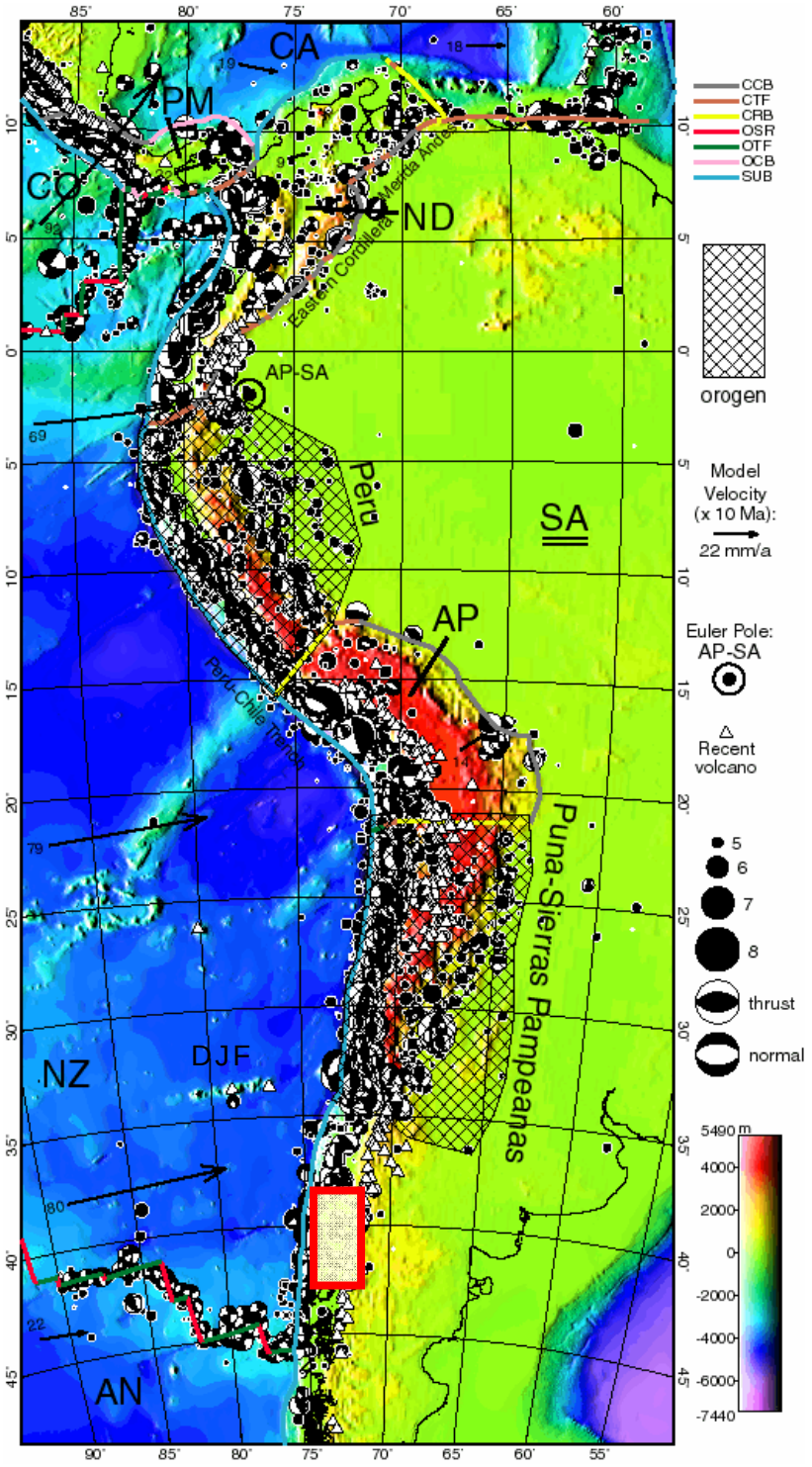

Fig. 1-3. Cadre géodynamique des Andes du Chili (Bird, 2003) et secteur d'étude (encadré).

de la crête de la Dorsale du Chili avec la fosse. La direction de convergence entre la plaque Nazca et la marge sud américaine est oblique (~20-30° d'après Jarrard, 1986; Dewey et Lamb, 1992) et la vitesse de convergence est de 7 à 9 cm/a (DeMets *et al*., 1994) ou un peu moins (~6 cm/a) d'après Angermann *et al*. (1999). L'âge de la plaque Nazca au contact de la fosse passe de 45 Ma dans le nord à 0 Ma dans le sud, au Point Triple du Chili. L'angle de subduction augmente de ~20° à l'extrémité nord des Andes du Sud à >25º au sud. Par conséquent, la distance de la fosse au front de l'arc volcanique actif diminue du nord au sud en passant de 290 kilomètres à moins de 270 km. L'épaisseur de la croûte diminue également de 55 à 60 kilomètres au nord de la ZVS à moins de 35 km au sud de 37°S. La croûte au-dessous de la ZVS se compose du socle paléozoïque/mésozoïque et des roches plutoniques mésozoïques/cénozoïques. La zone de subduction en face des Andes du Sud est caractérisée par un très fort couplage tectonique des plaques où des grands séismes sont localisés (Fig. 2-1). La déformation actuelle de l'avant arc est approximativement parallèle au vecteur de convergence, ce qui a été démontré par des mesures GPS (Klotz *et al*., 2001). Ceci suggère que l'accumulation intersismique de la transpression est localisée à la zone de couplage inter-plaques. La quantité de raccourcissement (jusqu'à 3.5 cm/a) diminue progressivement de la fosse vers l'est. Entre 37º et 42ºS, les vecteurs de vitesse GPS sont distribués de façon non uniforme, ce qui a été attribué à la déformation post-sismique suivant le tremblement de terre Chilien de 1960 (Klotz *et al*., 2001). Les données sismiques dans la croûte continentale disponibles sont limitées et suggèrent que l'avant-arc chilien entre 39ºS et 46ºS subit actuellement un raccourcissement perpendiculaire a la fosse tandis que l'arc volcanique absorbe une petite composante parallèle a la fosse (Chinn et Isacks, 1983; Cifuentes, 1989; Barrientos et Acevedo, 1992; Dewey et Lamb, 1992; Murdie, 1993). Cette composante parallèle a aussi, comme conséquence, le glissement parallèlement à l'arc du bloc de l'avant-arc (Cembrano *et al*., 1996, 2000; Lavenu et Cembrano, 1999; Arancibia *et al*., 1999).

1.6 Cadre géologique et évolution tectonique préquaternaire

L'orogène des Andes est très segmenté (*e.g.*, Tassara, 2005). La limite entre les Andes Centrales et les Andes du Sud à 33.5ºS est une transition tectonique importante (*e.g.*, Yáñez *et al.*, 2002). Au sud de cette latitude, les altitudes diminuent graduellement de ~4000 m dans la Cordillère Principale à moins de 2000 m dans la Cordillère de Patagonie. Cette diminution se corrèle également avec des variations du nord au sud de la déformation tectonique néogène. Les limites de l'inversion des bassins le long de la Cordillère Principale et la tectonique de socle (thick skinned) de l'avant-pays parallèle au système de Neuquén sont liées à des structures obliques à la fosse (Godoy *et al.*, 1999; Charrier *et al.*, 2002; Cobbold et Rossello, 2003).

Le segment 33-46ºS est caractérisé par trois morphostructures majeures: la Cordillère de la Côte, La Dépression Centrale et la Cordillère Principale (Fig.1-4). La Cordillère de la Côte est un orogène ancien constitué par des complexes d'accrétion paléozoïques-jurassiques et des séquences volcaniques et sédimentaires mésozoïques intrudées par des plutons triasiques à crétacés. La Dépression Centrale est un bassin tectonique formé par un remplissage de roches volcaniques et sédimentaires cénozoïques et des dépôts quaternaires d'origine volcanique et glaciaire. La Cordillère Principale est formée par des roches volcaniques et sédimentaires cénozoïques et par des plutons miocènes. Au sud de 38ºS, le Batholite de Patagonie Nord (BPN) occupe une bande de 1000 kilomètre de long (Hervé, 1994; Lavenu et Cembrano, 1999). La partie nord du BPN a été divisée en trois bandes approximativement nord-sud: une jurassique à l'ouest, une miocène au centre et une ceinture crétacée à l'est (Pankhurst *et al.*, 1992 ; 1999; SERNAGEOMIN, 2002).

Au sud de 42ºS, la Dépression Centrale est caractérisée par de nombreuses îles et fjords composés principalement de roches métamorphiques.

La déformation continentale cénozoïque de la marge des Andes centrales méridionales est la plupart du temps limitée à l'arc magmatique le long de la ZFLO (Hervé *et al.*, 1979; Forsythe et Nelson, 1985; Dewey et Lamb,

1992 ; Hervé, 1994 ; Cembrano *et al*., 1996). Les régions de l'avant-arc et d'arrière-arc montrent une très faible déformation régionale. Au sud de 47ºS, le développement d'une 'ceinture faillée et plissée' (thrust-and-fold belt) dans l'avant-pays est attribué à la migration vers le nord du Point Triple du Chili durant les 14 derniers Ma (*e.g*., Ramos et Kay, 1992). D'après Hervé (1994), l'absence de déformation au nord de 47ºS est le résultat d'une partition de la déformation concentrée significativement le long de la ZFLO.

L'identification des intrusions tardi-miocènes et des mylonites pliocènes le long de la ZFLO suggère que l'exhumation est associée à des failles. Cette exhumation est plus importante près de l'extrémité sud de la ZFLO et entre 42º et 46ºS, des taux de 1.3 à 2.7 mm/an entre 7 et 4 Ma ont été estimés sur la base des données thermo-géobarométriques (Parada *et al*., 2000; Cembrano *et al*., 2002) et des âges de traces de fission sur apatite et zircon (Thomson, 2002).

1.7 Tectonique du Pliocène-Quaternaire

Dans les Andes du Sud, entre 38° et 42º30'S, les terrains néogènes et quaternaires sont affectés par une déformation fragile peu développée, mais de grande extension géographique. L'analyse de la déformation fragile enregistrée dans la Dépression Centrale et près de la ZFLO montre qu'il existe deux événements tectoniques (Fig. 2-2). Des diagrammes de données des populations des failles montrent un stade tectonique pléistocène dans la Cordillère Principale dans la zone d'étude. Le stade pliocène se caractérise par un champ des contraintes compressif généralisé, enregistré dans les zones d'avant-arc et d'intra-arc actuelles représenté par σ_1 E-W avec σ_2 de direction N-S et σ_3 vertical (Lavenu et Cembrano, 1999).

Le stade quaternaire se caractérise par un champ de contraintes compressif N-S dans l'avant-arc représenté par σ_1 N-S avec σ_3 E-W (Lavenu et Cembrano, 1999). En revanche l'arc volcanique est caractérisé par un régime de transpression dextre avec σ_1 NE-SW, σ_3 perpendiculaire et σ_2 vertical.

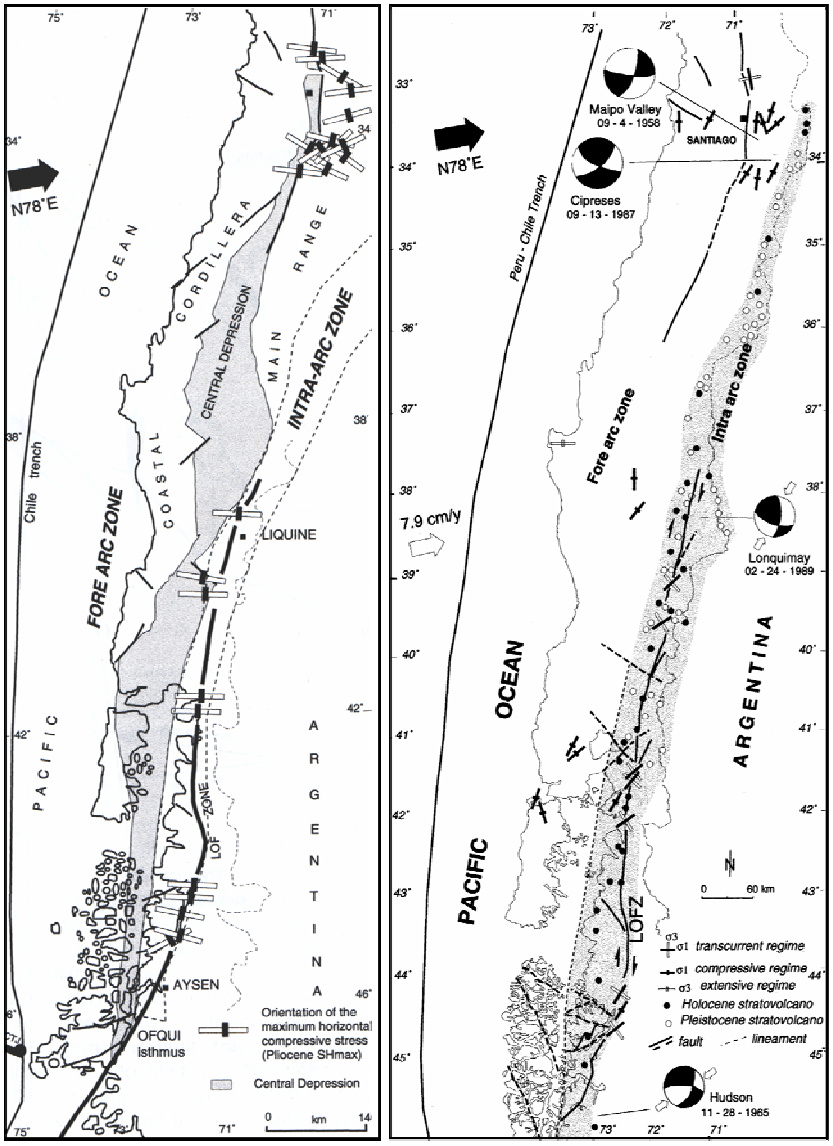

Fig. 1-4. Champs de contrainte déterminés par Lavenu et Cembrano (1999). Mécanismes au foyer des séismes dans la croûte de l'arc volcanique selon Chinn et Isaaks (1983) ; Cifuentes (1989) et Barrientos et Acevedo (1992). A gauche, orientation de la déformation principale pliocène en compression E-W. A droite, partition de la déformation principale en compression pleistocène N-S à NNE dans la Dépression Centrale et transpression NE-SW dans l'arc volcanique quaternaire.

1.8 Méthodologie

Vu la nature multiple du problème scientifique, on a utilisé une méthodologie combinée pour obtenir des données, les traiter et tester les hypothèses de travail. D'abord, on a construit une base de données pour le secteur d'étude qui inclut (voir annexe):

- Des Modèles Numériques de Terrain SRTM 90 d'accès public (www.seamless.nasa.gov) et corrigés ici.

- Des populations de failles pour l'analyse microtectonique, compilées de données publiées et nouvelles obtenues pendant cette étude.

- Une géologie de détail, généralement non publiée ou en processus de publication, aux échelles 1:25.000 à 1:75.000, digitalisée pour son analyse directe.

- Des données géochimiques à partir d'éléments majeurs et mineurs, spécialement les terres rares, publiées ou inédites.

- Des données géochronologiques K-Ar et $^{40}Ar/^{39}Ar$. Dans le premier cas, on a compilé principalement des données publiées; l'$^{40}Ar/^{39}Ar$, d'une plus grande résolution et avec possibilité d'obtenir des âges du Pléistocène supérieur en roche totale ou masse fondamentale, a été spécialement appliqué à un cas d'étude (Complexe Volcanique Puyehue-Cordón Caulle).

- Des données morphométriques des centres volcaniques. Directions d'alignement des cônes et des cratères, directions d'élongation de la base et du cratère ou d'effondrement latéral (breaching).

- Des images satellitaires Landsat TM7, Aster et Radarsat 1

Les Modèles Numériques de Terrain ont été corrigés au moyen d'itérations de Laplace en utilisant le programme Blackart ou en utilisant le logiciel ENVI 4.0. Postérieurement avec le logiciel RiverTools®, ils ont été reconvertis comme grilles sans dépressions (Depressionless DEM) grâce à l'algorithme D8 qui définit les directions de flux.

Les populations de failles ont été obtenues sur le terrain en suivant la méthodologie expliquée dans Lavenu et Cembrano (1999) et Lavenu (2006) dans des lieux choisis préalablement sur des images satellitaires, des cartes géologiques et des photographies aériennes où avaient été repérés des linéaments de premier ou second ordre avec une expression morphologique sur le terrain. Dans les emplacements choisis favorables à l'observation de plans de failles avec des indicateurs cinématiques nets et fiables, on a pu mesurer la direction et le pendage des plans ainsi que le rake (pitch) des stries en déterminant le sens de mouvement (Fig. 1-2).

Le concept de base du calcul de tenseurs provient de l'analyse vectorielle suivante. D'abord, sur chaque plan strié on définit deux vecteurs, un perpendiculaire au plan de faille n_i et un autre s_i parallèle au mouvement du bloc supérieur (Fig. 1-3). La contrainte σ_i appliqué à un plan de faille *i* correspond alors à la somme vectorielle tel que $\sigma_i = \sigma n_i + \tau_i$, où σn_i correspond à la composante perpendiculaire au plan de faille et τ_i à la composante de cisaillement. Cela implique que $(\tau_i, s_i)=0$ où τ_i est maintenant une relation de quatre paramètres qui définit le tenseur déviateur des contraintes. La relation de forme R de ces contraintes principales est égale à $\sigma'_2-\sigma'_1/\sigma'_3-\sigma'_1$ (Carey et Brunier, 1974) avec $\sigma'_1>\sigma'_2>\sigma'_3$ où σ'_1 est la contrainte déviatorique compressive, σ'_2 est la contrainte intermédiaire et σ'_3 est la contrainte déviatorique extensive. Les valeurs des quatre paramètres doivent satisfaire à $(\tau_i, s_i)\rightarrow 0$ et sont déterminées quand la relation $F= -\Sigma_{(i=1\rightarrow N)}\ k_i^* \cos^2(\tau_i, s_i)$ est minimale (Sébrier *et al*., 1985), où *N* correspond au nombre de plans de failles mesurés et $k_i=-1$ si $(\tau_i, s_i) \geq 90$ et $k_i=1$ si $(\tau_i, s_i) <90$.

À partir des approches initiales d'Anderson (1951), Wallace (1951), Bott (1959) et Price (1966), plusieurs auteurs ont proposé des méthodes de calcul numérique pour obtenir un tenseur des contraintes permettant d'interpréter la cinématique des failles dans un bloc de roche hautement fracturé. Dans toutes les méthodes, le résultat du calcul d'inversion fournit les axes $\sigma 1$, $\sigma 2$, $\sigma 3$ qui représentent le tenseur des contraintes. Ces méthodes se basent sur deux hypothèses alternatives: (1) la minimisation de la somme des erreurs de l'angle entre la direction de glissement observée pour chaque faille et l'effort de cisaillement calculé (Carey et Brunier, 1974; Carey, 1979; Armijo et Cisternas,

1978; Angelier et Goguel, 1979; Etchecopar *et al*., 1981; Angelier *et al*., 1982; Armijo *et al*., 1982; Michael, 1984; 1987; Reches, 1987; Gephart, 1988; Reches *et al*., 1992) et (2) la minimisation de la somme de l'angle de rotation entre chaque plan de faille observé et les plans qui font que la contrainte de cisaillement calculée coïncide avec la direction de glissement observée.

La fiabilité des tenseurs calculés numériquement a été statistiquement évaluée au moyen d'un histogramme des différences angulaires entre les directions de contraintes de cisaillement calculées et les stries mesurées, où une solution stable correspond à une différence <5º pour la majorité des

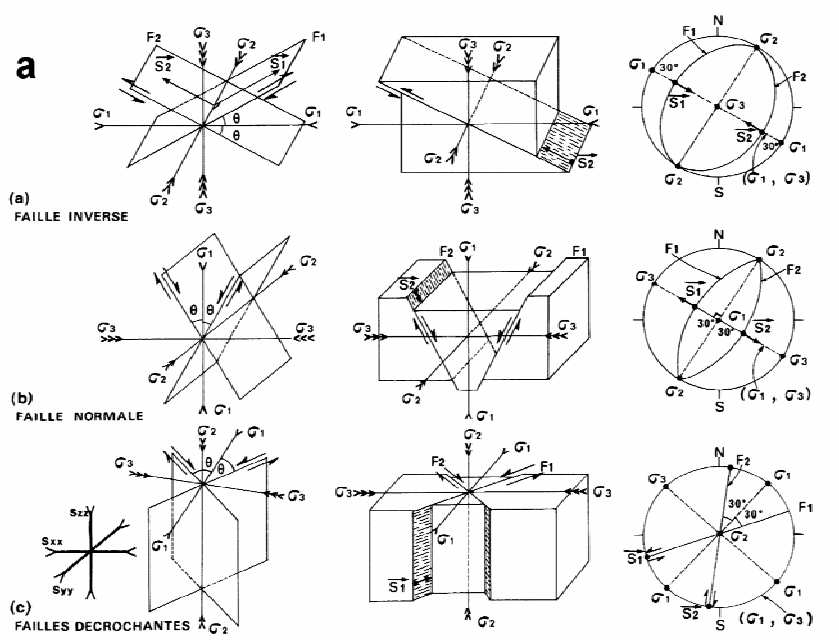

Fig. 1-5. (a) Failles selon Anderson (1951) et schéma des contraintes pour les différents régimes tectoniques. (b) Classification des tenseurs de contraintes et cercle de Mohr selon R (R=σ2-σ1/σ3-σ1) modifié d'après Ritz et Taboada (1993). σv peut être σ3 (régime compressif), σ2 (régime décrochant) ou σ1 (régime extensif).

données et <15º pour ce qui est des données restantes (Fig.1-3 ; 1-4).

D'autres auteurs comme Angelier et Mechler (1977), Pfiffner et Burkhard (1987), Marrett et Allmendinger (1990), Allmendinger *et al*. (1993) ont proposé une autre méthode semblable dans la façon mais conceptuellement différente pour effectuer l'analyse tectonique. À savoir, ils proposent le calcul des tenseurs de déformation (strain) et non des contraintes (stress) à partir de l'analyse des populations de failles. Avec quelques variations, le calcul d'ellipsoïdes de déformation se base sur la méthode des dièdres droits de manière semblable à celle utilisée pour obtenir des mécanismes focaux de séismes à partir de la polarité des ondes P.

Les deux méthodes donnent des résultats différents, bien qu'en néotectonique, et en assumant une rotation limitée des structures, ils soient proches et entraînent donc des interprétations parfois différentes. Finalement, quelques auteurs proposent un mélange des deux méthodes (Yin et Ranalli, 1993; Yin, 1996).

Quelques axiomes fondamentaux permettent d'interpréter les données cinématiques des plans de failles en termes de contraintes (Carey et Brunier, 1974): (1) pour chaque site de mesures, un événement tectonique observé se caractérise par un seul tenseur de contraintes homogène; (2) pour un événement tectonique donné, le glissement responsable de la striation se produit dans la même direction et le même sens que la projection de la contrainte de cisaillement sur chaque plan de faille et, en outre, la déformation est bref; et (3) la direction et le sens de l'indicateur cinématique sur le plan de faille, dépendent de l'orientation des contraintes et de la relation de forme R de l'ellipsoïde de contrainte.

La relation de forme R permet de déterminer les différents types de tenseurs et des régimes tectoniques qu'ils représentent. Ces différents régimes (compressif, décrochant et extensif) sont limités par quatre tenseurs de révolution qui représentent la compression uniaxiale, la compression radiale, l'extension uniaxiale et l'extension radiale (Ritz et Taboada, 1993). La superposition d'événements tectoniques, observable dans quelques sites de mesure, a été résolue en calculant des tenseurs indépendants pour chacun d'eux, après avoir effectué un essai de compatibilité et un filtrage manuel des plans incompatibles.

Dans ce travail, les tenseurs de contraintes ont été obtenus au moyen de l'algorithme inverse E.C.G.-GEOLDYNSOFT-5.0 de Carey et Mercier (1989), compilant un ensemble de sous-programmes. Dans des cas exceptionnels, comme par exemple quand on a enregistré seulement un système de failles dans le site de mesure, on a vérifié au moyen des dièdres droits les axes de raccourcissement et allongement en utilisant les programmes Faultkin 1.2.2© d'après Allmendinger *et al*. (1989; 1993) et TectonicsFP (www.tectonicsfp.com).

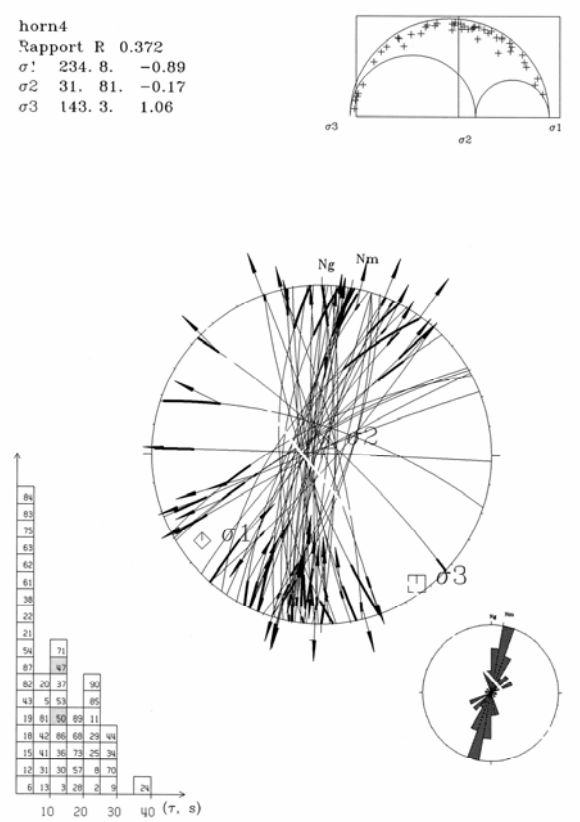

Fig. 1-6. Exemple du traitement des données par le logiciel E.C.G. GEOLDYNSOFT 5.0 d'analyse microtectonique.

À son tour, l'analyse des conditions de réactivation des failles anciennes a été ponctuellement pratiquée avec le programme Reactiva de Tolson *et al*. (2001).

Des antécédents géologiques ont été obtenus à partir des levers régionaux effectués simultanément par l'auteur et les collaborateurs faisant partie des programmes réguliers de SERNAGEOMIN. Entre autre, il faut souligner la carte 'Hoja Liquiñe-Neltume' (Lara et Moreno, 2004) d'échelle 1:100.000 qui couvre le secteur classique de définition de la ZFLO. De même, des études géologiques de détail ont été effectuées dans le cadre du

Programme de Risques Volcaniques de SERNAGEOMIN et ont permis de

Fig. 1-7. Photographies de plans striés a différentes échelles. (a) Long plan de faille dans des granites (Miocène) sur la ZFLO. (b) Détail de plan avec cisaillements de Riedel et mouvement dextre. (c) Roche volcanique avec stries glaciaires (volcan Mocho-Choshuenco, 40ºS) qui ne doivent pas être confondues avec des stries tectoniques, lesquelles ne sont pas superficielles mais pénétratives. (d) Exemple des failles (normales) peu abondantes dans des pyroclastiques du Pléistocène supérieur.

disposer d'une cartographie permettant de développer des études plus approfondies. Parmi celles-ci ils faut souligner les cartes géologiques d'échelle 1:50.000 ‘Géologie du Volcan Lanín' (Lara, 2004); ‘Géologie du Complexe Volcanique Puyehue-Cordón Caulle’ (Lara et Moreno, 2006) et ‘Géologie du Complexe Volcanique Mocho-Choshuenco’ (Moreno et Lara, 2006). Jusqu'à présent, les deux premières ont été à l'origine des articles scientifiques concernant l'évolution magmatique de ces centres (Lara *et al*., 2004a; Lara et al., 2004b; Lara *et al*., 2006b) et, en particulier, celui sur le Complexe Volcanique Puyehue-Cordón Caulle qui représente un cas d'étude abordé en détail pendant cette recherche.

Les données géochimiques ont été prises dans les publications ou préparées exclusivement pour les cas d'étude abordés. Elles ont consisté en analyse d'éléments majeurs et mineurs, particulièrement les terres rares, obtenus dans des échantillons de roche totale traités dans le Laboratoire de Chimie du SERNAGEOMIN. Des modèles de fusion partielle fractionnée et cristallisation fractionnée ont été construits à partir des données avec assistance partielle de programmes comme FC-Modeler (Keskin, 2002) par exemple.

Les données géochronologiques $^{40}Ar/^{39}Ar$ ont été obtenues dans le Laboratoire de Géochronologie du SERNAGEOMIN (Fig. 1-5) en suivant la méthode décrite par Arancibia *et al*. (2006). Les échantillons de roche pour datation ont été ensuite broyés manuellement et séparés entre 250-80 µm pour extraire les phénocristaux ou les surfaces altérées. Les fractions ont été mises dans le réacteur nucléaire de La Reina (Chili) pour une période de 48 heures. Postérieurement, l'analyse de fusion totale a été effectuée pour calculer le facteur J. La distribution de J dans deux dimensions sur chaque disque a été modelée avec un polynôme quadratique pour construire un plan de J pour chacun. À partir de cela, on a calculé un facteur J individuel pour chaque échantillon. Puis les échantillons ont été placés dans un disque d'aluminium de haute pureté avec un grain de sanidine de Fish Canyon (28.03±0.1 Ma; Renne *et al*., 1994) comme standard et postérieurement soumis au chauffage par des passages d'un laser de CO_2 à la puissance de 30 W. Tous les trois passages, on a analysé une ligne de blanc. Finalement, les gaz nobles ont été séparés des autres gaz au moyen d'un ‘piège froid’ à -133°C. Une fois purifiés, les gaz

nobles ont été introduits dans un spectromètre de masse de haute résolution MAP 215-50. La ligne de base a été analysée au début et à la fin et les 'pics' en ont été soustraits. Des erreurs du spectromètre ont été corrigées par des analyses périodiques d'échantillons d'air à partir desquelles un facteur de correction a été calculé. Finalement, en suivant Fleck (1977), on a obtenu des âges plateau avec au moins 3 passages rapprochés qui concentrent 50% du gaz libéré. Dans quelques cas, quand la précision analytique a été plus grande, on a préféré utiliser l'âge de l'isochrone inverse.

D'autre part, quelques âges complémentaires du Complexe Volcanique Puyehue-Cordón Caulle ont été obtenus à l'Université de Wisconsin-Madison par B. Singer (Lara *et al*., 2006b).

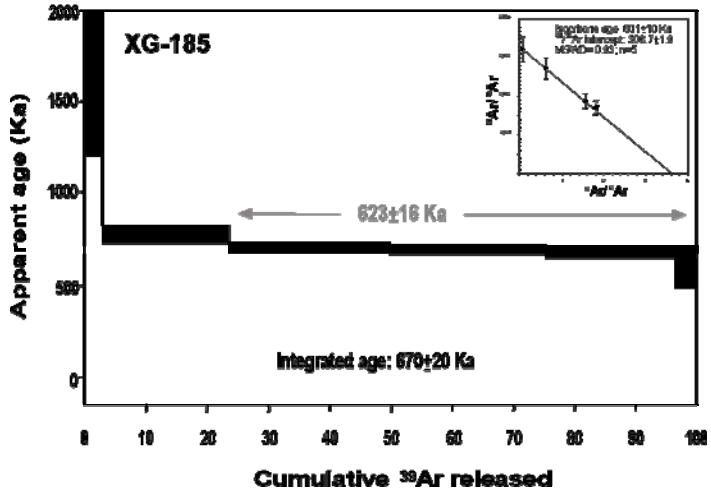

Fig. 1-8. Exemple de datation $^{40}Ar/^{39}Ar$ sur roche totale d'un basalte du volcan Chihuío (39.7ºS) réalisée dans le Laboratoire de Géochronologie de Sernageomin, Chili.

Une autre façon d'appréhender la géométrie des structures du socle et les composantes du tenseur de contrainte dans des régions couvertes par des volcans quaternaires est de faire une analyse morphométrique des cônes volcaniques. En premier lieu, comme l'avait déjà proposé antérieurement Nakamura (1977), l'alignement des cônes de flanc sur les stratovolcans est un indicateur de l'existence d'un champ de contrainte régional et la direction de l'alignement correspondrait à la direction de S_{Hmax}. Cette hypothèse est basée sur le fait que les cônes de flanc sont supposés être nourris par des dykes verticaux, qui se propagent perpendiculairement à $\sigma 3$, celui-ci étant orthogonal

à S_{Hmax}. Dans un régime décrochant, S_{Hmax} sera égal à $\sigma 1$ et dans un régime extensif il sera égal à $\sigma 2$.

Par ailleurs les expériences de modèles analogiques de Tibaldi (1995) étendent l'analyse antérieure à des groupes de cônes situés sur des surfaces en pente douce, et qui n'ont pas connexion directe avec les stratovolcans. Dans ce cas, les paramètres morphologiques tel que l'allongement de la base des cônes, l'allongement des cratères et la direction de la droite qui joint les points bas de ces cratères sont les paramètres les plus représentatifs de la structure sous-jacente. Les directions de 'breaching' (effondrement latéral) sont plus ambiguës et dépendent de la topographie. Par la suite, Adiyaman et al (1998) restreignent le critère des cônes ou des groupes de cônes monogéniques à ceux ayant des formes strictement elliptiques ou qui forment un groupe aligné avec le plus grand cône au centre et les cônes mineurs aux extrémités (Fig.1-9)

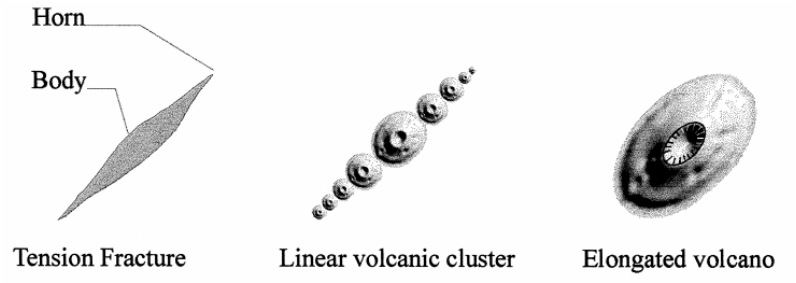

Fig. 1-9. Morphologie des cônes monogéniques comme indicateur de S_{Hmax} d'après Adiyaman *et al*. (1998). L'alignement ou l'allongement des cônes correspondrait à la direction de S_{Hmax}

1.9 Présentation des résultats

Les principaux sujets ont été abordés dans les chapitres 3 et 4 à partir des articles publiés ou à publier prochainement et qui les développent. Dans le *chapitre 1* on fait une présentation formelle concernant le problème scientifique, le secteur choisi pour l'étude, les principales hypothèses de travail et la méthodologie employée. Dans le chapitre 2 on fait une synthèse des principales caractéristiques de l'arc volcanique dans le secteur d'étude présentées comme

un résumé de deux chapitres d'un ouvrage élaboré en collaboration avec d'autres auteurs (Corbella et Lara, sous presse; Stern *et al*., sous presse) dans lesquels on souligne une synthèse du volcanisme du Cénozoïque supérieur dans la Patagonie et un résumé sur le magmatisme dans les Andes du Sud. On analyse aussi l'architecture et le raccourcissement de l'arc volcanique pliocène-quaternaire entre 37° et 42°S. Dans le *chapitre 3* on analyse la croûte fracturée et ses effets sur le volcanisme avec un cas d'étude concernant l'évolution magmatique du Complexe Volcanique Puyehue-Cordón Caulle (40°S). Dans le *chapitre 6* on discute du déclenchement à distance du volcanisme et de la déformation cosismique. Dans le *chapitre 4* on analyse les effets de la transpression et le champ de contraintes locales et on fait une discussion sur la relation entre la transpression et le volcanisme holocène le long de la ZFLO. Le *chapitre 5* présente une récapitulation des problèmes scientifiques abordés où on examine les résultats et les conclusions principales en posant les points de conflit et les conséquences des découvertes effectuées. Le *chapitre 6* synthétise de manière formelle les principales conclusions de cet ouvrage déjà contenues dans les articles présentés, les impacts prévisibles et les futures lignes de recherche qui apparaissent. Finalement, le *chapitre 7* contient la liste complète des références citées dans ce travail. Une annexe contient les données structurales obtenues dans cette étude en incluant celles utilisées dans les articles respectifs ainsi que celles qui n'ont pas permis le calcul de tenseurs fiables. On inclut aussi les données apportées par des études préalables pour structurer un ensemble complet. De même, on ajoute une liste des centres volcaniques inclus dans le secteur d'étude avec leurs principales caractéristiques.

Chapitre 2
Volcanisme Cénozoïque des Andes du Sud entre 37°et 42°S

L'éruption du volcan d'Antuco 1839 vu par Claude Gay (1800-1873)

Chapitre 2. Volcanisme Cénozoïque des Andes du Sud entre 37°et 42°S

2.1 Architecture de l'arc volcanique des Andes du Sud

Les volcans de la Zone Volcanique du Sud (ZVS: 33°-46°S) se localisent principalement au Chili et en Argentine. Au Chili centre-sud, la ZVS comprend 70 stratovolcans quaternaires et au moins neuf complexes de caldera, ainsi que des dizaines de petits centres éruptifs constitués par des cônes de scorie et des maars. Ceux-ci forment un segment d'arc volcanique continu de 1400 kilomètres de long de 33.3ºS à 46ºS. Entre 33.3º et 34.4ºS, l'arc est une chaîne étroite de volcans situés le long de la frontière Chili-Argentine, mais entre 34.4º et 39.5ºS l'arc s'élargit jusqu'à 200 kilomètres et se situe au Chili et en Argentine. Au sud de 39.5ºS, la ZVS se compose encore d'une chaîne relativement étroite de volcans et au sud de 42°S l'arc volcanique est situé complètement au Chili (Fig.1-1).

La ZVS a l'activité volcanique historique la plus importante, avec environ une éruption par an en moyenne. Les volcans Villarrica et Llaima (~39°S) sont les volcans les plus actifs dans la chaîne andine, avec chacun plus de 60 épisodes d'activité rapportés depuis 1558 (Simkin et Siebert, 1994). Parmi les 70 stratovolcans entre 33.3º et 46ºS, au moins 40 ont eu des éruptions durant l'Holocène et 20 ont eu des éruptions historiques. La plupart des centaines de cônes et maars monogéniques sont également holocènes, et trois d'entre eux (Riñinahue, Carrán et Mirador ; ~40°S) ont manifesté une activité pendant le siècle dernier. Diverses calderas ont été formées durant les derniers 200 ka.
Sur la base de considérations pétrologiques et géochimiques, l'arc volcanique quaternaire de la ZVS est divisé en quatre provinces ou segments principaux (Tormey *et al*., 1991; López-Escobar *et al*., 1995a; Stern, 2004). Ce sont les zones septentrionale (ZVSN : 33.3°-34.4°S), transitoire (ZVST : 34.4°-37°S), centrale (ZVSC : 37°- 42°S) et méridionale (ZVSS : 42°-46°S) (Fig.1-1).

Les taux des émissions magmatiques dans la ZVSN sont plus faibles que pour les segments méridionaux et les volcans ont des altitudes, au-dessus

de leur base, significativement plus faibles aussi. Dans ce segment il existe un groupe de volcans anciens profondément érodés (Caldera Nevado sin Nombre ; Nevado de Piuquenes ; Marmolejo ; Castillo, Caldera el Diamante, Listado et Picos del Barroso). Le groupe le plus jeune se compose des stratocônes actifs du Tupungato et du Tupungatito (5682 m), situés au-dessus du flanc de la Caldera Nevado sin Nombre, du complexe volcanique de San José (5.856 m) avec le volcan Marmolejo (López Escobar *et al.* 1985) et le volcan Maipo situé à l'intérieur de la Caldera de Diamante. Parmi eux, les volcans Tupungatito, San José et Maipo ont eu des éruptions historiques, les plus récentes en 1987, 1960 et 1912, respectivement. Tupungatito et San José montrent une activité solfatarique permanente.

De 34.4º à 37.0ºS, le front volcanique quaternaire de la ZVST a une direction N20ºE. L'arc s'élargit considérablement vers l'est en l'Argentine, avec des centres volcaniques situés sur des blocs élevés NW-SE séparés par des bassins extensifs contenant de petits cônes basaltiques (Muñoz et Stern, 1988, 1989). Les structures transversales induisent plusieurs complexes volcaniques au sud du volcan Planchón-Peteroa-Azufre. Ainsi, les volcans Descabezado Chico et San Pedro-Tatara-Pellado sont situés le long d'une structure NE-SW et les complexes Nevado de Longaví-Loma Seca-Resago et Nevados de Chillán sur une structure NW-SE.

La ZVST est caractérisée par de grands stratovolcans composés et des complexes volcaniques qui recouvrent les volcans basaltiques et les calderas. Du nord aux sud, les centres volcaniques les plus importants du Pléistocène-Holocène de la ZVST sont: Palomo (4850 m), Tinguiririca (4300 m), Planchón-Peteroa-Azufre (4101 m; Tormey *et al*., 1995; Naranjo et Haller, 2002), Descabezado Grande-Quizapu-Azul (3953 m; Hildreth et Drake, 1992), Descabezado Chico (3250 m), Caldera Calabozos (Hildreth *et al*., 1984), Del Medio (3508 m), San Pedro-Tatara-Pellado (3621 m; Dungan *et al*., 2001), Laguna del Maule (3175; Frey *et al*., 1984, Nevado de Longaví (3242 m; Sellés *et al*., 2004), Loma Blanca (2230 m), Resago (1890 m) et Nevado de Chillán (3216 m; Dixon *et al*., 1999; Naranjo et Lara, 2004). Les stratovolcans et les calderas fortement érodés et les plus anciens, probablement pliocènes-pléistocènes, forment la marge occidentale de la Caldera del Atuel et les complexes Alto del Padre- Sordo Lucas (3548 m) et Campanario (4020 m ;

Hildreth *et al*., 1998).

Les complexes volcaniques historiquement actifs sont Tinguiririca, Planchón-Peteroa-Azufre, Descabezado Grande-Quizapu-Azul, San Pedro-Tatara-Pellado et Nevados de Chillán.

Le secteur nord de la ZVSC (37°-39ºS), comme la ZVST, a près de 120 kilomètres de large, avec des bassins d'intra-arc et des volcans d'arc en Argentine (Muñoz et Stern, 1988, 1989; Lara et Folguera, 2006). Au sud de 39°S, le ZVSC se rétrécit en une chaîne de seulement environ 80 kilomètres de large sans bassin d'intra-arc. La ZVSC se trouve entièrement à l'ouest de la frontière Chili-Argentine, ceci dû à la réduction de la largeur de l'arc à partir du Pléistocène Supérieur (Lara *et al*., 2001; Lara et Folguera, 2006). Le front volcanique se compose d'édifices pliocènes et pléistocènes profondément érodés et des stratovolcans actifs les recouvrent. Au sud de 40.5ºS, les stratovolcans modernes se produisent le long de la marge occidentale de la Cordillère Principale.

Au sud de 38ºS, la ZFLO est le lieu de plusieurs centres volcaniques parmi les plus grands ainsi que de cônes monogéniques. Bien que l'arc volcanique ait presque une direction N-S, les alignements obliques induisent plusieurs des complexes volcaniques et des grands stratovolcans le long des structures NW-SE et NE-SW. Les édifices volcaniques de la ZVS atteignent leur taille maximum dans la ZVSC, montant jusqu'à 2600 m au-dessus de leur base et couvrant plus de 500 km2 bien que les altitudes du substratum continuent de diminuer au sud.

Le front volcanique de la ZVSC inclut les volcans Antuco (2979 m; López-Escobar *et al*., 1981 ; Lohmar, 2000), Callaqui (3100 m), Tolguaca (2806 m), Lonquimay (2865 m; Moreno et Gardeweg, 1989; Naranjo *et al*., 1992), Llaima (3179 m; Naranjo et Moreno, 1991; Moreno et Naranjo, 2003), Sollipulli (2282 m; Naranjo *et al*., 1993a; Gilbert *et al*., 1996), faisceau de Caburgua (998 m), Villarrica (2847 m; Moreno, 2000; Lara et Clavero, 2004; Moreno et Clavero, 2006), Mocho-Choshuenco (2422 m; Echegaray, 2004; Moreno et Lara, 2006), Cordillère Nevada (1799 m; Moreno, 1977; Lara *et al*., 2006b; Lara et Moreno, 2006), chaîne fissurale du Cordón Caulle (1793 m; Moreno, 1977; Lara *et al*., 2006a et 2006b; Lara et Moreno, 2006), Puyehue (2236 m; Moreno, 1977; Gerlach *et al*., 1988; Lara et Moreno, 2006), Antillanca (1990 m),

Puntiagudo-Cordón Cenizos (1668 m), Osorno (2.652 m; López-Escobar *et al*., 1992) et Calbuco (2003 m; Hickey-Vargas *et al*., 1995; López-Escobar *et al*., 1995b). Parmi eux on trouve des stratovolcans érodés du Pléistocène inférieur-moyen comme Sierra Velluda (3585 m), Lancú (2296 m), Sierra Nevada (2554 m), Llallicupe (1915 m), Quinquilil (2002 m), Quinchilca (1632 m), Mencheca (1840 m), Sarnoso (1630 m), La Picada (1715 m) et Hueñuhueñu (1207 m).

Entre 38° et 39.5ºS, la partie orientale de l'arc inclut le volcan Copahue (2952 m; Varekamp *et al*., 2001; Naranjo et Polanco, 2004) situé sur le bord occidental de la caldera El Agrio (Muñoz et Stern, 1988, 1989; Folguera et Ramos, 2000). Au sud ouest, les petits cônes holocènes recouvrent un plateau volcanique pliocène-pléistocène avec des stratovolcans érodés qui incluent la caldera pléistocène Pino Hachado (Muñoz et Stern, 1988; 1989). Au sud de 39.5ºS et derrière le front volcanique, l'arc inclut les volcans actifs Quetrupillán (2360 m) et Lanín (3774 m; Lara *et al*., 2004b; Lara, 2004), ainsi que les complexes Huanquihue, Chihuío (Lara et Moreno, 2004; Lara et Folguera, 2006), Pirehueico (Lara et Moreno, 2004; Lara et Folguera, 2006), Mirador, Pantoja, Tronador (Mella *et al*., 2005), Cerro Volcánico et Cuernos del Diablo. Les centres éruptifs mineurs tels que Caburgua, Huelemolles, Llizán, Fuy, Carrán-Los Venados, Cordón Cenizos, Cayutue et Ralún, parmi beaucoup d'autres, se produisent également à proximité des stratovolcans et le long de la ZFLO.

La ZVSC est le segment volcanique le plus actif de toutes les Andes et inclut deux des volcans les plus actifs en Amérique du Sud. Les complexes volcaniques ayant eu une activité historique sont brièvement décrits ci-dessous.

L'Antuco est un stratovolcan composé, actif depuis le Pléistocène supérieur, qui recouvre le centre érodé Sierra Velluda. Un premier édifice s'est effondré latéralement à l'ouest après une éruption de type Bandai il y a 6.2 Ka, laissant un cratère de 2 km de large et produisant une avalanche de débris de 5 km^3 qui a atteint la Dépression Centrale (Thiele *et al*., 1998). Le stratocône actuel s'est développé à l'intérieur de ce cratère d'avalanche. L'Antuco a eu au moins 17 éruptions historiques (Thiele *et al*., 1998). La dernière grande éruption s'est produite en 1853 et la dernière activité a été enregistrée en 1911. Actuellement, le volcan Antuco a une activité fumerolienne faible au sommet.

Le Callaqui est fortement commandé par une fissure NE-SW avec une

rangée de 11 km long de cratères et il possède un cratère principal rempli de glace au sommet. Il a été en activité depuis le Pléistocène supérieur La dernière éruption enregistrée a eu lieu en 1980. Actuellement, le Callaqui présente une activité solfatarique forte sur le flanc sud près du sommet.

Le Copahue est un stratovolcan composé d'âge pléistocène-holocène (Varekamp *et al*., 2001) situé à l'intérieur de la Caldera El Agrio (Pesce, 1989; Linares *et al*., 1999, 2001; Folguera et Ramos, 2000). L'édifice actuel a neuf cratères alignés et le plus oriental accueille un lac acide. Douze éruptions principalement phréatiques ont été rapportées pendant les trois derniers siècles (Naranjo et Polanco, 2004).

Le Lonquimay fait partie d'un alignement de cônes principalement actifs pendant l'Holocène (Moreno et Gardeweg, 1989). L'activité explosive holocène était abondante bien que seulement cinq éruptions historiques aient été signalées (Moreno et Gardeweg, 1989; Barrientos et Acevedo, 1992; Naranjo *et al*., 1992; Naranjo *et al*., 2000).

Le Llaima est un volcan composé pléistocène-holocène avec un cratère central et de nombreux cônes de flanc qui remplissent une caldera (Naranjo et Moreno, 2005). La succession des dépôts pyroclastiques inclut une ignimbrite basaltique de 24 km^3 formée vers *ca*.13.5 ka (Naranjo et Moreno, 1991; Moreno et Naranjo, 2003). Au moins 30 éruptions historiques ont été rapportées, la plus grande en 1640, et les fumerolles actives sont évidentes dans le cratère central. Le Villarrica est un volcan composé pléistocène-holocène situé dans une dépression constituée par deux calderas concentriques (Moreno et Clavero, 2004 *In* Lara et Clavero, 2004; Moreno et Clavero, 2006). Une séquence épaisse de dépôts pyroclastiques postglaciaires commence par une ignimbrite andésitique basaltique de 10 km^3 formée vers *ca*. 12.5. Une petite caldera plus récente a été probablement liée à l'éruption d'une ignimbrite vers *ca*. 3.5 ka (Clavero, 1996). Plus de trente éruptions historiques ont été rapportées, les plus récentes en 1948-49, 1963-64 et 1971-72. Des petites éruptions de type strombolien se produisent fréquemment en raison de la dynamique d'un lac de lave de cratère qui a persisté au moins depuis l'éruption de 1972 (Calder *et al*., 2004; et Witter *et al.*, 2004 *In* Lara et Clavero, 2004).

Le Quetrupillán est un complexe volcanique pléistocène-holocène situé sur la ZFLO et constitué par deux calderas concentriques et plusieurs dômes et

cônes pyroclastiques (Pavez, 1997). Une épaisse succession pyroclastique postglaciaire a été identifiée et de nombreuses éruptions historiques ont été observées, la plus récente en 1872.

Le Puyehue-Cordón-Caulle est un complexe volcanique pléistocène-holocène constitué par la Caldera Cordillère Nevada, des fissures de Cordón Caulle et le volcan de Puyehue sur un alignement NW-SE (Moreno, 1977; Lara *et al*., 2006a; Lara *et al*., 2006b). Ce complexe a émis des produits pyroclastiques de volume considérable à l'Holocène. Une éruption remarquable de rhyodacites à partir de fissures a suivi le grand tremblement de terre Mw: 9.5 en 1960 (Lara *et al*., 2004b).

L'Osorno est un stratovolcan pléistocène-holocène (Moreno *et al*., 1985) avec un champ de cônes pyroclastiques holocènes sur ses flancs. Au moins dix éruptions historiques ont été rapportées, la dernière en 1835 (Petit-Breuilh, 1999).

Le Calbuco est un volcan composé pléistocène-holocène (López-Escobar *et al*., 1992; 1995b). Il montre une avalanche qui a coulé vers le nord (Moreno *et al*., 1985). Un dôme andésitique s'est développé à l'intérieur de l'amphithéâtre. Onze éruptions historiques ont été enregistrées, la dernière en 1961 (Petit-Breuilh, 1999).

La ZVSS (42°-46°S ; Fig.1-1) se compose de 13 volcans quaternaires qui forment une chaîne étroite entièrement au Chili (Futa et Stern, 1988; López-Escobar *et al*., 1995a; D'Orazio *et al*., 2003; Naranjo et Stern, 2004). Quelques centres éruptifs mineurs se produisent également dans la ZVSS le long de la ZFLO. Les stratovolcans composés les plus grands de la ZVSS sont Yate, Hornopiren, Michinmahuida, Corcovado, Yanteles, Melimoyu, Mentolat, Cay, Maca et la caldera du volcan Hudson. Tous ont eu des éruptions holocènes (Naranjo et Stern, 2004), excepté peut-être le volcan Cay. Le Michinmahuida a eu des éruptions historiques en 1742 et 1834-35, et le volcan Hudson a eu une éruption qui a produit un grand lahar en 1971 (Best, 1992), suivi d'une grande éruption explosive en 1991 (Naranjo *et al*., 1993b). L'Hudson est anormal dans la ZVSS en ce qui concerne le nombre d'éruptions holocènes explosives de grand volume qu'il a produites, phénomène qui peut-être lié à sa proximité du Point Triple du Chili.

2.2 Pétrogenèse et évolution magmatique

Il existe d'importantes différences entre les magmas de la ZVSN et ceux des segments méridionaux. Ceci peut se produire pendant l'interaction des magmas, dérivés de l'asthénosphère, avec la lithosphère continentale (Rogers et Hawkesworth, 1989; Stern et Kilian, 1996; Hickey-Vargas *et al*., 2002), par assimilation dans la croûte (James, 1984; Hildreth et Moorbath, 1988; Davidson *et al*., 1991), et/ou par contamination de la source asthénosphérique par les composants continentaux (Stern *et al*., 1984; Stern, 1989 ; 1991; Stern et Skewes, 1995; Kay *et al*., 2005). De tels processus peuvent être attribués aux variations de l'épaisseur et de la composition de la croûte continentale (Hildreth et Moorbath, 1988; Dungan *et al*., 2001), à la nature de l'asthénosphère, à la contamination de la source par l'érosion tectonique de la marge continentale (Stern, 1991; 2004) et à une combinaison de ces paramètres.

Dans la ZVS centrale et méridionale, où la croûte est relativement mince (<35 km), les basaltes tholéïtiques à taux d'alumine élevé et les andésites basaltiques sont les roches dominantes issues des stratovolcans et de nombreux centres éruptifs mineurs (López-Escobar *et al*., 1995a; Hickey-Vargas *et al.*, 1984, 1986, 1989; Gerlach *et al*., 1988 ; Futa et Stern, 1988) ; les andésites, les dacites et les rhyolites sont aussi présentes.

Une différence importante qui distingue la ZVSS de la ZVSC est la présence, dans les roches de la ZVSC les plus siliciques, de minerais hydratés, comme la hornblende (dans les roches avec SiO_2 >59%) et la biotite. D'autre part, les données isotopiques de Sr, de Nd, de Pb et de O pour des basaltes de la ZVSC et de la ZVSS excluent toute assimilation significative de croûte continentale. Les basaltes de la ZVSC et de la ZVSS se forment par la fusion de l'asthénosphère contaminée par des fluides dérivés de la déshydratation de la lithosphère océanique y compris des sédiments (Morris *et al*., 1990; Sigmarsson *et al*., 1991; Hickey *et al*., 2002 ; Sigmarsson *et al*., 2002; Barreiro, 1984; MacFarlane, 1999) (Fig. 3-2).

Les taux décroissants de Ba/La, La/Nb et Ba/Nb dans les magmas émis progressivement à l'est du front volcanique dans la ZVSC suggèrent l'entrée décroissante des fluides dans la source des volcans en arrière du front en raison de la déshydratation progressive de la plaque océanique (Futa et Stern,

1988). Les taux de Ba/La et La/Nb décroissants à travers l'arc de la ZVSC sont associés à l'augmentation des Terres Rares légères (LREE) et sont interprété comme la réduction du degré de fusion partielle de l'asthénosphère (Hickey-Vargas *et al*., 1986, 1989; Muñoz et Stern, 1989 ; López-Escobar *et al*., 1995a).

Plus à l'est, dans la région de l'arrière-arc, les basaltes alcalins seraient générés par des degrés relativement bas de fusion asthénosphérique et ils montrent peu ou pas d'évidence de contamination par des composants dérivés de la plaque océanique (Skewes et Stern, 1979; Stern *et al*., 1990; Kay *et al*., 1993; Gorring *et al*., 1997).

Les andésites, les dacites et les rhyolites de la ZVSC et de la ZVSS ont généralement la même composition isotopique que les basaltes et les andésites basaltiques, indiquant qu'elles ont èté formées durant un processus FC (fractionnement et cristallisation) sans assimilation (Gerlach *et al*., 1988), ou ont assimilé une croûte jeune, isotopiquement semblable, telles que les roches plutoniques miocènes (McMillian *et al*., 1989).

Stern et Skewes (1995), Nyström *et al*. (2003) et Kay *et al*. (2005) ont démontré que la différence isotopique entre la ZVSN et la ZVSC s'est développée pendant le Miocène Supérieur et le Pliocène, avant la migration du

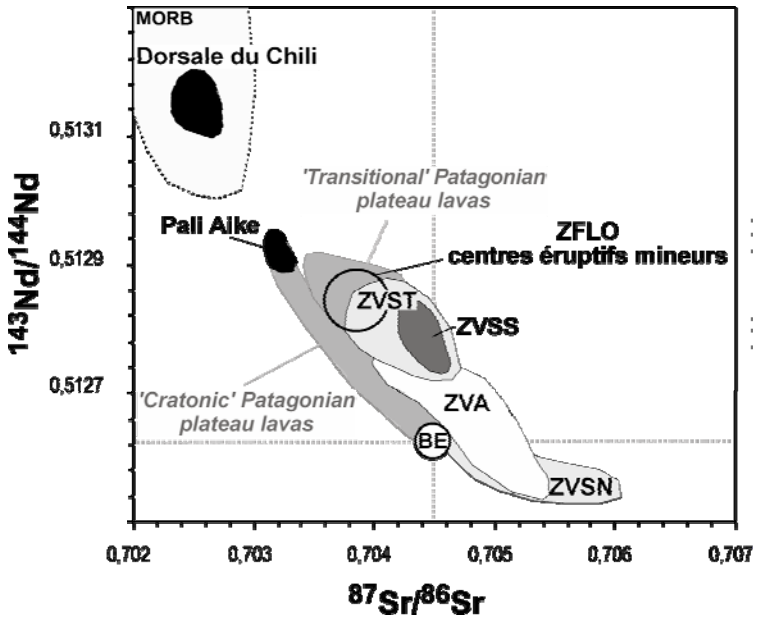

Fig. 2-1. Caractéristiques de la composition des magmas dans la Zona Volcaniques des Andes du Sud (33°-46°S) d'après Stern *et al*. (sous-presse) et références incluses.

front volcanique à sa position actuelle dans la Cordillère Principale au-dessus

d'une croûte relativement épaisse, supérieure à 45 km. À la latitude du volcan Maipo (34°S), les changements progressifs entre le Miocène et le Pliocène observés dans la composition isotopique des basaltes, impliquent des changements dans la composition isotopique de la région-source (Stern et Skewes, 1995). La migration diachronique vers le sud de ces derniers changements suit de près la migration vers le sud de la subduction de la Dorsale Juan Fernández et suggère qu'une partie importante de ces changements résulte de la contamination de la source provoquée par l'érosion tectonique.

2.3 Architecture de l'arc volcanique pliocène-quaternaire entre 37º et 42ºS

Dans cette section on analyse les conditions préexistantes de l'architecture actuelle de l'arc volcanique dans le segment 37°-42°S. En particulier, on révise la transition d'un arc volcanique exceptionnellement large à la fin du Pliocène à un arc volcanique étroit au début du Pléistocène (Lara et Folguera, 2006). On montre que cette transformation s'accompagnée d'un front volcanique essentiellement statique, dans la même position que l'actuel. Des âges $^{40}Ar/^{39}Ar$ démontrent que le front magmatique était dans la même position que'à l'actuel, et on peut vérifier qu'il était ici depuis le Miocène; ces âges écartent donc l'idée de la migration de ce front comme l'avaient suggérée des auteurs précédents (Muñoz et Stern, 1989). D'autre part, et malgré la difficulté à établir des limites chronologiques précises de la déformation quaternaire dans la région, Lavenu et Cembrano (1999) ont aussi établi un changement dans le régime de contraintes à la fin du Pliocène et on suggère ici que les deux processus (arc plus étroit et transition d'une compression E-W à une transpression dextre) ont pu être en rapport. En effet, on propose que les deux processus soient mis en rapport avec une réduction de la vitesse de convergence, produite immédiatement avant ces changements. Après cette transition la ZFLO concentrerait, le long de son axe, l'activité volcanique.

2.4 Le rétrécissement pliocène à quaternaire de l'arc volcanique dans les Andes du Sud entre 37° et 41°S

Un système complexe d'arrière-arc s'est développé sur la marge occidentale du bassin de Neuquén, au sud de 37ºS, pendant le Cénozoïque Supérieur. Au Miocène Moyen-Supérieur la déformation transpressive a affecté le front orogénique occidental (Zone de Faille Liquiñe-Ofqui, ZFLO) et les Andes orientales ont été soumises à une déformation compressive. Au sud de 38ºS, une physiographie dominée par des blocs élevés et des bassins allongés était le lieu du volcanisme intense du Pliocène ancien à l'Holocène. Un arc volcanique large s'est établi depuis le front orogénique occidental jusqu'au pied oriental des Andes pendant le Pliocène comme le démontrent les datations ^{40}Ar-^{39}Ar entre *ca*. 340 et 980 Ka. Cette phase volcanique était simultanée avec la déformation transpressive le long de l'arc frontal et des épisodes passagers d'extension dans l'arrière-arc intérieur. Les signatures géochimiques d'arc (taux élevé de Ba/La; taux faible La/Yb) se sont produites plus loin à l'est du front, montrant une subduction accrue dans le manteau situé au dessous de l'arc. Une diminution de la vitesse de convergence de la plaque de Nazca (antérieure à 2-3 Ma), avec un front volcanique stable a causé un rétrécissement progressif à l'ouest de l'arc volcanique quaternaire, probablement depuis *ca*. 1.6 Ma. A partir du Pléistocène Moyen-Supérieur, le volcanisme a été principalement concentré sur le Système de Faille Liquiñe-Ofqui, avec une activité holocène mineure dans la région andine orientale. Des signatures géochimiques d'arc sont alors limitées au front volcanique actuel. Morphologiquement, ceci a eu comme conséquence la création de bandes d'appareils volcaniques qui reflètent différentes étapes d'arc se rétrécissant plutôt que des arcs séparés comme cela a été précédemment proposé.

L'évolution de l'architecture de l'arc volcanique est dominée par des facteurs géodynamiques de premier ordre. Durant le Quaternaire, le système de failles d'intra-arc et la néotectonique de la région contrôlent l'évolution volcanique entre 37 et 42ºS.

Chapitre 3
Influence de la croûte fracturée et ses effets sur le volcanisme d’arc

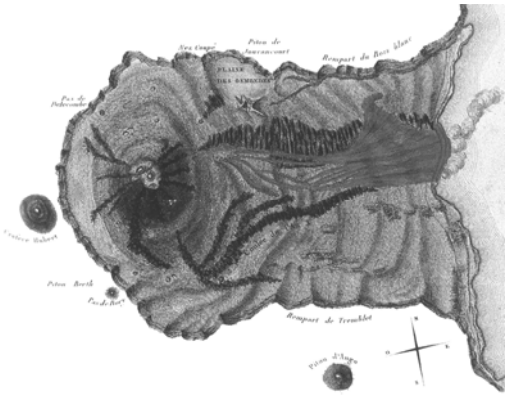

Chapitre 3. Influence de la croûte fracturée et ses effets sur le volcanisme d'arc

3.1 Introduction

Dans ce chapitre, on aborde, au moyen des articles publiés, l'influence de la structure sous-jacente aux complexes volcaniques. Elle pourra être vue comme le résultat de l'influence de la géométrie et de la cinématique des failles anciennes qui contrôlent effectivement la distribution des centres d'émission tant dans le long terme, à l'échelle de la vie d'un complexe volcanique, comme dans le court terme pendant des épisodes volcaniques plus courts. Dans le premier cas, l'article de Lara *et al*. (2006b) montre comment l'évolution magmatique du Complexe Volcanique Puyehue-Cordón Caulle est dominée par une structure NW identique à celles qui caractérisent l'avant-arc des Andes du Sud. Cette structure, réactivée pendant le Quaternaire, a servi comme canal d'acheminement et d'emplacement temporaire des magmas. Toutefois, une structure comme celle-ci constitue un domaine compressif dans le régime transpressif qui gouverne la néotectonique de l'arc; ces conditions ont déterminé des temps plus grands de résidence des magmas dans la croûte et des mécanismes de différenciation plus complexes qui accompagnent des styles éruptifs plus complexes aussi. La géochronologie $^{40}Ar/^{39}Ar$ de haute résolution a permis d'identifier les différents centres d'émission et de ratifier l'hypothèse de simultanéité en confirmant ainsi le fonctionnement d'un système de fissures long terme. Dans la section suivante on examine un cas ponctuel où des éruptions de fissures siliciques ont été causées à distance par des séismes éloignés de la zone de subduction.

En théorie, la déformation cosismique associée aux séismes de la zone de subduction affecterait principalement la région d'avant-arc sans conséquence dans l'arc volcanique, situé généralement à *ca*. 200 km de la fosse dans des zones à angle de subduction modéré. Toutefois, les grands séismes (magnitudes supérieures à Mw: 9) peuvent transmettre une contrainte dynamique à plusieurs kilomètres à l'intérieur de la marge convergente. Des

exemples disponibles dans la littérature ont été analysés par Linde et Sacks (1998). La modification du champ de contraintes régional en raison d'un séisme a été examinée, entre autres, par Harris (1998). Dans ce chapitre on analyse le cas de l'éruption fissurale du Cordón Caulle (40ºS) dans les Andes du Sud au Chili, produite 38 heures après le plus grand séisme instrumentalement enregistré (Valdivia, Mw: 9,5) et analysé dans l'article de Lara *et al*. (2004a). Des données paléosismologiques de Cisternas *et al*. (2005) montrent que les grands séismes auraient une récurrence de *ca*. 300 ans dans le segment 38º-42ºS. Ainsi, le séisme de 1575 AD a pu aussi être responsable d'une éruption volcanique dans la zone en faisant de ce mécanisme un important facteur dans la relation entre néotectonique et volcanisme.

3.2 Evolution magmatique du Complexe Volcanique Puyehue-Cordón Caulle (40ºS), Zone Volcanique des Andes du Sud : d'un volcanisme de plateau à un volcanisme fissural rhyolitique anormal

Entre les latitudes 37º et 46ºS, les volcans quaternaires des Andes Centrales méridionales sont la source de magmas principalement basaltiques et andésitiques. Par exemple, le Complexe Volcanique Puyehue-Cordón Caulle (CVPCC ou PCCVC en anglais; 40ºS) montre une évolution magmatique singulière due à l'évacuation anormale des rhyolites, particulièrement dans les derniers 100 Ka. D'autre part, le CVPCC est le résultat de la juxtaposition des produits de l'alignement NW de la caldera Cordillère Nevada, des fissures du Cordón Caulle et du stratocône du volcan Puyehue. En utilisant la géochronologie $^{40}Ar/^{39}Ar$ et ^{14}C on peut établir qu'ils ont évolué depuis *ca.* 500 ka comme des centres volcaniques simultanés mais séparés par une première étape de volcans de plateau, suivie d'effondrements répétés qui ont formé un graben intérieur allongé de direction NW. Après *ca*. 100 Ka, l'activité volcanique s'est produite selon un système de fissures (Cordón Caulle) et un volcan central (Puyehue). Les éruptions explosives holocènes, principalement dans le cratère de Puyehue, ont accompagné le dôme croissant le long d'un système de fissures NW. Les dernières éruptions historiques ont eu lieu en 1921 et 1960 quand les fissures du Cordón Caulle ont alimenté des laves rhyodacitiques. En

1960, l'éruption de fissure a été déclenchée par un tremblement de terre (Valdivia, Mw : 9,5) dans la zone de subduction. La caldera Cordillère Nevada présente une gamme de composition réduite (52-63% SiO_2) et des caractéristiques géochimiques du mélange et de l'assimilation crustale à basse pression. Au lieu de cela, les volcans du Cordón Caulle et Puyehue présentent un taux élevé de silice (48-71% SiO_2) et une géochimie inhabituel qui peuvent être reliés à la cristallisation partielle à haute pression initiale, le mélange modéré de magma et la cristallisation partielle à basse pression d'une source parentale commune. L'évolution magmatique exceptionnelle et le modèle éruptif du CVPCC dans les Andes méridionales pourraient être liés à la physique du système d'ascension et à sa mise en place, qui peuvent être contrôlées aussi bien par des facteurs externes que par la nature de la croûte continentale et le régime des contraintes.

Available online at www.sciencedirect.com
ScienceDirect
Journal of volcanology and geothermal research
ELSEVIER
Journal of Volcanology and Geothermal Research 157 (2006) 343–366
www.elsevier.com/locate/jvolgeores

Magmatic evolution of the Puyehue–Cordón Caulle Volcanic Complex (40° S), Southern Andean Volcanic Zone: From shield to unusual rhyolitic fissure volcanism

L.E. Lara [a,b,*], H. Moreno [a], J.A. Naranjo [a], S. Matthews [a], C. Pérez de Arce [a]

[a] *Servicio Nacional de Geología y Minería, Av. Santa María 0104 Santiago, Chile*
[b] *IRD-LMTG, Laboratoire des Mécanismes de Transfert en Géologie, IRD–UMR 5563, 14 Avenue Edouard Belin, 31400 Toulouse, France*

Received 5 July 2005; received in revised form 10 March 2006; accepted 6 April 2006
Available online 14 August 2006

Abstract

Magmas erupted from Quaternary volcanoes of Southern Andes between 37° and 46° S latitude are mainly basaltic to andesitic. However, PCCVC (40° S) shows a singular magmatic evolution due to the abnormal evacuation of rhyolites, especially in the last 100 ka. In addition, PCCVC is the result of juxtaposing products from the NW-trending alignment of Cordillera Nevada caldera, Cordón Caulle fissure volcano and the Puyehue stratocone. Using $^{40}Ar/^{39}Ar$ and ^{14}C geochronology it can be established that they evolved since ca. 500 ka as coeval but separated vents with a first stage of shield volcanism, followed by repeated collapses that formed an internal NW-elongated graben. From ca. 100 ka, volcanic activity occurred in both a fissure system (Cordón Caulle) and a central volcano (Puyehue). Holocene explosive eruptions, mainly in the Puyehue crater, accompanied the dome growing along a NW-trending fissure system. Last historical eruptions were in 1921 and 1960 when NW fissures of Cordón Caulle fed rhyodacitic lava flows. In 1960, the fissure eruption was triggered by a remote Mw: 9.5 thrust earthquake.

Cordillera Nevada caldera presents a reduced compositional range (52–63% SiO_2) and geochemical features of low-pressure magma mixing and assimilation. Instead, Cordón Caulle and Puyehue volcanoes have a wide silica range (48–71% SiO_2) and an outstanding affinity, which can be modelled with initial high-pressure fractional crystallization, moderate magma mixing and subsequent low-pressure fractional crystallization from a common parental source.

The exceptional magmatic evolution and eruptive style of PCCVC in Southern Andes could be related with the physics of the plumbing system, which in turn can be controlled by external factors as the structure of the continental crust and the ongoing stress regime.

Keywords: rhyolitic fissure volcanism; geochronology; Southern Andes

1. Introduction

The Puyehue–Cordón Caulle Volcanic Complex (PCCVC) is a cluster of Pleistocene to recent volcanic vents at 40.5° S, 72.2° W that are aligned in a northwest–southeast trend oblique to the main volcanic front of the Southern Volcanic Zone (SVZ) of the Chilean Andes (Fig. 1) (Table 1). At this latitude, the Chile–Perú trench trends 10° E, and convergence between the Nazca and South American plates occurs at 7.9 cm/yr toward 79° E (DeMets et al., 1994; Tamaki, 2000). The volcanic front parallels the trench, the arc is 60–70 km wide, the crust is about 38–40 km thick beneath the arc front (Hildreth and Moorbath, 1988; Tassara and Yáñez, 2003), and the

* Corresponding author. Servicio Nacional de Geología y Minería, Av. Santa María 0104 Santiago, Chile.
E-mail address: lelara@sernageomin.cl (L.E. Lara).

0377-0273/$ - see front matter © 2006 Elsevier B.V. All rights reserved.
doi:10.1016/j.jvolgeores.2006.04.010

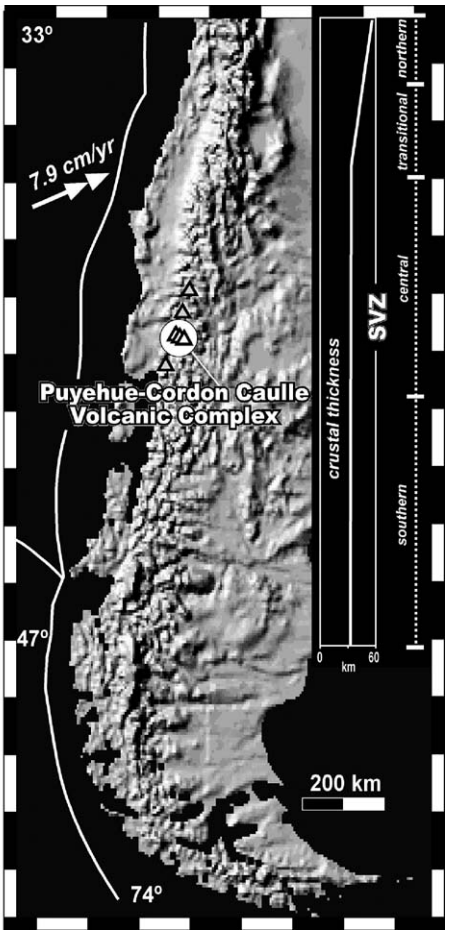

Fig. 1. Southern Volcanic Zone (SVZ) of the Andes and magmatic segments after López-Escobar et al. (1995a). Puyehue–Cordón Caulle Volcanic Complex is shown in the white circle. Right box shows approximate variation of crustal thickness after Tassara and Yáñez (2003) inferred from Bouguer anomaly. Convergence vector after DeMets et al. (1994).

Wadatti–Benioff zone dips 30° E (Cahill and Isacks, 1992). Within the SVZ, and especially among the largely basalt to basaltic andesite-dominated southern SVZ complexes between 37 and 46° S, the PCCVC is unusual in that it comprises abundant basaltic and silicic lavas, domes, and pyroclastic flow and fall deposits. Moreover, the PCCVC houses the second largest geothermal field in the SVZ (Sepúlveda et al., 2004).

A close spatial relationship between PCCVC vents and crustal structure seems clear, but especially during post glacial time, i.e., the last 14,000 yr (Lowell et al., 1995; Bentley, 1997; Denton et al., 1999). Of particular interest are two rhyodacitic fissure eruptions that occurred during 20th century, one of them only 38 h after the largest earthquake instrumentally recorded, the great Mw: 9.5 Chilean earthquake centred <240 km to the northwest of the PCCVC (e.g., Kanamori and Cipar, 1974; Lara et al., 2004). In addition, the PCCVC rests upon the trace of the Liquiñe–Ofqui fault, a long-lived intraarc structure, ca. 1000 km long, related with a dextral transpressive regime during the Quaternary (Lavenu and Cembrano, 1999).

From the beginning of 20th century, the PCCVC area has drawn the attention of many reconnaissance studies due to the unusual petrologic features and the persistent, occasionally explosive, volcanic activity (Steffen, 1922; Krumm, 1923, Hantke, 1940; Klohn, 1955; León and Polle, 1956; Müller and Veyl, 1957; Illies, 1959; Wetzel, 1959; Veyl, 1960; Saint Amand, 1961; Casertano, 1962; Weischet, 1963; Katsui and Katz, 1967). The first geologic mapping by Moreno (1977) was based on aerial photographs and field-stratigraphic observations. Gerlach et al. (1988) studied the petrology of postglacial lavas and pyroclastic deposits. Ongoing research deals with high resolution geochronology (e.g., Harper et al., 2004), neotectonics of the entire system (Lara et al., in press), geothermal properties (e.g., Sepúlveda et al., 2004), 1:50,000 scale mapping by the Servicio Nacional de Geología y Minería (Lara and Moreno, 2006) and U–Th isotope disequilibria studies (e.g., Singer et al., 2004).

The goal of this paper is to establish the basic geology and chronostratigraphy of the PCCVC, as it has been constrained on the basis of twelve new $^{40}Ar/^{39}Ar$ age determinations, as well as fifteen ^{14}C ages. In turn, these temporal constraints bear on better understanding the magmatic and morphostructural evolution of this long-lived volcanic system that forms an unusual chain transverse to the main SVZ frontal arc. The role of basement structures and the ongoing stress regime are also explored. Late Pleistocene to Holocene high resolution $^{40}Ar/^{39}Ar$ chronostratigraphy, focused mainly on Cordón Caulle and Puyehue volcanoes, is the subject of a complementary study (Harper et al., 2004; B. Singer, written communication).

2. Overview

PCCVC is a cluster of eruptive centres that extends between the Cordillera Nevada caldera (1799 m a.s.l.) and the Puyehue stratovolcano (2236 m a.s.l.) with a fissure system, Cordón Caulle (1793 m a.s.l.), between them. The PCCVC forms a 15-km-long, by 4-km-wide ridge of 135° azimuth direction that includes a nested graben (Fig. 2). Mencheca volcano, an eroded centre, is located to the north of PCCVC but its lavas overlap mainly those from Puyehue volcano. Several monogenetic centres, pyroclastic cones and maars, are widely distributed around the PCCVC in northeast- or north–

Table 1
General data for Cordón Caulle Volcanic Complex

	Cordillera Nevada caldera	Cordón Caulle fissure system	Puyehue volcano
SiO_2 range of products	52.2–63.1	50.9–71.2	48.1–71.3
Age of activity (ka)	>376–50?	>430–present	>180–2.3?
Elevation (m)			
Summit	1799	1793	2236
Caldera floor	1328		1950
Area (km^2)			
Total	700	290	160
Caldera at rim	56.75		3.8
Caldera at floor	33.18		2.14
Volume (km^3)			
Present (eroded)	120	15	50
Maximum (restored)	235	60	70

Note: compositional range of products analysed is given in wt.% SiO_2 and include dikes and sills of each unit. Estimates of volumes are no better than ±20% and consider only the present cone for Puyehue volcano.

south-trending alignments. Although silica-rich products exist in several volcanoes from Southern Andes, they are unusually abundant in PCCVC, especially in the younger units. However, no postglacial ignimbrites exist and fissure fed eruptions are volumetrically important. The most silica-rich magmas were erupted as domes throughout the Cordón Caulle fissure system and intermediate compositions dominate on Puyehue stratocone. Mafic lavas were mainly erupted in the early stages along the entire complex. Volcanic activity was nearly coeval along the PCCVC but collapse events and erosion of the volcanic edifices had their proper timing. Magmatic evolution, eruptive styles and morphostructural features makes the PCCVC a unique volcanic centre in the SVZ.

3. $^{40}Ar/^{39}Ar$ and ^{14}C geochronology

3.1. $Ar/^{39}Ar$ samples, methods and results

From the first geological map by Moreno (1977), the main evolutionary units were recognised in the field and samples were collected as representatives of these stratigraphic elements. When possible, samples were collected in sections for having a stratigraphic control of geochronological results. Fresh whole-rocks were crushed to 250–180 μm grain sizes and handy-picked for extract major phenocrysts or weathered surfaces. Single aliquots were analysed by incremental heating with a CO_2 laser at SERNAGEOMIN (Servicio Nacional de Geología y Minería, Chile) and three samples were repeated at University of Wisconsin-Madison for comparison. Procedures and methods for the latter laboratory were as published by Singer et al. (1997, 2002). At SERNAGEOMIN, the method was as follows: the selected whole-rocks were first placed in a disk of high purity aluminium, which holds up to a maximum of twenty-one different samples in small orifices. The dimensions of the disk are: 18.5 mm diameter, 4.8 mm high, with sample holes of 3 mm diameter and a depth of 3 mm. In each hole, besides the sample to be dated, is placed a monitor grain of Fish Canyon sanidine (28.03 ± 0.1 Ma; Renne et al., 1994). The complete disc is sealed with an aluminium disc plate and sent for irradiation to La Reina nuclear reactor (Chile), operated by the Comisión Chilena de Energía Nuclear. This is a 5 MW pool reactor of Herald type. Given the requirements of the samples to be irradiated, we have assigned a stable position inside the reactor, which is surrounded by a cadmium shield (Position A-09). The samples studied in this paper were irradiated for a period of ca. 48 h. Once the samples were received from the reactor, individual total fusion analyses were performed for all the monitors from the disk, and *J* factors are calculated for each grain, which represents an individual position in the disc. The distribution of *J* in 2 dimensions across the disc is modelled by a 2-dimensional quadratic fit to the data, resulting in a '*J* surface' for the disc (Pérez de Arce et al., 2003). Individual *J* factors for each sample are thus calculated depending upon the coordinates of the sample. Once cooled, the samples are introduced into a disk of Cu with capacity for ten different samples, covered with a transparent disk of potassium bromide, and the disk introduced into a sample chamber, connected to an ultra high vacuum line. The sample chamber is covered by a Zn–Se window, which is transparent to the CO_2 laser. The samples were analysed by successive heating with increments of temperature by increases in the power of the laser using an integrative lens, which allows even heating of a plane of 6 × 6 mm (each sample hole has a diameter of 5 mm). The CO_2 laser has a maximum power of 30 W. Following each three heating steps a line blank was analysed. Then, the

Fig. 2. (a) Panorama of Cordillera Nevada caldera, view to the NW. At the foreground, the graben infill of Cordón Caulle can be observed, widely covered by 1960 pumice tephra. (b) Rhyodacitic lava flows and still active fumaroles on El Azufral crater (Cordón Caulle) where 1960 eruption took place, view to southeast. At the background, Puyehue volcano. (c) Puyehue volcano, view to the north. (d) Puyehue volcano, view to the south. A lateral crater with an inner spine-shaped dome can be observed at the northern flank. (e) Cordón Caulle 2 unit (cc2w); (f) Cliff on Puyehue 1 unit (p1), dykes and tephra layer of p2 eroded vent; (g) Laccolith in Cordón Caulle 2 unit (cc2w); (h) Tilted flood layer over the external flank of the graben (cc3); (i) Eastern wall of Puyehue crater; reddish and yellowish pyroclastic layers overlying rhyolitic lavas; (j) Distal facies of ash-fallout, which are older than ca. 2.3 ka; (k) Holocene spine-shaped dome; (l) Holocene dome; (m) pumice cone of the 1990(?) AD eruption. Selected $^{40}Ar/^{39}Ar$ ages are also shown (Table 2).

noble gases were separated from the other evolved ones by means of a cold trap at −133 °C and a ST101 getter operated at 2.2 A. Once purified the noble gases were introduced into a high resolution MAP 215-50 mass spectrometer (Pérez de Arce et al., 2000) in electron multiplier mode. The isotopes ^{36}Ar, ^{37}Ar, ^{38}Ar, ^{39}Ar and ^{40}Ar were analysed in 10 cycles, and the $^{36/40}$Ar, $^{37/40}$Ar, $^{38/40}$Ar and $^{39/40}$Ar ratios were calculated for time zero (moment of introduction of the gas into the spectrometer) to eliminate the effects of isotope fractionation during the analysis. The baseline was analysed at the beginning and the end of the analysis, for each step, and subtracted from the peak heights. Spectrometer bias was corrected using periodic analyses of air samples, from which a correction factor (discrimination factor) was calculated.

Twelve reproducible results were obtained from the step heating experiments with CO_2 laser. Each apparent age considers the corrections corresponding to isotopes of Ar associated with atmospheric argon, and argon that results from the irradiation of K, Ca and Cl. Plateaus were defined using the approach of Fleck et al. (1977). For a plateau to be valid, it must comprise three or more serial steps containing at least 50% of the total liberated ^{39}Ar, and the 2σ errors of these steps must overlap. When ^{40}Ar excess was detected, the isochrone age was preferred if available. In some cases, when the heating steps did not define a clear isochrone, total fusion ages on individual grains were performed with low temperature steps for cleaning. When concordant plateau and isochrone ages were obtained, the plateau age was preferred because of its low uncertainty (Table 2). Three concordant ages were also obtained with the furnace at UW-Madison. One of them gave the youngest age of 16.5±3.8 ka. Another was concordant with the obtained through CO_2 laser considering 2σ uncertainty, but more precise. The last one does not match with the CO_2 laser being considerably younger.

3.2. ^{14}C samples, methods and results

After a detailed study of ca. 25 stratigraphic sections in the distal and proximal area of the PCCVC, a first physical correlation was made between those postglacial pyroclastic deposits. After that, a selection of key layers allows to collect charcoal samples for ^{14}C standard radiometric dating at Beta Analytic Inc. (Miami, USA). Usually, charcoal fragments were contained in massive pyroclastic layers that bracketed tephra fallout deposits. Sampling pretreatment for wood included hot HCI acid washes to eliminate carbonates, and alkali washes (NaOH) to remove secondary organic acids. The alkali washes were followed by a final acid rinse to neutralize the solution prior to drying (details and dating procedures described at www.radiocarbon.com). The results were 16 conventional ages that range from 5890±79 to 180±50 yBP. Recalibrated ages were obtained with Calib 5.0 package (Stuiver and Reimer, 1993). Dates were reported as radiocarbon years before present (i.e., 1950 A.D.), using the Libby ^{14}C half life (5568 years). All reported ages (Table 3) have quoted errors that represent the 95.4% confidence limit.

4. Geology of the PCCVC

4.1. Basement

The basement of PCCVC is important not only as a substrate of volcanic products but also because it hosts many structural discontinuities that constrain the local tectonic regime and the foci of volcanic activity. This basement is mainly formed by granitoids comprising the North Patagonian Batholith characterized by K–Ar cooling ages of ca. 10–6.5 Ma (Campos et al., 1998). Granitic rocks crop out from the base level of the major lakes (60–520 m a.s.l.) to altitudes of ca. 1300 m a.s.l. Locally, Oligocene–Miocene roof-pendants of volcanosedimentary sequences cap hills near, or crop out along the shoreline of Ranco Lake. These units are partially covered by a thick subhorizontal succession of Pliocene (5–4 Ma) volcanic and sedimentary beds (Estratos de Pitreño; Campos et al., 1998). Estratos de Pitreño are exposed from the bottom of the major glacial valleys up to ca. 1290 m a.s.l., where they are deeply eroded and overlain by pre-caldera basaltic lavas from Cordillera Nevada and Mencheca volcanoes (Fig. 3).

4.2. Cordillera Nevada Caldera

Cordillera Nevada is a collapsed shield volcano whose products (basaltic andesites to dacites) cover an area of ca. 700 km^2 at the NW border of PCCVC. The caldera is a subcircular structure with a diameter of 8.5 km open to the southeast where a graben extends southward to Puyehue volcano. Volcanism evolved from a shield stage followed by collapse and subsequent eruption along the ring faults.

4.2.1. Shield volcanism and pre-caldera sequence

4.2.1.1. Cordillera Nevada 1 unit: the basal shield (>ca. 377 ka). The pre-caldera sequence (cn1) is a thick volcanic succession, radially and gently dipping, formed by basaltic andesite lava flows, gravels and scarce crystalline mafic ignimbrites, locally welded and reomorphic. Silica contents of this unit are from 52.5 to

Table 2
Summary of $^{40}Ar/^{39}Ar$ incremental heating experiments

Furnace UW-Madison

Sample	Geological unit	Material	wt. (mg)	K/Ca Total	Total fusion Age (ka)±2σ	Age spectrum Increments used, °C	^{39}Ar %	Age (ka) ±2σ	MSWD	*N*	Isochron analysis Sums (*N*−2)	$^{40}Ar/^{36}Ar_i$ ±2σ	Age (ka) ±2σ
Experiment	Lat S/Long W (°)												
LL-160201-1	Cordón Caulle, cc4												
UW36H21	40.54°/72.15°	GM	247	0.832	11.9±6.0	1030–1410	99.1	13.2±4.9	0.72	5 of 7	0.93	294.8±4.8	14.8±9.9
UW36H20		GM	230	0.818	21.1±7.2	730–1350	94.6	21.4±6.0	0.21	7 of 9	0.15	296.6±3.2	18.8+9.2
Weighted mean plateau and combined isochron:								**16.5±3.8**	1.7	12 of 16	0.35	296.0±2.6	16.9±6.6
LL-150201-7	Cordón Caulle, cc2w												
UW36I30	40.55°/72.18°	WR	263	0.101	100.7±7.7	800–1380	100.0	**96.8±6.1**	0.57	6 of 6	0.31	298.0±3.9	93.4±8.1
XG-77A	Cordillera Nevada, cn1												
UW36I26	40,46°/72.20°	GM	345	0.223	128.3±14.5	740–1285	100.0	**128.4±10.9**	0.18	7 of 7	0.19	296.5±5.4	124.3±24.3

CO_2 laser SERNAGEOMIN

Sample	Geological unit	Material	K/Ca Total	Age spectrum Increments used, Pw/°C	^{39}Ar %	Age (ka) ±2σ	MWSD	*N*	Isochron analysis Sums (*N*−2)	$^{40}Ar/^{36}Ar_i$ ±2σ	Age (ka) ±2σ
Experiment	Lat S/Long W (°)										
LL-150201-6	Cordón Caulle, cc2w (dike)										
10356-01	40.55°/72.18°	WR	6.772	1–28	74.9	**24.0±13.0**	0.86	8 of 15	0.57	295±4	25.0±22.0
Combined isochron (3 total fusion included):					74.9			14 of 18	0.49	295.0±4.0	28.0±20.0
LL-150201-7	Cordón Caulle, cc2w										
10429-01	40.55°/72.18°	GM	1.346	1–18	96.6	**74.0±18.0**	0.87	6 of 8	0.95	295.0±7.0	74.0±36.0
LL-160201-3	Cordón Caulle, cc2e										
10354-01	40.52°/72.15°	WR	10.951	1–20	61.0	340.0±130.0		12 of 17			
		WR	12.133	1–20	100.0			17 of 17	1.30	296.5±0.2	130.0±60.0

Possible age:						**<100**					
LL-160201-4	Cordón Caulle, cc2e										
	40.52°/72.15°	WR	0.725	1–24	100.0	**70.0 ± 20.0**	0.66	15 of 15	0.38	296.4 ± 1.2	60.0 ± 26.0
LL-140201-1	Cordón Caulle, cc1										
10433-01	40.48°/72.17°	GM	1.360	6–30	98.6			4 of 5	0.23	307.6 ± 1.2	**430.0 ± 60.0**
XG-081	Cordillera Nevada, cn3										
10445-01	40.44°/72,21°	GM	1.152	3–20	100.0	**25.0 + 15.0**	1.79	4 of 4			
10439-01		GM	1.093	3–20	88.8			4 of 5	0.38	301.0 ± 2.0	50.0 ± 40.0
XG-070	Cordillera Nevada, cn2										
10358-01	40.41°/72.27°	WR	6.203	0.5–20	100.0	**110.0 ± 30.0**	0.78	11 of 11			
Combined isochron (4 total fusion included):					100.0			15 of 15	0.51	297.0 ± 2.0	100.0 ± 40.0
XG-005	Cordillera Nevada, cn2										
10357-01	40.34°/72.79°	WR	2.426	1–22	100.0	**160.0 ± 40.0**	0.98	11 of 11			
Combined isochron (5 total fusion included):					100.0			14 of 14	0.78	299.0 ± 7.0	130.0 ± 80.0
XG-77A	Cordillera Nevada, cn1										
10438-01	40.46°/72,20°	GM	1.610	3–22	100.0	**330.0 + 140.0**	1.56	6 of 6	1.56		
XG-071	Cordillera Nevada, cn1										
10448-01	40.43°/72.29°	WR	6.156	1–17	100.0	**377.0 ± 7.0**	0.85	8 of 8	0.72	294.0 ± 2.0	379.0 ± 10.0
LL150201-1	Puyehue, p2b										
10448-01	40.55°/72.10°	WR	2.451	1–14	100.0	**30.0 ± 20.0**	0.73	8 of 8	0.56	298.0 ± 4.0	19.0 ± 20.0

WR = whole rock wafer drilled from rock GM = groundmass material free of phenocrysts.
Preferred ages in bold (see text for explanation). All uncertainties reported at 2 s precision.
(*) Samples analysed at University of Wisconsin-Madison and calculated relative to 1.194 Ma sanidine from Alder Creek Rhyolite (Renne et al., 1998).
Others analysed at SERNAGEOMIN (Servicio Nacional de Geología y Minería, Chile), calculated relative to 28.03 Ma Fish Canyon sanidine (Renne et al., 1994).

Table 3
Summary of radiocarbon ages of charcoal in pyroclastic deposits from CCVC

Sample	Lat S/Long W (°)	Locality, distance to CCVC	Age (BP)[a] ± 2 s	Cal BC/AD age range (95.4% confidence level)	Pbb
XM0064	40.53°/72.45°	Rucatayo, 20 km W	180 ± 50	Cal AD 1667–1788	0.447
				Cal AD 1791–1951	0.553
XM0065	40.53°/72.45°	Rucatayo, 20 km W	240 ± 50	Cal AD 1513–1544	0.026
				Cal AD 1623–1817	0.825
				Cal AD 1827–1893	0.095
				Cal AD 1916–1951	0.054
110299-5C	40.75°/71.60°	Cerro Bayo	830 ± 60	Cal AD 1052–1076	0.021
				Cal AD 1148–1311	0.955
				Cal AD 1359–1379	0.024
070599-1B	40.43°/72.53°	Vivanco, 20 km W	830 ± 60	Cal AD 1052–1076	0.021
				Cal AD 1148–1311	0.955
				Cal AD 1359–1379	0.024
250198-7	40.68°/71.77°	Totoral lake	950 ± 60	Cal AD 1021–1229	0.990
				Cal AD 1251–1260	0.010
171297-6	40.66°/72.10°	Pajaritos, 8 km S	1520 ± 60	Cal AD 433–494	0.121
				Cal AD 505–664	0.879
050699-1	40.31°/72.22°	Riñinahue, 16 km N	1630 ± 60	Cal AD 344–373	0.028
				Cal AD 376–613	0.972
070399-2	40.30°/72.97°	Río Bueno, 120 km NW	1970 ± 80	Cal BC 109–AD 260	0.972
				Cal AD 281–324	0.026
240198-3N	40.48°/71.58°	Falkner lake, 60 km E	2260 ± 80	Cal BC 401–49	1.000
060300-3	40.31°/72.22°	Riñinahue, 16 km N	2400 ± 40	Cal BC 729–692	0.039
				Cal BC 659–653	0.004
				Cal BC 543–356	0.904
				Cal BC 287–234	0.053
100295-1	40.31°/72.22°	Riñinahue, 16 km N	2400 ± 60	Cal BC 750–687	0.090
				Cal BC 667–640	0.028
				Cal BC 593–349	0.745
				Cal BC 316–208	0.137
240198-3	40.48°/71.58°	Falkner lake, 60 km E	2430 ± 80	Cal BC 768–353	0.940
				Cal BC 293–230	0.057
				Cal BC 218–214	0.003
070599-1A	40.43°/72.53°	Vivanco, 20 km W	3270 ± 60	Cal BC 1660–1654	0.004
				Cal BC 1637–1377	0.984
				Cal BC 1337–1321	0.012
110299-5B	40.75°/71.60°	Cerro Bayo	5470 ± 70	Cal BC 4440–4425	0.011
				Cal BC 4370–4045	0.989
240198-3D	40.48°/71.58°	Falkner lake, 60 km E	5890 ± 70	Cal BC 4878–4871	0.005
				Cal BC 4848–4500	0.995

Note: All data obtained at Beta Analytic Inc. (Miami, USA) from charcoal. Pbb: relative area under probability distribution. Conventional ages recalibrated with Calib 5.0 (Stuiver and Reimer, 1993), electronic 5.0.1 version at http://radiocarbon.pa.qub.ac.uk/calib/calib.html. Calibration data set was shcal02.14 c (McCormac et al., 2004), more suitable for samples from Southern hemisphere.
Quoted cal BC/AD range represent up to 90% of the relative area under probability distribution.
[a] Present = 1950 AD.

57.3% SiO_2. This sequence reaches 200 km thickness in some glacial valleys. Upper Pliocene–Pleistocene poor constrained K–Ar ages for basalts were reported by Lara et al. (2001) and Lara and Moreno (2006). Nevertheless, a new $^{40}Ar/^{39}Ar$ age of a sample dated before by Lara et al. (2001), yield a Middle Pleistocene age of 377 ± 7 ka (Table 2). This sample is from the older part of the caldera rim and the age matches with the scarce ages reported for other eroded stratovolcanoes of the region. For example, oldest lavas from Mencheca volcano (Fig. 1) were K–Ar dated by Moreno (1977) at ca. 530 ka. Other neighbouring eroded volcanoes, including Mirador and Pantoja to the east, show similar morphology being part of the wide Late Pliocene–Early Pleistocene volcanic arc (Lara et al., 2001; Lara and Folguera, 2006).

4.2.1.2. Cordillera Nevada 2 unit: the upper shield (ca. 377–117 ka). The younger section of the pre-caldera sequence is represented by a volcanic sequence (cn2)

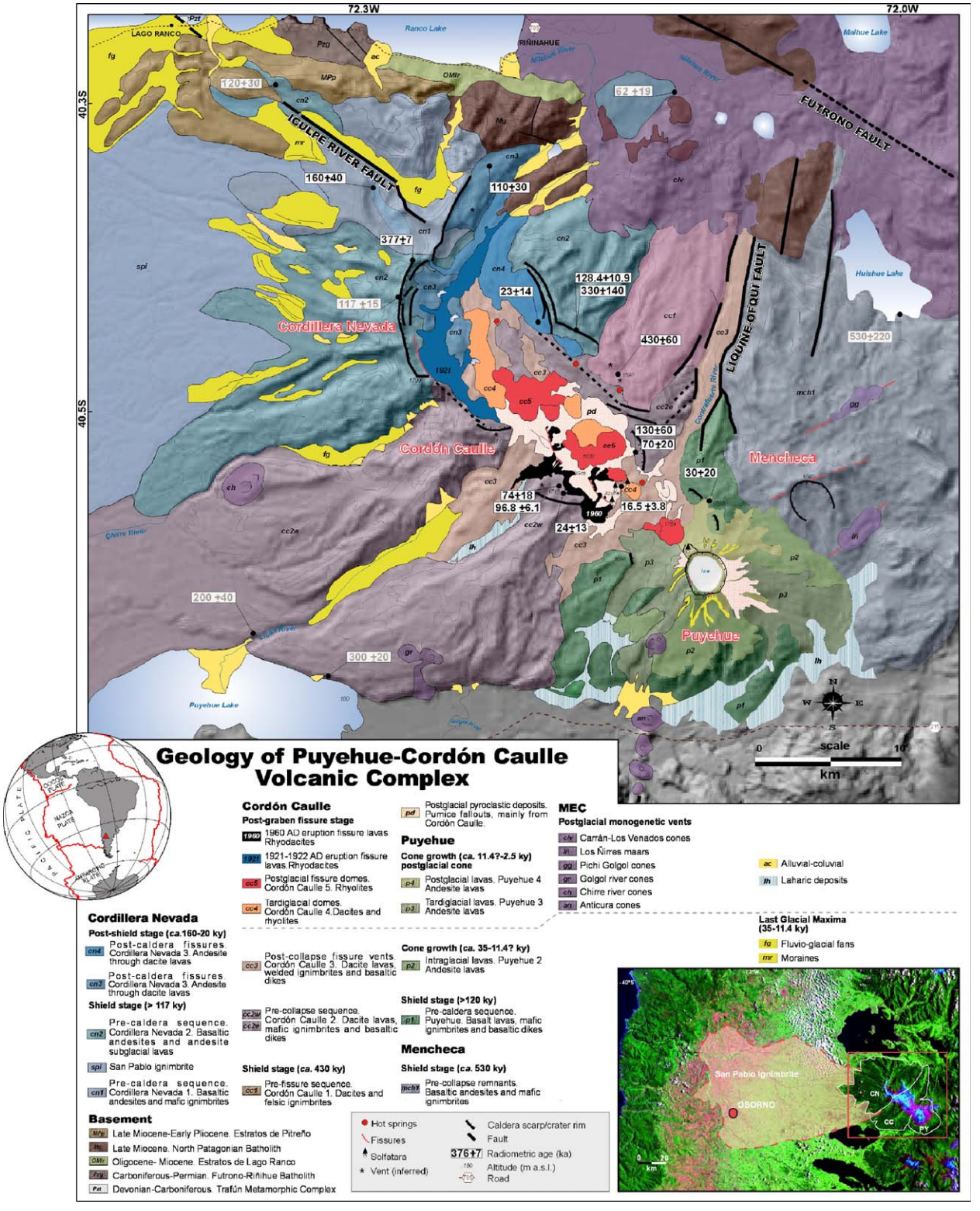

Fig. 3. Geological map of PCCVC over a shaded relief of the area, simplified from a 1:50,000 scale map by Lara and Moreno (2006) and modified from Moreno (1977). Inserts show both, general location in South America and lateral extension of San Pablo ignimbrite. Previous $^{40}Ar/^{39}Ar$ ages from Sepúlveda et al. (2005) and Sepúlveda (2006) are shown in grey. SVZ: Southern Volcanic Zone.

that both partially covers the glacially eroded basal shield, and occurs as a pile of thick lava flows ponded within the major glacial valley of Iculpe river. Deep glacial erosion has also modified this subhorizontal sequence.

Lavas from this unit are dominantly basaltic andesites, containing 53.4–57.2% SiO_2, and have been evacuated from a central conduit, yet other vents occur slightly outside of the caldera rim (Fig. 3). This unit, and specially the valley-ponded lavas, show remarkable subglacial features including hackle joints and horizontal megacolumns (e.g., Lescinsky and Fink, 2000). Two $^{40}Ar/^{39}Ar$ ages from lava flows in the Iculpe river valley gave 160±40 ka and 120±30 ka (Sepúlveda et al., 2005) (Fig. 3; Table 2). Sepúlveda et al., 2005 dated the upper part of the pre-caldera sequence in 117±15 ka along the western rim. A sample from the eastern caldera rim yield 128.4±10.9 ka (UW-Madison furnace) and a poor and older age of 330±140 ka (SERNAGEOMIN CO_2 laser). Considering the youngest age, caldera collapse should be strictly younger than 132 ka.

4.2.1.3. San Pablo ignimbrite and caldera collapse. A high volume, low aspect ratio ignimbrite is part of a conspicuous volcanoclastic succession widely recognised in valleys west of the PCCVC and crosses the entire width of the Central Valley. The San Pablo ignimbrite covers an area of ca. 1500 km^2 (Fig. 3) with a thickness of ca. 1 m near the city of Osorno, 80 km to west of the PCCVC. Remarkably, at a similar 80 km from the PCCVC, channel facies of this pyroclastic flow reach 70 m in thickness in the Pilmaiquén and Bueno river valleys. The distal facies of the San Pablo ignimbrite are widely covered by till deposits, mainly from the last Llanquihue Glaciation (90–32 ka; Clapperton, 1993). Moreover, in the main valleys the San Pablo Ignimbrite buries till from the penultimate Santa María glaciation (262–132 ka; Porter, 1981; Clapperton, 1993), thus its maximum age is roughly 130 ka. Distal facies of the San Pablo ignimbrite are characterised by a massive indurated flow unit, without sedimentary structures, composed by pumice and scarce scoria pyroclasts in a fine yellowish ash matrix. At many places, the deposit includes ca. 10% of possible juvenile lithic clasts, sub-spherical 3–8 cm in diameter with incipient prismatic fractures and dacitic in composition. In addition, the distal facies are lithic-rich and comprise a wide compositional range including andesites, siltstones and diatomaceous clasts. Scarce granitic clasts are completely argillized. A lapilli tuff deposit rests upon the ignimbrite, and is buried by an epiclastic succession of reworked pyroclastic materials. On top of the latter bed, silts, sands and gravels related to the LGM crop out. This till deposit forms the upper main aquifer in the Central Valley being isolated by the waterproof level of San Pablo ignimbrite. On the other hand, the proximal facies of this ignimbrite are not well exposed because the postglacial pyroclastic cover although in some places, such as the Chirre river valley, a lithic-poor massive deposit with well-preserved PJB bombs crops out.

From the total area covered by San Pablo ignimbrite and its average thickness in both distal and proximal facies, a maximum restored volume of ca. 15 km^3 can be estimated. If the entire volcaniclastic sequence is considered, including the channel facies, the maximum volume could be closer to 20 km^3.

The San Pablo ignimbrite has eluded radioisotopic dating, despite attempts using $^{40}Ar/^{39}Ar$ incremental heating on both plagioclase from large single pumice blocks and glassy dacite clasts that yielded no radiogenic argon. However, as the San Pablo ignimbrite is interbedded between till deposits related to the last and penultimate glaciations, a minimum age contained in the last glaciation timespan and a maximum of 132 ka should be accepted following the glacial stratigraphy of Clapperton (1993). If as we suspect the San Pablo Ignimbrite formed in response to collapse of the Cordillera Nevada caldera, the collapse may have occurred after the termination of the penultimate glaciation (ca. 132 ka), but prior to the beginning of the last glacial advance (ca. 90 ka) and the oldest intra-caldera lava flows that we have $^{40}Ar/^{39}Ar$ dated at 110±30 ka (Fig. 4).

4.2.2. Ring faults and post-caldera volcanism

4.2.2.1. Cordillera Nevada 3 unit: partial caldera infilling (<ca. 117 ka). This unit (cn3) crops out as a caldera infill composed of fissure-fed andesitic lavas probably extruded from the ring faults (Fig. 3). In addition, a pile of dacitic lavas forms a conical outcrop at the centre of the caldera. Dacitic composition prevails over andesites (56% to 67% SiO_2), where glacial erosion can be observed as well as features of subglacial emplacement. An andesite from the Nilahue river valley yield an $^{40}Ar/^{39}Ar$ age of 110±30 ka and Sepúlveda et al. (2005) dated a distal isolated pile in 62±19 ka.

4.2.2.2. Cordillera Nevada 4 unit: late activity of the ring faults (<ca. 40 ka?). Andesitic to dacitic lavas (cn4) were extruded from the inner ring faults. A poor $^{40}Ar/^{39}Ar$ *plateau* age of 25±15 ka was obtained for an andesite from the eastern caldera wall. Lava flows from this unit were weakly eroded by glaciers, some of them showing surficial striaie. This unit is morphologically

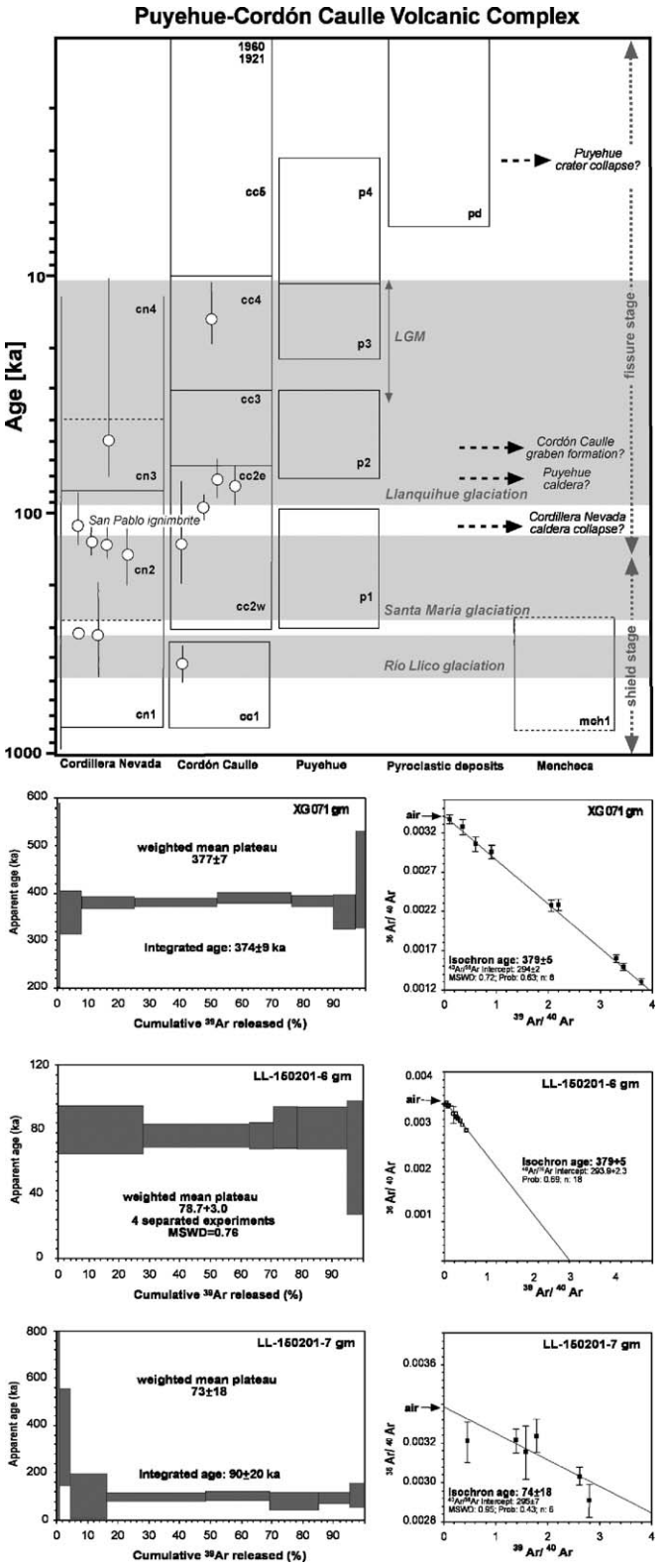

Fig. 4. Stratigraphic chart of PCCVC, main glacial periods at the region from Clapperton (1993), Lowell et al. (1995) and Bentley (1997). Below, selected step-heating spectra and isochrone analysis for selected reproducible experiments. LL150201-6 and LL150201-7 are duplicates of the same sample, upper panel show lower accuracy result obtained with CO_2 laser (SERNAGEOMIN, Chile) and below the high accuracy value with a resistance furnace (UW-Madison, USA).

equivalent to cc3 unit from Cordón Caulle, both representing the post-collapse stage with dominant fissure-fed eruptions in the northern section of the PCCVC.

4.3. Cordón Caulle fissure system: shield to fissure volcanism

Cordón Caulle is a 9-km-long, 5-km-wide fissure system that contains an asymmetric graben defined by two northwest trending main escarpments. Inside, a suite of postglacial domes and a fissure ridge comprise the more recent vents. At the graben walls, isolated vents can be recognised (Fig. 3).

4.3.1. Pre-graben sequence: shield volcanism

4.3.1.1. Cordón Caulle 1 unit: eastern shield complex (>ca. 430 ka). This unit (cc1) crops out at the northeastern wall of the graben as a pile of silicic lavas, welded ignimbrites, sills and laccoliths, and coarse gravel beds juxtaposed to pre-caldera lavas from Cordillera Nevada and Mencheca volcanoes. An $^{40}Ar/^{39}Ar$ age of 430±60 ka was obtained from a dacitic lava in the upper part of this unit. This age is similar to that of the older pre-caldera sequence in Cordillera Nevada and roughly matches that reported for the eroded Mencheca volcano (ca. 530 ka; Moreno, 1977; Fig. 3). Although Plio–Pleistocene shield volcanoes of the region are dominantly basaltic in composition (Lara et al., 2001; Lara and Folguera, 2006), some cc1 rocks are rhyolites with SiO_2 contents among the highest of the entire PCCVC suite.

4.3.1.2. Cordón Caulle 2 unit: shield to fissure transition (ca. 300–70 ka). Volcanism previous to the present graben is also recognised in two isolated lava sequences that potentially represent different feeder systems. The western sequence (cc2w) is divided by the Licán stream in two volcanic piles. The northernmost is a succession 60 m thick that forms a concave escarpment to the northeast. This pile crops out attached to cn1 unit of Cordillera Nevada and have deep glacial incisions and valleys filled by lavas from cc3 unit. Pyroclastic breccias and debris flows with oxidised matrix and andesitic lavas are exposed at the main escarpment where basaltic andesite dykes and sills intruded. The dykes from the lower part of the sequence were dated in ca. 167 and ca. 173 ka (Harper, 2003). A basal lava flow from this pile was $^{40}Ar/^{39}Ar$ dated in 200±40 ka near the Puyehue lake (Sepúlveda et al., 2005). The southwestern pile is a suite of lavas and pyroclastic rocks that reach 150 m thickness on the wall that form a subvertical escarpment. Lavas, breccias and massive mafic ignimbrites are subhorizontal or slightly deflected around a basaltic andesite laccolith that intrudes them. Vertical basaltic dykes cut the entire suite as well. An $^{40}Ar/^{39}Ar$ age of 74±18 ka was obtained for the laccolith using the CO_2 laser at the SERNAGEOMIN, and is remarkably consistent with the age of 96.8±6.1 ka obtained at UW-Madison using a resistance furnace (Table 2; Fig. 3). A poorly constrained age of 23±14 ka was also obtained from a basaltic dyke (Fig. 3). Subhorizontal lava flows of the main sequences are between ca. 112 and 107 ka (Fig. 3; Harper, 2003). A basal lava flow from this pile was $^{40}Ar/^{39}Ar$ dated in 300±20 ka near the Puyehue lake shoreline (Sepúlveda et al., 2005).

The eastern sequence (cc2e) is a succession 120 m thick that covers with unconformity the cc1 unit. This sequence form a concave escarpment, 8 km long and open to the west, and is composed by dacitic lavas gently dipping to the east and cut by dacitic domes and sills. The overall sequence show regular joints and NW-trending faults being widely intruded by basaltic dykes. A poor $^{40}Ar/^{39}Ar$ isochrone of 130±60 (preferred age <100 ka) and a plateau age of 70±20 ka were obtained from two dacitic lava flows (Fig. 3; Table 2). B. Singer (written communication) reported an age of ca. 73 ka for the upper dacitic lava.

4.3.2. Intra-graben fissure volcanism (<70 ka–present)

4.3.2.1. Cordón Caulle 3 unit: ignimbrites and lavas (<70 ka). Partially welded ignimbrites, massive or having weak sedimentary structures and locally indurated, together with dacitic lavas, form packages that can reach 250 m thick. This unit cc3 crops out as a graben infill or surpassing this basin. Whereas the most external volcaniclastic beds show inner-graben dips, the internal ones appear subhorizontal. Long outer lava flows from this unit extend toward the north in the glacial valley of Nilahue and Contrafuerte rivers and fill the Licán river valley to the south (Fig. 3).

Where this unit ponded against the previous cc2w, Harper (2003) dated a lava pile widely intruded by dikes and sills in ca. 54 to 32 ka. These lava flows show slight glacial erosion on surface and their vent were obscured by the recent domes and tephra fallout.

4.3.2.2. Cordón Caulle 4 unit: intra-postglacial domes and coulées (<32 ka). A first generation of domes and coulées (cc4) lie in the centre of the graben. They are mainly dacitic and have typical aspect ratios near 2.5, being slightly elongated in NW direction. Crease structures (Anderson and Fink, 1992) are parallel to the longer axis of the domes. They show an incipient surficial

erosion at the flanks and have a meter thick cover of pyroclastic deposits. One of them shows solfatara activity over its flank (Fig. 2) and a $^{40}Ar/^{39}Ar$ age of 16.5± 3.8 ka was obtained for it (Fig. 4).

4.3.2.3. Cordón Caulle 5: postglacial domes and coulées (Holocene). A younger suite of dacitic to rhyolitic domes and lava-domes (cc5) with fresh morphology lie inside the graben. A huge viscous lava-dome, whose vent is near the scarp of the graben, occurs in the northwestern sector and its blocky-lava invades the Cordillera Nevada caldera. Two rhyodacitic coulées located at the central part of the graben were also emitted from vents located next to the southern escarpment. Their surficial morphology is so fresh that crease and 'ropy' structures can be recognised. They are covered mainly by tephra fallout from the 1960 eruption. A singular rhyolitic dome, 1.5 km in diameter with an inner 'crater' that is filled by a spine-shaped plug also forms this unit (Fig. 3).

The age of these postglacial domes is unknown, as radioisotopic dating experiments failed to reveal detectable amounts of radiogenic ^{40}Ar. However, we can speculate that they can be vent facies of the explosive eruptions recorded by the pyroclastic succession in the distal area (Fig. 5). As we show later, the recognised pyroclastic sequence of PCCVC is mainly younger than 6 ka, a range consistent with the fresh morphology of the domes.

4.3.2.4. Historic fissure lavas of A.D. 1921. An eruptive cycle began on December 13, 1921 and was active until February, 1922. Following the scarce written reports (e.g., Hantke, 1940 and references therein), an initial eruptive stage formed a Plinian column 6.2 km high during the first seven days accompanied by cyclic explosions and noticeable seismic activity. In this initial stage, eight aligned vents were formed over ring faults inside the Cordillera Nevada caldera reaching 8 km long. They allowed the drainage of several dacitic flows during the second more effusive stage. The most active vent was the northern one, where a long lava flow reached the Riñinahue river valley. The total volume of lava and tephra emitted in 1921–1922 reached ca. 0.4 km^3.

4.3.2.5. Historic fissure lavas of A.D. 1960. The 1960 earthquake-triggered eruptive cycle occurred on a ca. 5.5-km-long fissure located near the SW margin of the PCCVC and formed by two sub-parallel segments. Each segment included alignments oriented N135° and N160–165°. Twenty-one identifiable vents emitted pyroclastic ejecta and lava flows of rhyodacitic composition (68.9–70.01% SiO_2) with ca. 0.25 km^3 of total DRE volume. The eruptive cycle began on May 24 (09:00 h GMT), 38 h after the main shock of May 22, starting with an explosive subplinian phase and the formation of an eruptive column of about 8 km high, together with emission of water vapour from other vents along the fissure system (Lara et al., 2004). The most active centre in this phase was the Gris crater, followed by El Azufral crater (Fig. 3), both at the southern end of each segment. The pyroclastic plumes were dispersed toward the southeast forming a white pumice deposit with thickness up to 10 cm at 30–40 km of the vents. An accumulation of 'bread crust' bombs and coarse lapilli pumice around the Gris crater formed a low aspect ratio pyroclastic cone. An effusive phase, with emission of aa and blocky rhyodacitic lava flows followed the previous stage. The eruptive vents evolved to a N160–165° alignments, as the first phase culminated. As the vents were sealed by viscous lava flows, a quiescence period followed and renewed activity started with an explosive phase characterised by the accumulation of 'bread crust' bombs around the Gris and El Azufral craters, apparently the only active ones during this latest phase. A coarse lapilli pumice-fallout deposit represents the proximal facies of the eruptive column during the last phase, which ended on July 22 after two months of activity.

4.4. Puyehue Volcano: central volcanism

Puyehue volcano (2236 m a.s.l) is a stratocone located at the southeast end of the PCCVC. It covers an area of ca. 160 km^2 and has an open crater of ca. 2.4 km diameter now filled with ice.

4.4.1. Pre-caldera sequence (ca. 245–96 ka)

4.4.1.1. Puyehue 1 unit: shield volcanism. Ancient volcanic sequences of an ancestral Puyehue volcano (p1) are partially buried by younger flows, or exposed in concave cliffs that surround the present stratocone. The westernmost remnant is a succession up to 150 m thick composed by andesitic lavas and breccias gently dipping to the west. Harper (2003) has obtained ages of ca. 193 ka at the base and ca. 131 at the top of the pile. The eastern succession is composed by basalts and mafic andesites cross-cut by numerous vertical dikes. B. Singer (written communication) have obtained ages of ca. 245 ka at the base and ca. 103 ka at the top of the sequence with ca. 96 ka in the mafic dykes, the latter constraining the maximum age for the collapse on this ancestral volcano. Another mostly buried basaltic andesite on the southern

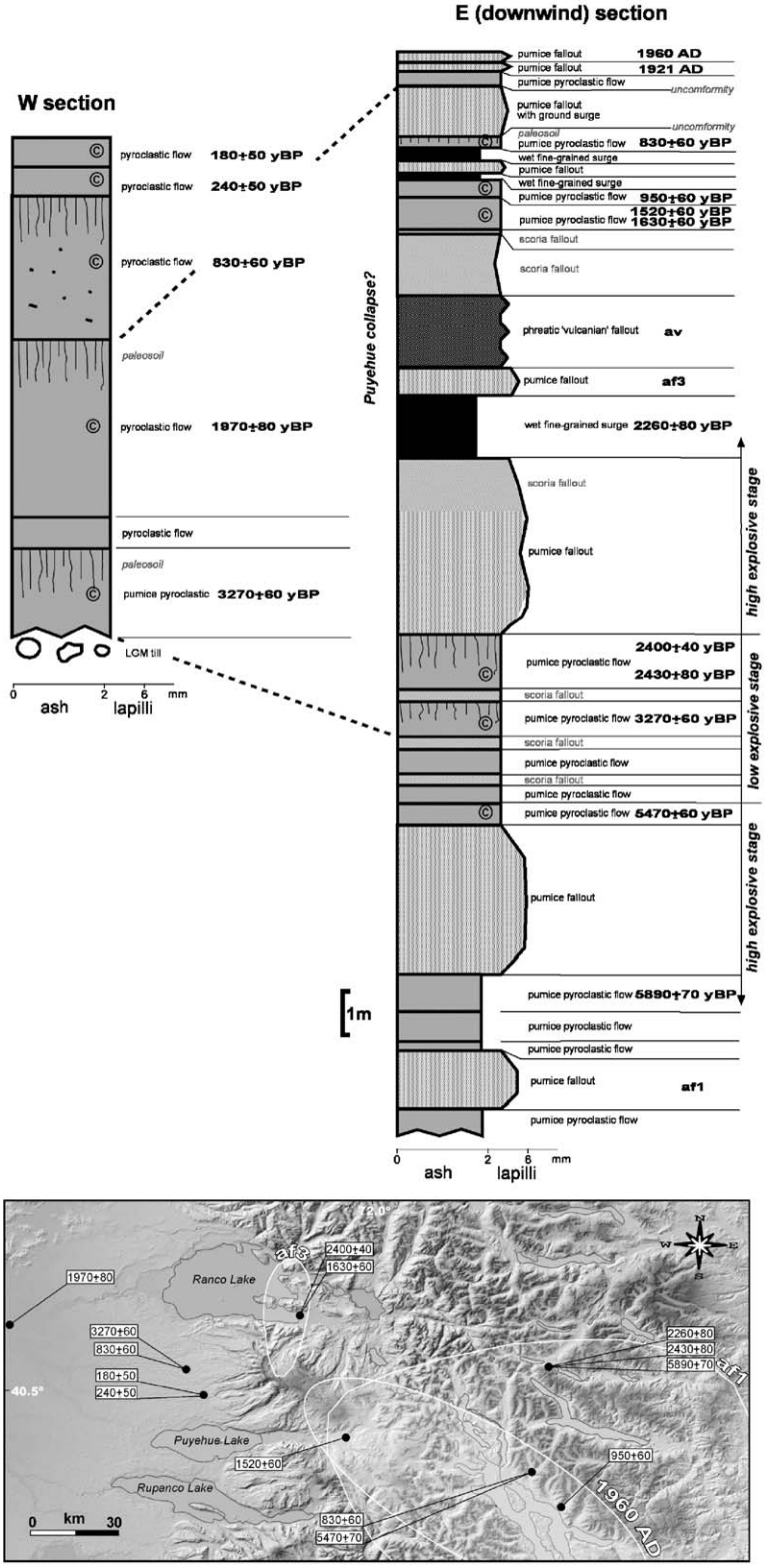

Fig. 5. General stratigraphic section for western (a) and eastern downwind (b) sectors with ^{14}C ages quoted in Table 3. Grey labelled scoria fallouts are mainly from Antillanca volcanic complex, south of Puyehue, and from Carrán–Los Venados group, to the northeast. Isopach map of main pumice-fallouts (c) show thickness in cm for the main tephra layers. Two distinctive vents can be inferred on Cordón Caulle fissure system matching with the sites of historical eruptions.

flank of Puyehue volcano gave ca. 224 ka (B. Singer, written communication).

4.4.2. Post-caldera stratovolcano (ca. 69–2.3 ka)

4.4.2.1. Puyehue 2 unit: englacial volcano (ca. 69–34 ka). Heavily eroded andesitic lavas (p2) crop-out at the base of the present stratocone or juxtaposed to p1 sequence. At the eastern cliff of p1, a complex of mafic and aphyric andesites cross-cut by dikes represents vent facies of a lateral vent. A poor defined $^{40}Ar/^{39}Ar$ plateau age of 30±20 ka was obtained for an andesitic dike. Harper (2003) have obtained ages of ca. 68 ka and ca. 45 ka for the lava flows. A scarp cut this vent exposing its core and postdating the ancient caldera collapse.

On the flank of the present Puyehue volcano, andesitic to rhyolitic lavas with heavy glacial erosion marked by striae on surface and hackly joints are exposed. These lava flows are interbedded with indurated gravel layers that include 'pop corn' bombs in a sandy matrix that resemble the 'mixed avalanches' (Pierson and Janda, 1994). Two ages of ca. 34 ka were obtained by Harper (2003) for a rhyolite on the flank and dacite of the inner wall of the crater, respectively. B Singer (written communication) reported and age of ca. 63 ka at the inner wall of the crater.

4.4.2.2. Puyehue 3 unit: tardiglacial lavas (ca. 19–11 ka). Basaltic to rhyodacitic multiple lava flows with only weak glacial erosion form p3 unit on the western flank of Puyehue volcano. Harper (2003) has obtained ages of ca. 19 and ca. 15 ka for an aphyric rhyodacite and a dacite respectively. Unglaciated basalts from this unit were dated in ca. 13–11 ka (B. Singer, written communication). Slight surface erosion can be observed on these lava flows that should be older than the complete ice retreat from the flanks. In fact, a minimum age for this unit could be indirectly constrained by the ice retreat during the Last Glacial Maxima (sensu Lowell et al., 1995) in the eastern shoreline of the Puyehue lake (~190 m a.s.l.), inferred by Bentley (1997) in ca. 12.2 ka. This is slightly younger than the ca. 13.9 ka proposed by Lowell et al. (1995) for the massive ice retreat from the western shoreline of Llanquihue lake (~51 m a.s.l. and 80 km southward). Puyehue cone prior to the crater collapse could have reached ~3000 m a.s.l. keeping ice remnants onto the flanks.

4.4.2.3. Puyehue 4 unit: postglacial lavas (ca. 7–2.5 ka). Mostly rhyolitic lava flows and domes form the p4 unit at the eastern flank of Puyehue volcano. They are well exposed in the crater wall, where at least 150 m of glassy rhyolites are overlain by an indurated tephra layer. Lava flows from this unit are completely postglacial. Harper (2003) obtained ca. 6.4 ka for a rhyolite of the crater rim and B. Singer (written communication) reported $^{40}Ar/^{39}Ar$ ages of ca. 5.2 to 6.9 ka. Maximum age for the crater-forming eruption of Puyehue volcano is given by the age of ca. 6.4 ka, but the overlying lavas and tephra force to consider it younger. A candidate is a vulcanian eruption, which age is bracketed between ca. 1630 and ca. 2260, at the beginning of a highly explosive cycle (Fig. 5).

4.5. Lateral vents

Holocene postglacial flank or peripheral vents are widely distributed around the PCCVC (Fig. 3). They are mainly pyroclastic cones and maars that fed small lava flows whose ages are not directly constrained. On the southern flank of Puyehue volcano, a double scoria cone (an) is aligned with the Anticura cones that are sitting on the main trace of Liquiñe–Ofqui Fault system. At the distal flank, over cc2w lavas from Cordón Caulle, another paired Golgol cones (gr) appear atop the ca. 1200 m thick preglacial sequence reaching their lavas the Golgol river valley. Similar stratigraphic exposure shows a third group of double cones (ch) near the Chirre river valley. Towards the northeast, several peripheral postglacial cones partially cover the oldest units of Cordillera Nevada or Mencheca shield volcanoes. The more conspicuous is the Carrán–Los Venados group, a NE-trending alignment of 48 Holocene scoria cones and maars with historic eruptions. In addition, over the eroded lavas of Mencheca shield volcano, the northeast alignments of Los Ñirres maars (lñ) and Pichi Golgol cones (gg) lie. Finally, the most remarkable flank vent is the explosion parasitic crater on the northwestern flank of Puyehue volcano. It has near 600 m diameter and shows a spine-shaped dome inside with solfatara activity. The age of formation is unknown, but must be younger than ca. 2.2 ka, the maximum age of the main crater forming eruption.

4.6. Pyroclastic deposits

A sequence of pyroclastic deposits is recognised nearby the PCCVC (<60 km). As in other volcanoes of the Southern Andes, tropospheric winds cause a mainly southeastern dispersion of tephra, thus the most complete sections are preserved downwind in Argentina (Fig. 5). Although not all layers are present in the overall sites, as is the case of some topographically constrained pyroclastic flows, the physical features, stratigraphic position and ^{14}C geochronology allow a generalized correlation. The succession starts with pumice pyroclastic

horizons older than ca. 5.9 ka, the age of the lowermost dated deposit. In the western downwind section four plinian or subplinian pumice-fallout appear. The older pumice ash-fall deposit (>ca. 5.9 ka) can be recognised only at few localities eastward and no reliable isopachs can be drawn. Another ash-fall deposit has an age between ca. 5.5 and 5.9 ka. Remarkable thickness up to 80 km eastward describes high-volume eruptions during this high explosive cycle. After that, a low-explosive cycle began with long quiescence periods that can be inferred from paleosoil horizons, the latter dated in ca. 2.4 ka. Upward in the section, a major plinian eruption (ca. 4 km^3 DRE volume) mark the renewal of explosive activity. Surprisingly, the isopach map rejects a provenance from PCCVC suggesting a source located further south. This event is characterised by a lower amphibole-bearing pumice fallout that gradually passes to a mafic ash-fall covered by a wet fine-grained surge or a massive pyroclastic flow deposit. Charcoal from an overlying surge layer gave an age of ca. 2.26 ka. Above this wet surge deposit, a pumice fallout has an isopach map, which indicates provenance from Cordillera Nevada caldera or Cordón Caulle with an unusual dispersion to the north. Upward in the section, a phreatic 'vulcanian' fallout indicates a strong erosion of a conduit, which could be assumed as a crater collapse event of Casablanca volcanic complex further south. Renewal of the activity is represented by scoriaceous ash-fallouts and a massive pyroclastic flow deposit dated in ca. 1.6 ka, which is covered by humid surges, another pumice ash-fallout and a pyroclastic flow deposit of ca. 830 yBP (1170–1265 cal AD). This local abundance of phreatomagmatic facies is slightly older than the Little Ice Age event (ca. 1300–1900 AD after Soon and Baliunas, 2003), also recognised in Southern Andes by Clapperton (1993) and recently dated for the Puyehue lake area in ca. 1490–1700 AD (Bertrand et al., 2005).

A new quiescence period is deduced from the deep paleosoil on a ca. 830 yBP flow deposit and the local erosive unconformity between the latter and the overlying beds. Historical explosive activity is recorded by two thin pyroclastic flow deposits dated at 180 ±50 yBP and 240±50 yBP, respectively. Explosive activity was renewed during the 20th century by subplinian eruptions that produce two pumice fallouts, the first in 1921 AD and the younger in 1960 AD. In proximal facies, this pumice layers onlap in a sharp erosive unconformity a succession formed by epiclastic levels, bomb agglomerates, accretionary lapilli beds and the thick white pumice fallout whose age is younger than ca. 830 yBP. Reworked layers formed by lahars and floods are commonly interbedded with the pyroclastic horizons. Recent renewal corresponds to the construction of a small pumice cone aligned with the youngest postglacial domes in Cordón Caulle. Local inhabitants inform that this cone born in 1990 AD, but there is no additional confirmation except the fact that until 1977 AD the cone did not exist (Moreno, 1977).

4.7. Historical and current activity

The historical eruptive activity of PCCVC (Fig. 6), referred as historical the period span after the Spanish conquest (i.e., the last ~500 years), is only partially known and the record appears poor compared to another volcanoes from Southern Andes (e.g., Moreno and Petit-Breuilh, 1999; Petit-Breuilh, 1999). This lack of information is especially critical for 16th and 19th centuries. This fact can be explained by the isolation of the PCCVC from the main cities during the Hispanic period. Osorno city, 80 km west of PCCVC in the Central Valley, was established in 1553 AD being rebuilt in 1558 AD and left in 1604 AD because of the strong siege of Indians, the so called *mapuches* (e.g., Bengoa, 2003). After two centuries, the ruins were discovered and the city repopulated in 1796 AD. Until the late 19th century, *mapuches* resisted both the Spanish colonisation and the Chilean domain, forcing a virtual border in the Cautin river, 200 km to the north. Even on 1850 AD, when German colonisation was stimulated by the Chilean government, the access to the eastern Andean area was restricted and no connection existed from Osorno to Puerto Montt, 100 km towards the south. This fact is important because it made difficult the access for the historians, naturalists and Jesuit priests, main source for the historical chronicles in Chile. Although Indians maintained an active pass to the extra-Andean plains, only in the 20th century the international pass throughout the Golgol river (Fig. 3), south of Puyehue volcano, was established and the access facilitated. However, the northern access to PCCVC area is still difficult. Fig. 6 shows the recorded historical eruptions, some of them with doubts.

Two pyroclastic deposits whose calibrated ^{14}C ages span the Hispanic period can be related to historical chronicles, perhaps the possible eruptions of 1759 AD and 1893 AD. Subplinian eruptions occurred in 1921 AD and 1960 AD and the more recent renewal corresponds to the small pumice cone of Cordón Caulle, probably built in 1990 AD.

Current activity corresponds to visible fumaroles on several points along the PCCVC and frequent perceptible earthquakes but presently there is no instrumental monitoring. A recent crisis was reported on May 1994

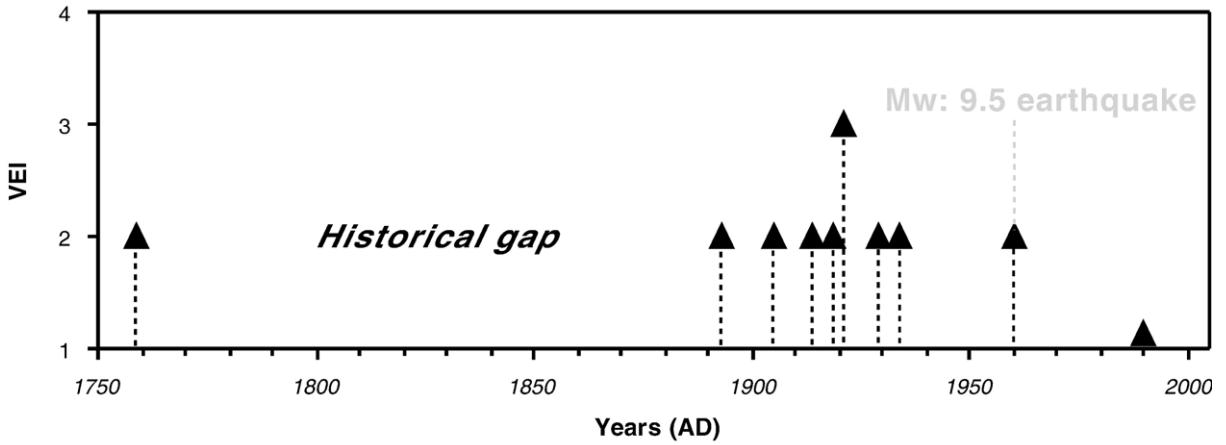

Fig. 6. Historical record of eruptions at PCCVC (modified from Moreno and Petit-Breuilh, 1999). VEI: Volcanic Explosiveness Index (Newhall and Self, 1982), estimated from chronicle reports as follows:1759?: Garavito (1759, in Moreno and Petit-Breuilh, 1999); 1893?: Sapper (1927), Ayala (1956); 1905?: von Wolff (1929), Stone and Ingerson (1934), Salmi (1941), Saint Amand (1961); 1914/Feb 08: Rimbach (1930), Hantke (1961); 1919–1920: Brüggen (1950); 1921–1922/Dec 12–Feb12: Krumm (1923), Sapper (1927), Stone and Ingerson (1934), Stone (1935), Brüggen (1950), Meyer Rusca (1955), Klohn (1955), Ayala (1956), Illies (1959), Casertano (1962); Katsui and Katz (1967), Moreno (1977); 1929/Jan 07: Saint Amand (1961), Hantke (1961), Moreno (1980); 1934/Mar 06: Vogel (1934), Hantke (1961), Moreno (1980); 1960/May 24–Jul 30: Casertano (1960), Weischet (1963), Saint Amand (1961), Veyl (1960), Casertano (1962), Katsui and Katz (1967), Moreno (1977), Lara et al. (2004); 1990?: local inhabitants (personal communication).

when a temporal seismic network recorded small to moderate earthquakes and subterranean noises. The detected harmonic tremor and earthquakes were centred north of Puyehue volcano, probably located at Cordón Caulle fissure system. Tremor shook with Mercalli-scale intensity IV and V forcing scientists and civil authorities to form an emergency action committee whose first mandate was to review and update the emergency plans.

The Chilean volcano observatory (www2.sernageomin.cl/ovdas) displayed another 1 Hz seismometer on March 1999 during a field work, receiving a rich seismic signal with harmonic tremor, long period and volcano-tectonic events (Peña and Fuentealba, 2000).

4.8. Geothermal activity

The graben of PCCVC hosts one of the most important geothermal fields of Southern Andes (Sepúlveda et al., 2004). Many hot springs, geysers and solfatara fields are widely distributed inside the graben or above its margins. At the northwestern end of the graben is located Trahuilco hot spring (1000 m a.s.l.), a suite of geysers, vapour steams and boiling HCO_3 water ponds with surface temperature of ca. 93 °C and an average flow rate of ca. 100 l/seg. Around the discharge points there are sulphur deposits and geyserites that suggest a high geothermal gradient. The HCO_3 waters have a pH of 8.64–9.38 at 19.5 °C (Pérez, 1999). Na/K and Na–K–Ca geothermometers indicate shallow temperatures of 100–140 °C but corrected Quartz and Chalcedony geothermometers gave 170–180 °C suggesting a steam-heated aquifer overlying the main vapour-dominated system (Sepúlveda et al., 2004). At the middle point of the graben, Las Sopas hot spring (1560 m a.s.l.) is a suite of geysers, fumaroles, boiling water pools and mud ponds with high surficial temperatures of 83–93 °C. They have a flow rate higher than 10 l/seg and the water steam produces an intense acid–sulphate alteration. A low pH of 2.23–2.76 at 17.3 °C was obtained for these acidic-SO_4 waters (Pérez, 1999). No reliable subsurface temperatures were obtained because the effect of dissolution processes. Next to the NW flank of Puyehue volcano, on the fluvial terrace of Nilahue river, Los Baños hot spring (1425 m a.s.l.) is located. This is a small area of water ponds with surface temperatures of 43–70 °C. The HCO_3 waters have a flow rate lower than 1 l/seg with a pH of 6.85 at 18 °C. Another site with fumaroles or warm spring waters is located at the heads of Los Venados river. Active solfataras appear in some Holocene domes, the El Azufral crater of 1960 AD eruption, the small pumice cone of 1990 AD and the parasitic crater on the northern flank of Puyehue volcano. Geochemical data by Pérez (1999) and Sepúlveda et al. (2004) suggest a major hydraulic connected vapour-dominated system where topography constrains the water flow and the locus of hot springs.

5. Geochemistry

General geochemical features of postglacial lavas and domes from Cordón Caulle and Puyehue were discussed in detail by Gerlach et al. (1988). The aim of this section is to characterize the geochemical evolution of the PCCVC and document potential magmatic relations between individual centres of the complex and provide some brief comparison with the neighbouring stratovolcanoes of this SVZ segment (Figs. 1 and 7). Thus, we measured with ICP-MS seventy one new samples from Cordillera Nevada, Cordón Caulle and Puyehue volcano, in order to describe the entire suite. In addition, we include some samples of postglacial pyroclastic deposits that complete a representative set of volcanic rocks from PCCVC (140 samples including published data).

For the complete set, Al_2O_3, Fe_2O_3, MgO and CaO contents decrease and Na_2O and K_2O increase with increasing SiO_2 as differentiation index. P_2O_5 and TiO_2 contents show a maximum value in basaltic andesites or andesites. Despite the scatter in the contents, the overall Harker diagrams define clear linear trends although K_2O content show some departure at high silica content, mainly for the youngest samples. Cordillera Nevada suite show a more restricted silica content (52.2–63.11%) and Puyehue volcano includes the end-members of the entire set in a continue trend. With exception of cc1 unit from Cordón Caulle, the older units are mainly basalt to basaltic andesite in composition. From Late Pleistocene, Cordón Caulle emitted only rhyodacites and rhyolites but Puyehue has interbedded basalts. Holocene basalts were emitted only from flank or isolated monogenetic centres. Postglacial pyroclastic deposits have mainly rhyodacitic composition. A first difference with the southern SVZ magmas arises because most of the Quaternary magmas of this segment show a narrow range of silica content and rhyolitic magmas are rare. K_2O contents are higher than the neighbouring SVZ magmas as well.

Abundances of the trace elements Co, Ni, Cr and Sr decrease and Ba, Cs, Rb, Zr, Nb, Ta, Hf, Th, Y, Zn and Pb increase with increasing SiO_2 content. Sc and V contents increase from basalts to basaltic andesites but decrease thereafter. Basalts are relatively enriched in light REE with respect to the chondrite (Fig. 7). La/Sm and La/Yb ratios increase with increasing SiO_2 content in the entire suite and only rhyolites from Cordón Caulle show negative Eu anomalies (Fig. 7). Sr and Nd isotopic compositions for Cordón Caulle and Puyehue appear as one end of the trend defined by lavas from Southern Andean Volcanic Zone (Gerlach et al., 1988 and references therein).

REE patterns for end-members samples suggests a prevailing fractional crystallization process in a closed system (Fig. 7). Nevertheless, when ratios of incompatible elements are considered (Ba/Rb vs. Rb), Cordillera Nevada appears as a non cogenetic suite, or as having an isolated magmatic evolution. In general terms, Pleistocene magmas from Cordillera Nevada can be modelled by mixing and re-assimilation at low pressures, probably accompanied by a limited amount of fractional crystallization of plagioclase, olivine and piroxene. In turn, mafic to intermediate magmas from Cordón Caulle and Puyehue volcanoes fit the mixing curve between the end-members of each subset, but dacites to rhyolites should be modelled by fractional crystallization of plagioclase and piroxene from silicic andesites. Rhyolites from Cordón Caulle have Fe-olivine as a residual phase. The more recent magmas from Cordón Caulle are very similar and can be also explained by fractional crystallization. For example, a 1960 AD magma can be obtained from a 1921 AD composition throughout crystallization (<10%) of plagioclase, augite, orthopiroxene, magnetite, ilmenite and apatite. As was proposed by Gerlach et al. (1988), magmatic evolution seem to occur in two stages of different pressures. The first one should occur in conditions near 8 kb, being basalts or basaltic andesites produced from the parental source. The second stage should be near 1 kb in anhydrous conditions. Extended assimilation would have occurred at Cordillera Nevada, where middle compositions were obtained, and fractional crystallization would have occurred at Cordón Caulle and Puyehue, where high silica magmas were emitted. Since ca. 2.3 ka, only rhyolites erupted from fissures of Cordón Caulle. Evolved products of PCCVC have geochemical signatures of relative long residence in the shallow reservoirs but there are not evidences of crustal interactions as occur in the northern province of Southern Andes (33°–37° S; e.g., Hildreth and Moorbath, 1988; Dungan et al., 2001). Scarce published data of radiogenic isotopes (Tormey et al., 1991; Sigmarsson et al., 1991) suggest rapid ascent from the mantle source and short residence times compared to the northernmost volcanoes.

6. Neotectonics

The most remarkable structural feature in the Andean orogen of SVZ is the Liquiñe–Ofqui Fault, a ca. 1000 km long-lived fault, which crosses the PCCVC area under Puyehue volcano. Different authors have proposed a right-lateral or dextral-inverse Plio–Quaternary kinematics for the master fault imbedded in an overall transpressive regime of the entire arc (Lavenu and Cembrano, 1999). On the other hand,

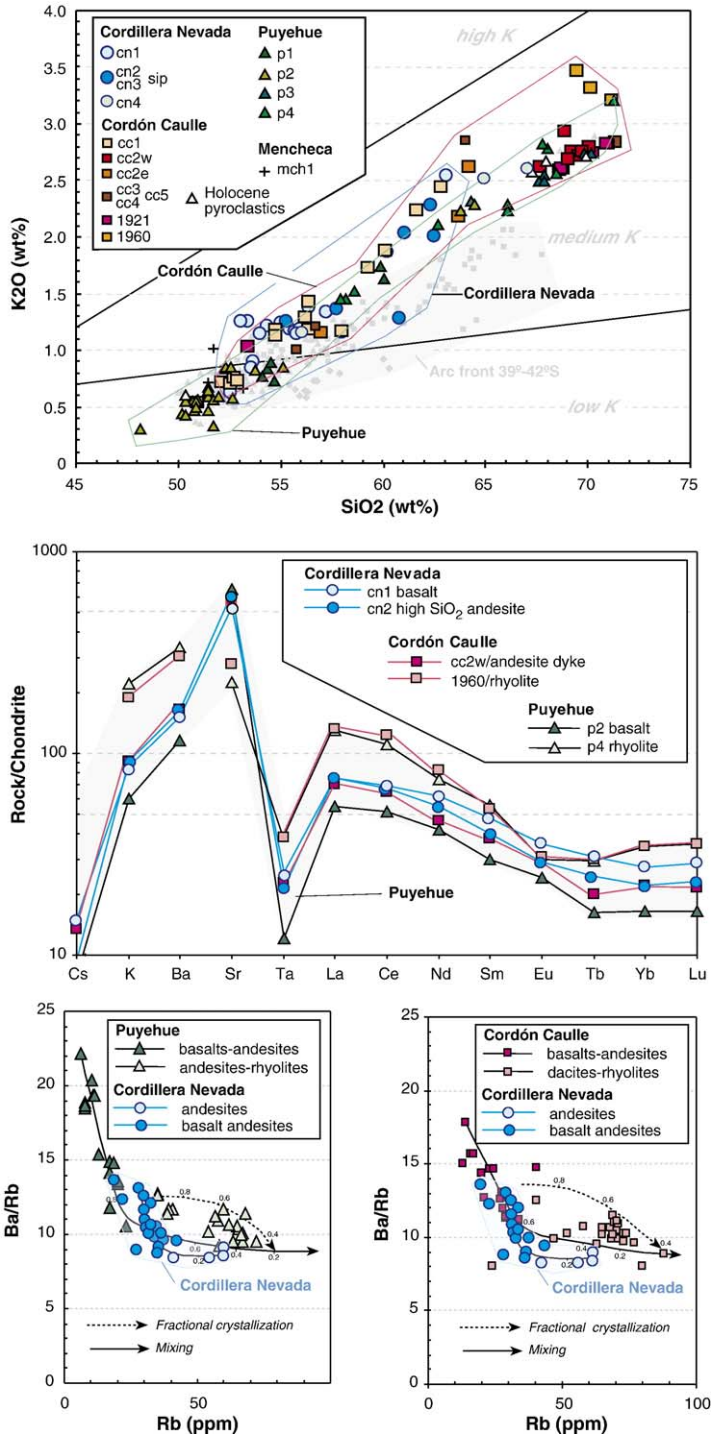

Fig. 7. (a) K_2O vs. SiO_2 contents for products of Cordón Caulle Volcanic Complex. Major elements were normalised to volatile-free totals of 99.6 wt. % (leaving 0.4 wt.% for trace elements and halogens). Light grey field is for other volcanoes from the arc front (39°–42° S): Villarrica (triangles; Hickey-Vargas et al., 1989; Lara and Clavero, 2004); Mocho-Choshuenco (squares; McMillan et al., 1989; Echegaray, 2004); Calbuco (diamonds; López-Escobar et al., 1995b). (b) Multielement diagram for selected end-member samples from PCCVC, normalised to chondritic values after Sun and McDonough (1989). (c) Plots of Ba/Rb vs. Rb. Mixing curves between end-members and fractional crystallisation trends (dashed lines) are shown for three intervals. Bulk partition coefficient values are from Hickey-Vargas et al. (1989) as follows: $F=1.0$ to 0.7: $D^{Rb}=0.01$; $D^{Ba}=0.06$; $F=0.7$ to 0.4: $D^{Rb}=0.05$; $D^{Ba}=0.16$; $F=0.4$ to 0.17: $D^{Rb}=0.12$; $D^{Ba}=0.51$.

several emission centres of PCCVC roughly overlap the trace of Iculpe River Fault, which is part of a regional suite of structural northwest-trending alignments that cross from the coastal range to the Andean range (Lara et al., in press). Although these northwest alignments are pre-Andean in origin, some authors have proposed for them a Cenozoic reactivation as strike-slip faults related to the opening of Tertiary basins (Duhart et al., 2001 and references therein) or as the westernmost expression of the Gastre Fault System (Coira et al., 1975; Rapela and Pankhurst, 1992; Brasse and Soyer, 2001). Quaternary kinematics for the overall northwest structures is poorly constrained. Some of them, such a Futrono Fault, show mesoscale features of sinistral displacement. Others seem to be at least crustal discontinuities that control the nucleation of seismic foci (Bohm et al., 2002).

Along the Iculpe River Fault there are no Quaternary surface markers of displacement, although it is a border between geological units at the Ranco lake shoreline (Campos et al., 1998). In addition, both the 1921–22 AD and 1960 AD fissure eruptions occurred along a possible blind northwest trace of this fault and its reshearing ability was proposed by Lara et al. (2004). In spite of the kinematics, Iculpe River Fault would have been a long-live ascent pathway for magmas from PCCVC.

7. Discussion

7.1. Stratigraphy and vents distribution

Based on field mapping and geochronology, a time and spatial sequence of volcanic events can be outlined as well as a transition from shield to unusual fissure rhyolitic volcanism. First, a nearly coeval evolution was recognised for Cordillera Nevada, Cordón Caulle, Puyehue and Mencheca volcanoes since the early stages. This is slightly different from the previous assumptions based on general morphology that suggested a time polarity with younger vents located towards the southeast (e.g., Moreno, 1977). Older units (ca. 450–100 ka) from Cordillera Nevada, Cordón Caulle, Puyehue and Mencheca have physical and chemical features of a widespread construction of shield volcanoes. High volume stratovolcanoes, mainly basaltic or basaltic andesite in composition evolved as nearly synchronous but separated vents (Fig. 7). After that, a succession of collapses gave rise to a graben morphology, which was the site for fissure eruptions of domes and the construction of Puyehue volcano. An interplay between fissure and central eruptions of mainly silica-rich magmas dominated the last ca. 100 ka (Fig. 4).

7.2. Magmatic evolution

Geochemical signature based on major oxide contents shows a clear affinity between Cordón Caulle and Puyehue magmas. Instead, magmas from Cordillera Nevada exhibit a more restricted compositional range (Fig. 7). Fractional crystallization appears as an appropriate model for the transition from basalts to andesites, and from andesites to rhyolites, in Cordón Caulle and Puyehue volcanoes. Instead, mixing or assimilation curves fit better the transition from basaltic andesites to andesites in Cordillera Nevada. This behaviour is independent of the age or the eruptive style and suggests a singular plumbing system for Cordillera Nevada that permitted successive replenishment of a shallow magma reservoir. In turn, high pressure basalts would have passed throughout the crust up to the shallow magma chambers, where fractional crystallization gave rise to the evolved products. Thus, rhyodacitic to rhyolitic magmas were emitted from Puyehue and Cordón Caulle by means of both effusive and explosive eruptions according to the external controls exerted to the conduits.

7.3. Eruptive style

The eruptive style have changed in space and time. The first stage of shield volcanism recognised at the entire PCCVC should be part of a regional event in Southern Andes that culminated in the Middle Pleistocene (Lara and Folguera, 2006). Once the successive collapses occurred, central and fissure eruptions build up both a stratocone and a fissure volcano that partially filled the graben. Moreover, the fissure system invaded the Cordillera Nevada where ring faults were reactivated. This stage occurred as an interplay of both effusive and explosive eruptions. The Holocene record is an example of alternating lava emissions with dome growing and explosive eruptions mainly from Puyehue volcano. This eruptive dynamics is not related with the major geochemical features, which are similar for Cordón Caulle and Puyehue volcanoes, but to the vent morphology that in turn could reflect the physics of the plumbing systems.

7.4. Tectonic control of volcanism

The PCCVC is perhaps the best example of spatial relationship between basement faults and volcanic vents in Southern Andes (López-Escobar et al., 1995a; Lara et al., in press). Moreover, the singular fissure eruptive style of silicic magmas along the Cordón Caulle also suggests

a causal relation between the structural setting and volcanism. However, the precise way in which tectonics of the upper crust influences the magma eruption is still obscure. For example, remote triggering after a great subduction earthquake was proposed by Barrientos (1994) for the 1960 AD eruption of Cordón Caulle. For the same event, Lara et al. (2004) discussed a model of fault reshearing of an underlying fault as a consequence of dynamic stresses transmitted during the coseismic period. Seismic pumping would have drained a shallow silicic magma to the surface. However, in the most dominant state of stress along the volcanic arc, which is a dextral transpression after Lavenu and Cembrano (1999), a contractional regime should act over the northwest oblique volcanic chains (e.g., Cembrano and Moreno, 1994). Thus, longer residence times and subsequent complex volcanic interactions are expected along these structural domains. In contrast, northeast chains would be tensional and mafic magmas would be drained from the deep sources without significant crustal residence. Following Takada (1994), despite the regional stress regime, volcanic morphology and eruptive style depend on the relation between the strain ratio and magma input from the subarc mantle source.

8. Conclusions

After the analysis of $^{40}Ar/^{39}Ar$ and ^{14}C geochronology merged with a detailed field mapping and geochemical data for PCCVC, some remarkable facts arise:

(1) PCCVC is located atop of first order orogenic faults that played a significant role on the vent distribution and magmatic processes.
(2) An early stage of shield volcanism older than ca. 100 ka is recognised at the entire PCCVC although individual centres evolved as separated systems. This stage correlates with a regional shield volcanism recognised in SVZ south of 38° S, which lasted until the end of the Middle Pleistocene. After that, episodic collapses created a graben morphology.
(3) A subsequent stage fissure and central volcanism built the Cordón Caulle fissure system and the Puyehue central volcano. Andesitic to rhyolitic lavas were emitted from Puyehue cone while mainly evolved magmas erupted as lava-domes from Cordón Caulle.
(4) Magmas from Cordillera Nevada have geochemical signatures of an isolated evolution with evidences of shallow magma mixing. Cordón Caulle and Puyehue volcanoes, despite the range of silica contents, define similar trends that can be related with fractional crystallization processes from a common parental source.
(5) Eruptive style, effusive or explosive, seems to be independent of the geochemical signatures.
(6) Magmatic evolution of PCCVC appears singular in the SVZ and seems to be related to local factors involving the underlying basement. The local stress regime of the upper crust could be the external control of magmatic evolution but this hypothesis need to be tested.

Acknowledgements

Field support and chemical and $^{40}Ar–^{39}Ar$ laboratory facilities are acknowledged to SERNAGEOMIN (Servicio Nacional de Geología y Minería, Chile). ^{14}C geochronology was carried out throughout funds from Fondecyt projects 1960186 and 1960885. B. Singer performed three $^{40}Ar–^{39}Ar$ analysis at the University of Wisconsin-Madison in duplicated samples and kindly shared unpublished data. D. Welkner reviewed an early version of the manuscript. Constructive criticism of M. Gorring and an anonymous reviewer greatly improved the article. This is a contribution to Volcanic Hazard Programme from SERNAGEOMIN.

References

Anderson, S.W., Fink, J.H., 1992. Crease structures: indicators of emplacement rates and surface stress regimes of lava flows. Geol. Soc. Amer. Bull. 104, 615–625.
Ayala, A., 1956. La erupción del Riñinahue. Rev. Geogr. Chile, Terra Australis 14, 52–64.
Barrientos, S., 1994. Large thrust earthquakes and volcanic eruptions. Pure Appl. Geophys. 142, 225–237.
Bengoa, J., 2003. Historia de los antiguos Mapuches del sur, Catalonia, Santiago.
Bentley, M.J., 1997. Relative and radiocarbon chronology of two former glaciers in the Chilean Lake District. J. Quat. Sci. 12, 25–33.
Bertrand, S., Boës, X., Castiaux, J., Charlet, F., Urrutia, R., Espinoza, C., Lepoint, G., Charlier, B., Fagel, N., 2005. Temporal evolution of sediment supply in Lago Puyehue (Southern Chile) during the last 600 yr and its climatic significance. Quat. Res. 64, 163–175.
Bohm, M., Lüth, S., Asch, G., Bataille, K., Bruhn, C., Rietbrock, A., Wigger, P., 2002. The Southern Andes between 36°S and 40°S latitude: seismicity and average velocities. Tectonophysics 356, 275–289.
Brasse, H., Soyer, W., 2001. A magnetotelluric study in the Southern Chilean Andes. Geophys. Res. Lett. 28, 3757–3760.
Brüggen, J., 1950. Fundamentos de Geología de Chile. Instituto Geográfico Militar, Santiago.
Cahill, T., Isacks, B., 1992. Seismicity and shape of the subducted Nazca plate. J. Geophys. Res. 97, 17503–17529.
Campos, A., Moreno, H., Muñoz, J., Antinao, J., Clayton, J., Martin, M., 1998. Area de Futrono-Lago Ranco, Región de los Lagos.

Servicio Nacional de Geología y Minería, Mapas Geológicos No. 8, 1 mapa escala 1:100.000. Santiago.

Casertano, L., 1960. Relación entre vulcanismo y sismicidad. Universidad de Chile, Boletín, vol. 12, pp. 23–27.

Casertano, L., 1962. Sui fenomeni sismo-vulcanici del Sud del Chile. Annali Osservatorio Vesubiano, vol. 4 (serie 6). Naples.

Cembrano, J., Moreno, H., 1994. Geometría y naturaleza contrastante del volcanismo cuaternario entre los 38°S y 46°S: ¿Dominios compresionales y tensionales en un régimen transcurrente?. Congreso Geológico Chileno No. 7, Actas Vol. 1, 240–244.

Clapperton, C., 1993. Quaternary Geology and Geomorphology of South America. Elsevier Science Publishers, Amsterdam.

Coira, B., Nullo, F., Proserpio, C., Ramos, V., 1975. Tectónica de basamento de la región occidental del Macizo Nordpatagónico (provincias de Río Negro y Chubut) Republica Argentina. Rev. Asoc. Geol. Argent. 30, 361–383.

Denton, G.H., Heusser, C.J., Lowell, T.V., Moreno, P.I., Andersen, B.G., Heusser, L.E., Schluchter, C., Marchant, D.R., 1999. Interhemispheric linkage of paleoclimate during the last glaciation. Geogr. Ann. 81, 107–153.

DeMets, C., Gordon, R., Argus, D., Stein, S., 1994. Effect of recent revisions to the geomagnetic reversal time scale on estimates of current plate motions. Geophys. Res. Lett. 21, 2191–2194.

Duhart, P., McDonough, M., Muñoz, J., Martin, M., Villeneuve, M., 2001. El Complejo Metamórfico Bahía Mansa en la cordillera de la Costa del centro-sur de Chile (39°30′–42°00′S): geocronología K–Ar, $^{40}Ar/^{39}Ar$ y U–Pb e implicancias en la evolución del margen sur-occidental de Gondwana. Rev. Geol. Chile 28, 179–208.

Dungan, M.A., Wulff, A., Thompson, R., 2001. Eruptive stratigraphy of Tatara–San Pedro complex, 36°S, Southern Volcanic Zone, Chilean Andes: reconstruction meted and implications for magma evolution at long-lived arc volcanic centres. J. Petrol. 42, 555–626.

Echegaray, J., 2004. Evolución geológica y geoquímica del centro volcánico Mocho-Choshuenco, Andes del Sur, 40°S. Unpublished MSc thesis, Universidad de Chile.

Fleck, R.J., Sutter, J.F., Elliot, D.H., 1977. Interpretation of discordant $^{40}Ar/^{39}Ar$ age-spectra of Mesozoic tholeiites from Antarctica. Geochim. Cosmochim. Acta 41, 15–32.

Gerlach, D., Frey, F., Moreno, H., López, L., 1988. Recent volcanism in the Puyehue–Cordón Caulle Region, Southern Andes, Chile (40.5°S): petrogenesis of evolved lavas. J. Petrol. 29, 333–382.

Hantke, G., 1940. Das Vulkangebeit zwischen den Seen Ranco und Puyehue in Süd Chile. Annali Osservatorio Vesubiano, vol. 7 (series 2). Naples.

Hantke, G., 1961. Der Vulkanismus in Chile. Smithsonian Institution, Washington.

Harper, M.A., 2003. $^{40}Ar/^{39}Ar$ Constraints on the Evolution of the Puyehue–Cordon Caulle Volcanic Complex, Andean Southern Volcanic Zone, Chile. Unpublished MSc thesis, University of Wisconsin-Madison.

Harper, M.A., Singer, B.S., Moreno-Roa, H., Lara, L.E., Naranjo, J.A., 2004. $^{40}Ar/^{39}Ar$ Constraints on the Evolution of the Puyehue–Cordón Caulle Volcanic Complex, Andean Southern Volcanic Zone, Chile, IAVCEI General Assembly, Abstracts, Pucón.

Hickey-Vargas, R., Moreno, H., López Escobar, L., Frey, F., 1989. Geochemical variations in Andean basaltic and silicic lavas from the Villarrica–Lanín volcanic chain (39.5°S): an evaluation of source heterogeneity, fractional crystallization and crustal assimilation. Contrib. Mineral. Petrol. 103, 361–386.

Hildreth, W., Moorbath, S., 1988. Crustal contributions to arc magmatism in the Andes of Central Chile. Contrib. Mineral. Petrol. 98, 455–489.

Illies, H., 1959. Die entstehungsgeschichte eines Maars in Süd Chile. Geol. Rundsch. 28, 232–247.

Kanamori, H., Cipar, J.J., 1974. Focal process of the great Chilean earthquake, May 22, 1960. Phys. Earth Planet. Inter. 9, 128–136.

Katsui, J., Katz, H., 1967. Lateral fissure eruptions in the Southern Andes of Chile. Fac. Sci. Ser. 4, 433–448 (Hokkaido).

Klohn, C., 1995. Informe geológico sobre el volcán Pillanilahue. CORFO. 61 p. Santiago.

Krumm, F., 1923. Topographische und geologische Nachrichten über die Gegend stlich des Ranco Sees in Süd Chile, im Besonderen über den jüngsten Vulkanausbruch 'Los Azufres' (Dezember 1921). Geol. Rundsch. 14, 146–150.

Lara, L.E., Clavero, J. (Eds.), 2004. Villarrica volcano (39.5°S), Southern Andes, Chile. Servicio Nacional de Geología y Minería Boletín, vol. 61, 66 pp.

Lara, L.E., Folguera, A., 2006. The Pliocene to Quaternary narrowing of the Southern Andean volcanic arc between 37° and 41°S latitude. In: Kay, S.M., Ramos, V.A. (Eds.), Evolution of an Andean margin. A tectonic and magmatic view from the Andes to the Neuquén Basin (35°–39°S lat). Geol. Soc. Am. Spec. Pap., 407, pp. 299–315.

Lara, L.E., Moreno, H., 2006. Geología del Complejo Volcánico Puyehue–Cordón Caulle, X Región de Los Lagos. Servicio Nacional de Geología y Minería, Carta Geológica de Chile, Serie Geología Básica, 1 mapa escala 1:50.000.

Lara, L.E., Rodríguez, C., Moreno, H., Pérez de Arce, C., 2001. Geocronología K–Ar y geoquímica del volcanismo plioceno superior-pleistoceno de los Andes del Sur (39°–42°S). Rev. Geol. Chile 28, 67–90.

Lara, L.E., Naranjo, J.A., Moreno, H., 2004. Rhyodacitic fissure eruption in Southern Andes (*Cordón Caulle*; 40.5°S) after the 1960 (Mw: 9.5) Chilean earthquake: a structural interpretation. J. Volcanol. Geotherm. Res. 138, 127–138.

Lara, L.E., Lavenu, A., Cembrano, J., Rodríguez, C., in press. Structural controls of volcanism in transversal chains: resheared faults and neotectonics in Cordón Caulle–Puyehue area (40.5°S), Southern Andes. J. Volcanol. Geotherm. Res.

Lavenu, A., Cembrano, J., 1999. Compressional and transpressional-stress pattern for Pliocene and Quaternary brittle deformation in fore arc and intra-arc zones (Andes of Central and Southern Chile). J. Struct. Geol. 21, 1669–1691.

Lescinsky, D., Fink, J., 2000. Lava and ice interaction at stratovolcanoes: use of characteristic features to determine past glacial events and future volcanic hazards. J. Geophys. Res. 105, 23,711–23,726.

León, L., Polle, E., 1956. Las capas volcánicas de Carrán y la erupción del Nilahue. Comunicaciones 7, 24.

López-Escobar, L., Cembrano, J., Moreno, H., 1995a. Geochemistry and tectonics of the Chilean Southern Andes basaltic Quaternary volcanism (37°–46°S). Rev. Geol. Chile 22, 219–234.

López-Escobar, L., Kempton, P.D., Moreno, H., Parada, M.A., Hickey-Vargas, R., Frey, F.A., 1995b. Calbuco volcano and minor eruptive centers distributed along the Liquiñe–Ofqui fault zone, Chile (41°–42°S): contrasting origin of andesitic and basaltic magma in the Southern Volcanic Zone of the Andes. Contrib. Mineral. Petrol. 119, 345–361.

Lowell, T.V., Heusser, C.J., Andersen, B.G., Moreno, P.I., Hauser, A., Heusser, L.E., Schluchter, C., Marchant, D.R., Denton, G.H.,

1995. Interhemispheric correlation of late Pleistocene glacial events. Science 269, 1541–1549.
McCormac, F.G., Hogg, A.G., Blackwell, P.G., Buck, C.E., Higham, T.F.G., Reimer, P.J., 2004. SHCal04 Southern Hemisphere Calibration 0–1000 cal BP. Radiocarbon 46, 1087–1092.
McMillan, N.J., Harmon, R.S., Moorbath, S., Lopez-Escobar, L., Strong, D., 1989. Crustal sources involved in continental arc magmatism: a case study of Volcan Mocho-Choshuenco, southern Chile. Geology 17, 1152–1156.
Meyer Rusca, W., 1955. Diccionario geográfico-etimológico indígena de las provincias de Valdivia, Osorno y Llanquihue. Editorial Universitaria (2ª edición), Temuco, 299 p.
Moreno, H., 1977. Geología del área volcánica Puyehue-Carrán en los Andes del sur de Chile. (unpublished thesis). Universidad de Chile, Santiago.
Moreno, H., 1980. La erupción del volcán Mirador en abril–mayo de 1979, Lago Ranco-Riñinahue, Andes del Sur. Comunicaciones 28, 1–23.
Moreno, H., Petit-Breuilh, M.E., 1999. El volcán fisural Cordón Caulle, Andes del Sur (40.5°S): geología general y comportamiento eruptivo histórico. 14th Congreso Geológico Argentino, Actas, vol. 2, pp. 258–260. Salta.
Müller, G., Veyl, G., 1957. The birth of Nilahue, a new maar type volcano at Riñinahue, Chile. 20th International Geological Congress, Proceedings I–II, pp. 375–396. Ciudad de México.
Newhall, C.G., Self, S., 1982. The volcanic explosivity index (VEI): an estimate of explosive magnitude for historical volcanism. J. Geophys. Res. 87, 1231–1238.
Peña, P., Fuentealba, G., 2000. Antecedentes preliminares de sismicidad asociada al complejo volcánico activo Cordón Caulle, Andes del Sur (40,5°S). 9th Congreso Geológico Chileno, Actas, vol. 2, pp. 52–53. Puerto Varas.
Pérez, Y., 1999. Fuentes de aguas termales de la Cordillera Andina del Centro-Sur de Chile (39°–42°S). Servicio Nacional de Geología y Minería, Boletín No. 54, 65 p., 2 anexos, 1 mapa escala 1:500.
Pérez de Arce, C., Becker, T., Roeschmann, C., 2000. El nuevo sistema de datación ^{40}Ar–^{39}Ar equipado con láser de CO_2 en el SERNAGEOMIN. 9th Congreso Geológico Chileno, Actas, vol. 1, p. 675. Puerto Varas.
Pérez de Arce, C., Matthews, S., Klein, J., 2003. Geochronology by the $^{40}Ar/^{39}Ar$ method at the SERNAGEOMIN Laboratory, Santiago, Chile. International Conference on Research Reactor, Utilization, Safety, Decommissioning, Fuel and Waste Management, Actas, Santiago.
Petit-Breuilh, M.E., 1999. Cronología eruptiva histórica de los volcanes Osorno y Calbuco, Andes del Sur (41°–4°°30′S). Servicio Nacional de Geología y Minería, Boletin, vol. 53. 46 pp. Santiago.
Pierson, T., Janda, R., 1994. Volcanic mixed avalanches: a distinct eruption-triggered mass-flow process at snow-clad volcanoes. Geol. Soc. Amer. Bull 106, 1351–1358.
Porter, S.C., 1981. Pleistocene glaciation in the Southern Lake District of Chile. Q. Res. 16, 263–292.
Rapela, C., Pankhurst, R., 1992. The granites of northern Patagonia and the Gastre Fault System in relation to the break-up of Gondwana. In: Alabaster, T., Pankhurst, R. (Eds.), Magmatism and Causes of Continental Break-up, Storey, B. Geological Society, Special Publication, vol. 68, pp. 209–220.
Renne, P.R., Deino, A.L., Walter, R.C., Turrin, B.D., Swisher, C.C., Becker, T.A., Curtis, G.H., Sharp, W.D., Jaouni, A.R., 1994. Intercalibration of astronomic and radioisotopic time. Geology 22, 783–786.
Renne, P.R., Swisher, C.C., Deino, A.L., Karner, D.B., Owens, T.L., DePaolo, D.J., 1998. Intercalibration of standards, absolute ages, and uncertainties in $^{40}Ar/^{39}Ar$ dating. Chem. Geol. 145, 117–152.
Rimbach, C., 1930. Kurze Mitteilungen über einige chilenische Vulkane mit 9 Textfigure. Zeitschrift für Vulkanologie, Band, vol. XVVV, pp. 105–108.
Saint Amand, P., 1961. Observaciones e interpretación de los terremotos chilenos de 1960. Comunicaciones 2, 1–54.
Salmi, M., 1941. Die postglacialen Eruptansschichten Patagoniens und Feuerlands. Ann. Acad. Sci. Fenn. (Serie A), Helsinski, 116 p. (2 folding plates).
Sapper, K., 1927. Vulkankunde. Stuttgart.
Sepúlveda, F., 2006. El sistema geotérmico de Cordón Caulle, sur de Chile. Caracterización geológica y geoquímica. Unpublished PhD thesis (Universidad de Chile).
Sepúlveda, F., Dorsch, K., Lahsen, A., Bender, S., Palacios, C., 2004. Chemical and isotopic composition of geothermal discharges from the Puyehue–Cordón Caulle area (40.5°S), Southern Chile. Geothermics 33, 655–673.
Sepúlveda, F., Lahsen, A., Bonvalot, S., Cembrano, J., Alvarado, A., Letelier, P., 2005. Morphostructural evolution of the Cordón Caulle geothermal region, Southern Volcanic Zone, Chile: insights from gravity and $^{40}Ar/^{39}Ar$ dating. J. Volcanol. Geotherm. Res. 148, 165–189.
Sigmarsson, O., Condomines, M., Morris, J.D., Harmon, R.S., 1991. Uranium and ^{10}Be enrichments by fluids in Andean arc magmas. Nature 346, 163–165.
Singer, B.S., Thompson, R.A., Dungan, M.A., Feeley, T.C., Nelson, S.T., Pickens, J.C., Brown, L.L., Wulff, A.W., Davidson, J.P., Metzger, J., 1997. Volcanism and erosion during the past 930 ka at the Tatara–San Pedro complex, Chilean Andes. Geol. Soc. Amer. Bull. 109, 127–142.
Singer, B.S., Relle, M.R., Hoffman, K.A., Battle, A., Guillou, H., Laj, C., Carracedo, J.C., 2002. $^{40}Ar/^{39}Ar$ ages of transitionally magnetized lavas on La Palma, Canary Islands, and the geomagnetic instability timescale. J. Geophys. Res. 107 (B11), doi:10.1029/2001JB001613.
Singer, B.S., Jicha, B.R., Harper, M.A., Moreno, H., Naranjo, J.A., Lara, L.E., 2004. Genesis of basalt and rhyolite erupted in the last 35 ka at Volcán Puyehue Chilean SVZ: initiation of a U–Th Isotope study. IAVCEI General Assembly, Abstracts, Pucón.
Soon, W., Baliunas, S., 2003. Proxy climatic and environmental changes of the past 1000 years. Clim. Res. 23, 89–110.
Steffen, H., 1922. Nachrichten aus den vulkangebieten der Kordilleren von Mittel—Chile. Z. Ges. Erdkunde 273–277.
Stone, J., 1935. The volcanoes of Southern Chile. Zeitschrift für Vulkanologie, vol. 16, pp. 81–97.
Stone, J., Ingerson, E., 1934. Algunos volcanes del sur de Chile. Boletín de Minas y Petróleo, vol. 5, No.40.
Stuiver, M., Reimer, P.J., 1993. Extended ^{14}C database and revised CALIB radiocarbon calibration program. Radiocarbon 35, 215–230.
Sun, S.S., McDonough, W.F., 1989. Chemical and isotopic systematics of oceanic basalts: implications for mantle composition and processes. In: Saunders, A.D., Norry, M.J. (Eds.), Magmatism in the Ocean Basins. Geological Society Special Publications 42, 313–345.
Takada, A., 1994. The influence of regional stress and magmatic input on styles of monogenetic and polygenetic volcanism. J. Geophys. Res. 99, 13,563–13,573.
Tamaki, K., 2000. Nuvel 1-A Calculation Results. Ocean Research Institute, University of Tokio. http://ofgs.ori.u-tokyo.ac.jp/~okino//rate_calc_new.cgi.

Tassara, A., Yáñez, G., 2003. Relación entre el espesor elástico de la litósfera y la segmentación tectónica del margen andino (15–47°S). Rev. Geol. Chile 30, 159–186.

Tormey, D., Schuller, P., López, L., Frey, F., 1991. Uranium–thorium activities and disequilibria in volcanic rocks from the Andes (33°–46S): petrogenetic constraints and environmental consequences. Rev. Geol. Chile 18, 165–175.

Veyl, C., 1960. Los fenómenos volcánicos y sísmicos de fines de Mayo de 1960 en el sur de Chile. Universidad de Concepción, Concepción. 42 pp.

Vogel, M., 1934. Caulle (Chile). Zeitschrift für Vulkanologie, vol. 16, p. 128.

von Wolff, F., 1929. Der Vulkanismus. Stuttgart.

Weischet, W., 1963. Further observations of geologic and geomorphic changes resulting from the catastrophic earthquake of May 1960, in Chile. Seism. Soc. Am. Bull. 53, 1237–1257.

Wetzel, W., 1959. Informe sobre investigaciones efectuadas durante el segundo semestre de 1958. Universidad Austral, Valdivia, 11 pp.

3.3 L'éruption fissurale du Cordón Caulle (40.5ºS) après le séisme (Mw: 9.5) de 1960 AD : une interprétation structurale

L'éruption rhyodacitique de 1960 AD d'une fissure dans le Complexe Volcanique de Puyehue-Cordón Caulle (CVPCC), situé dans les Andes méridionales (40.5ºS) était un épisode volcanique unique. Cette éruption remarquable a été déclenchée par le plus grand tremblement de terre enregistré dans la zone de subduction et cela a commencé 38 h après le choc principal, 240 kilomètres à l'intérieur du continent. Le comportement structural (deux fissures composées s'ouvrant le long d'une structure NW-SE oblique à la marge continentale sont reliées à l'évolution quaternaire du CVPCC) suggère que la nature fracturée de la croûte supérieure dans les Andes du Sud a été un paramètre influent pour les éruptions volcaniques. A partir des données historiques et de l'analyse morphologique et structurale, nous proposons que les structures de direction NW-SE constituent des voies d'ascension et de mise en place magmatique régulières. Ainsi, pendant le grand événement sismique, et catalysé par la pression du liquide autour de la faille, cette préfracturation aurait été réactivée en permettant, au commencement, la propagation d'un dyke non-Andersonien. Puis, le magma silicique aurait atteint la surface par le 'pompage' sismique. Quand l'activité tectonique initiale dans les segments réactivés a cessé, le champ de contraintes local aurait changé, favorisant la formation de nouvelles fractures, cette fois presque parallèles à la contrainte horizontale maximum N-S, et favorisant le transport de magma comme des dykes Andersoniens. Bien que les caractéristiques rhéologiques des laves siliciques émises ainsi que le comportement structural et les dispositifs sismiques de ce cycle éruptif constituent des conditions plutôt exceptionnelles dans les Andes du Sud, la nature fracturée de la croûte supérieure et la propagation de dykes Andersoniens et non-Andersoniens fournissent un cadre théorique pour analyser la néotectonique de l'arc volcanique dans une marge convergente.

Available online at www.sciencedirect.com

SCIENCE DIRECT®

Journal of Volcanology and Geothermal Research 138 (2004) 127–138

Journal of volcanology and geothermal research

www.elsevier.com/locate/jvolgeores

Rhyodacitic fissure eruption in Southern Andes (*Cordón Caulle*; 40.5°S) after the 1960 (Mw:9.5) Chilean earthquake: a structural interpretation

L.E. Lara[a,b,*], J.A. Naranjo[a], H. Moreno[a]

[a]*SERNAGEOMIN, Servicio Nacional de Geología y Minería, Chile*
[b]*Université Paul Sabatier, Toulouse III, France*

Received 16 October 2003; accepted 22 June 2004

Abstract

The 1960 rhyodacitic fissure eruption in the *Cordón Caulle* Volcanic Complex (CCVC), located in Southern Andes (40.5°S) was a unique volcanic episode. The remarkable eruption was triggered by the greatest recorded subduction-zone earthquake, starting 38 h after the main shock, 240 km inland. The structural behaviour, two compound fissures opening along a margin-oblique (NW) structure related to the Quaternary evolution of the CCVC, suggests that the prefractured nature of the upper crust in the Southern Andes was an influential condition for volcanic eruptions. From historical data and morphologic and structural analysis, we suggest that NW structures constitute pathways of steady magmatic ascent. Thus, during the great seismic event, and catalysed by the fluid pressure around a fault, it would have been reactivated allowing, initially, the propagation of a non-Andersonian dyke. Then, the silicic magma would have reached the surface by 'seismic pumping'. Once the initial activity in the reactivated segments ceased, the local stress field would have changed, favouring the formation of new failures, this time almost parallel to the maximum horizontal stress, and promoting magma transport as Andersonian dykes. Although the rheologic characteristics of the silicic lavas erupted together with the structural behaviour and seismic features of this eruptive cycle constitute rather exceptional conditions in the Southern Andes record, the prefractured nature of the upper crust and the shifting propagation of Andersonian and non-Andersonian dykes provide a theoretical framework to analyse the neotectonics of the volcanic arc in a convergent margin.

Keywords: fissure eruption; rhyodacitic magma; 1960 Chilean earthquake; fault reactivation

1. Introduction

The relationship between volcanism and tectonics has been a controversial topic for many years. The early recognition of close spatial relationships

* Corresponding author. Av. Santa Maria 0104, Providencia-Santiago, Chile.
E-mail address: lelara@sernageomin.cl (L.E. Lara).

0377-0273/$ - see front matter © 2004 Elsevier B.V. All rights reserved.
doi:10.1016/j.jvolgeores.2004.06.009

between faults and volcanic centres has led to construction of models that try to explain the pattern of regional deformation as well as the distribution, evolution and morphostructure of the volcanic centres in different geodynamic settings (Takada, 1994; Bellier and Sébrier, 1994; Dhont et al., 1998). For example, Nakamura (1977) suggested that the parasitic cones of stratovolcanoes are aligned according to the maximum horizontal stress (σ_{hmax}). Other authors have shown direct links between the geometry of the faults that are used as pathways for magmatic ascent (Tibaldi, 1995), their displacements (e.g., Delaney et al., 1986; Alaniz-Alvarez et al., 1998), and some morphologic characteristics of the volcanic centres. Although that is a key topic of research in the Southern Andes Volcanic Zone (SAVZ: 33–46°S), we want to focus on two less discussed aspects: (1) the reactivation of structures allowing the emplacement of 'non-Andersonian' dykes (i.e. dykes not parallel to σ_{hmax} and therefore not correspond to 'Andersonian' structures; Anderson, 1951; Bahar and Girod, 1983; Delaney et al., 1986) and (2) injection resulting from coseismic deformation during large earthquakes in subduction zones. The concept of fault reactivation was mainly developed by Sibson (1985, 1987, 1996, 2000) and Sibson et al. (1988) to explain cycles of mineralization in several tectonic settings and is an important framework for understanding prefractured convergent margins with regional-scale active faults. This is the case of the South Southern Volcanic Zone (SSAVZ: 37–46°S) where the Quaternary volcanic arc has been built close to trench-parallel Cenozoic structures such as the Liquiñe-Ofqui Fault (e.g., Cembrano et al., 1996; Lavenu and Cembrano, 1999), as well as, older NW–SE structures, possibly formed previous to the Mesozoic Andean cycle.

In addition, coseismic deformation propagated inland for 250 km would be an unlikely fact, although it is possible in the context of the largest earthquake instrumentally recorded in the world (rupture zone around 1000 km long) (Fig. 1). The relation between subduction earthquakes and volcanic eruptions has been analysed by Blot (1965), Acharya (1982) and Linde and Sacks (1998), among others, although with very different data sets. Although the instantaneous deformation in the volcanic arc in the Southern Andes was not monitored during the 1960 eruptive cycle,

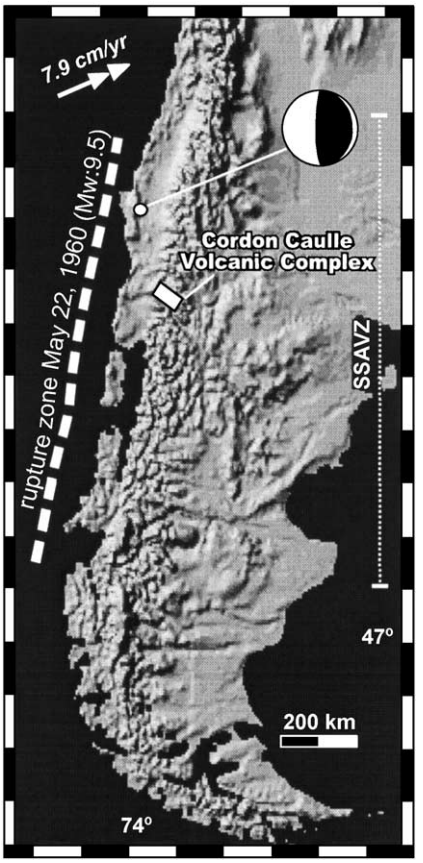

Fig. 1. Shaded relief of South America. White box shows the CCVC. Rupture zone of 1960 Chilean earthquake after Plafker and Savage (1970) and relocated epicentre (Cifuentes, 1989) are shown. Current subduction velocity after DeMets et al. (1994) is also indicated. A focal mechanism solution for 1960 earthquake by Cifuentes (1989) is at upper right corner (black region corresponds to compression on lower hemisphere diagram).

some morphologic features, as well as the analysis of several technical reports and papers (Veyl, 1960; Saint Amand, 1961; Casertano, 1962; Katsui and Katz, 1967) about the eruptive process, allow a more comprehensive explanation of the eruptive event as a whole. A structural analysis based on the classic theory of fractures and brittle rupture criteria (e.g., Anderson, 1951; Hubbert and Rubey, 1959; Byerlee, 1978) together with new approaches on fault reshearing (e.g., Sibson, 1985, 1987, 1996, 2000; Sibson et al., 1988) may explain the relationship between the coseismic deformation and the fissure eruption of a rhyodacitic magma.

2. Cordón Caulle Volcanic Complex (CCVC)

Cordón Caulle Volcanic Complex (CCVC) is a cluster of eruptive centres that extends between the Cordillera Nevada caldera (1799 m a.s.l.) and the Puyehue stratovolcano (2236 m a.s.l.) from NW to SE (Fig. 2). It consists of various fissure vents with aligned domes and pyroclastic cones (Moreno, 1977). The CCVC, located 240 km east of the Chile–Perú trench, forms a transversal 15 km long by 4 km wide ridge of 135° azimuthal direction, including a nested graben. On the northwestern end is located the Cordillera Nevada caldera, a collapsed Pleistocene stratovolcano (Campos et al., 1998; Lara et al., 2001, 2003) while on the southeastern end, the Puyehue stratovolcano appears as a prominent truncated cone that has a 2.5-km diameter summit caldera intermittently active during the last 10,000 years with noticeable explosive pulses. The chemical composition of the CCVC has been mainly rhyodacitic to rhyolitic (68–71% SiO_2; Gerlach et al., 1988), with subordinated basaltic to andesitic types among the earlier lavas. The abundance of silicic types is unique among the mostly bimodal centres along the SSAVZ

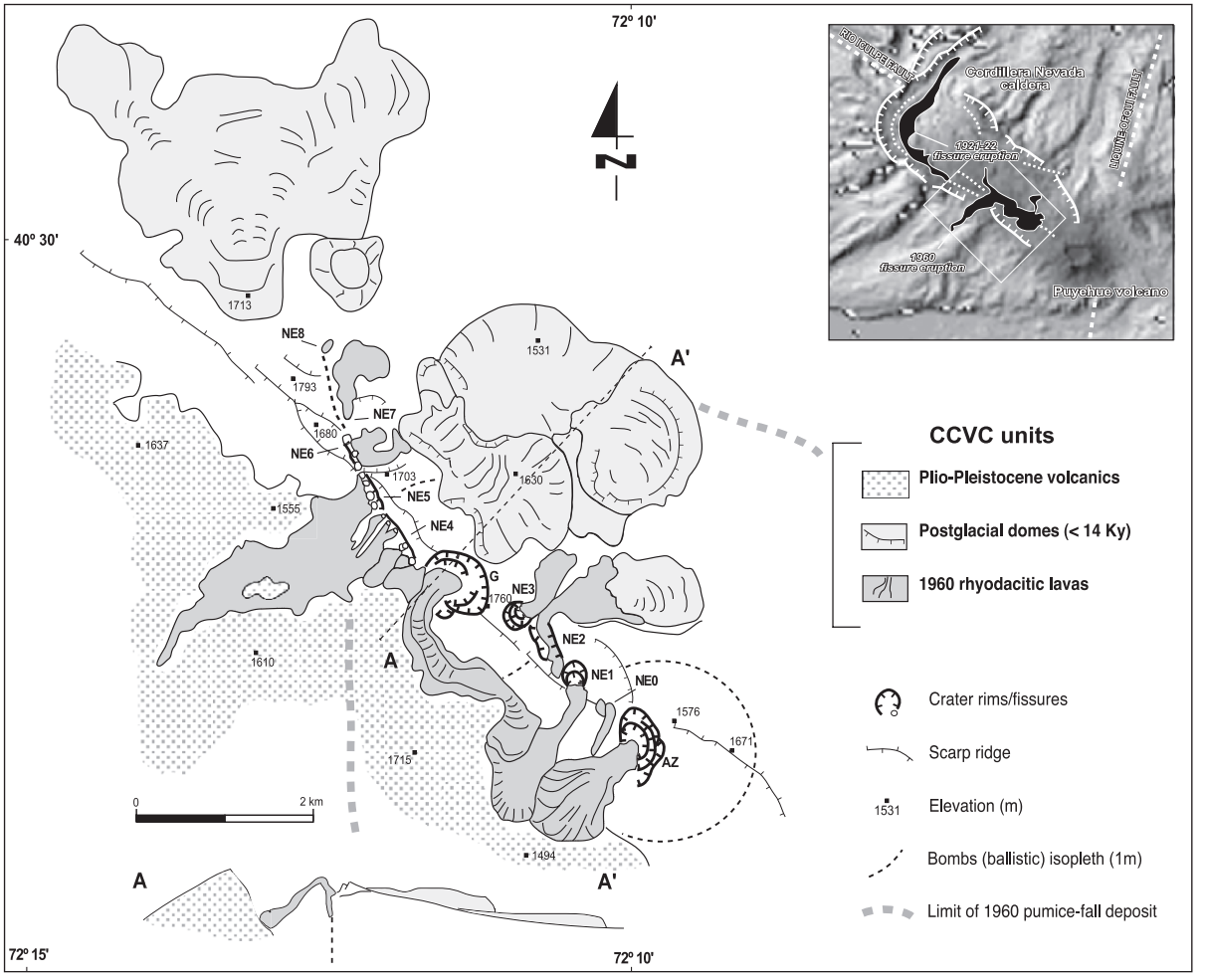

Fig. 2. Geologic map of 1960 fissure in the CCVC. Main crater, fissure or vents are labelled (G: Gris crater; AZ: El Azufral crater; NE0, NE1, NE3, NE7 and NE8 vents; NE2, NE4; NE5 and NE6 fissures). Insert sketch shows CCVC as a whole (white box is the map area) and 1921–22 and 1960 fissure vents. Regional long-lived faults are also indicated.

(37–46°S), where basalts widely predominate over more silica-rich rocks.

The tectonic control of the CCVC seems to be remarkable. The entire volcanic complex was built on a pre-Andean NW structure that limits geological domains at regional scale. For example, the overall construction of Puyehue volcano was coeval with the early stages of lava domes eruptions along the internal NW graben in the CCVC (Moreno, 1977). Moreover, another fissure eruption of rhyodacitic magma in 1922 is recognized in the northwestern end of the CCVC where NW fissures bend as ring faults inside the Cordillera Nevada caldera. On the other hand, several hot springs, forming the most important active geothermal field of the SSAVZ, are located inside the graben that joins Cordillera Nevada caldera with the Puyehue stratovolcano (Fig. 2). In the CCVC, microseismic volcanotectonic events, together with long period and low frequency signals and a sustained tremor may be related to the opening and closing of the hydrothermal and magma conduits inside the structural system (Peña and Fuentealba, 2000).

3. The 1960 earthquake (Mw=9.5)

The 1960 Chilean earthquake is the largest instrumentally recorded in the world. The magnitude of the released energy saturated the conventional scale when the dimension of the rupture zone exceeded the wavelength of the seismic waves used for its calculation (Kanamori and Cipar, 1974). Thus, Kanamori (1977) proposed a new scale that considers the seismic moment for the equation of energy of Gutenberg–Richter (Gutenberg, 1956). In this modified scale, the Chilean earthquake of 1960 reaches Mw=9.5, followed by the Alaska 1964 (Mw=9.2), Aleutians 1957 (Mw=9.1) and Kamchatka 1952 (Mw=9.0) earthquakes. The rupture zone (Fig. 1), determined by Plafker and Savage (1970) considering coseismic intensities and land deformations, reaches 1000 km in length, with the CCVC located approximately in front of the middle of this segment. Some of the effects of the earthquake were worldwide and, for example, Smylie and Mansinha (1968) described a shift of the terrestrial axis of rotation that followed the earthquake and Eaton et al. (1961), Sievers et al. (1963), and Berninghausen (1962) described destructive tsunamis that affected the coasts of the western Pacific Ocean. In addition, Duda (1963) and Plafker and Savage (1970) made a detailed compilation of the sequence of seismic events that began on May 21st (10:03 GMT), with a first shock located in the north end of the rupture zone, and culminated on May 22nd (19:11 GMT) with the main shock, whose epicentre was located 140 km toward the southwest of the first one. More recently, Cifuentes (1989) analysed the foreshock and aftershock sequences constraining the source mechanism of the main thrust event. Many authors (e.g., Veyl, 1960; Weischet, 1963) report huge topographic changes along the Pacific shoreline where up to 5.7 m of uplift and 2.7 m of subsidence occurred after the main earthquake. Subsequently, using a local geodetic network, Plafker and Savage (1970) characterized the coseismic deformation in the coastal area and inland. In addition to uplift and subsidence along the shoreline, spontaneous water springs, 'mud volcanoes' and cracks, took place on the unconsolidated deposits. Fractures up to 500 m long with orthogonal directions of N45° and N135° were recognized in the coastal area. Landslides located along the main trace of the Liquiñe–Ofqui Fault were the easternmost morphologic effects of the 1960 earthquake.

Only 38 h after the main shock, an eruptive cycle of the CCVC began. Although the Chilean seismic network available in 1960 was too sparse to suitably characterize the earthquake sequence, the zone of continental surficial deformation was at least 150 km wide according to the local geodetic network (Plafker and Savage, 1970). With these data, Barrientos and Ward (1990) obtained the displacement in the rupture zone. Using this displacement, Barrientos (1994) made a bidimensional analysis of the deformation and applied a static propagator matrix (Ward, 1984) to obtain the displacements in the CCVC area, assuming a 25° west vergent thrust plane in the rupture zone. If their assumptions were correct, horizontal displacements of ca. 20 m in the coastal area, close to the rupture zone, suitably fit the measured vertical variations and could have produced EW horizontal displacement of ca. 2 m in the main cordillera, where the CCVC is located. Following this analysis, displacements sufficiently large to reactivate shallow

structures and to trigger the CCVC eruption seem plausible.

4. 1960 fissure CCVC eruption

The isolated area where CCVC is located made the direct observation of the 1960 eruptive cycle difficult. In addition, because of the fatalities and the huge damage caused by the earthquake itself, there were few recorded reports of the eruption. Nevertheless, the reviews of newspaper articles, technical reports (Veyl, 1960; Saint Amand, 1961; Casertano, 1962; Katsui and Katz, 1967), an unpublished thesis (Moreno, 1977) and new precise geomorphologic field observations, have allowed its characterization.

The 1960 eruptive cycle (Table 1) occurred on a ca. 5.5-km long N135° fissure located near the SW margin of the CCVC and was formed by two sub-parallel segments. Each of these segments has secondary alignments oriented N160–165°. Twenty-one identifiable vents emitted pyroclastic ejecta and lava flows of rhyodacitic composition (68.9–70.01% SiO_2) with a ca. 0.25 km^3 of DRE volume. The eruptive cycle began on May 24th (09:00 h GMT), 38 h after the main shock of May 22nd, starting with an explosive subplinian phase and the formation of an eruptive 'mushroom-like' column about 8 km high, together with the emission of water vapour from other vents along the fissure system. The most active centre in this phase (stage 1) was the Gris crater (Figs. 2 and 3), followed by El Azufral crater (Fig. 2), both at the tips of the fissure. The pyroclastic plumes were dispersed toward the southeast forming a white pumice deposit with thickness up to 10 cm at 30–40 km of the Gris crater. An accumulation of 'bread crust' bombs and coarse lapilli pumice around the Gris crater formed a low aspect ratio pyroclastic cone.

Table 1
Summary of 1960 eruptive cycle

	May 21st (10:03 GMT)	Foreshock in the north end of rupture zone of 1960 earthquake
	May 22nd (19:11 GMT)	Main shock of 1960 earthquake
Stage 1	May 24th (09:00 GMT)	Subplinian phase on N135 alignments: pyroclastic ejecta from Gris and Azufral craters
Stage 2	May 26th?	Effusive phase on N135 alignments: rhyodacitic lava from Gris, NE1 and Azufral craters
Stage 3	June?	Effusive phase on N165 alignments: rhyodacitic lava from NE2 to NE8 vents; rhyodacitic lava from Gris, NE1 and Azufral craters continued
	June	Effusive ongoing phase
	July?	Quiescence period
	pre-July 22nd	Renewed pyroclastic phase: ballistic ejecta from Gris and Azufral craters
	post-July 22nd–present	Quiescence period/Solfataric and microseismic activity

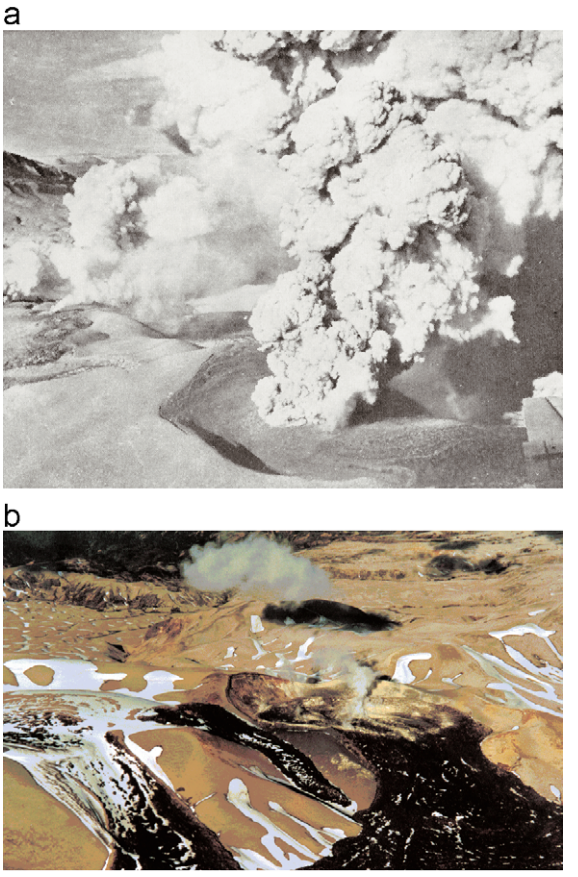

Fig. 3. (a) Aerial photograph of the 1960 eruptive cycle in the CCVC (P. Saint Amand in Casertano, 1962). This picture, taken toward the southwest, shows the Gris crater in close-up view and the coeval water vapour columns through northeastern vents (NE2; NE3) during the third eruptive stage. (b) Current aerial view of El Azufral crater, NE0 and NE1 vents with a still active solfatara, 44 years later.

An effusive phase, with emission of *a′a* and blocky rhyodacitic clinopyroxene and Fe-olivine lava flows followed the previous stage. The first blocky lava flow was produced by NE1 crater (Fig. 2), followed by the coeval flows from the Gris and El Azufral craters. The eruptive vents evolved to a N160–165° (stage 3) alignments (NE2 and NE4 vents), as the first phase culminated. A compound *a′a* lava flow, fed from NE5 craters, was emplaced toward the SW of the fissure. As these vents were sealed by viscous lava flows, a quiescence period followed and renewed activity started with an explosive phase characterized by the accumulation of 'bread crust' bombs (0.5–1.0 m diameter) around the Gris and El Azufral craters, apparently the only active ones during this latest phase. Ballistic ejecta cover a coarse lapilli pumice-fall deposit that represents the proximal facies of an eruptive column during the last phase, which ended on July 22nd after 2 months of activity.

5. Morphometric analysis

To better understand the structural conditions during each eruptive cycle, we measured such morphometric parameters as vent alignments, elongation axes of pyroclastic cones and craters, cone breaching or collapse directions (Fig. 4) and then, we interpreted them within the context of existing analogue models (e.g.,Tibaldi, 1995).

The alignment of the major craters along the N135° direction arises as a first order feature. All vents lie on a ridge which flanks slope 40–50° southwest and 10–20° northeast, the axis of which parallels the alignments of larger emission centres and postglacial rhyolitic domes. The elongation of Gris pumice cone is parallel to the main direction (135°) and the crater elongation of major vents (Gris and El Azufral), as well as their internal depressions, is parallel to both the main N135° and the secondary N160–165° directions. All the emission centres without open craters are

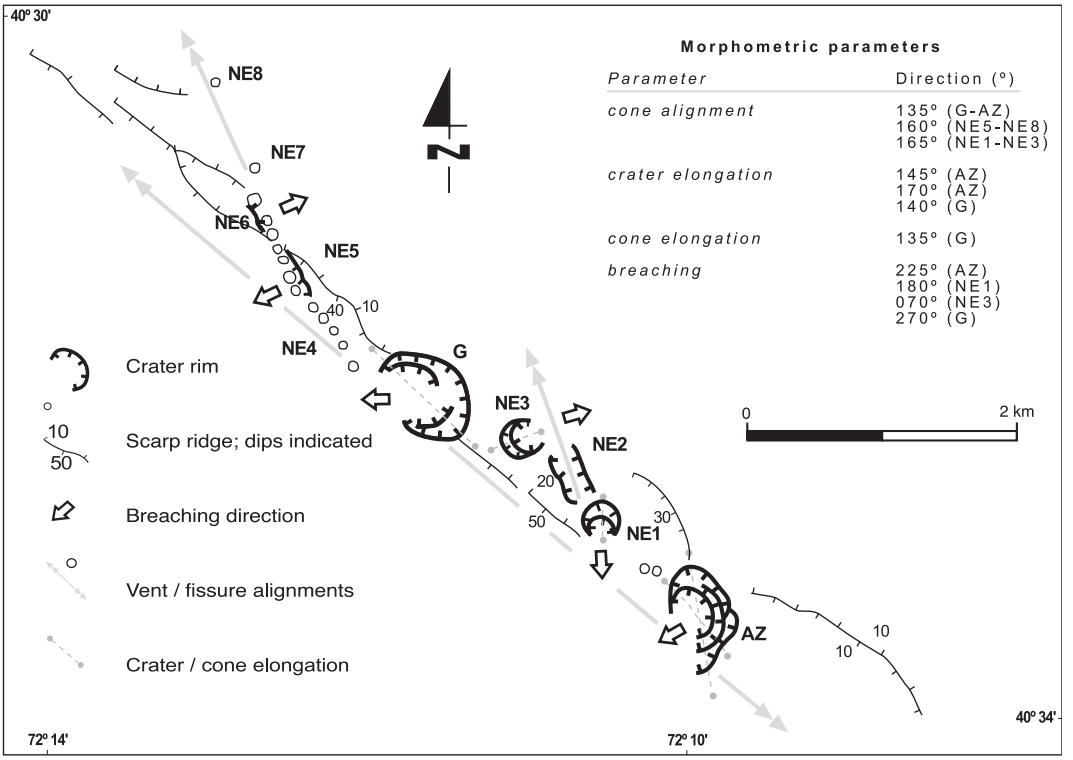

Fig. 4. Geomorphologic map of 1960 fissure in the CCVC and attached values for morphometric parameters. Key as Fig. 2.

aligned in N160–165° direction (Fig. 2). The breaching directions are usually orthogonal to the vent alignments and to the elongation of the corresponding craters. Those located on the main N135° alignment are open toward the south or southwest. The main exception is the Gris crater, the opening of which is toward the west. However, the centres located in N160–165° alignments, on the internal flank of the ridge (NE2; NE4), are open toward the northeast or constitute only fissures without individual craters.

6. Structural analysis

In the absence of data gathered from direct instrumental monitoring, we used the morphologic characteristics of the vents to rebuild the structural conditions during the eruptive cycle. Traditionally, authors such as Nakamura (1977) have considered that the alignment of volcanic centres to be parallel to the maximum horizontal stress (σ_{hmax}). Assuming that the volcanic centres are the surface expression of near vertical feeder dikes, the $\sigma 3$ (minimum stress axis) should be horizontal (and perpendicular to the dikes) with σ_{hmax} corresponding to $\sigma 1$ or $\sigma 2$ (Emmerman and Marrett, 1990). If σ_{hmax} corresponds to $\sigma 2$, the arc tectonics is extensional; if σ_{hmax} corresponds to $\sigma 1$ (with $\sigma 3$ lying on the horizontal plane), the arc tectonics is strike-slip. The focal mechanism deduced by Cifuentes (1989) for 1960 thrust earthquake (Fig. 1) and the related coseismic deformation (Plafker and Savage, 1970) suggests that $\sigma 3$ was E–W, and therefore, σ_{hmax} would have been NS. If σ_{hmax} corresponds to $\sigma 2$ or $\sigma 1$ is hard to constrain. Nevertheless, the small amount of shortening near the N–S direction recorded in the geodetic network after the 1960 earthquake (Plafker and Savage, 1970), the absence of N–S normal faults at the first eruptive stage and the parallel array of secondary fissures suggest a horizontal N–S $\sigma 1$ and then, a strike-slip stress regime. The latter is different to the widespread Quaternary transpressional setting of the entire volcanic arc described by Lavenu and Cembrano (1999) for Southern Andes.

On the other hand, recent works show that volcanic alignment parallel to σ_{hmax} is only the simplest scenario, applicable primarily to isotropic materials showing, for example, good correlations in flank cones on stratovolcanoes (e.g., Delaney et al., 1986; Emmerman and Marrett, 1990; Lister and Kerr, 1991; Glazner et al., 1999). Nevertheless, ancient faults could act as ascent pathways for magmas modifying the geometry of volcanic alignments and their morphological features. The faults related to volcanic vents are commonly blind but analogue models developed by Tibaldi (1995) show good empirical correlation between several morphologic parameters of the cones and craters (alignment, breaching directions, elongation of crater and cone base) and the geometry of the underlying fault plane. This relationship is stronger if the elongation of craters is considered, together with the ellipticity of the cone bases and of the nested craters. The relationship is less evident with respect to the displacement of the faults or the stress regime (Tibaldi, 1995) although there is a good correspondence of normal faults to perpendicular breaching directions of the cones and strike-slip faults to parallel breaching directions. Then, vent morphometry is not enough to interpret the state of stress of a region, but it provides some insight into it in absence of direct measures. Applying Tibaldi's results, we can assume that the 1960 fissure eruption was controlled by a structure composed of two subvertical bent segments in which concavity to the northeast suggests a slight northeast dipping geometry. In addition, some breaching directions oblique to the fissure could be related to an early shear-extensional condition (oblique opening) at the first eruptive stage while they suggest almost pure extensional behaviour (orthogonal opening) at the final effusive phase. The breaching direction of the Gris crater, the first active one and the largest of the entire eruption, may indicate the sense of the oblique displacement at the early stage of the eruptive cycle (Fig. 4). In addition, on the near N160–165° segments (stage 3), small normal fault scarps can be observed. Then, we can assume that, despite the topographic conditions, the geomorphological criteria provide some partial information about the coeval state of stress. In the CCVC, the main 1960 crater alignment (N135°) is parallel to a chain of postglacial domes so that the prior topography was constrained by the position of their feeder dikes and the overall Holocene vents lie on the western scarp of the graben which coincides with the trace of a regional fault (Río Iculpe fault). Thus, from the geodetic data and the strain model of

Barrientos (1994) together with the morphometric analysis, we can assume that the underlying fault was an ancient reactivated structure, at least at the first eruptive stage. For proposing a dynamical model, we appeal to some concepts derived from the theory of fractures and hydraulic fracturing. If the propagation of strain from the coastal zone toward the interior of the continent during the earthquake actually occurred as Barrientos (1994) calculated (Fig. 5), then the CCVC area was affected by an E–W extension with small N–S contraction defining a strike-slip regime, as it was stated before. Then, the instantaneous stress axis would be E–W ($\sigma 3$) and N–S ($\sigma 1=\sigma_{hmax}$).

Following the simple model proposed by Byerlee (1978) and Sibson (1985), improved after by Ivins et al. (1990), Yin and Ranalli (1992), Huyghe and Mugnier (1992) and Morris et al. (1996), an oblique NW structure (N135°) is moderately well oriented for a reactivation with an angle of $\theta r=45°$ from $\sigma 1$. This conclusion is confirmed by a quantitative analysis made throughout a software developed by Tolson et al. (2001) that considers other physical conditions for reactivation. The optimal angle of reactivation (angle between the maximum stress axis and the fault plane) is $\theta r=26.5°$ for a coefficient of static friction $\mu=0.75$ (Fig. 6a; Sibson, 1985). We stated for the 1960 earthquake that in the horizontal

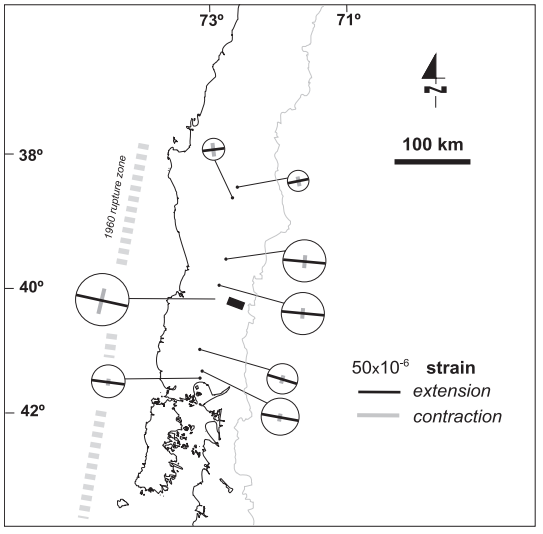

Fig. 5. Deviatoric strains for coseismic deformation calculated by Plafker and Savage (1970) from a geodetic triangulation along the Central Valley of Chile, in front of the rupture zone of 1960 earthquake. Circles are proportional to the amount of extension (adimensional scale bar for 5×10^{-6} strain for reference); orthogonal contraction at the same scale.

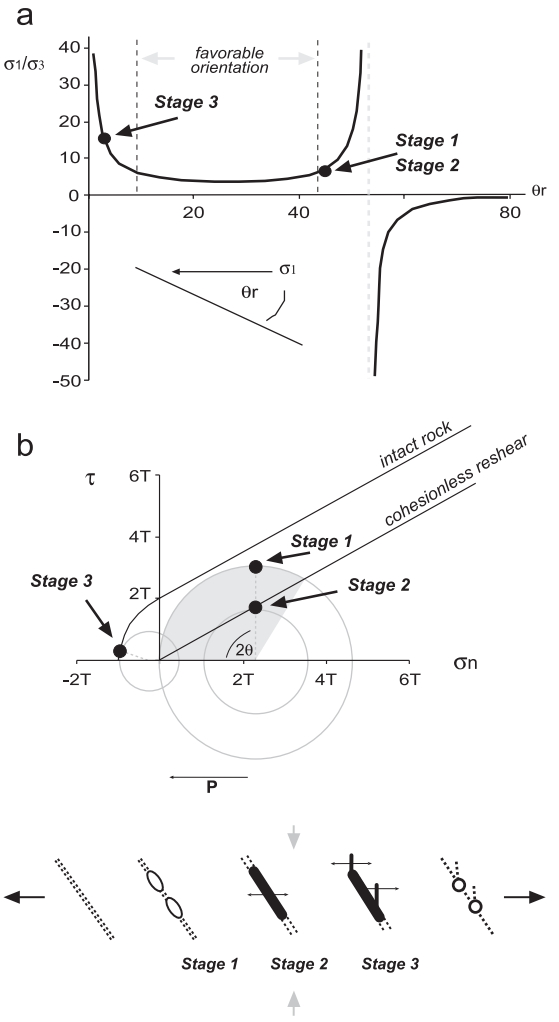

Fig. 6. (a) Effective stress diagram (modified from Sibson, 1985) showing the way of eruptive cycle and the structural conditions from reshear (stage 1 to stage 3). (b) Mohr diagram (shear stress [τ] against effective normal stress [σ_n] normalized to tensile strength [T]) with composite failure envelope for intact rock, reshear condition (Sibson, 1985) for a cohesionless fault and possible macroscopic modes of brittle failure at stage 1, stage 2 (shear-extensional; oblique opening) and stage 3 (extensional-shear, orthogonal opening). Decreasing and increasing effect of fluid (magma) pressure is indicated. Stage 1 correspond to a critical condition but dashed line circle shows a more general scenario for the first stage where all planes between 0 and 2θ (grey shaded) could be reactivated. Sketch below shows the evolution of the fissure (see text for details). Black arrows indicate ongoing tension ($\sigma 3$) and grey arrows correspond to compression ($\sigma 1$) according to geodetic data (Plafker and Savage, 1970).

plane, $\sigma 1=\sigma_{hmax}$ is N–S and $\sigma 3$ is E–W. In the case of 1960 eruption, the condition of reactivation would be reached with a ratio of effective stress of $\sigma 1'/\sigma 3'$ near 7 (with $\sigma 1'=\sigma 1-P$; $\sigma 3'=\sigma 3-P$ with P being the fluid pressure and $\mu=0.75$) (Fig. 6b). This condition can be reached more easily with small values for the coefficient of static friction and the presence of a fluid pressure, a typical feature in an active geothermal field. Other physical conditions, as the depth, were considered by Tolson et al. (2001). Then, assuming a linear relationship between stress and strain, we can obtain a maximum value for $\sigma 3$ of -4 MPa if we consider a 40×10^{-6} strain as Barrientos (1994) calculated and a Young modulus of 1×10^{10} Pa (Turcotte and Schubert, 1982). Barrientos (1994) only considered the main contribution of displacement in E–W direction over the thrust plane for the strain propagation. Nevertheless, the weak N–S compressive stress increases the dextral shear component over the NW fault. Fig. 6b shows a major Mohr's circle that does not reach the Navier–Coulomb envelope for fracture intact rocks. For this non-optimum state of stress, faults with $0<\theta r<60^\circ$ ($0<2\theta r<120^\circ$) could be reactivated depending of their cohesion. At the second eruptive stage, the stress drop and the magma injection along the fault plane would favour the condition for extensional-shear allowing magma drainage to the surface. The arrest of the dyke could increase the fluid pressure favouring new, near pure extensional hydraulic fractures. The dynamic solution would be, initially (stage 1), the reactivation of a NW fault as a dextral shear-extensional failure. However, once the magma occupies the fissure and the explosive phase of the eruptive cycle begins, the pressure drops allowing effusive magma drainage (stage 2) and after a quiescence period, the conditions would vary until they allow the generation of a new, near pure extensional failure, this time near parallel to the σ_{hmax} of NS direction as an hydraulic (magma) fracture (Stage 3; Fig. 6b).

7. Discussion

An instrumental analysis of the instantaneous coeval deformation during an eruptive cycle is the only way to directly constrain the feasibility of the morphologic and structural analysis commented herein. Therefore, our analysis is based on inferences and the argumentative line is robust but speculative. On the other hand, the studied event represents a unique case in the geodynamic context of the SSAVZ (37–46°S) of the Andes and the kinematics considerations cannot extend to the 'normal' state of the volcanic arc. In fact, the microtectonic analysis (*striae*) of mesoscopic structures and focal mechanism of crustal earthquakes suggests opposite conditions of strain (dextral N–S transpression in the volcanic arc as a whole, with dextral strike-slip in the Liquiñe–Ofqui Fault and sinistral strike-slip in NW structures (e.g., Assumpçao, 1992; Lavenu and Cembrano, 1999), that would have been reversed during the 1960 earthquake.

7.1. 1921–1922 eruption

A point of additional conflict is indicated by the December 1921–February 1922 fissure eruption. That eruption also produced rhyodacitic lava flows (68–71% SiO_2) with vents aligned on a NW fissure joined with the ring faults inside the Cordillera Nevada caldera. Nevertheless, in December 1921, there was no record of any noticeable earthquake in the region and that eruption should be assumed as an event that took place during the 'normal' stress regime of the volcanic arc. However, the expected extensional fractures in the dextral–transpressional regime must be in NE direction. Then, local deviations of a complex stress field or a fluid pressure-controlled behaviour of the magma ascent giving a non-Andersonian setting can be assumed as well. So, as in other natural phenomena, similar effects can be obtained from different causes.

7.2. '*Valve*' *faults and seismic pumping*

The application of the reshear criterion of Byerlee (1978) and Sibson (1985) raises additional questions. For example, the coseismic deformation during the 1960 earthquake found other volcanic alignments that had an equivalent orientation ($\theta r=45^\circ$) to the reshear criterion. In fact, NE–SW-oriented structures that align the monogenic cones at Carrán–Los Venados (40°S) or Antillanca (41°S) groups are located only about 10 km north and south of the CCVC,

respectively. In an even more favourable orientation for reactivation would be the Liquiñe–Ofqui Fault, which parallels the Chile–Peru trench and the expected maximum horizontal stress. Nevertheless, both types of structures did not demonstrate reactivation during the 1960 event. We suppose then that these faults were sealed and would act like 'valves' (Sibson et al., 1988) by dynamic loading during other types of seismic events such as those that characterise the current stress field as a dextral transpressional regime (e.g., Chinn and Isacks, 1983; Barrientos and Acevedo, 1992). So, we propose that the NW–SE fault systems, where the CCVC is located, are regionally favourable to steady-state magma transport, storage and their subsequent differentiation, an idea enunciated before in other terms by Cembrano and Moreno (1994). Thus, the magma is maintained in the upper crust levels, where the faults could act as 'pumps' (Sibson et al., 1988) during seismic events. In that way, the upper level processes (fractional crystallization; hydrothermalism) would increase the fluid pressure near the structure facilitating its reactivation and the renewal of the magma ascent.

7.3. Remote seismic triggering of seismicity and volcanism

The relationship between distant earthquakes, remote remote seismicity and volcanic eruptions has been analysed from different perspectives. From a statistical approach, Blot (1965), Acharya (1982) and Linde and Sacks (1998) studied data collections of major subduction (thrust) earthquakes and volcanic eruptions with contradictory results. Despite the biased sample method, Blot (1965) and Acharya (1982) conclude an unidirectional relation from big eruptions to earthquakes. On the other hand, Linde and Sacks (1998) proposed a causal relationship between Mw>7 earthquakes and eruptions in a radius of 250 km from the seismic source based on a bubble rising model for propagation of dynamic stress. Nevertheless, these authors neglect the pair earthquake-eruption discussed herein, maybe the clearest example of a causal relation between this type of events. A more complete revision of earthquake interactions was published in a special issue of the Journal of Geophysical Research (Stress triggers, stress shadows, and implications for seismic hazard, 1998, V.101, No.B10). There, several papers (e.g., Harris, 1998; Toda et al., 1998; Harris and Simpson, 1998; Nostro et al., 1998) demonstrate Coulomb stress change and other methods for a calculation of dynamic and static stress over active fault as consequence of an earthquake. Although we do not have any seismic parameter of the shear-extensional or extensional faults in the CCVC eruption, the strong spatial and time relationship between the thrust earthquake and the fissure eruption can be analysed as a consequence of dynamic stress propagation. Dynamic strain could be translated to static strain, at local scale, by rectified diffusion (Brodsky et al., 1998) increasing magma pressure that allows reshearing of an ancient fault. In this conceptual framework, the brittle failure theory helps to understand the geometry and evolution of this special but unknown fissure eruptive event.

8. Conclusions

Almost 2 days after the largest instrumentally recorded earthquake registered in the world, in May 1960, a noticeable fissure eruption of rhyodacitic magma took place in the CCVC, ca. 240 km to the east of the rupture zone. The dynamic stress and the general extension propagated toward the continent as a result of the thrust in the subduction zone would have favoured the structural conditions for the evacuation of magma stored in a shallow reservoir. The presence of remarkable NW structures, oblique to the margin, which is typical of the SAVZ and particularly of the CCVC, necessarily forces one to look for a mechanism to explain their reactivation as a response of the whole structural system. In addition, in 1960, new structures were not generated in other places of the volcanic arc, according to the direction of the E–W extension inferred from the geodetic record. Besides, in the CCVC, the fluid pressure increased by the presence of silicic magma near the surface would have facilitated the reactivation of the NW structure, moderately well oriented for the displacement. Hence, the eruptive cycle would have begun by 'seismic pumping' of magma after a dextral shear-extensional displacement of the NW structure as a consequence of a strike-slip regime. After the blockage of first displacement (E–W opening), the

deformation continued with the opening of NNW near pure extensional failure, this time nearly parallel to the expected maximum horizontal stress as hydraulic fractures. Although the lack of instrumental record precludes possibilities to verify the inferences presented herein, the morphometric, structural and volcanological analysis allows reconstruction of the most likely prevailing structural condition during the 1960 fissure eruption. The causal relationship described, although exceptional in the geodynamic evolution of the western South American margin, indicates the relevance of peculiar episodes in the construction of the geologic record.

Acknowledgements

This work is part of a research of the first author on the relationship between volcanism and tectonics in the Southern Andes, a collaborative project of SERNAGEOMIN (Chile) and IRD-Université Paul Sabatier (France). Fieldwork has been supported by Fondecyt 1960885 (HM, LL) grant. Stratigraphic data of the 1960 tephra-fall have been also obtained through Fondecyt 1960186 (JN, HM, LL) grant. The authors are grateful to R. Scandone, P. Segall, and D. Hill for their critical revision of an early version. M. Neri, E. Parfitt and specially S. Alaniz-Alvarez are kindly acknowledged as reviewers. This work is a contribution to the Volcanic Hazards Project of SERNAGEOMIN (Chile).

References

Acharya, H., 1982. Volcanic activity and large earthquakes. J. Volcanol. Geotherm. Res. 86, 335–344.

Alaniz-Alvarez, S., Nieto-Samaniego, A., Ferrari, L., 1998. Effect of strain rate in the distribution of monogenetic and polygenetic volcanism in the Transmexican volcanic belt. Geology 26, 591–594.

Anderson, E.M., 1951. The Dynamics of Faulting, 2nd ed. Oliver and Boyd, pp. 1–191.

Assumpçao, M., 1992. The regional intraplate stress field in South America. J. Geophys. Res. 97, 11,889–11,903.

Bahar, I., Girod, M., 1983. Controle structural du volcanisme indonesien (Sumatra, Java–Bali); application et critique de la methode de Nakamura. Bull. Soc. Geol. Fr. 7, 609–614.

Barrientos, S., 1994. Large thrust earthquakes and volcanic eruptions. Pure Appl. Geophys. 142, 225–237.

Barrientos, S., Acevedo, P., 1992. Seismological aspects of the 1988–1989 Lonqimay (Chile) volcanic eruption. J. Volcanol. Geotherm. Res. 53, 73–87.

Barrientos, S., Ward, S.N., 1990. The 1960 Chile earthquake: coseismic slip from surface deformation. Geophys. J. Int. 103, 589–598.

Bellier, O., Sébrier, M., 1994. Relationship between tectonism and volcanism along the Great Sumatran Fault deduced by SPOT image analyses. Tectonophysics 233, 215–231.

Berninghausen, W.H., 1962. Tsunamis reported from the west coast of South America. Seismol. Soc. Am., Bull. 52, 915–921.

Blot, C., 1965. Relation entre les séismes profonds et les éruptions volcaniques au Japon. Bull. Volcanol. 28, 25–64.

Brodsky, E.E., Sturtevant, B., Kanamori, H., 1998. Earthquakes, volcanoes, and rectified diffusion. J. Geophys. Res. 103, 23827–23838.

Byerlee, J.D., 1978. Friction of rocks. Pure Appl. Geophys. 116, 615–626;
Byerlee, J.D., 1978. Friction of rocks. J. Geophys. Res. 103, 23,827–23,838.

Campos, A., Moreno, H., Muñoz, J., Antinao, J., Clayton, J., y Martin, M., 1998. Area de Futrono-Lago Ranco, Región de los Lagos. Servicio Nacional de Geología y Minería, Mapas Geológicos No. 8, 1 mapa escala 1:100.000. Santiago.

Casertano, L., 1962. Sui fenomini sismo-vulcanici del Sud del Chile. Annali Osservatorio Vesuviano 4 (serie 6) Nápoles.

Cembrano, J., Moreno, H., 1994. Geometría y naturaleza contrastante del volcanismo cuaternario entre los 38°S y 46°S: Dominios compresionales y tensionales en un régimen transcurrente? Congr. Geol. Chil. Actas 1 (7), 240–244.

Cembrano, J., Hervé, F., Lavenu, A., 1996. The Liquiñe–Ofqui fault zone: a long-lived intra-arc fault system in southern Chile. Tectonophysics 259, 55–66.

Chinn, D., Isacks, B., 1983. Accurate source depths and focal mechanisms of shallow earthquakes in Western South America and the New Hebrides Island arc. Tectonics 2, 529–563.

Cifuentes, I.L., 1989. The 1960 Chilean earthquakes. J. Geophys. Res. 94, 665–680.

Delaney, P.T., Pollard, D.D., Ziony, J.I., Mckee, E.H., 1986. Field relations between dykes and joints: emplacement processes and paleostress analysis. J. Geophys. Res. 91, 4920–4938.

DeMets, C., Gordon, R., Argus, D., Stein, S., 1994. Effect of recent revisions to the geomagnetic reversal time scale on estimates of current plate motions. Geophys. Res. Lett. 21, 2191–2194.

Dhont, D., Chorowicz, J., Yürür, T., Froger, J.L., Köse, O., Gündogdu, N., 1998. Emplacement of volcanic vents and geodynamics of Central Anatolia, Turkey. J. Volcanol. Geotherm. Res. 62, 207–224.

Duda, S.J., 1963. Strain release in the circum-Pacific belt, Chile, 1960. J. Geophys. Res. 68, 5,531–5,544.

Eaton, J.P., Richter, D.H., Ault, W.U., 1961. The tsunami of May 23, 1960, on the island of Hawaii. Seismol. Soc. Am., Bull. 51, 135–157.

Emmerman, S., Marrett, R., 1990. Why dikes? Geology 18, 231–233.

Gerlach, D., Frey, F., Moreno, H., López, L., 1988. Recent

volcanism in the Puyehue–Cordón Caulle Region, Southern Andes, Chile (40.5°S): petrogenesis of evolved lavas. J. Petrol. 29, 333–382.
Glazner, A., Bartley, J., Carl, B., 1999. Oblique opening and noncoaxial emplacement of the Jurassic Independence dike swarms. J. Struct. Geol. 21, 1275–1283.
Gutenberg, B., 1956. The energy of the earthquakes. Q. J. Geol. Soc. London. 112, 1–14.
Harris, R., 1998. Introduction to special section: stress triggers, stress shadows, and implications for seismic hazard. J. Geophys. Res. 103, 24,347–24,358.
Harris, R., Simpson, R., 1998. Suppression of large earthquakes by stress shadows: a comparison of Coulomb and rate-and-state failure. J. Geophys. Res. 103, 24,439–24,451.
Hubbert, M.K., Rubey, W.W., 1959. Role of fluid pressure in the mechanics of overthrust faulting. Geol. Soc. Am. Bull. 70, 115–205.
Huyghe, P., Mugnier, J.L., 1992. The influence of the depth on reactivation in normal faulting. J. Struct. Geol. 14, 991–998.
Ivins, E.R., Dixon, T.H., Golombek, M.P., 1990. Extensional reactivation of an abandoned thrust: a bound on shallowing in the brittle regime. J. Struct. Geol. 12, 303–314.
Kanamori, H., 1977. The energy release in great earthquakes. J. Geophys. Res. 82, 2981–2987.
Kanamori, H., Cipar, J.J., 1974. Focal process of the great Chilean earthquake, May 22, 1960. Phys. Earth Planet. Inter. 9, 128–136.
Katsui, J., Katz, H., 1967. Lateral fissure eruptions in the Southern Andes of Chile. Faculty of Science Series, vol. 4, pp. 433–448. Japan.
Lara, L., Rodriguez, C., Moreno, H., Pérez de Arce, C., 2001. Geocronología K–Ar y geoquímica del volcanismo plioceno superior-pleistoceno de los Andes del Sur (39°–42°S). Rev. Geol. Chile 28, 67–90.
Lara, L.E., Matthews, S., Pérez de Arce, C., Moreno, H., 2003. Evolución morfoestructural del Complejo Volcánico Cordón Caulle (40°S): evidencias geocronlógicas $^{40}Ar/^{39}Ar$. Congreso Geológico Chileno, vol. 10. Actas, Concepción.
Lavenu, A., Cembrano, J., 1999. Compressional and traspressional-stress pattern for Pliocene and Quaternary brittle deformation in fore arc and intra-arc zones (Andes of Central and Southern Chile). J. Struct. Geol. 21, 1669–1691.
Linde, A.T., Sacks, I.S., 1998. Triggering of volcanic eruptions. Nature 395, 888–890.
Lister, J.R., Kerr, R.C., 1991. Fluid-mechanical models of crack propagation and their application to magma transport in dikes. J. Geophys. Res. 96, 10,049–10,077.
Moreno, H., 1977. Geología del área volcánica Puyehue-Carrán en los Andes del sur de Chile. Memoria para optar al título de geólogo. Departamento de Geología, Universidad de Chile.
Morris, A., Ferril, D.A., Hendeson, D.B., 1996. Slip-tendency análisis and fault reactivation. Geology 24, 275–278.
Nakamura, K., 1977. Volcanoes as possible indicators of tectonic stress orientation: principle and proposal. J. Volcanol. Geotherm. Res. 2, 1–16.
Nostro, C., Ross, S., Cocco, M., Belardinelli, M.E., Marzochi, W., 1998. Two-way coupling between Vesuvius eruptions and southern Apennine earthquakes, Italy, by elastic stress transfer. J. Geophys. Res. 103, 24,439–24,451.
Peña, P., Fuentealba, G., 2000. Antecedentes preliminares de sismicidad asociada al complejo volcánico activo Cordón Caulle, Andes del Sur (40,5°S). Congreso Geológico Chileno, vol. 9, pp. 52–53. Actas 2.
Plafker, G., Savage, J.C., 1970. Mechanism of Chilean earthquakes of May 21 and May 22, 1960. Geol. Soc. Am. Bull. 81, 1001–1030.
Saint Amand, P., 1961. Los Terremotos de Mayo-Chile 1960, an eyewitness account of the greatest natural catastrophe in recent history. U.S. Naval Ordinance Test Station, Technical article 14, 39 p. China Lake.
Sibson, R., 1985. A note on fault reactivation. J. Struct. Geol. 7, 751–754.
Sibson, R., 1987. Earthquake rupturing as a mineralizing agent in hydrothermal systems. Geology 15, 701–704.
Sibson, R., 1996. Structural permeability of fluid-driven fault-fracture meshes. J. Struct. Geol. 18, 1031–1042.
Sibson, R., 2000. A brittle failure mode plot defining conditions for high-flux flow. Econ. Geol. 95, 41–48.
Sibson, R., Robert, F., Poulsen, K.H., 1988. High-angle reverse faults, fluid-pressure cycling, and mesothermal gold–quartz deposits. Geology 16, 551–555.
Sievers, H., Villegas, G., Barros, G., 1963. The seismic sea wave of 22 May 1960 along Chilean Coast. Seismol. Soc. Am., Bull., 1125–1190.
Smylie, D.E., Mansinha, L., 1968. Earthquakes and the observed motion of rotation pole. J. Geophys. Res. 73, 7,661–7,663.
Takada, A., 1994. The influence of regional stress and magmatic input on styles of monogenetic and polygenetic volcanism. J. Geophys. Res. 99, 13,563–13,573.
Tibaldi, A., 1995. Morphology of pyroclastic cones and tectonics. J. Geophys. Res. 100, 24,521–24,535.
Toda, S., Stein, R., Reasenberg, P., Dietrich, J., Yoshida, A., 1998. Stress transferred by 1995 Mw=6.9 Kobe, Japan shock: effect on the aftershocks and future earthquake probabilities. J. Geophys. Res. 103, 24,543–24,565.
Tolson, G., Alaniz-Alvarez, S.A., Nieto-Samaniego, A., 2001. ReActiva, a plotting program to calculate the potential of reactivation of preexisting planes of weakness. Instituto de Geología, Universidad Autónoma de México. http://geologia.igeolcu.unam.mx/Tolson/Software/ReActivaV24En.exe.
Turcotte, D., Schubert, G., 1982. Geodynamics, Application of Continuum Physics to Geological Problems. John Wiley and Sons, New York.
Veyl, C., 1960. Los fenómenos volcánicos y sísmicos de fines de Mayo de 1960 en el sur de Chile. Universidad de Concepción, Instituto Central de Química, Concepción, 42 pp.
Ward, S.N., 1984. A note on lithospheric bending calculations. Geophys. J. R. Astron. Soc. 78, 241–253.
Weischet, W., 1963. Further observations of geologic and geomorphic changes resulting from the catastrophic earthquake of May 1960, in Chile. Seismol. Soc. Am., Bull. 53, 1237–1257.
Yin, Z.M., Ranalli, G., 1992. Critical stress difference, fault orientation and slip direction in anisotropic rocks under non-Andersonian stress systems. J. Struct. Geol. 14, 237–244.

Chapitre 4
Transpression et volcanisme quaternaires: effets du champ de contrainte local

Chapitre 4. Transpression et volcanisme quaternaires: effets du champ de contrainte local

4.1 Introduction

Dans le cas le plus simple d'un arc volcanique lié à une marge convergente, la déformation active serait contrôlée par l'angle de séparation entre le vecteur de convergence oblique et la normale à la fosse. Autrement dit, s'il y avait une partition complète, la situation serait bien représentée par le modèle de Dewey et Lamb (1992) qui suggère que la composante latérale soit complètement absorbée dans l'arc. Selon ce scénario, les domaines d'extension et de compression seraient ceux envisagés dans un modèle de cisaillement simple (*e.g*., Cembrano et Moreno, 1994). Si la partition n'est pas complète et si une partie du raccourcissement orthogonal à la marge est aussi transféré à l'arc, alors le modèle le plus approprié est celui de transpression (Sanderson et Marchini, 1984) comme l'ont déjà suggéré López Escobar *et al*. (1995a) pour les Andes du Sud. Un cas le plus proche de la réalité est celui où il existe une déformation triclinique (c'est-à-dire, la déformation n'est pas plane mais présente une composante verticale) et qui est analysé dans la section suivant. Une complication additionnelle est celle qui introduit la nature fracturée de la croûte supérieure et qui détermine la réactivation de structures préalables en induisant une rotation du champ de contraintes régional. Dans l'article de Lara *et al*. (2006a) on analyse comment la distribution des centres éruptifs est contrôlée et déterminée, finalement, par le champ de contrainte local.

L'existence des tenseurs de contrainte compressifs (σ_3 vertical avec σ_1 d'orientation NE-SW comme reconnu dans les ellipsoïdes de transpression) et certaines caractéristiques morphologiques du relief de premier ordre témoignent d'importants déplacements verticaux, on suggère que la déformation soit triclinique et qu'il existerait un transport de masse vertical. Comme l'ont démontré des auteurs précédents par de traces de fission sur zircons et apatites du Batholite Nord

Patagonien (*e.g*., Thomson, 2002; Adriasola *et al*., 2005), ce transport vertical s'est effectué principalement à l'occasion des failles les plus grandes de l'arc magmatique (ZFLO). Au moins une fraction du soulèvement et l'exhumation totale peuvent s'être produits pendant le Quaternaire. Toutefois, ce soulèvement n'est pas associé strictement ou exclusivement au régime de transpression. En effet, comme suggèrent Thomson (2002) et Seifert *et al*. (2005), une partie de ce soulèvement a été provoquée par des facteurs climatiques, particulièrement induits par l'érosion glaciaire intense qui a accompagné la Grande Glaciation de la Patagonie durant le Pliocène (*e.g*. Singer *et al*., 2004) et les quatre suivantes du Pléistocène (e.g. Clapperton, 1993; Lowell *et al*., 1995). Additionnellement, le rebond isostatique attendu comme ajustement à la disparition rapide d'un important volume de glace apparaît aussi comme un facteur à considérer. Dans ce chapitre l'article de Lara *et al*. (soumis) on analyse le régime de contraintes pendant l'Holocène à partir de l'analyse microtectonique et de la morphométrie des centres volcaniques et on discute le cas des cônes monogéniques construits sur la ZFLO. On conclut que les magmas émis par ces cônes, et dont la pétrogenèse indique une contribution d'éléments de la zone de subduction peu importante, sont produits par décompression adiabatique. Cette décompression serait adéquatement expliquée par des mouvements sporadiques de la ZFLO comme ceux qui seraient associés aux déplacements verticaux du socle. Ces épisodes coexistent pendant l'Holocène avec ceux mieux expliqués par la transpression de l'arc en suggérant des ajustements temporaires de la ZFLO en marge du cycle transpressif. De cette manière, l'architecture finale de l'arc volcanique résulte de la conjonction de facteurs tectoniques et climatiques qui opèrent de manière diverse en temps et un espace bien définis.

4.2 Contrôle structural du volcanisme dans les chaînes obliques : failles réactivées et néotectonique dans la zone de Puyehue-Cordón Caulle (40.5ºS), Andes du Sud

La nature du rapport entre la tectonique et le volcanisme dans un secteur spécifique de l'arc volcanique est le résultat de l'interaction entre les structures de la croûte supérieure et le champ de contrainte régional actif. Dans les Andes du sud,

les différents environnements cinématiques représentés par deux systèmes de fissures volcaniques, actifs et presque orthogonaux, montrent des alignements de directions apparemment incompatibles. D'ailleurs, un régime compressif quaternaire local est compatible avec des failles du substratum. Cependant, ces chaînes, orthogonales l'une à l'autre et qui sont également obliques à la direction du front volcanique, ont une évolution magmatique et des styles éruptifs différents qui peuvent être reliés à leur arrangement tectonique. Considérant que des cônes monogéniques holocènes de direction approximative NE-SW (Carrán-Los Venados) peuvent être interprétés comme le lieu de l'ascension magmatique liée au régime de tension régionale dans un domaine transpressif/compressif, le système de fissures NW-SE (Complexe Volcanique de Puyehue-Cordón Caulle) peut être le résultat de la réactivation de failles et de la longue résidence de magma dans la croûte supérieure. Les différents environnements cinématiques sont la cause de l'évolution magmatique contrastée et des différents styles éruptifs. Un mécanisme bi-directionnel de couplage est suggéré pour expliquer la déviation locale du champ de contraintes régional, de la géométrie des dispositifs d'extension et de l'évolution magmatique dans ces domaines volcaniques des Andes méridionales.

Available online at www.sciencedirect.com
ScienceDirect
Journal of Volcanology and Geothermal Research 158 (2006) 70–86
Journal of volcanology and geothermal research
www.elsevier.com/locate/jvolgeores

Structural controls of volcanism in transversal chains: Resheared faults and neotectonics in the Cordón Caulle–Puyehue area (40.5°S), Southern Andes

Luis E. Lara [a,b,*], Alain Lavenu [b], José Cembrano [c], Carolina Rodríguez [d]

[a] Servicio Nacional de Geología y Minería. Av. Santa María 0104, Providencia, Santiago, Chile
[b] IRD-LMTG, Laboratoire de Mecanismes de Transferts en Géologie-Université Paul Sabatier-Toulouse III. 14 Avenue Edouard Belin, 31400 Toulouse, France
[c] Universidad Católica del Norte. Chile. Angamos 0610, Antofagasta, Chile
[d] Université de Genève, Département de Minéralogie. Rue des Maraîchers 13, CH 1205 Genève, Switzerland

Received 25 February 2005; accepted 10 April 2006
Available online 7 July 2006

Abstract

The nature of the relationship between tectonics and volcanism in a specific area is the result of the interaction between the crustal structures of the basement and ongoing regional stress field. In the Southern Andes, different kinematic environments represented by two nearly orthogonal active fissure systems show apparently incompatible arrays of volcanic chains. Moreover, a local Quaternary compressive regime is inferred from basement faults. However, these mutually orthogonal chains, which are also oblique to the volcanic front, have contrasting magma evolution and eruptive styles that can be related with their tectonic setting. Whereas northeast-trending monogenetic cones (Carrán–Los Venados) can be interpreted as resulting from magma upwelling along regional tension cracks in a Quaternary dextral transpressive/compressive domain, northwest-striking fissure system (Cordón Caulle Volcanic Complex) can be the result of extensional fault reactivation and long magma residence in the upper crust. Different kinematic environments cause contrasting magma evolution and eruptive styles. A two-way coupling mechanism is suggested for to explain local depart of the regional stress field, geometric array of extensional features, and final magmatic evolution in these volcanic domains of the Southern Andes.

Keywords: basement tectonics; resheared faults; local stress fields

1. Introduction

The causal relationship between volcanism and tectonics is a key topic in the overall tectonic settings. The early recognition of close spatial association between faults and volcanic centres has led to the construction of models that try to explain the pattern of regional deformation as well as the distribution, evolution and morphostructure of the volcanic centres in different geodynamic frameworks (e.g., Takada, 1994; Bellier and Sébrier, 1994; Dhont et al., 1998). At convergent margins with oblique subduction, transversal volcanic chains are believed to describe different structural domains controlled by the plate boundary-

* Corresponding author. Servicio Nacional de Geología y Minería. Av. Santa María 0104, Providencia, Santiago, Chile.
E-mail address: lelara@sernageomin.cl (L.E. Lara).

0377-0273/$ - see front matter © 2006 Elsevier B.V. All rights reserved.
doi:10.1016/j.jvolgeores.2006.04.017

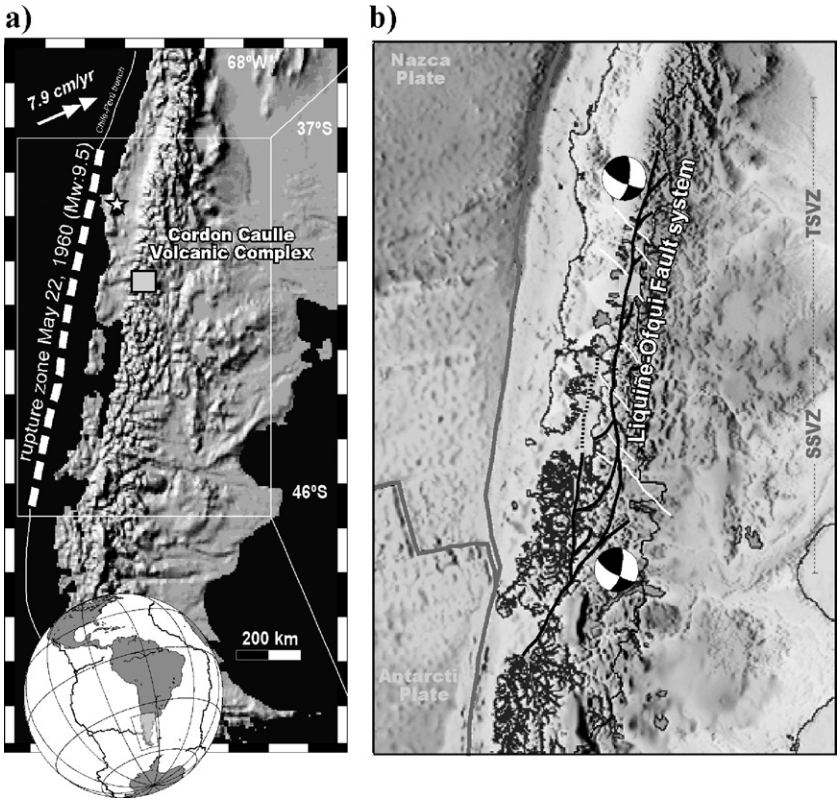

Fig. 1. (a) Shaded relief of South America. White box shows the Cordón Caulle Volcanic Complex (CCVC) and monogenetic fields in the surrounding area. Current subduction vector after DeMets et al. (1994). Rupture zone of 1960 earthquake after Plafker and Savage (1970) and relocated epicentre (star) are shown (Cifuentes, 1989). (b) Detail with Liquiñe–Ofqui Fault system after Cembrano et al. (2000). CSVZ: Central Southern Volcanic Zone; SSVZ: South Southern Volcanic Zone; are volcanic provinces as defined by López-Escobar et al., 1995).

scale stress field (e.g., Nakamura, 1977; Nakamura and Uyeda, 1980; Zoback and Zoback, 1980). However, continental margins with long-lived subduction processes show first and second-order tectonic features, most of them inherited, that control volcanism without a simple relation with the ongoing stress field. The Southern Andes are a special example of volcanic chains aligned at least in three different directions (north–south, northeast and northwest) with close spatial association with ancient and Quaternary fault systems (Fig. 1). Quaternary dextral transpression has been inferred for the arc domain from microtectonic data (Lavenu and Cembrano, 1999), compatible with earthquake focal mechanisms along the volcanic arc (Barrientos and Acevedo, 1992) and the intraplate stress field proposed for South America (Assumpçao, 1992). These studies document a horizontal northeast-trending $\sigma 1$ (greatest principal stress). Contrasting geochemical features and eruptive styles are present in some of the three structural trends. One end-member will be the case of a northwest oblique-to-the-arc volcanic chain with long-lived evolution over an ancient fault. Another could be a newly-formed northeast tension crack. In this contribution, we address the problem of kinematic compatibility between nearly coeval extensional domains of a long-lived transpressive to compressive tectonic regime where the local stress field seems to sporadically depart of the regional pattern. Fault population analysis, pyroclastic cones morphometry and geochemical features were combined for to clarify this issue.

2. Tectonic and structural features of the Southern Andes

Inherited northwest-trending lineaments and Quaternary northeast trends define an oblique geometry that controls the first-order structural pattern of the study area, as can be observed on geological maps and specially in the magnetic structure (Fig. 2). The northwest-trending structural pattern appears to be a consequence of the geological evolution of the Southern Andes, where a long-lived subduction system added an accretionary prism and magmatic arcs to the South American (Gondwana) margin since the Upper

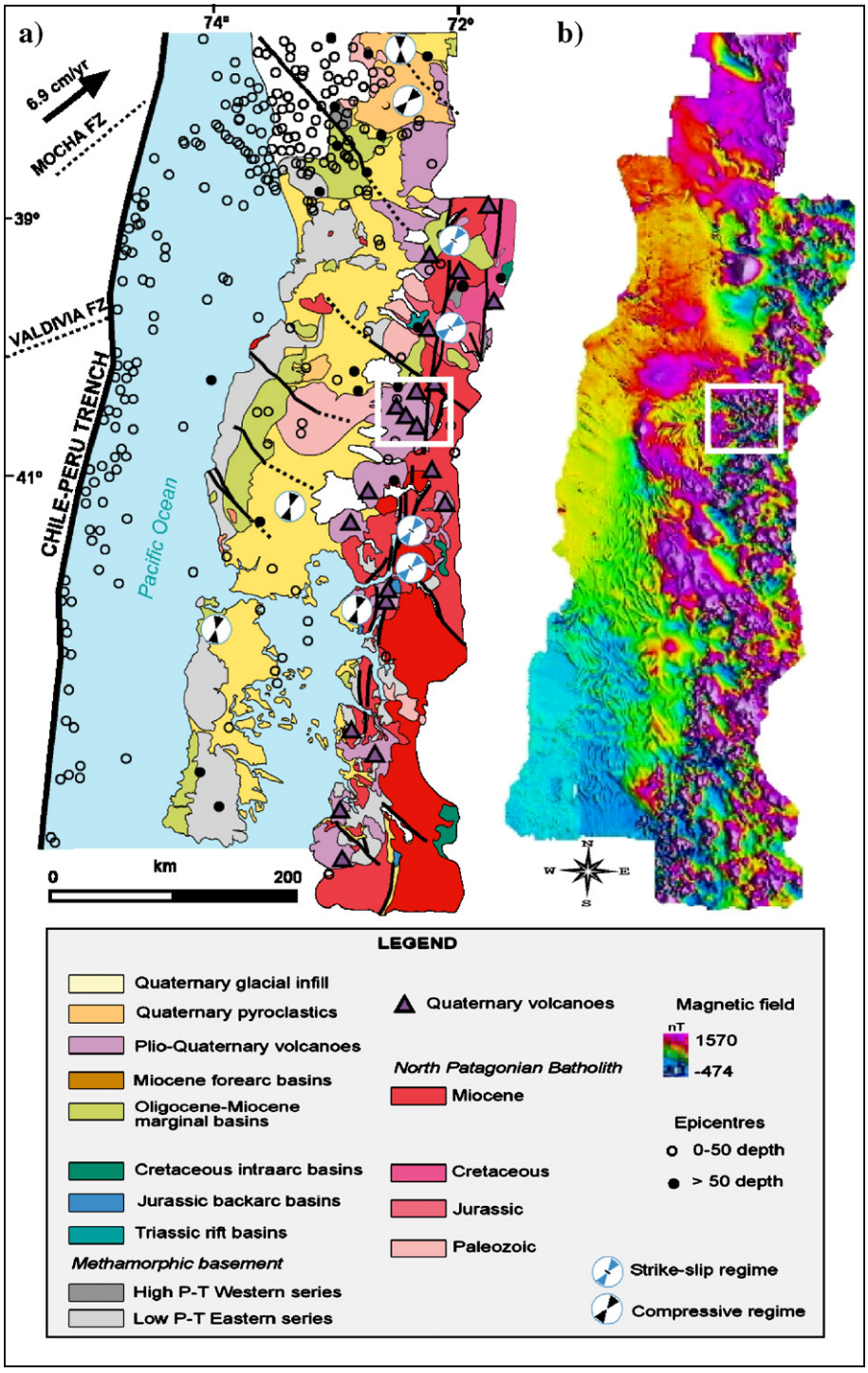

Fig. 2. (a) Geological sketch for South American margin (modified from SERNAGEOMIN, 2002 and references therein). Crustal seismicity taken from CMT Harvard catalogue. (b) Total magnetic field for the same region (taken from SERNAGEOMIN, 1998). Note the northwest–southeast first order magnetic pattern that match with the main geological boundaries from west to east.

Palaeozoic. Thus, this pattern (Fig. 2) was inherited from the pre-Andean cycle (Franzese, 1995; Martin et al., 1999) and resulted mainly from Palaeozoic and Triassic events. A Carboniferous accretionary prism intruded by Permian plutons was metamorphosed and deformed until the Triassic forming the core of the present Coastal Range and some transversal blocks, which merge with the main cordillera (e.g., Loncoche block; Chotin, 1975). In addition, a Triassic rift was developed on the western margin of Gondwana and is represented by northwest-trending magmatic belts and forearc sedimentary sequences (e.g., Rapela and Pankhurst, 1992). This geometry was subsequently resumed during the opening and inversion of the Oligocene–Miocene marginal basins (Jordan et al., 2001). Both sedimentary growth and Miocene basin inversion were controlled by margin-parallel normal and reverse faults but subbasin arrays were defined by northwest-trending structures (Jordan et al., 2001).

In turn, the Andean cycle in the Southern Andes was characterised by the establishment of margin-parallel magmatic arcs from the Early Cretaceous followed by orogenic uplift, whose main phase began in the Late Miocene. Instead, northeast-trending features are defined by Late Cenozoic, mainly Holocene, volcanic alignments. Thus, geodynamic evolution of the Southern Andes is a combined result of geological inheritance and Neogene tectonic regimes.

3. Overview of the Cordon Caulle region

In the Cordón Caulle region the main structural features recognised for the overall Southern Andes are associated with specific volcanic chains and tectonic structures. A brief description of the main geological features of them is presented in this section.

3.1. Northwest-trending volcanic chains and tectonics

3.1.1. Cordón Caulle Volcanic Complex and Iculpe River Fault

The Cordón Caulle Volcanic Complex (CCVC), located 240 km east of the Chile–Perú trench, is a transversal volcanic chain formed by a cluster of eruptive centres that extends *ca*. 15 km between the Cordillera Nevada caldera and the Puyehue stratovolcano (Fig. 3). On the northwestern end, Cordillera Nevada caldera represents a collapsed Pleistocene stratovolcano (Campos et al., 1998; Lara et al., 2001, 2003) whilst on the southeastern boundary, the Puyehue stratovolcano appears as a prominent truncated cone that has a 2.5-km-wide summit caldera. They are connected by a Pleistocene–Holocene fissure system (Cordón Caulle) whose older units crop out along the escarpment of a graben. Gravity measurements (Sepúlveda et al., 2005) suggest an extensional origin of this depression and Pritchard and Simons (2004) propose a possible ongoing subsidence. Postglacial domes, lavas and pyroclastic deposits fill this graben (Fig. 4).

^{40}Ar–^{39}Ar ages for the last 200 ka (Lara et al., 2003 and unpublished data) document a nearly coeval volcanism along several vents on the CCVC. After a generalized shield stage, CCVC evolved as both fissure and central system with active vents from Cordillera Nevada to the ancestral Puyehue volcano. The Late Pleistocene–Holocene period is characterized by an enhancement of fissure activity inside the graben and the building and erosion of the present Puyehue volcano.

The chemical composition of the CCVC products covers the wide range of Southern Andes magmas. However, while basalts and andesites predominate in the early shield stage, an unusual frequency of rhyodacitic to rhyolitic magmas (Gerlach et al., 1988) occurs in the Late Pleistocene to Holocene units of the Cordón Caulle and Puyehue volcanoes. The abundance of silica-rich types is unique among the mostly basaltic–andesitic centres along the Central Southern Volcanic Zone (CSVZ: 37°–42°S) and South Southern Volcanic Zone (SSVZ: 42°–46°S) (López-Escobar et al., 1995; Fig. 1).

The CCVC is emplaced along the Iculpe River Fault, a *ca*. 20 km long, northwest-striking structure, which is part of a conspicuous set of oblique pre-Andean faults that start in the Coastal Range and run eastward to the main cordillera. Some of these regional-scale structures are thought to have mainly left-lateral displacements along the geological history (e.g., Spalletti and Dalla Salda, 1996; Martin et al., 1999; Jordan et al., 2001; Bohm et al., 2002). In addition, a branch of the NNE-striking Liquiñe–Ofqui Fault system, the most outstanding tectonic feature of Southern Andes (Hervé, 1994; Cembrano et al., 1996) crosses the area being morphologically identified in the Contrafuerte and Nilahue river valleys (Fig. 3) and in the Anticura cones alignment. The history of this long-lived margin-parallel fault system is that of a Late Cenozoic transpressive regime in the magmatic arc domain where right-lateral and vertical displacements have been observed (Lavenu and Cembrano, 1999; Cembrano et al., 2002).

3.2. Northeast-trending volcanic chains

3.2.1. Carrán–Los Venados pyroclastic cones

The Carrán–Los Venados group is a cluster of 60 minor eruptive centres that form a northeast-trending

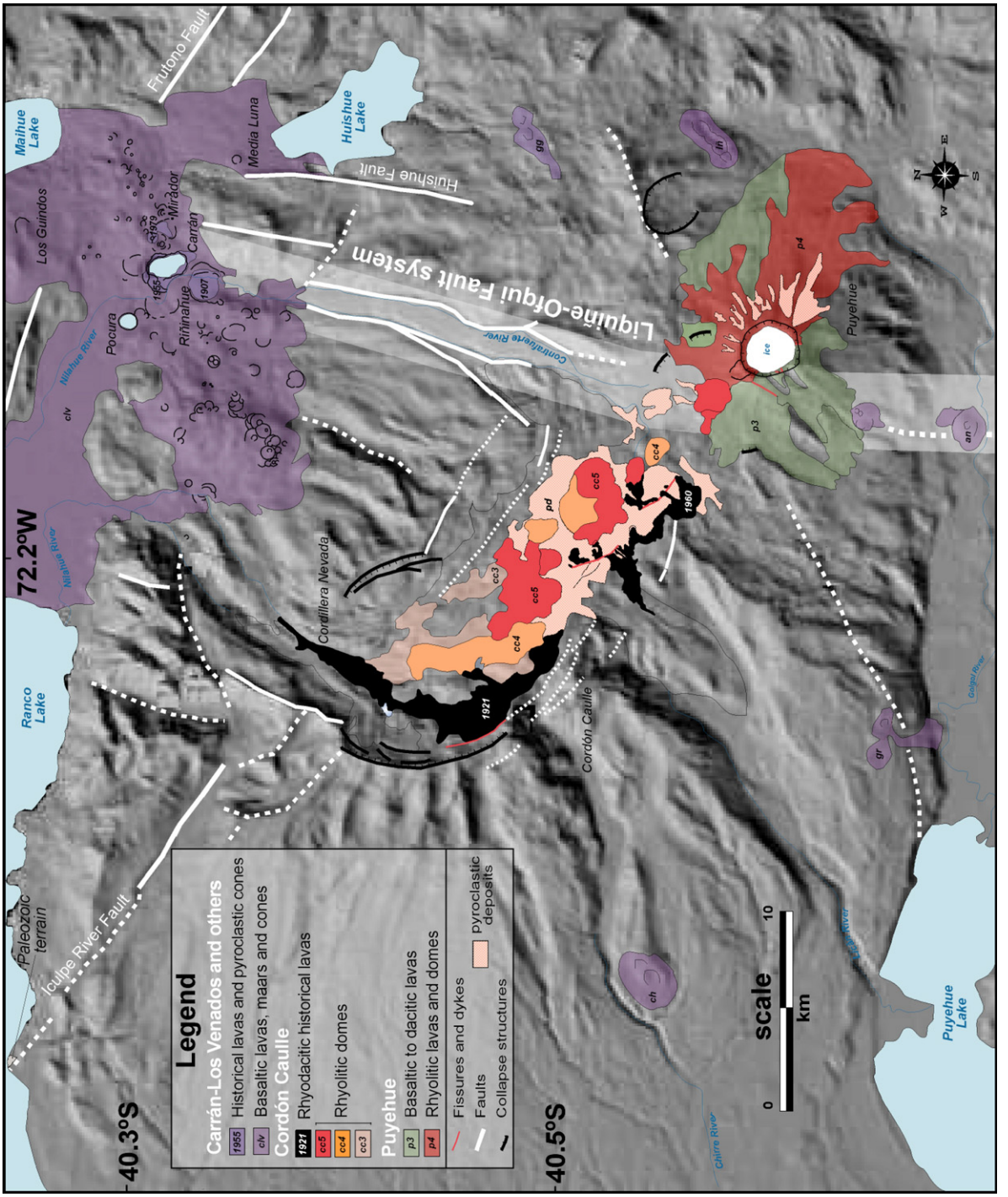
Legend
Carrán-Los Venados and others
1955 Historical lavas and pyroclastic cones
clv Basaltic lavas, maars and cones
Cordón Caulle
1921 Rhyodacitic historical lavas
cc5
cc4
cc3 Rhyolitic domes
Puyehue
p3 Basaltic to dacitic lavas
p4 Rhyolitic lavas and domes
Fissures and dykes
Faults
Collapse structures
pyroclastic deposits
scale
0
10
km
72.2°W
40.3°S
40.5°S
Paleozoic terrain
Icalpe River Fault
Ranco Lake
Maihue Lake
Huishue Lake
Puyehue Lake
Los Guindos
Mirador
Carrán
Pocura
Riñinahue
Media Luna
Frutono Fault
Huishue Fault
Liquiñe-Ofqui Fault system
Cordillera Nevada
Cordón Caulle
Puyehue
Nilahue River
Contrualelfe River
Chirre River
Golgol River
1921
1960
1907
clv
cc5
cc4
cc3
pd
p3
p4
ice
gg
th
an
gr
ch

volcanic alignment, nearly orthogonal to the CCVC. With the exception of Los Guindos volcano, all pyroclastic cones are Holocene and some of them have had historical eruptions. Olivine-rich basalts and basaltic andesites are the dominant compositions.

Although some northeast-striking branches of the Liquiñe–Ofqui Fault, which depart eastward from the master fault, are recognisable along the CSVZ segment (37°–42°S), the northeast-trending monogenetic clusters are not aligned above them and appear isolated as a Quaternary feature (e.g., López-Escobar et al., 1995). More active historical maars (Carrán) and pyroclastic cones (Riñihahue, Mirador) are located at the centre of the volcanic alignments (Fig. 4). Los Guindos is a Late Pleistocene to Holocene stratocone located to the north of the main cluster, where Futrono and Liquiñe–Ofqui fault systems converge. Another peripheral cone (Media Luna) is sitting on top of the Huishue Fault, which is parallel to the main Liquiñe–Ofqui Fault and shows a vertical separation with a western hanging block (Fig. 3).

3.2.2. Los Ñirres and Golgol clusters

The Los Ñirres (lñ) and Golgol (gg) groups are northeast-trending clusters of pyroclastic cones and maars located east of Puyehue volcano. They are Holocene in age and basaltic in composition and does not appear spatially related with faults or surface lineaments (Fig. 3).

3.2.3. Golgol River and Chirre peripheral cones

Golgol River cones (gr) are paired pyroclastic cones located west of the CCVC. They are Holocene and basaltic and are located above a stair-like morphology defined by a northeast-trending lineament defined on the Pleistocene volcanic units of CCVC. Chirre cones (ch) are nested Holocene pyroclastic cones, basaltic in composition and not spatially related with basement structures (Fig. 3).

3.3. North–south-trending volcanic chains

3.3.1. Anticura cones

Anticura cones (an) constitute a north–south-trending alignment of five pyroclastic cones, which are located along the master fault of the Liquiñe–Ofqui Fault system, morphologically defined as a sharp lineament further south. They are Holocene and basaltic in composition (Fig. 3).

4. Neogene kinematics in the CCVC area: coeval compressive, extensional and transpressive regimes

In this section we asses the current tectonic regime in the CCVC area based on spatial arrays of structures, fault kinematic indicators and morphometry of volcanoes and volcanic clusters.

The first step was to identify some surface markers as lineaments on aerial 1:50,000 scale photographs, Landsat ETM7 optical images, topographic 1:50,000 charts and Radarsat 1 images in negative view. Afterwards, field sites were selected for a tectonic study of fault populations following the method of Carey and Brunier (1974) and the procedure developed by Carey and Mercier (1987). Only those faults with well constrained kinematics were selected for further analysis, which explains the limited number of faults in these sites. In addition, aerial photographs were used to examine the volcanic morphology in order to obtain parameters such as cone alignment, cone breaching, cone elongation, crater elongation or saddle-like morphologies on volcanic craters for to infer geometry of underlying faults or possible orientation of the stress axis following the method of Tibaldi (1995) and the conceptual framework provided earlier by Nakamura (1977). The alignment of flank cones in stratovolcanoes was proposed by Nakamura (1977) as evidence of maximum horizontal stress direction but this concept can be extended to isolated elliptical cone clusters (e.g., Dhont et al., 1998). In addition, analogue experiments by Tibaldi (1995) showed a direct relation of some morphometric parameters with the geometry of underlying faults and possible kinematic regimes. Of course, the array of monogenetic cones and cone morphologies also depends of magmatic inputs (Takada, 1994), among the underlying structures and stress regimes, but this factor can be considered as constant for a small area. A summary of results is shown in Fig. 3, where an 'unwrapped' interferogram obtained by Pritchard and Simons (2004) showing possible subsidence, overlain the Radarsat 1 image (positive view) with the identified structures.

4.1. Northwest-trending structural features

At regional scale, previous works have proposed mainly a left-lateral displacement for the northwest-

Fig. 3. Late Pleistocene–Holocene volcanic units from Cordón Caulle area (modified from Moreno, 1977). Middle Pleistocene units, which form the graben walls are omitted as well as the basement. ***clv***: Carrán–Los Venados cones; ***gg***: Golgol cones; ***lñ***: Los Ñirres cones and maars; ***an***: Anticura cones; ***gr***: Golgol river cones; ***ch***: Chirre cones; ***cc***3, ***cc***4 and ***cc***5 are successive dome generations; 1921 and 1960 are fissure historical lavas from Cordón Caulle and 1907, 1955 and 1978 are pyroclastic cones and historical lavas from Carrán, Riñinahue and Mirador cones.

striking faults. Palaeozoic and Triassic shear zones in the forearc (Franzese, 1995; Martin et al., 1999) as far as Oligocene–Miocene basin opening and subsequent inversion along the arc and backarc regions (Spalletti and Dalla Salda, 1996; Jordan et al., 2001) constitute the evidences. In addition, some of these faults could have played a role in the Quaternary, as suggested by Folguera et al. (2004) and Lara and Folguera (2006) for the CSVZ. Present seismicity in the coastal area suggests an increased yet local activity for some of these oblique structures (Bohm et al., 2002).

In addition, in a long-term dextral transpressive regime, as proposed by Lavenu and Cembrano (1999) for Southern Andes, northwest-striking structures should be contractional domains because they are orthogonal to the maximum horizontal stress axis (Cembrano and Moreno, 1994; López-Escobar et al., 1995).

Along the volcanic arc region, northwest-striking structures are morphologically well-defined but kinematically poorly-constrained. For the Futrono Fault (Fig. 2), exposed along the northern shoreline of Ranco and Maihue lakes, scarce kinematic indicators on Miocene granitoids suggest left-lateral displacement without a clear age constraint. Instead, small-scale faults on a secondary west-northwest fault that splays from the Futrono Fault (site 2, Fig. 5) shows two stress tensors of compressive regime with both a northeast-trending $\sigma 1$ and an east–west $\sigma 1$.

The Iculpe River Fault, which underlies the CCVC, has a fresh morphology with a clear eroded scarp in the northern wall of the Iculpe river valley. Several landslide deposits can be recognised at the footwall. These lobed deposits appear mainly in front of inflections or steps of the fault trace and geometry, a non-conclusive argument, suggest a left-lateral displacement. In the Ranco Lake shoreline, the Iculpe River fault is the western boundary of an exhumed block of Palaeozoic–Triassic metasedimentary rocks. There, several small-scale left-lateral faults cut the cleavage and connect northwest quartz-veins. In turn, kinematic analysis on the scarce mesoscopic faults, observed on Pliocene volcanic rocks (*ca*. 5–4 Ma; Campos et al., 1998) near the trace,

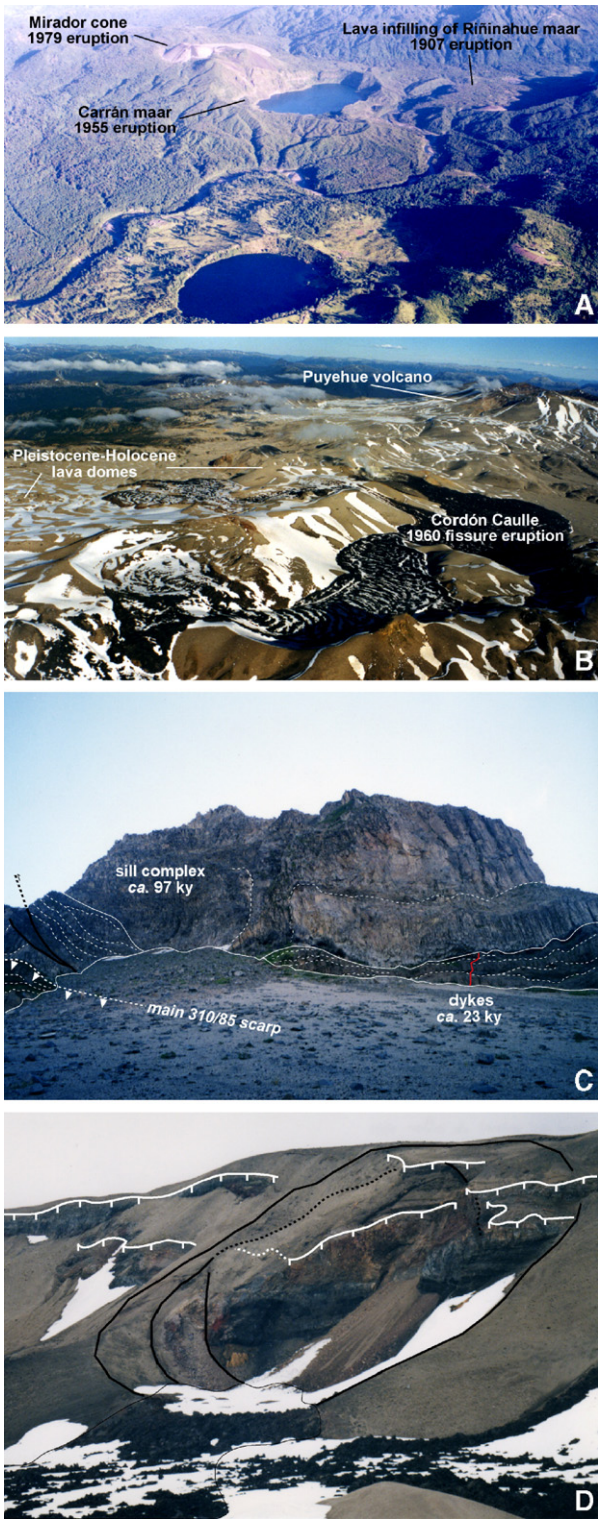

Fig. 4. (A) Photo of Carrán–Los Venados monogenetic cones, view to the northeast along the volcanic alignment. Pucura Holocene maar in the foreground and vents of the historical eruption in the background. (B), Cordón Caulle–Puyehue area, view to southeast along the volcanic alignment. Main crater and pumice cone of 1960 eruption in the foreground. This area is a graben, whose margins are scarps formed on the ancient Pleistocene volcanic units from the same volcanic complex. The main scarp in (C) exposes a dacitic sill (*ca*. 97 ka in age) that intrudes thrusted volcaniclastic beds (*ca*. 100 ka). Younger (*ca*. 23 ka) vertical basaltic dikes cut the basal sequence and show the alternating mechanism of magma emplacement. (D), a crater of the 1921–22 eruption built on the fault scarps that grew from the ring faults of Cordillera Nevada caldera.

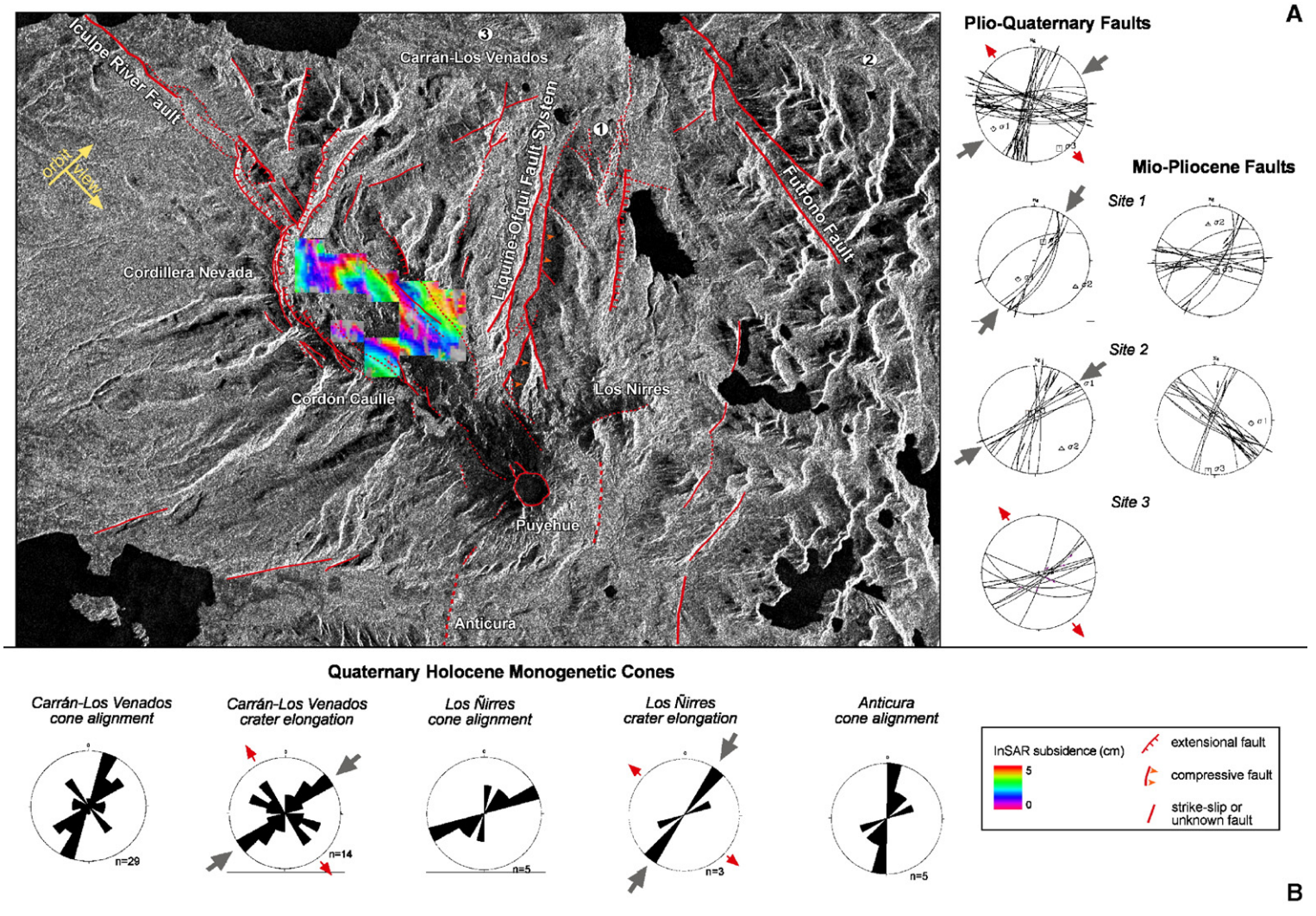

Fig. 5. Structural interpretation over a Radarsat image (Radarsat 1 Scan SAR Narrow image, August 6, 1996/3942 descending orbit, positive view). Coloured area shows an expanded interferogram by Pritchard and Simons (2004) where a possible subsidence pattern can be observed (maximum 8 cm for the period 1996–1999). Stereoplots for mesoscopic faults are shown to the right. Stress tensors are calculated with the method of Carey and Mercier (1976). Quaternary $\sigma 1$ corresponds to σhmax in all diagrams and is shown with dark grey arrows. When horizontal, $\sigma 3$ is indicated by red arrows. Morphometric features of Quaternary monogenetic cones are used as stress indicators, as an analogue to dike intrusion (e.g., Tibaldi, 1995). A double apparent contradiction arises because the two orthogonal extensional domains for volcanic areas and the transpressive–compressive regime recorded at the basement (see the text for discussion). (For interpretation of the references to colour in this figure legend, the reader is referred to the web version of this article.)

indicates an east–west shortening. This partial result is compatible with the regional east–west compressive Miocene–Pliocene event recognised by Lavenu and Cembrano (1999).

In addition, the prominent scarps of the CCVC graben and some secondary lineaments outside the depression are oriented northwest. The most recent historical fissure eruptions (1921–22 and 1960 AD) were produced on concave structures whose main trace follows a northwest trend (Lara et al., 2004). The 1921–22 northwest fissure merges with the ring faults of Cordillera Nevada caldera and 1960 fissure system is composed of two bent segments, each one with a minor north–south tail. Vertical displacement can be observed on some scarps preserved on the western hanging walls (Fig. 5).

Minor reverse faults are oriented northwest as well. They were observed on Middle Pleistocene volcanic units where mafic lavas and ignimbrites are juxtaposed (Lara et al., 2003).

4.2. Northeast-trending structural features

At regional scale, northeast-trending alignments of monogenetic centres are thought to represent extensional domains in a bulk dextral transpressive regime (Cembrano and Moreno, 1994; López-Escobar et al., 1995). All of them have erupted mainly primitive basalts and show some field evidences of surficial extension as fissures and dike swarms. A focal mechanism obtained from the Harvard Centroid Moment Tensor (CMT) catalogue for a Mw: 5.3 earthquake (Fig. 1), which accompanied the 1989 eruption of Lonquimay volcano (39°S), shows a northwest *T* axis that is compatible with extension on northeast domains. At the beginning of the 1989 eruption of Lonquimay volcano, a northeast fissure was formed and subsequently covered by ejecta that finally formed the Navidad pyroclastic cone (Moreno and Gardeweg, 1989).

In the CCVC area, the Carrán–Los Venados volcanic cluster forms a first-order northeast-trending alignment. Larger and most active pyroclastic cones are located in the middle of the chain. Secondary, yet frequent cone alignment strikes N35°E while others are N60°E and even N40°W. Crater elongation shows a dominant N45°E orientation, which is thought to represent a more reliable σhmax (Fig. 5). Los Ñirres cones and maars are east-northeast aligned. Instead, crater elongations of them are N42°E, which is also interpreted as σhmax orientation. Golgol and Chirre cones form northeast-trending alignments but their crater elongation and breaching direction seem to be controlled by the topographic slope.

In addition, scarce northeast-trending faults observed on the basement of Carrán–Los Venados cones show an extensional component that defines a northwest-oriented minimum horizontal stress, which is consistent with the analysis of cone morphology.

4.3. North–south-trending structural features

At regional scale, the Liquiñe–Ofqui Fault presents evidences of both, strike–slip and vertical displacements. From striae on mesoscopic faults observed along the main trace between 39° and 46°S, Lavenu and Cembrano (1999) proposed a dextral transpressive regime for the post-Pliocene period. These authors obtained a consistent northeast-trending maximum horizontal stress, which is also the major axis of the stress tensor (σ1). However, the vertical axis of the stress tensor can be either σ2 (transpression–transtension) or σ3 (compression) as can be observed on published (e.g., Lavenu and Cembrano, 1999) and new data.

In the CCVC area, the Liquiñe–Ofqui Fault is represented by a set of north-northeast lineaments, the best-defined of which is the Contrafuerte river where a west-facing eroded scarp is recognisable on Quaternary rocks (<500 ka). Along this trace, a secondary set produces a geometric pattern of possible Riedel shears (Fig. 5). No lateral displacement can be deduced from surface markers but an important vertical separation is observed on the eastern hanging block. Further east, on a parallel trace that cut Miocene granites (*ca*. 5.4 Ma; $^{40}Ar/^{39}Ar$ age by Sepúlveda et al., 2005), several mesoscopic faults indicate two incompatible stress tensors. The first one defines a N42.5° maximum horizontal stress axis, similar as the bulk Quaternary dextral transpression proposed by Lavenu and Cembrano (1999) but with vertical σ3 (compression). The second tensor is compressive as well but show an east–west σ1, same as the Miocene–Pliocene event described by Lavenu and Cembrano (1999). For reference, the nearest site outside the area is shown above in Fig. 5, which represents a transpressive regime for the master fault some kilometres north (Lavenu and Cembrano, 1999).

Anticura cones are nearly circular centres with round craters aligned north–south along the master fault of the Liquiñe–Ofqui Fault system. However, following Dhont et al. (1998) they cannot be used as stress indicators or evidence for σ1.

A summary of these results is shown in Table 1, where a clear consistency can be observed between fault population analysis on basement rocks and volcanic morphology studied on Holocene pyroclastic cones. The

Table 1
Stress tensors inferred from microtectonic data and cone morphometry

Site		n	σ1		σ2		σ3		R
			Azimuth	Dip	Azimuth	Dip	Azimuth	Dip	
	Liquiñe–Ofqui fault zone	28	238°	12°	034°	76°	147°	05°	0.593
1	Liquiñe–Ofqui fault zone	06	219°	41°	123°	07°	025°	48°	0.536
2	Futrono Fault Zone	10	049°	01°	139°	19°	315°	71°	0.773
3	Carrán–Los Venados cones	14	045°	00°	00°	90°	315°	00°	
4	Los Ñirres cones	03	042°	00°	00°	90°	312°	00°	

σhmax is northeast-trending (~N39–60°E) and the vertical axis can be either σ2 (transpression) or σ3 (compression).

5. Discussion

The scarce focal mechanisms and the published microtectonic data by Lavenu and Cembrano (1999) suggest mainly a Quaternary transpressive regime for the volcanic arc region in Southern Andes, with an horizontal northeast-trending σ1. Morphometric analysis of monogenetic cones in the CCVC area is consistent with this regional setting. In addition, extensional conditions have accompanied both basaltic eruptions along northeast domains and rhyodacitic eruptions on the northwest trends. Therefore, there is an apparent contradiction that poses a problem of kinematic compatibility. Theoretical structures expected in both transpressive and compressive regimes are shown in Fig. 6, where reshear ability of fault planes is also represented. Obviously, these regimes cannot coexist in space and time, although they may alternate. Therefore, the age uncertainty of the deformation must be established previous to a dynamic analysis. Next, we show possible relations between these tectonic regimes and first we discuss the origin of a local compressive setting. Then, we analyse magma ascent and volcanism in compressive and transpressive regimes and finally, we try to explain how alternant extension occurs in orthogonal domains.

5.1. Age uncertainty for Quaternary events

The precise age of Quaternary deformation in Southern Andes can be established only by regional criteria although local data is generally lacking (Lavenu and Cembrano, 1999). Because of the small amount of displacements and high erosion rates precluding preservation of surface markers, fault planes are usually studied in basement rocks. In turn, Late Quaternary structural features are mainly expressed in volcanic alignments or fissure systems. However, Lavenu and Cembrano (1999) found a regional consistency between two Neogene events of deformation: a Miocene–Pliocene east–west compressive event and the superposed Plio-Quaternary northeast dextral transpression/compression. The present regime would have a maximum age of *ca*. 3.6 Ma in the CSVZ (37°–42°S) and *ca*. 1.6 Ma along the SSVZ (42°–46°S). In the CCVC area, stress tensors were obtained mainly in Late Miocene to Early Pliocene rocks, where the two regional events were recognised (Fig. 5) and their age thus assumed (Table 1).

5.2. Low strain partitioning and compressive regimes in the volcanic arc

The regional northeast dextral transpressive regime described by Lavenu and Cembrano (1999) seems to alternate with local compressive conditions, as occur in

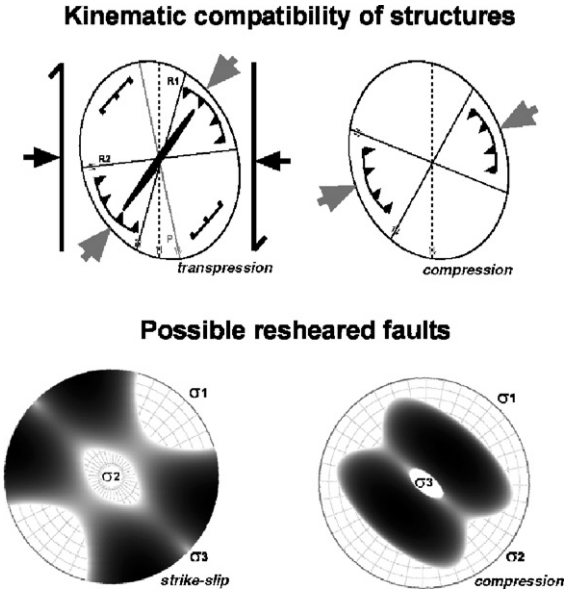

Fig. 6. Theoretical structures with kinematic compatibility are shown for both transpressive and compressive regimes. Possible planes for reshearing (black area) in both strike–slip and compressive regimes, are plotted on a polar net using the method of Tolson et al. (2001).

CCVC area. However, a northeast-trending $\sigma 1$ appear constant at both regional and local scale. Compressive regimes (northeast $\sigma 1$ and vertical $\sigma 3$) are especially clear where vertical separation occurs along the Liquiñe–Ofqui Fault (e.g., Lara and Moreno, 2004; Lara et al., 2005). In addition, no clear lateral displacement with surface expression has been observed along this fault.

A plausible explanation comes from a margin-scale analysis of the strain field, which can be considered an analogue of the stress field in active tectonics. Following Teyssier et al. (1995), a small amount of partitioning for the strike–slip component can be deduced for a nearly orthogonal convergence, as occur in Southern Andes (Fig. 1). In turn, highly oblique convergent margins should produce wrench-dominated regimes with very active margin-parallel strike–slip faults (Withjack and Jamison, 1986; Richard and Cobbold, 1990).

In the CCVC area, the small component of lateral displacement (<5%) could be absorbed either by small-scale faults along the Liquiñe–Ofqui Fault system, in the diffuse zone of deformation or as oblique tension cracks, perhaps represented at arc-scale by the monogenetic clusters.

5.3. Magmatism in a transpressive–compressive environments

Evolved magmatism in CCVC requires long residences times and complex differentiation processes, which should be enhanced in compressive regimes. Primitive basaltic magmas of Carrán–Los Venados cluster suggest direct ascent from the mantle source, which can be facilitated by extensional or transpressive conditions of the crust.

Authors such as Ramsay and Huber (1987) and Rebaï et al. (1993) suggested that under general contractional regimes, the deep part of the crust undergoes compression, whereas the shallower part is submitted to extension. However, as many authors have already noted (e.g., Sibson et al., 1988), transpressive and even pure contractional regimes are able to localize magmatic fluids under adequate conditions. Local compression with vertical $\sigma 3$ suppress magmatic ascent and promotes horizontal sheet intrusions and longer residence in the crust at different crustal levels. In that condition, magma ascends because sheeted-dikes can cancel the differential stress generating a neutral local stress against the regional compressive field (Takada, 1994). In turn, high magma pressures could displace misoriented thrust faults that can connect the horizontal tensional domains (sills) or magma chambers in a bulk compressive environment favouring magma ascent (after the Amonton's Law; see Byerlee, 1978; Sibson et al., 1988).

In volcanic areas, the level of neutral buoyancy can occur below the crustal compression/extension interface and magmatic fluids are arrested in compressive environments precluding eruptions. However, magmatic fluids overpressurized by, for example, trapped bubbles can reshear subvertical ancient faults making connections between horizontal neutral buoyancy levels (Sibson, 1985, 1987; Sibson et al., 1988) allowing the magma to reach the surface.

Because the differentiation processes are sensible to pressure conditions, some geochemical features can be used to test the structural settings. Here, incompatible elements describe similar asthenospheric sources for Cordón Caulle fissure system, Puyehue volcano and Carrán–Los Venados cones but different ascent pathways for each one. Basalts from Carrán–Los Venados can be derived from low degrees (5–10%) of partial melting with a stage of high pressure fractional crystallisation dominated by olivine and clinopiroxene (Fig. 7). More evolved basaltic andesites are typically recognised in the most active (*i.e.*, polygenetic) pyroclastic cones. A plausible scenario, which explain both the different magma compositions and eruptives modes, is that coalescent channels and small magma chambers are the feeding systems for the polygenetic cones, while isolated channels lacking crustal residence are the feeders of the strictly monogenetic ones.

On the other hand, rhyolites and rhyodacites of Cordón Caulle and Puyehue volcanoes are derived from advanced fractional crystallization of basalts without significant crustal assimilation. Andesites can be derived by magma mixing between basalts and rhyolites (Gerlach et al., 1988). Both processes require a long residence time, probably higher than previously proposed by Sigmarsson et al. (1990, 1998) from radioactive $^{238}U/^{230}Th$ disequilibria for the most active stratovolcanoes of Southern Andes, which erupted scarce rhyolites. The primary Fo-rich olivines and Ca-rich plagioclases in rhyolites are in disequilibria with silica-rich liquids (Gerlach et al., 1988), suggesting that silica enrichment is a late low pressure process.

5.4. Extension in misorientated domains by dynamic and static stress change

In a transpressive/compressive regime with horizontal northeast-trending $\sigma 1$, northwest-trending structural

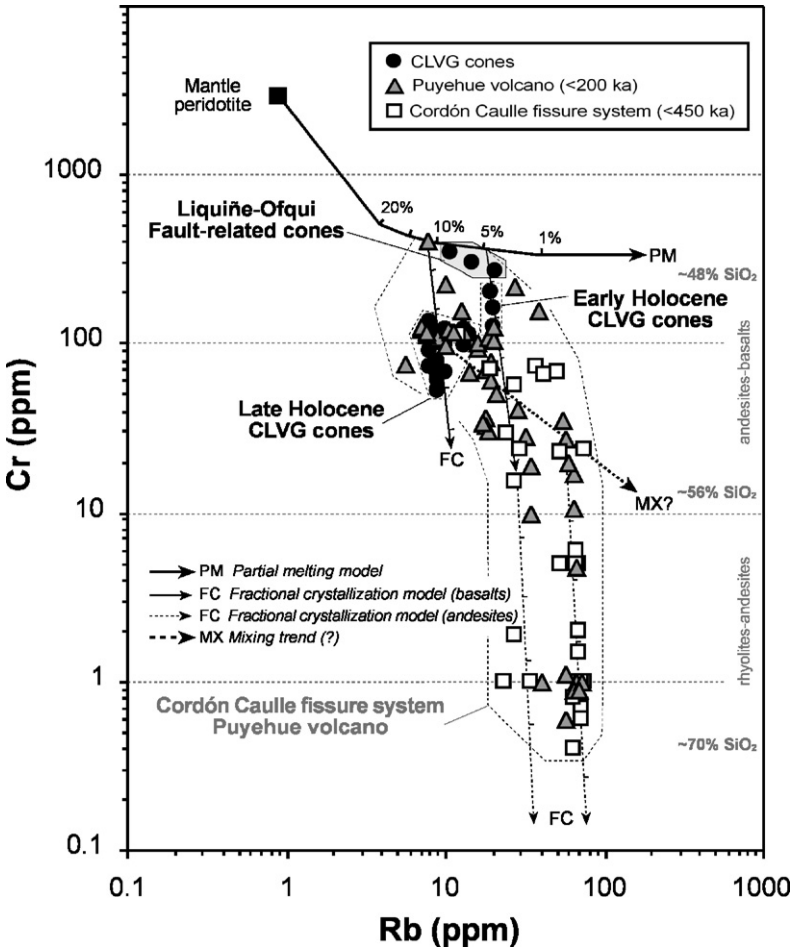

Fig. 7. Selected geochemistry of Carrán–Los Venados monogenetic cones (CLVG) and Cordón Caulle Volcanic Complex (CCVC). Data taken from Gerlach et al., 1988; Rodríguez, 1999 and unpublished data from the authors). Pearce (1982) diagram was modified preferring Rb than Y as a more incompatible element plotted against Cr. Raleigh fractional crystallization vectors were obtained by means of 'FC modeler' by Keskin (2002). Partial melting was calculated with a non-modal batch-melting model. Parental predictive contents taken from McDonough et al. (1991) and Wood et al. (1979). Basalts from CLVG evolved from different basaltic end-members following a simple fractional crystallization processes of olivine and piroxene. Hypothetic mixing trend is shown to emphasize that intermediate compositions in Cordón Caulle–Puyehue are not simple evolved products from basaltic sources. Low pressure fractional crystallization model fits the silica-rich compositions as evolved products from intermediate ones in Cordón Caulle–Puyehue. This pattern can be interpreted as a direct ascent of basaltic dikes in CLVG and trapped, mixed and pressurized cooling magmas in CCVC.

domains are strongly misorientated for extension or strike–slip displacements. In such a case, extension on these domains requires local rotation of the stress field. Here, we present three different options that could explain local reorientation of the instantaneous stress tensors (Fig. 8).

One possible explanation is that change in the dynamic stresses caused from large, distant subduction earthquakes could reshear ancient faults that are not, otherwise, favourably oriented within the regional stress field. This idea was posed by Lara et al. (2004) for the 1960 eruption on Cordón Caulle, which occurred 38 hours after the large Mw: 9.5 Chilean earthquake. There, the authors proposed that dynamic stresses propagated 200 km inland from the epicentral area and resheared a northwest ancient fault, where the magma would have been already emplaced near the surface. The mechanism was first a shear extensional failure allowing a non-Andersonian dyke (Anderson, 1951), and a pure extension after, with a dyke parallel to the current $\sigma 1$ (Lara et al., 2004).

This hypothesis fails in that not all eruptions can be correlated with large subduction earthquakes. Strong motions caused by earthquakes with Mw>8.5 have recurrence periods of 147–211 year in the area (Nishenko, 1985). Giant Mw>9.0 earthquakes as the

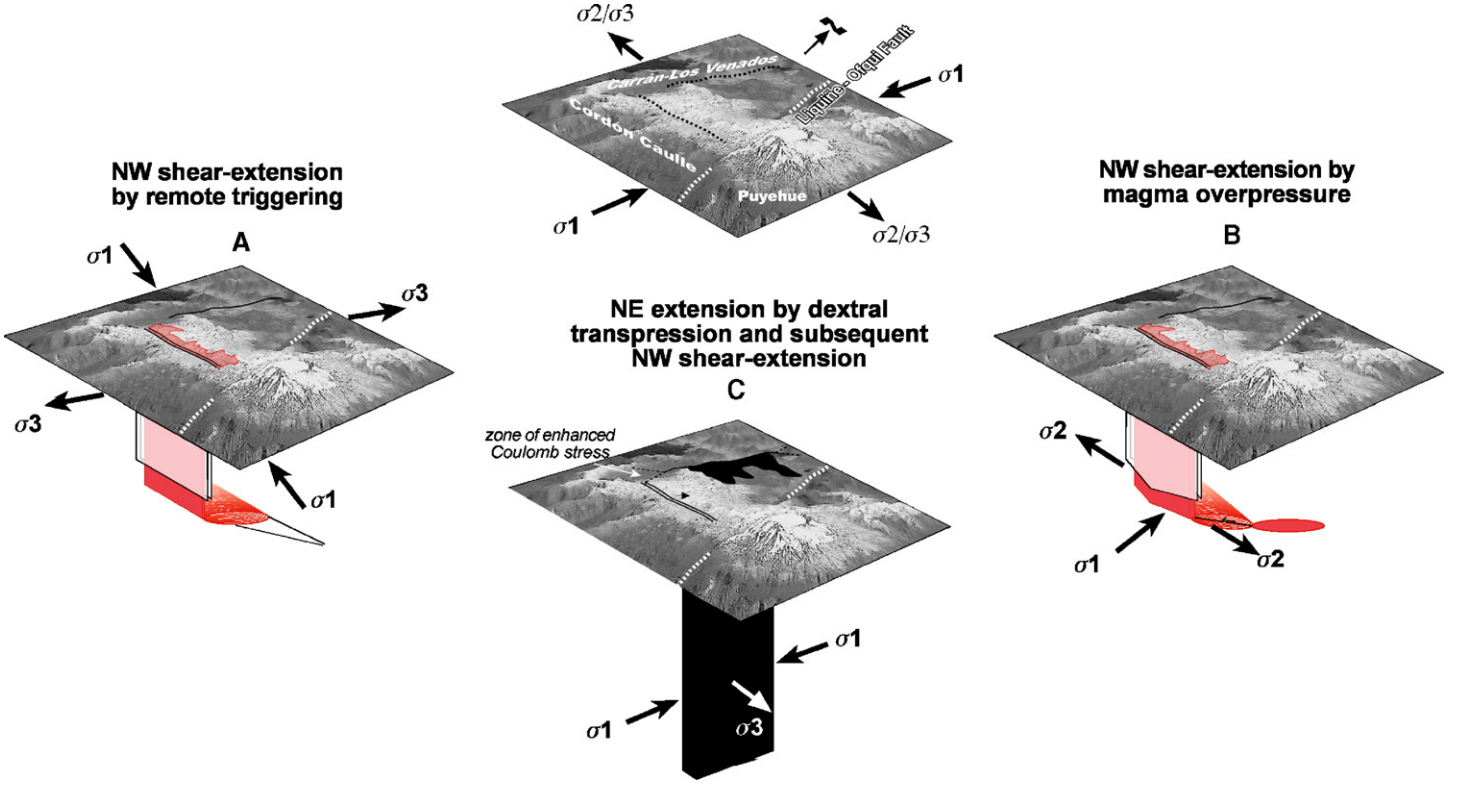

Fig. 8. Cartoons for hypothetical non-exclusive mechanisms of extension in misorientated NW domains. (A) Shear extension triggered by remote subduction earthquakes; (B) shear extension caused by magmatic overpressure and (C) shear extension caused by the emplacement of orthogonal Andersonian dikes (see the text for discussion).

1960 event have periods of *ca*. 300 years (Cisternas et al., 2005). Historical subduction earthquakes recorded in the area were 1575, 1737, 1837 and the last 1960. Two ^{14}C unpublished ages (cal AD 1668–1955 and cal AD 1624–1955) on pyroclastic deposits identified to the west of Puyehue volcano partially cover the time span of these great earthquakes. This suggests a similar triggering mechanism as for the 1960 eruption. However, the 1921–22 fissure eruption of Cordón Caulle cannot be linked to any large historic subduction earthquake.

A second option is to assign a key role to the magmatic stresses produced around arrested sills. This mechanism is supported by several seismic surveys in other volcanic areas where sharp changes in stress tensors were observed before, during and after eruptions (e.g., Legrand et al., 2002; Roman et al., 2004). Most of these changes are directly related to magma movement along the conduits or volumetric effects on the country rock. For example, volcanic seismicity on Crater Peak, a mafic parasitic vent of Mount Spurr (Alaska), showed a 90° clockwise rotation of the local stress tensor with respect to the background in the precursory period of the 1992 eruptions, recovering the regional trend afterwards (Roman et al., 2004). Phreatic 1998–1999 eruptions and dome growth in Guagua Pichincha volcano (Ecuador) were accompanied by a seismic swarm whose stress tensor departs (83° rotation of $\sigma 1$ with an horizontal $\sigma 3$) from the compressive regional stress field (Legrand et al., 2002). For the 1989 eruption of Lonquimay volcano (Chile, 39°S), the strike–slip focal mechanism (Barrientos and Acevedo, 1992) was compatible with the regional stress regime obtained by Lavenu and Cembrano (1999) but different from the CCVC area. The difference implies a shift between $\sigma 3$ and $\sigma 2$ maintaining the trend of the horizontal $\sigma 1$. Thus, the CCVC area can represent a locus for magma ascent and storage because of compression (*i.e.*, horizontal $\sigma 1$ with vertical $\sigma 3$) allow growing of sill complexes until they can reshear faults that connect these neutral buoyancy levels. This would cause transient stress field rotation that permits the final magma ascent to the surface with coeval extensional conditions. This mechanism can explain the eruptive dynamics at andesitic–dacitic volcanoes with shallow levels of neutral buoyancy. Residence in the upper crust causes an increase in silica contents by low pressure fractional crystallization. Consequently, the magma would expand deforming the country rock, suppressing the regional stress and promoting vertical dikes that drain the lateral part of the chamber. Finally, silica-rich remnant can be extruded through the central vent. In Southern Andes, this can be the case of Calbuco volcano (42°S); Lanín (39.5°S) and Quetrupillán (39.4°S) volcanoes (Lara et al., 2004).

A third, perhaps more speculative option, could be that emplacement of Andersonian dikes in northeast domains trigger reshearing of northwest faults and subsequent extension and eruption. This argument follows the rationale that fault rupture and dike intrusion changes the static stress around neighbouring faults (see e.g. Harris, 1998 and references therein). As was shown by Toda et al. (2002), emplacement of a vertical dyke produces a 'dog-bone' pattern of seismicity that roughly follows the Hill's mesh model (Hill, 1977), which is a consequence of symmetric changes of the static stress around the dike.

Table 2
Historical and Holocene eruptive events

Carrán–Los Venados
1907 AD
April 7: perceptible earthquakes
April 8: phreatomagmatic eruption followed by cyclic seismic swarms and pulsatory eruptive column
April 24: strombolian phase with emission of a basaltic lava flow. After that, a pyroclastic cone was built. Gas emission lasted until February 1908
1955 AD
Perceptible earthquakes
July 27: seismic swarm with strong ground motion. Phreatomagmatic eruption. Pulsatory pyroclastic ejecta lasted until November 12. Column height reached 5 km at paroxysmal phase
1979 AD
March 15: perceptible earthquakes
April 4: increasing seismic swarm
April 14: strombolian eruption with a increasing pulsatory phase; Eruptive column height reached 3 km. A pyroclastic cone was built
April 17: rupture cone and lava flow emission and decreasing activity
May 12: renewal of strombolian activity and new lava flow emission
May 20: decreasing activity
Cordón Caulle
1921–22 AD
Perceptible seismic swarm
December 13: explosive eruptions; cyclic phase with fissure active vents
December 19: effusive phase
1960 AD
May 22: Mw:9.5 earthquake in the subduction zone
May 24: subplinian phase along fissure vents
May 26?: effusive phase followed by a renewed pyroclastic phase on major craters
2000 AD?
Perceptible seismic swarm
Unreported small eruption; a pumice cone was built

If the static stress change is computed for a northwest dextral fault, perpendicular to a 15-km-long vertical northeast dyke, an orthogonal to the tips area of increased static stress would result. This is an enhanced domain for future displacement. After the northeast dyke emplacement, northwest domains become favourable areas for dextral strike–slip and subsequent extension that permit eruptions. Once a northwest fault is relaxed, the regional stress field recovers its prevalence and these faults remain as contractional domains. Some clue for this two-way coupling between these incompatible extensional domains could be the eruptive record for 20th century (Table 2). This reduced amount of data preliminary suggests an alternating behaviour and, perhaps the effect of this triggering mechanism.

6. Conclusions

In the CCVC area, there is a clear tectonic control on volcanism. The entire CCVC was built on a pre-Andean northwest structure and Carrán–Los Venados and other clusters of monogenetic cones follow regional trends as occur along the entire CSVZ.

In this work we have reviewed the available geological knowledge about this volcanic area and conducted a microtectonic analysis of fault populations, together with a morphological study of volcanic features that serve as kinematic indicators. This was complemented with a review of selected geochemical signatures that describes magmatic evolution of both, northwest and northeast volcanic trends.

The results can be summarized as follows:

(a) A compressive regime was obtained along the Liquiñe–Ofqui Fault system with a horizontal northeast-trending $\sigma 1$. This differs from the regional transpression previously inferred at arc scale although $\sigma 1$ direction is equivalent.
(b) A horizontal northeast-trending $\sigma 1$ was obtained from volcanic kinematic indicators on Carrán–Los Venados and other clusters of pyroclastic cones. Because of the fissure eruptive style and primitive magmas erupted along these alignments, they likely correspond to extensional domains and thus agree with the regional transpression previously documented at arc scale.
(c) Geochemical features of Carrán–Los Venados group suggest that basalts ascended directly from the mantle source without intracrustal pauses. Instead, CCVC evolved magmas requires a long residence time, which is thought to be favoured by more compressive regimes.
(d) An apparent inconsistency arises because at local scale there is evidence of compressive and transpressive regimes and two orthogonal extensional volcanic domains exist.

We propose that the small strike–slip component expected at the Southern Andes is mainly absorbed on northeast-trending volcanic domains that act as tensional cracks in a general transpressive regime. The Liquiñe–Ofqui Fault system in these areas patially reflect the coaxial component of the deformation and thus, a spatial strain partitioning arises.

To explain extension in the northwest misorientated domains we propose three non-exclusive processes that take into account in the interplay between deformation and magmatism:

(a) Shear extension (oblique opening) triggered by dynamic stress imparted by great subduction earthquakes, as would have been the case of 1960 AD eruption.
(b) Shear extension caused by magma driven pressures when arrested sills suppress the regional stress field, reshearing faults or feeding vertical dikes to the surface, as could be the case reported for the ancient Cordón Caulle unit (Fig. 6) and many described seismic swarms that accompanied eruptions.
(c) Shear extension induced by static stress change after the emplacement of Andersonian NE dikes, as could be hypothetically the case of the alternant eruption of 20th century.

Regardless of the dominant spatial and temporal mechanism, the Quaternary magmatic evolution of the CCVC area shows a great variety of eruptive, compositional and structural features of the vents dynamics, which is controlled by local rotations of the regional stress field and the inherited basement structures. Although some first-order structural patterns are related to the regional-scale architecture of the volcanic arc, the actual tectonic control of volcanism is also dependant of the local kinematic conditions as arising from the interplay between the tectonic stress field and magma forces.

Acknowledgements

This work is part of a research on the relationships between tectonics and volcanism in Southern Andes, a collaborative effort of the SERNAGEOMIN (Chile) and IRD-Université Paul Sabatier (France). Fieldwork and geochemistry was mainly supported by Fondecyt grants

No. 1960885 and 1930164, and ECOS C01U03 grant. We are indebted to H. Moreno for the long lasted and helpful discussion on these issues. P. Villamor is kindly thanked for her constructive criticism and useful suggestions. D. Dhont made sharp observations and A. Tibaldi is acknowledged as special editor. This is a contribution to the UNESCO-IUGG-IGCP project No.455 and the Volcanic Hazards Programme of SERNAGEOMIN (Chile).

References

Anderson, E.M., 1951. The Dynamics of Faulting, 2nd ed. Oliver and Boyd, pp. 1–191.

Assumpçao, M., 1992. The regional intraplate stress field in South America. J Geophys. Res. 97, 11,889–11,903.

Barrientos, S., Acevedo, P., 1992. Seismological aspects of the 1988–1989 Lonqimay (Chile) volcanic eruption. J. Volcanol. Geotherm. Res. 53, 73–87.

Bellier, O., Sébrier, M., 1994. Relationship between tectonism and volcanism along the Great Sumatran Fault deduced by SPOT image analyses. Tectonophysics 233, 215–231.

Bohm, M., Lüth, S., Echtler, H., Asch, G., Bataille, K., Bruhn, C., Rietbrock, A., Wigger, P., 2002. The Southern Andes between 36° and 40°S latitude: seismicity and average seismic velocities. Tectonophysics 356, 275–289.

Byerlee, J.D., 1978. Friction of rocks. Pure Appl. Geophys. 116, 615–626.

Campos, A., Moreno, H., Muñoz, J., Antinao, J., Clayton, J. y Martin 1998. Area de Futrono-Lago Ranco, Región de los Lagos. Servicio Nacional de Geología y Minería, Mapas Geológicos No. 8, 1 sheet, 1:100.000 scale. Santiago.

Carey, E., Brunier, B., 1974. Analyse théorique et numérique d'un modèle élémentaire appliqué à l'étude d'une population de failles. C. R. Acad. Sci., Paris, D 269, 891–894.

Carey, E., Mercier, J.L., 1987. A numerical method for determining the state of stress using focal mechanisms of earthquake populations: application to Tibetan teleseisms and microseismicity of Southern Peru. Earth Planet. Sci. Lett. 82, 165–179.

Cembrano, J., Moreno, H., 1994. Geometría y naturaleza contrastante del volcanismo cuaternario entre los 38°S y 46°S: ¿Dominios compresionales y tensionales en un régimen transcurrente? Congreso Geológico Chileno No. 7, Actas, vol. 1, pp. 240–244.

Cembrano, J., Hervé, F., Lavenu, A., 1996. The Liquiñe–Ofqui fault zone: a long-lived intra-arc fault system in southern Chile. Tectonophysics 259, 55–66.

Cembrano, J., Shermer, E., Lavenu, A., Sanhueza, A., 2000. Contrasting nature of deformation along an intra-arc shear zone, the Liquiñe–Ofqui fault zone, southern Chilean Andes. Tectonophysics 319, 129–149.

Cembrano, J., Lavenu, A., Reynolds, P., Arancibia, G., López, G., Sanhueza, A., 2002. Late Cenozoic transpressional ductile deformation north of the Nazca–South America–Antarctica triple junction. Tectonophysics 354, 289–314.

Chotin, P., 1975. Los Andes Meridionales et la Termination du Basin Andin. De Lonquimay (Chili) et le Neuquén (Argentine) (lat.38°45′S) [Ph.D. Thesis]: Paris, Université Pierre et Marie Curie. 306 pp.

Cifuentes, I.L., 1989. The 1960 Chilean earthquakes. J. Geophys. Res. 94, 665–680.

Cisternas, M., Atwater, B., Torrejón, F., Sawai, Y., Machuca, G., Lagos, M., Eipert, A., Youlton, C., Salgado, I., Kamataki, T., Shishikura, M., Malik, J.K., Rizal, Y., Rajendran, C.P., Husni, M., 2005. Incubation of the giant 1960 Chile earthquake through multiple recurrence intervals. Nature 437, 404–407.

DeMets, C., Gordon, R., Argus, D., Stein, S., 1994. Effect of recent revisions to the geomagnetic reversal time scale on estimates of current plate motions. Geophys. Res. Lett. 21, 2191–2194.

Dhont, D., Chorowicz, J., Yürür, T., Froger, J.L., Köse, O., Gündogdu, N., 1998. Emplacement of volcanic vents and geodynamics of Central Anatolia, Turkey. J. Volcanol. Geotherm. Res. 62, 207–224.

Folguera, A., Ramos, V.A., Hermanns, R., Naranjo, J.A., 2004. Neotectonics in the foothills of the southernmost central Andes (37°–38°S): Evidence of strike–slip displacement along the Antiñir–Copahue fault zone. Tectonics 23 (TC 5008) (23 pp.).

Franzese, J., 1995. El Complejo Piedra Santa (Neuquén, Argentina): parte de un cinturón metamórfico neopaleozoico del Gondwana suroccidental. Rev. Geol. Chile 22 (2), 193–202.

Gerlach, D., Frey, F., Moreno, H., López-Escobar, L., 1988. Recent volcanism in the Puyehue–Cordón Caulle Region, Southern Andes, Chile (40.5°S): petrogenesis of evolved lavas. J. Petrol. 29, 333–382.

Harris, R., 1998. Introduction to special section: stress triggers, stress shadows, and implications for seismic hazard. J. Geophys. Res. 103, 24,347–24,358.

Hervé, F., 1994. The Southern Andes between 39° and 44°S latitude: the geological signature of a transpressive tectonic regime related to a magmatic arc. In: Reutter, K.J., Scheuber, E., Wigger, P.J. (Eds.), Tectonics of the Southern Central Andes, pp. 243–248.

Hill, D., 1977. A model for earthquake swarms. J. Geophys. Res. 82, 1347–1352.

Jordan, T.E., Burns, W.M., Veiga, R., Pángaro, F., Copeland, P.I., Kelley, S., Mpodozis, C., 2001. Extension and basin formation in the southern Andes caused by increased convergence rate: a mid-Cenozoic trigger for the Andes. Tectonics 20, 308–324.

Keskin, M., 2002. FC-Modeler: a Microsoft® Excel© spreadsheet program for modelling Rayleigh fractionation vectors in closed magmatic systems. Comput. Geosc. 28 (8), 919–928.

Lara, L.E., Folguera, A., 2006. The Pliocene to Quaternary narrowing of the Southern Andean volcanic arc between 37° and 41°S latitude. In: Kay, S.M., Ramos, V.A. (Eds.), Evolution of an Andean Margin: A Tectonic and Magmatic View from the Andes to the Neuquén Basin (35°–39°S lat), Geological Society of America Special Paper 407, pp. 299–315.

Lara, L.E., Moreno, H., 2004. Geología preliminar del área Liquiñe-Neltume: Servicio Nacional de Geología y Minería Carta Geológica de Chile, Serie Geología Básica No. 83, scale 1:100,000, 1 sheet. 101 pp.

Lara, L.E., Rodríguez, C., Moreno, H., Pérez de Arce, C., 2001. Geocronología K-Ar y geoquímica del volcanismo plioceno superior-pleistoceno de los Andes del Sur (39°–42°S). Rev. Geol. Chile 28, 67–90.

Lara, L.E., Mathews, S., Pérez, C., Moreno, H., 2003. Evolución morfoestructural del Complejo Volcánico Cordón Caulle (40°S): evidencias geocronológicas 40Ar–39Ar. Proceedings, Congreso Geológico Chileno, 10th: Concepción, Electronic Files.

Lara, L.E., Naranjo, J.A., Moreno, H., 2004. Rhyodacitic fissure eruption in Southern Andes (Cordón Caulle; 40.5°S) after the 1960 (Mw: 9.5) Chilean earthquake: a structural interpretation. J. Volcanol. Geotherm. Res. 138, 127–138.

Lara, L.E., Cembrano, J., Lavenu, A., Darrozes, J., 2005. Holocene volcanism and vertical displacements along the major intraarc

transpressive system in Southern Andes. 6th International Symposium on Andean Geodynamics, Extended Abstracts, Barcelona.

Lavenu, A., Cembrano, J., 1999. Compressional and transpressional-stress pattern for Pliocene and Quaternary brittle deformation in fore arc and intra-arc zones (Andes of Central and Southern Chile). J. Struct. Geol. 21, 1669–1691.

Legrand, D., Calahorrano, A., Guillier, B., Rivera, L., Ruiz, M., Villagómez, D., Yepes, H., 2002. Stress tensor analysis of the volcanic swarm of Guagua Pichincha volcano, Ecuador. Tectonophysics 344, 15–36.

López-Escobar, L., Cembrano, J., Moreno, H., 1995. Geochemistry and tectonics of the Chilean Southern Andes basaltic quaternary volcanism (37–46°S). Rev. Geol. Chile 22 (2), 219–234.

Martin, M.W., Kato, T., Rodríguez, C., Godoy, E., Duhart, P., McDonough, M., Campos, A., 1999. Evolution of the Palaeozoic accretionary complex and overlying forearc–magmatic arc, south central Chile (38°–41° S): constraints for the tectonic setting along the southwestern margin of Gondwana. Tectonics 18 (4), 582–605.

McDonough, W., Sun, S., Ringwood, A., Jagoutz, E., Hofmann, A., 1991. K, Rb and Cs in the Earth and Moon evolution of the Earth's mantle. Geochemical and Cosmochemical Acta, Ross Taylor Symposium Volume.

Moreno, H. 1977. Geología del área volcánica Puyehue–Carrán en los Andes del sur de Chile. Universidad de Chile, thesis (unpublished). 181 pp.

Moreno, H., Gardeweg, M.C., 1989. La erupción en el complejo volcánico Lonquimay (Diciembre 1988-), Andes del Sur. Rev. Geol. Chile 16 (1), 93–117.

Nakamura, K., 1977. Volcanoes as possible indicators of tectonic stress orientation: principle and proposal. J. Volcanol. Geotherm. Res. 2, 1–16.

Nakamura, K., Uyeda, S., 1980. Stress gradient in arc–back arc regions and plate subduction. J. Geophys. Res. 85, 6419–6428.

Nishenko, S., 1985. Seismic potential for large and great interplate earthquakes along the Chilean and Southern Peruvian margins of South America: a quantitative reappraisal. J. Geophys. Res. 90 (B5), 3589–3615.

Pearce, J., 1982. Trace elements characteristics of lavas from destructive plate boundaries. In: Torpe, R. (Ed.), Andesites. John Wiley & Sons.

Plafker, G., Savage, J.C., 1970. Mechanism of Chilean earthquakes of May 21 and May 22, 1960. Geol. Soc. Amer. Bull. 81, 1001–1030.

Pritchard, M.E., Simons, M., 2004. Geophys. Res. Lett. 31, L15610.

Ramsay, J., Huber, M., 1987. The techniques of Modern Structural Geology. Folds and Fracturs, vol. 2. Academic Press, London. 462 pp.

Rapela, C., Pankhurst, R., 1992. The granites of northern Patagonia and the Gastre Fault System in relation to the break-up of Gondwana. In: Alabaster, T., Pankhurst, R. (Eds.), Magmatism and Causes of Continental Break-Up, Storey, B. Geological Society, Special Publication, vol. 68, pp. 209–220.

Rebaï, S., Phillip, H., Dorbath, L., Borissoff, B., Haessler, H., Cisternas, A., 1993. Active tectonics in the lesser Caucasus: coexistence of compressive and extensional structures. Tectonics 12, 1089–1114.

Richard, P., Cobbold, P., 1990. Experimental insights into partitioning of fault motions in continental convergent wrench zones. Ann. Tecton. IV, 35–44.

Rodríguez, C. 1999. Geoquímica del Grupo Carrán–Los Venados, Andes del Sur (40.3°S). Universidad de Chile, thesis (unpublished). 133 pp. Santiago.

Roman, D., Moran, S.C., Power, J.A., Cashman, K.V., 2004. Temporal and Spatial Variation of Local Stress Fields before and after the 1992 Eruptions of Crater Peak Vent, Mount Spurr Volcano, Alaska. Bull. Seismol. Soc. Am. 94 (6) (p.).

Sepúlveda, F., Lahsen, A., Bonvalot, S., Cembrano, J., Alvarado, A., Letelier, P., 2005. Morpho-structural evolution of the Cordón Caulle geothermal region, Southern Volcanic Zone, Chile: Insights from gravity and $^{40}Ar/^{39}Ar$ dating. J. Volcanol. Geotherm. Res. 148, 165–189

SERNAGEOMIN, 1998. Estudio geológico-económico de la X^{a} región norte, Chile. Servicio Nacional de Geología y Minería, Informe Registrado IR-9815, 6 Vols., 13 sheets 1:100,000 scale. Santaigo.

SERNAGEOMIN, 2002. Mapa Geológico de Chile, escala 1:1.000.000. Servicio Nacional de Geología y Minería, Carta Geológica de Chile. Santiago.

Sibson, R., 1985. A note on fault reactivation. J. Struct. Geol. 7, 751–754.

Sibson, R., 1987. Earthquake rupturing as a mineralizing agent in hydrothermal systems. Geology 15, 701–704.

Sibson, R., Robert, F., Poulsen, K.H., 1988. High-angle reverse faults, fluid-pressure cycling, and mesothermal gold-quartz deposits. Geology 16, 551–555.

Sigmarsson, O., Condomines, M., Morris, J.D., Harmon, R.S., 1990. Uranium and ^{10}Be enrichments by fluids in Andean arc magmas. Nature 346, 163–165.

Sigmarsson, O., Martin, H., Knowles, J., 1998. Melting of a subducting oceanic crust from U–Th disequilibria in austral Andean lavas. Nature 394, 566–569.

Spalletti, L.A., Dalla Salda, L.H., 1996. A pull-apart volcanic related Tertiary basin, an example from the Patagonian Andes. J. South Am. Earth Sci. 9 (3–4), 197–206.

Takada, A., 1994. The influence of regional stress and magmatic input on styles of monogenetic and polygenetic volcanism. J. Geophys. Res. 99, 13,563–13,573.

Teyssier, C., Tikoff, B., Markley, M., 1995. Oblique plate motion and continental tectonics. Geology 23 (5), 447–450.

Tibaldi, A., 1995. Morphology of pyroclastic cones and tectonics. J. Geophys. Res. 100, 24,521–24,535.

Toda, S., Stein, R.S., Sagiya, T., 2002. Evidence from the AD 2000 Izu islands earthquake swarm that stressing rate governs seismicity. Nature 419, 58–61.

Tolson, G., Alaniz-Alvarez, S.A., Nieto-Samaniego, A. 2001. ReActiva, a plotting program to calculate the potential of reactivation of preexisting planes of weakness. Instituto de Geología, Universidad Autónoma de México. http://geologia.igeolcu.unam.mx/Tolson/Software/ReActivaV24En.exe.

Withjack, M.O., Jamison, W.R., 1986. Deformation produced by oblique rifting. Tectonophysics 13, 1061–1078.

Wood, D., Joron, J., Treuil, M., Norry, M., Tarney, J., 1979. Elemental and Sr isotope variations in basic lavas from Iceland and the surrounding ocean floor. Contrib. Mineral. Petrol. 70, 319–339.

Zoback, M.L., Zoback, M., 1980. State of stress in the conterminous United States. J. Geophys. Res. 85, 6113–6156.

4.3 Mouvements verticaux holocènes et volcanisme contemporain dans la ZFLO

La Zone de Faille de Liquiñe-Ofqui (ZFLO) est une structure d'intra-arc parallèle à la marge qui a été impliquée dans la croissance orogénique et le magmatisme pendant le Cénozoïque. Des déformations ductiles représentées par des mylonites suggèrent un cisaillement latéral important en régime de transpression et des déformations fragiles superposées se sont développées en réponse aux régimes de transpression et/ou aux régimes de compression. En outre, les failles mésoscopiques principales N-S de la ZFLO avec des traces de stries horizontales abondantes suggèrent également une déformation fragile avec un déplacement décrochant dextre. Ainsi, on a largement pensé que durant la majeure partie de son existence, la ZFLO montrait un glissement décrochant dextre important. Néanmoins, il n'y a pas que des miroirs de faille ou des évidences morphologiques pour un mouvement dextre dans le Quaternaire. D'ailleurs, la séparation verticale est le caractère le plus exceptionnel observable le long des failles principales. Le réseau de rivières montre également des discontinuités locales quand il est coupé par ces failles de premier ordre. En climat humide, l'équilibre topographique devrait être rapidement reconstitué, une partie au moins du déplacement vertical étant Holocène. Les mouvements et les soulèvements verticaux du substratum peuvent être provoqués par les forces tectoniques mais être également augmentés par le rebond isostatique régional, induit par l'érosion climatique et le soulèvement postglaciaire. Ce dernier aurait été intense pendant le Pléistocène et particulièrement après les derniers maximums glaciaires dans les Andes méridionales entre 38º et 46ºS. Les cônes monogéniques localisés sur la ZFLO ont des signatures géochimiques que l'on ne peut pas associer avec des fluides de la zone de subduction et seraient le résultat de la décompression adiabatique indiquée par des mouvements sporadiques possiblement verticaux de la ZFLO.

Article soumis a Tectonophysics (2006)

Quaternary vertical displacement along the Liquiñe-Ofqui Fault Zone: relative uplift and coeval volcanism in Southern Andes?

L.E. Lara [1, 2,*], A. Lavenu [2, 3], J. Cembrano[4], J. Darrozes[2]

(1) Servicio Nacional de Geología y Minería. Chile

(2) Laboratoire de Mécanismes de Transferts en Géologie-Université de Toulouse III. France

(3) IRD (Institut pour le Recherche en Développement). France

(4) Universidad Católica del Norte. Chile

** corresponding author: Luis E. Lara/ lelara@sernageomin.cl*

Abstract

The Liquiñe-Ofqui Fault Zone (LOFZ) is a long-lived, margin-parallel, intraarc megastructure, which has been involved in both orogenic growth and magmatism during the Late Cenozoic. Ductile and superimposed brittle deformations have been developed as a response to mainly dextral transpressional or compressional regimes. Late Miocene to Early Pliocene mylonites record dextral shear localised along the master faults. In addition, mesoscopic faults in the main north-south traces have plenty of horizontal striae suggesting also a brittle right-lateral displacement of them. Thus, the LOFZ has been widely thought as a mostly right-lateral strike-slip fault zone imbedded in a transpressional setting. Nevertheless, there are scarce slickensides or morphological evidences for such a dextral movement during the Late Quaternary. Moreover, vertical separation is the more outstanding feature observable along the master faults. The river network also shows local discontinuities when cut by these first-order faults. In humid climates, topographic equilibrium should be fast restored and then, at least a part of the vertical displacement would be Holocene. Vertical movements can be caused by tectonic forces but also enhanced by the regional isostatic rebound, driven either by climatically-controlled erosion or postglacial uplift. The latter would have been intense during the Pleistocene-Holocene and especially after the Last Glacial Maxima in the Southern Andes between 38º and 46ºS. In addition, vertical movements with localized gravitational collapse could be related to coseismic deformation after giant subduction earthquakes.

A consistent Quaternary NE-oriented maximum horizontal stress accompanies both compressional and transpressional tensors along the volcanic arc, which support that part of this vertical displacement could be tectonic in origin. However, strike-slip (or transpressional) regimes can be also inferred from both the NE-trending flank cones alignments on stratovolcanoes and the isolated NE-trending volcanic clusters, which are widespread in the northern segment (38º-42ºS) of the LOFZ.

Therefore, competing transpressional and compressional regimes, with both strike-slip and vertical displacement, occur along the entire intraarc zone and are spatially and causatively related with a wide variety of volcanic outspurs. The most primitive Holocene basaltic magmas, which sample an aged mantle wedge, are related to mostly vertical offsets across the LOFZ and seem to ascend directly to the surface. In turn, NE-striking oblique-to-the-margin chains would be fed from an enriched mantle source, which has undergone an incipient differentiation and subsequent ascent and eruption controlled by transpression.

Compression and transpression can alternate (by shifting $\sigma 2$ and $\sigma 3$, with the same $\sigma 1$) because of local or regional factors as rock strength, inherited discontinuities and/or variations of the angle between the convergence vector and the margin trend. This shifting should be common in lowly oblique subduction zones, which show low strain partitioning and 'pure shear-dominated' strain regimes (cf. Tikoff and Teyssier, 1994). Arc volcanism would occur and evolve by the activity of 'valve faults' (cf., Sibson *et al*., 1988) in a bulk transpressional regime. Instead, sporadic vertical adjustments along the LOFZ either tectonic or exogenous in origin, would trigger monogenetic volcanism after induced decompressional melting. Thus, volcanic and orogenic processes seem to be coupled and that should be considered for understanding the arc architecture and the coeval relief building.

Keywords: Transpression, bedrock uplift, arc volcanism, Southern Andes

1. Introduction

The Southern Andes (33°-46°S) is a Quaternary volcanic arc located between the Pampean flat slab segment and the Nazca-Antarctic-South America triple junction (Fig.1). They overlap a Late Cenozoic orogenic relief that is a result of contrasting tectonic regimes that thickened the crust in the north but not so far in the south. The austral segment of the Southern Andes (37°-46°S) is a narrow yet imposing cordillera where episodic magmatic belts have been active along margin-scale intraarc fault zones. Magmatic fronts have been static from the Miocene and arc architecture was dominated by magma extrusion rates and tectonic regimes of the upper crust. The most outstanding feature of the southernmost provinces of the Southern Andean Volcanic zone (SSVZ) is the presence of a margin-parallel intraarc fault, the Liquiñe-Ofqui Fault Zone (LOFZ). The LOFZ is *ca*. 1000 km long-lived structure, which has evolved mainly in a transpressional setting coeval with pluton emplacement and superimposed Quaternary brittle deformation. LOFZ domain is bounded by two Cenozoic fold-and-thrust belts. East of LOFZ deformation is weak or completely absent (Fig. 1). Therefore, most of the intraplate strain should be absorbed along the intraarc structures. Rock uplift or lateral transport should be also localized along the LOFZ.

The most recent history of LOFZ include an EW contractional stage which was coeval with a broadening of the arc towards the east followed by a transpressional episode since *ca*. 1.6 Ma and subsequent arc narrowing (Lavenu and Cembrano, 1999; Lara and Folguera, 2006). While the Quaternary transpressional regime is widely inferred from fault populations, which include mesoscopic faults with horizontal striae, scarce displacement markers can be observed in the field or remote sensing images. In addition, a few focal mechanism of crustal earthquakes that accompanied eruptions define strike-slip regimes with the same NE-trending Maximum Horizontal Stress axis (S_{Hmax}). Instead, the first order lineaments, which are master faults of the LOFZ, coincide mostly with vertical distortions of the topography that are not always related with distinctive geological units. On the other hand, flank vents on stratovolcanoes are consistently aligned in a NE-SW trend, which can be interpreted as the S_{Hmax} direction following Nakamura (1977). This argument can be extended to the NE-striking alignments as proposed by Dhont *et al*. (1998). If cone alignments are supposed surface evidence of tension cracks, the overall regime should be dextral strike-slip. Thus, the LOFZ has been thought as a major strike-slip fault but no significant horizontal displacement has been actually observed, even in the southernmost segment near the Chile Triple Junction where Nazca, Antarctic and South America plates meet (*e.g*., Forsythe and Diemer, 2006). In addition, as was noted by Lara *et al*. (2006a) for the Cordón Caulle-Puyehue case-study (40°S), stress tensors define both contractional or transpressional regimes with R values ($R=\sigma2-\sigma1/\sigma3-\sigma1$) ranging from *ca*. 0.2 to 0.9. In this article we make a review of published structural data mostly by Lavenu and Cembrano (1999) and new studied sites providing a complete panorama of the along-arc variation of the Quaternary tectonic regimes in the 38°-42°S segment in Southern Andes. The latter is complemented with a morphometric study of volcanic centres and transversal chains obtaining independent estimates of the S_{Hmax}. A numerical approach is used to describe geomorphological discontinuities as vertical separation along the LOFZ master faults or river network anomalies. After that, these evidences are confronted with some first order features of the convergent margin (obliquity, trench direction, first-order relief) searching a dynamic cause of the nearly coeval Holocene compression and transpression together with the related arc volcanism. Finally, some key geochemical features of Holocene magmas are explored to understand the effects of such competing tectonic styles along the arc.

2. Methodological issues

Because of the nature of the problem, we use a combined approach to understand the effect of crustal tectonics on relief building and coeval volcanism in the central Southern Andes. First, considering the widely recognised influence of climate on the orogenic evolution, a regional-scale inspection of first order features was based on digital elevation models, after a GIS-assisted numerical correction. Published exhumation rates were used to constrain erosive and tectonic effects. Vertical separation along the master faults was analysed in detail over SRTM digital elevation models (3 arc-second/90-meter horizontal resolution; 15 meter vertical resolution) for selected areas by means of automatic extraction of the river network (D8 algorithm in RiverTools® package) and calculation of some key morphometric parameters of the streams. On the other hand, published and new stress tensors were numerically derived from microtectonic analysis of fault populations using an inverse algorithm

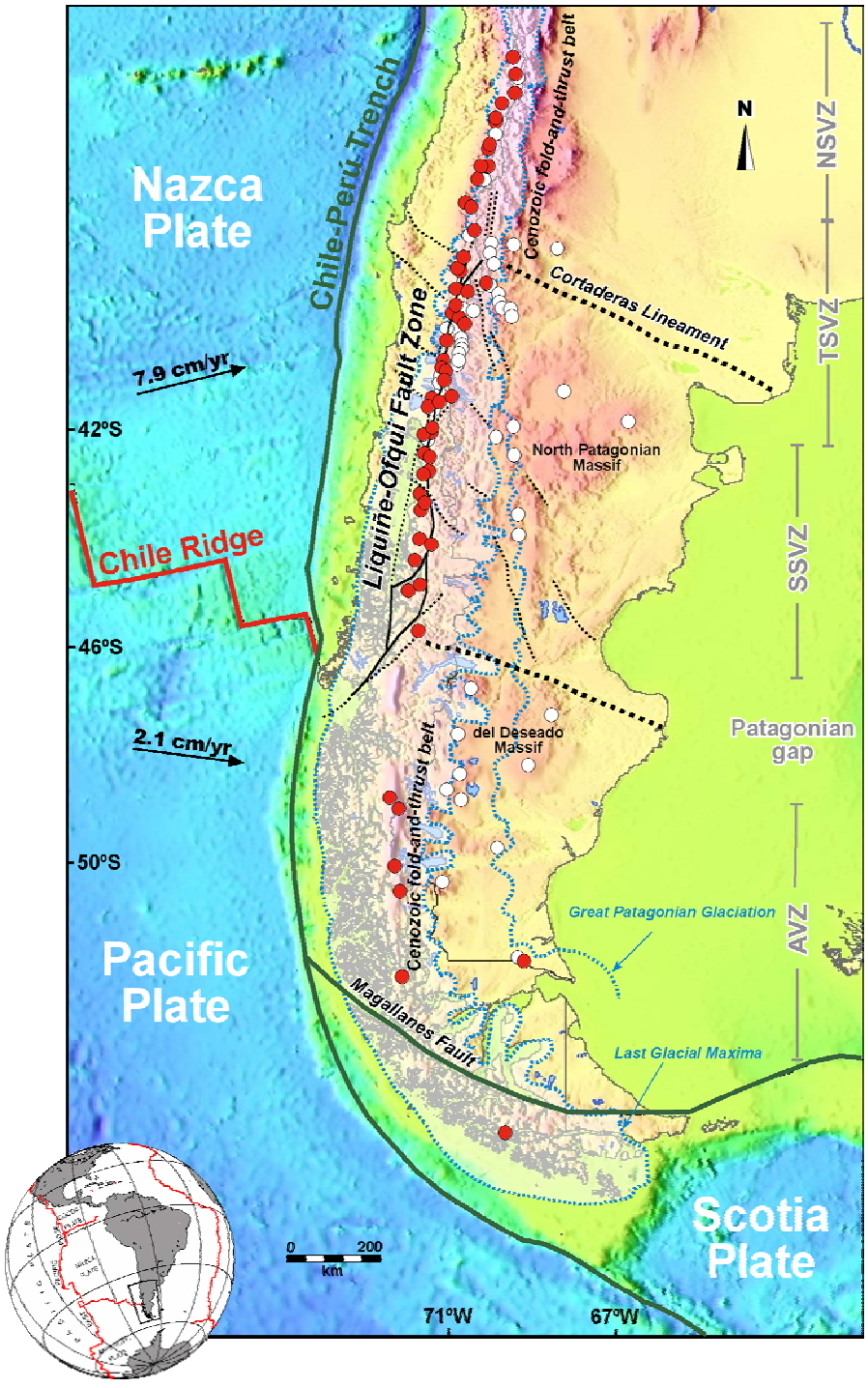

Fig. 1. Liquiñe-Ofqui Fault Zone (LOFZ) and Cenozoic volcanic provinces of Southern Andes. Upper Pliocene-Early Pleistocene (white) and Pleistocene-Holocene volcanoes (black/red) are also indicated. Extension of glacial ice during the Last Glacial Maxima (~32-14 ka) and the Great Patagonian Glaciation taken from Hulton *et al*., (1994) and Singer *et al*., (2004). Convergence vector from DeMets *et al*. (1994). Foreland Cenozoic fold-and-thrust belts are also indicated bounding the undeformed backarc block east of LOFZ.

by means of the ECG-Geoldynsoft software (Carey and Mercier, 1987). Test of compatibility were carried-out before numerical computation. Incompatible faults or having dubious slip sense were removed and only with up to 10 faults from two antithetic sets a stress tensor was calculated. As was noted by Lavenu and Cembrano (1999), a pre-Quaternary EW compressional event was recorded at several sites and excluded in this study. Stress tensors were analysed for instability of secondary axis and the ellipsoid shape ratio R, which allow to

distinguish between compressional and transpressional regimes even whether they have similar σ1. As a complement, S_{Hmax} (Maximum Horizontal Stress axis direction) was inferred from the volcanic morphology of flank cones and oblique-to-the-margin monogenetic cone alignments (*e.g.*, Tibaldi, 1995; Dhont *et al.*, 1998; Lara *et al.*, 2006a). Geochemical patterns of both, LOFZ-related cones and oblique NE-striking volcanic alignments are discussed in order to understand the effect of tectonics on volcanic evolution of primitive magmas.

3. Regional-scale geomorphology: climate and tectonic effect on rock uplift

As discussed noticeably by Rosenau (2004) and references therein, both tectonic and isostatic uplift (due to erosional unloading) act on a regional scale (10^3 - 10^4 km^2) and a time scale of about 10^4 years. Consequently, even high rates of regional erosion do not force the mean elevation of an area to depart from its isostatically balanced level by more than a few tens of meters (England and Molnar, 1990; Burbank and Anderson, 2001). However, isostatic uplift due to postglacial rebound, especially after a fast ice retreat of a thick glacial cover could produce a near instantaneous surface uplift (*e.g.*, Montgomery *et al.*, 2001), even accompanied by seismic renewal as observed in North America or Greenland (*e.g.*, Thorson, 1996; Grollimund and Zoback, 2001)

Rosenau (2004) also compared exhumation patterns of the North Patagonian Batholith along the 38°-42°S segment in Southern Andes with the mean elevation trend and he notice that high exhumation rates derived from Al-in-hornblende geothermobarometry and zircon and apatite fission-tracks (Cembrano *et al.*, 2002; Thomson, 2002; Seinfert *et al.*, 2005, Adriasola *et al.*, 2005) correspond to zones of low mean elevation. This suggests that rock uplift is controlled significantly by erosion. In this arc segment, elevation decreases from *ca.* 1200 m at 37°S to *ca.* 700 m at 43°S whereas the level of erosion) increases from *ca.* 3 km to *ca.* 15 km (Thomson, 2002; Seinfert *et al.*, 2005).

On the other hand, postglacial rebound that causes surface uplift can be also a key factor for understanding vertical movements in Southern Andes. In fact, ice-cover during the last Pleistocene glacial advance (Llanquihue glaciation after Porter, 1981) between 90-14 ka (Laugenie, 1982; Mercer, 1976, 1983; Heusser, 1990; Lowell *et al.*, 1995; Denton *et al.*, 1999) widely extended in the region where ice thickness reached up to 1 km along the valleys and the Equilibrium Line of Altitude (ELA) was

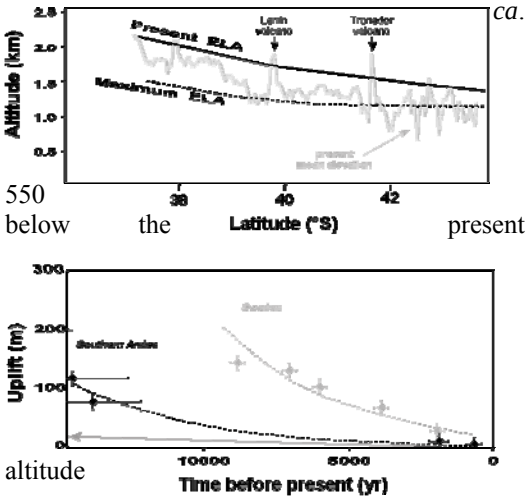

(a) Mean elevation, present Equilibrium Line of Altitude (ELA) and maximum ELA during the Last Glacial Maxima (taken from Hulton *et al.*, 1994). South of 39°S, increasing vertical displacement caused by both erosionally and tectonically driven uplift can be observed (see text for details). **(b)** Post Last Glacial Maxima isostatic rebound (<13 ka) calculated using Holocene emerged shells strata at Reloncaví estuary (41.5°S; Ota and Hervé, 1993) and archaeological sites at Calafquen Lake (39.2°S; Pino *et al.* 2004 *In* Lara and Clavero, 2004). A characteristic relaxation time (4400 yr; Turcotte and Schubert, 2002) was used assuming a fast ice retreat. For comparison, Holocene isostatic rebound in Sweden, where a thick glacial coverage was rapidly removed (Turcotte and Schubert, 2002).

(Hulton *et al.*, 1994). After the Last Glacial Maxima during the Llanquihue Glaciation (32-14 ka; Lowell *et al.*, 1995) the ice retreat was very fast (*e.g.*, Clapperton, 1993; Hulton *et al.*, 1994; Bentley, 1997) calling for an isostatic disequilibria. A rough estimation of the postglacial isostatic rebound can be made considering the ^{14}C age of Holocene uplifted sites and the exponential decay of surface displacement as material viscously flows from regions of elevated topography to areas of depressed topography ($\omega(t)=\omega_m e^{-t/\zeta r}$; where ω_m is the initial maximum vertical uplift and ζr is a possible characteristic time relaxation constant after Turcotte and Schubert (2002). Up to 100 meters of surface uplift can be due to such adjustment at 39-41°S but *ca.* 200-550 meters (Fig. 2) of vertical separation can be measured on mean elevations across the Andean cordillera. The point here is that a regional surface uplift due to postglacial rebound could change the mechanical state of faults and thus be resheared.

Considering some features of the river network, part of the total vertical separation observed in the average topography could be

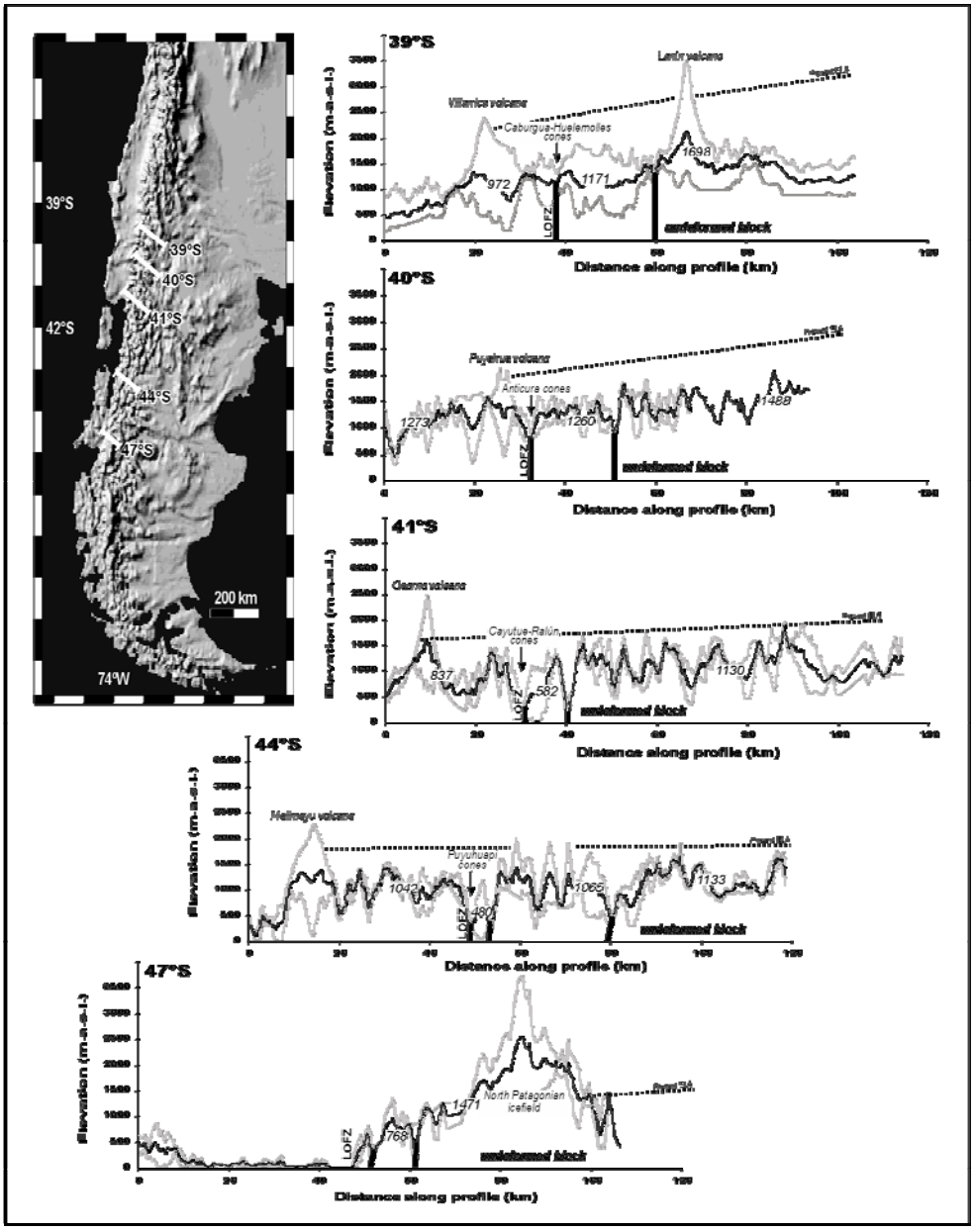

Fig. 3. Topographic swath profiles from SRTM Digital Elevation Models. Mean elevation is the altitude over which the area enclosed by positive relief equals the negative one along a segment.

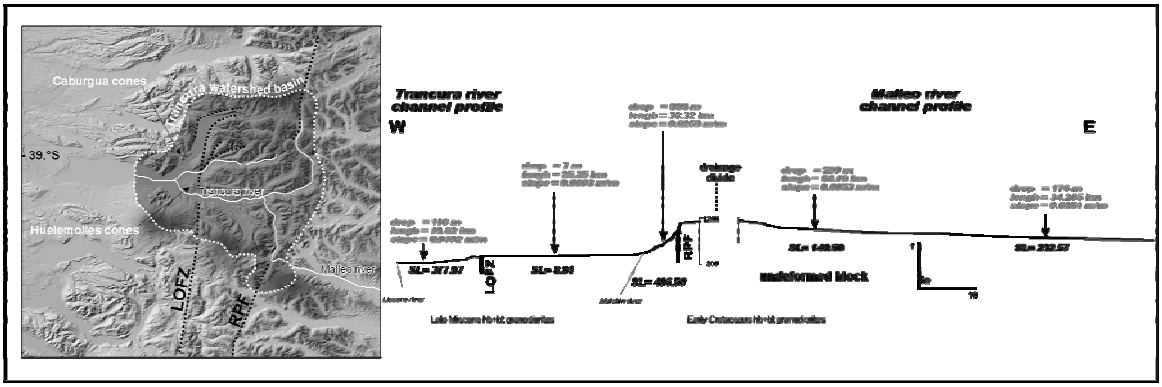

Fig. 4. Trancura watershed basin and along-channel profile (not to scale) for Trancura River with main stream indexes as sinuosity and stream power index (*SL*) shown. Note sharp contrast between structural blocks limited by LOFZ master faults not related to lithological boundaries.

in zircon FT ages across the LOFZ is another evidence for a significant component of post-Miocene vertical displacement, at least the depth of the zircon partial annealing zone (*ca*. 60 ºC or 1.3-2.6 km; Thomson, 2002).

Anyhow, whatever the relative amount of erosionally and tectonically driven uplift, differential vertical transport of rock masses occurs across the LOFZ master faults as demonstrated by the contrasting thermal histories and relief patterns across the structural system. Such a process provides the reason and circumstance for the deep-fed arc volcanism along the LOFZ.

4. Local-scale vertical displacement across the LOFZ

Suggesting but non conclusive evidences have been presented for Quaternary dextral block displacement along the LOFZ (*e.g*., Folguera *et al*., 2004; Rosenau *et al.* 2006). Moreover, where morphological features observed on surface can be linked with measured fault planes, they are related to tensional or transtensional tectonics (*e.g*., horse tails, tail cracks), mostly in the northern end of the LOFZ (e.g., Folguera et al., 2004; Rosenau et al., 2006). Normal faulting was also recognised by Forsythe and Diemer (2006) near the Chile Triple Junction on both surface morphology and submarine acoustic profiles. Although these features are compatible with a right-lateral displacement in a strike-slip (or transpressional-transtensional) regime, they are not a proof of a significant northward transport of forearc blocks.

Caburgua Lake (39°S): Near the northern terminus of the LOFZ, NE-striking secondary faults depart from the NS master fault, which is also cut by a NW-striking oblique structure that limits the Loncoche block (Chotin, 1975; Fig. 1). Eroded scarps facing west define the NS master fault. There, up to 200 m of vertical separation can be recorded from the mean altitudes. Farther east, the Reigolil-Pirihueico fault (Lara and Moreno, 2004) juxtaposes the easternmost undeformed block, which mean altitude is *ca*. 245 m higher (Fig. 3). The along channel profiles in the Trancura watershed basin also records changes across the master faults that are not related to geological limits (*e.g*., Lara and Moreno, 2004). Eastern and western blocks have rivers with steep profiles, low sinuosity (along channel length divided by straight-line length) and high SL stream-gradient indexes (Hack, 1973) (Fig. 4). In contrast, Trancura River on the central block meanders along a wide flat valley (Fig. 4). Considering the high regime of precipitation in the area (*ca*. 2000 mm/yr annual average) and the consequent high river flow (>250 m^3/s), high erosion rates should be expected and therefore, such a fluvial anomalies should be young, probably Holocene. A mostly compressional stress tensor was obtained by Lavenu and Cembrano (1999) in this site. There are some field evidences of Holocene surface uplift as subaqueous facies of *ca*. 14 ka ignimbrites from Villarrica volcano now exposed ~80 m above the present lake level (Moreno and Clavero, 2006); archaeological sites where estuarine beds are up to 100 m above the present shoreline of the Calafquen lake (Pino *et al*., *In* Lara and Clavero, 2004) and emerged lacustrine fluvioglacial deltas commonly found along the eastern shorelines of both lakes. Caburgua volcanic centers (5 pyroclastic cones) and Huelemolles (3 pyroclastic cones) lie above the hanging wall just in front of the scarp of the LOFZ .

Nilahue-Golgol river valleys (40°S):
North of Puyehue volcano, the LOFZ master fault appears as a NNE-striking lineament that run along the Nilahue river valley. It forms a west-facing eroded scarp on Pleistocene (*ca*. 500 ka) lavas from the Mencheca volcano (Lara *et al*., 2006a, b). In detail, this structure is defined by a Riedel shears array that limits the hanging wall to the east. Farther east, a parallel normal fault cuts these volcanic beds forming a horst that involves granitic basement (*ca*. 5 Ma; Sepúlveda *et al*., 2005) and where mostly compressional stress tensors have been obtained (Lara *et al*., 2006b). A significant vertical offset of *ca*. 230 meters occurs across an eastern branch of the LOFZ, which run farther east (Fig. 3). To the west, subaqueous Holocene lava flows appear now emerged at the shoreline of the Ranco Lake. South of the Puyehue volcano, the Anticura cluster (4 pyroclastic cones) lies on top of the master fault of LOFZ, which has not a sharp morphological expression.

Reloncaví estuary and fjord (41°S):
Along southern shoreline of Todos los Santos Lake the NS LOFZ master fault juxtaposes Miocene (*ca*. 10 Ma) to Late Cretaceous granitic rocks of the North Patagonoian Batholith (*ca*. 120 Ma; Adriasola *et al*., 2005 and references therein). Above the flat glacial valley the Cayutue volcanic cluster (11 pyroclastic cones) is located. Two isolated cones are located south along the master fault. Farther south, along the Reloncaví fjord, the LOFZ separates a central block with a mean elevation *ca*. 250 meters lower than the western block (Fig. 3). The Ralun cluster (3 pyroclastic cones) includes cones juxtaposed to the western

wall of the fjord or located in the middle of it. On the eastern wall of the fjord, emerged marine shell beds dated by Hervé and Ota (1993) as *ca*. 2050 and 750 yBP crop-out 3-7 meters above the present sea level. In that place an oblique NNE-striking fault departs from the main LOFZ trace and extends northward. Another uplifted *ca*. 550 meters above the central block occur to the east where the Tronador volcano is emplaced. Fission track thermochronology by Adriasola *et al*. (2005) show a Late Cenozoic differential transport between basement blocks.

Puyuhuapi fjord (44ºS):

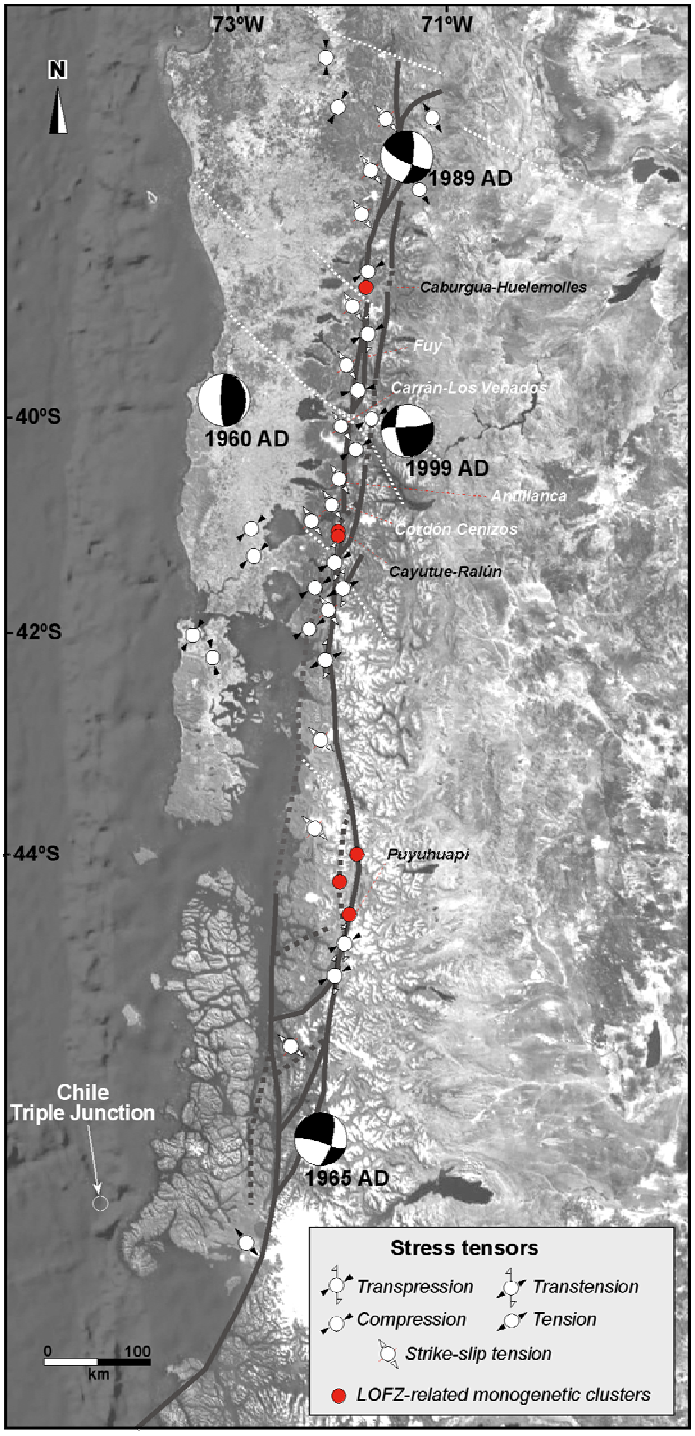

Fig. 5. (a) Stress tensors along the LOFZ domain (taken from Lavenu and Cembrano, 1999; Arancibia *et al*., 1999; Lara *et al*., 2006 and new unpublished data). Maximum horizontal stress axis inferred from volcanic morphometry. Local tensional regime only inferred from strain tensors in the northern end (Potent and Reuter, 2001; Rosenau *et al*., 2006) and acoustic submarine profiles or geomorphic features in the southern end (Forsythe and Diemer, 2006). Focal solutions for historical earthquakes taken from Chinn and Isacks (1983); Cifuentes (1989), Barrientos and Acevedo (1992) and the CMT-Harvard database.

As in the Relocaví fjord, a deeply eroded and narrow central block is bounded by two LOFZ master faults with mean elevation *ca*. 550 meters lower than the lateral blocks (Fig. 3). The Puyuhuapi cluster (9 pyroclastic cones) is located along the western LOFZ master fault. Farther east, another conspicuous master fault (Azul-Tigre Fault) limits the eastern undeformed block that is *ca*. 70 m higher than the westernmost ones. Fission track thermochronology by Thomson (2002) show a Late Cenozoic differential uplift between basement blocks but in the opposite sense the Holocene supposed separation.

San Rafael fjord (47°S):
Near to the southern end of the LOFZ, glacial erosion is extreme and the forearc block has been deeply flattened. The LOFZ master fault crops-out as a 25 km long fresh scarp with sag ponds on the hanging wall. This place was buried in *ca*. 0.5 meters during the last Mw:9.5 Chilean earthquake (Plafker y Savage, 1970; Muir-Wood, 1989; Barrientos y Ward, 1990; Barrientos et al., 1992) and at the present experiences the postseismic uplift evidenced by emerged died trees. The easternmost block, which is covered by the North Patagonian Icefield, is *ca*. 700 meters above the westernmost ones (Fig. 3). Fission track thermochronology by Thomson (2002) show a Late Cenozoic differential uplift in an east-vergent flower structure with exhumation rates decreasing eastward.

5. Transpressional and compressional regimes inferred from microtectonic analysis

Lavenu and Cembrano (1999) provided a complete dataset of fault populations for the 38°-44°S segment and performed a numerical inversion for stress tensors. Potent and Reuter (2001) and Rosenau *et al*. (2006) obtained strain tensors by means of the P-T diedra method for the 38º-42ºS segment. Although these conceptually different methods hamper a comparison, they yield a stable shortening axis striking roughly NE, which is compatible with the NE-striking S_{Hmax} deduced for the dextral transpression along the arc if plane strain is assumed. However, because of the triaxial nature of the transpressional regime and the observed vertical offsets along the LOFZ, we prefer the inverse algorithm for obtaining stress tensors and we have added some new measures that generate a representative set for a regional-scale analysis (Fig. 5).

A remarkable fact not discussed by Lavenu and Cembrano (1999) is that the Quaternary S_{Hmax} is always σ1 and roughly constant (N45-60°E) but the second horizontal axis is alternatively σ2 or σ3. Thus, the stress regime could be compressional (radial to unixial compression) or strike-slip (transpressional to transtensional as can be also observed in the R value (Ritz and Taboada, 1993). Three types of stress ellipsoids were obtained (see discussion and figure 8).

Stress regimes and their R values are spatially distributed and do not show a close relation with the basement geology or some first order features of the continental margin. Instead, high R values that characterize compressional regimes that are always found in places defined by abrupt relief changes related to vertical separation of structural blocks (Fig. 3).

6. Tensional domains inferred from volcanic morphology

A remarkable feature along the Southern Andes, mostly in the 38-42°S segment, is the presence of clusters of Holocene monogenetic pyroclastic cones, which are roughly NE aligned. In addition, several flank vents on top of the large stratovolcanoes show the same general trend. After the pioneer work of Nakamura (1977), the alignment of flank cones can be used as evidence of S_{Hmax} because it is thought that the flank vents are tension cracks fed by vertical dykes from the shallow magma reservoirs. According to Lister and Kerr (1991) deviatoric stress plays a key role in the initiation and orientation of dikes. For low viscosity magmas, dikes are expected to be oriented perpendicular to the minimum principal

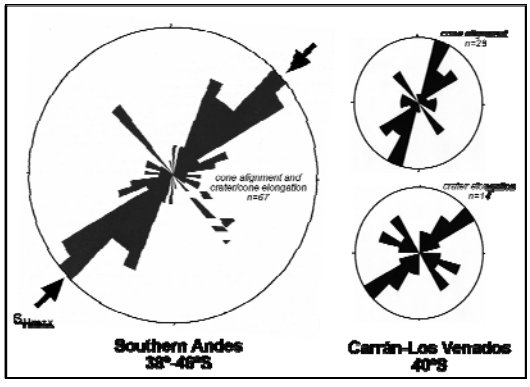

Fig. 6. (a) Rose diagram with average $S_{\square max}$ directions inferred from volcanic morphology, mostly first-order volcanic alignments and fissure trends, according to Nakamura (1977) and Tibaldi (1995). In a local-scale analysis not only cone alignment should be measured but also crater elongation and cone breaching directions. (b) Detail for Carrán-Los Venados cluster (40ºS) where cone alignment and cone elongation present some deviation (Lara *et al*., 2006). According to Tibaldi (1995), crater elongation presents a best correlation with the underlying faults and hence is preferred as

stress axis at all depths within the lithosphere (Emerman and Marrett, 1990). Hence, spatially associated volcanic alignments would reflect the direction of S_{Hmax}, which may be either $\sigma 1$ or $\sigma 2$ but in a strike-slip regime (transpression or transtension) S_{Hmax} must be $\sigma 1$. Analogue modelling by Tibaldi (1998) showed that monogenetic cones alignments can be also used for inferring S_{Hmax} when secondary morphometric features as cone breaching direction, cone elongation and crater elongation are considered. Thus, throughout a statistical treatment of the measured directions, a near NE-striking S_{Hmax} arise.

Characteristically, LOFZ-related monogenetic cones form random clusters and, yet aligned along the underlying faults, they have circular shapes without any elongation or anisotropy neither in the crater nor the basal contour. In addition, virtually all of them evolved from an early fissure stage with effusive volcanism to strombolian eruptions that built the pyroclastic cones with ballistic ejecta. As shown by Dhont *et al*., (1998), this kind of volcanic alignment reflect the trace of the underlying fault but no kinematic inferences can be made from them. East of the easternmost branch of LOFZ (Reigoli-Pirihueico Fault; Lara and Moreno, 2004), composite volcanoes present only radial distribution of flank cones (Lara *et al*., 2004), which is consistent with prevailing magmatic pressures inside the mostly undeformed backarc block.

7. Geochemical features and tectonic regimes

Basalts and basaltic andesites from the NE-striking volcanic chains, which are thought to represent tension cracks in a transpressional regime, were compared to mostly NS-striking volcanic clusters sitting on top of the master faults of the LOFZ. Sharp differences arise in

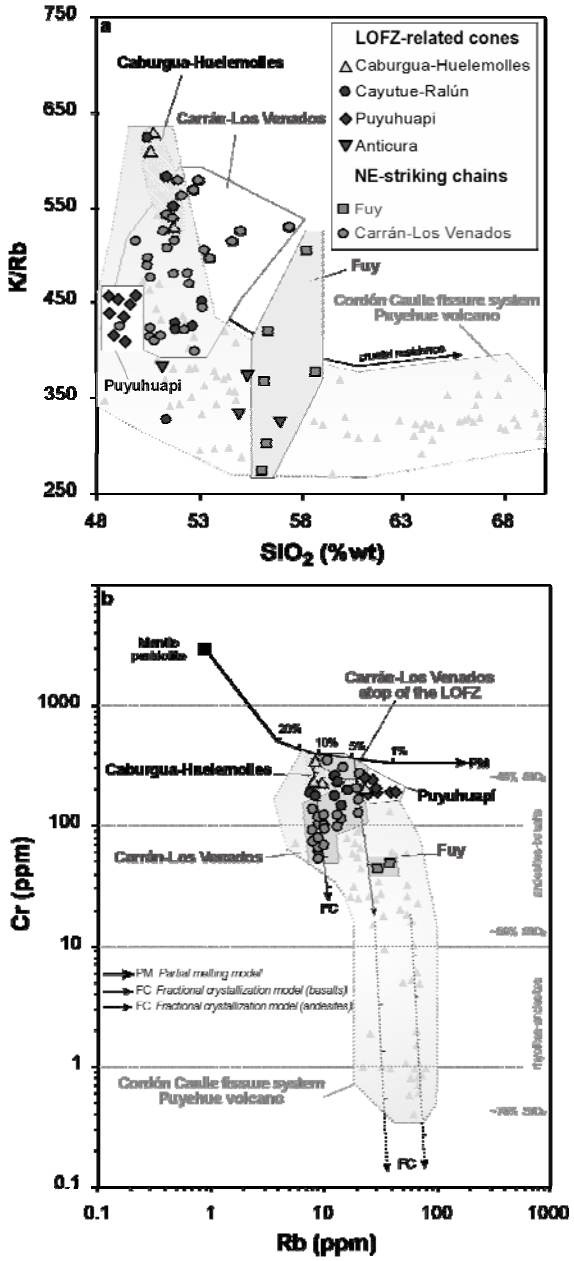

Fig. 7. Contrasting geochemical signatures of NE-striking volcanic clusters and LOFZ-related monogenetic cones based on highly incompatible elements. (a) High K/Rb ratios denote poor crustal interactions and probably rapid magma ascent of pristine LOFZ basalts while NE chains cover a wide compositional range with incipient crustal signature. Stratovolcanoes show the lowest K/Rb ratios, probably related with larger residence times in the uppermost magma chambers AFC (assimilation, fractionation, crystallization) processes take place. (b) Modified diagram by Pearce (1982). Raleigh fractional crystallization vectors were obtained by means of 'FC modeler' by Keskin (2002). Partial melting was calculated with a non-modal batch-melting model. Parental contents taken from McDonough *et al*. (1991) and Wood *et al*. (1979). LOFZ-related basalts are mostly obtained by lower degrees of partial melting. NE volcanic chains evolve from different basaltic end-members but following simple fractional crystallization processes of olivine and pyroxene. This pattern can be interpreted as direct ascent of basaltic dykes along the LOFZ and partially trapped magmas subsequently erupted from NE transversal chains (data taken from Gerlach *et al*., 1988; López *et al*., 1995; González-Ferrán *et al*., 1996; Rodríguez, 1999; Echegaray, 2004; Lara *et al*., 2006a).

major oxides contents and trace elements. For instance, LOFZ-related cones are mostly basalts but magmas from NE-striking chains have a wider compositional range (Fig.7). Basalts atop of the LOFZ are characterized by higher LREE/HREE (light rare earth elements/heavy rare earth elements), lower abundances of fluid-mobile elements like B, Cs, Rb, U, Pb, Ba and K, and lower $^{87}Sr/^{86}Sr$ ratios compared with the dominant basalt type erupted from stratovolcanoes or NE-striking volcanic clusters. Despite the possible differences in the subarc mantle source (*e.g*., Hickey-Vargas *et al*., 1989; López *et al*., 1995; Hickey-Vargas *et al*., 2002), magmas from LOFZ-related cones are derived from a depleted source by different degrees of partial melting followed by low pressure crystallization processes (Hickey-Vargas *et al*., 2002). Crustal interaction is scarce or occurs at shallow depths in phreatic eruptions as is a common feature in the Southern Andes (*e.g*., Hickey-Vargas *et al*., 1989).

In addition, contrasting differentiation patterns can be observed between NE chains and LOFZ basalts (Fig. 7). Once again, magmas from LOFZ-related cones seem to be more primitive liquids while NE-striking cones exhibit more evolved trends, which can suggest slightly larger residence times although their initial degree of mantle melting can be similar. Eruptive styles are also contrasting: whereas monogenetic LOFZ-related cones were built by effusive and weak strombolian eruptions, cones from the NE-striking chains erupted repeatedly in vigorous strombolian and vulcanian cycles.

A plausible explanation is that LOFZ-related cones were fed by mantle melts that ascended directly from the source to the surface. Hickey-Vargas *et al*. (2002) proposed that these basalts were mostly formed by a small degree of decompression melting of an aged mantle wedge. Such a process, which requires a transient tension drop, should be triggered by local or regional adjustments along the LOFZ, which would be probably fast and without significant wrenching. In turn, the predominant basalt type that fed stratovolcanoes or NE-striking chains formed by flux melting of mantle wedge with significant input from the active subduction zone.

8. Discussion

The uncertainty of age and rates of deformation

The age and evolution of Late Cenozoic deformation in the Southern Andes can be established only by regional criteria because local geochronological data is generally lacking (Lavenu and Cembrano, 1999). By correlation along the intraarc domain, the Quaternary dextral transpressional event can be constrained with a maximum age of *ca*. 3.6 Ma for the 37º-42ºS segment and *ca*. 1.6 Ma for the southernmost portion of the LOFZ (42º-46ºS). But actually, most stress fault populations were measured on granitic rocks with cooling $^{40}Ar/^{39}Ar$ ages between *ca*. 15 Ma and 4.5 Ma (Lavenu and Cembrano, 1999; Lara *et al*., 2006a, b). Because an EW Late Miocene-Early Pliocene compressional event was also widely recognised in the arc and forearc domains (Lavenu and Cembrano, 1999), fault populations were sorted and fault planes selected for the least-square statistical treatment. Thus, all bulk stress tensors are stable and represent the youngest tectonic event, which assumed to be Quaternary based on regional geochronological constrains.

On the other hand, regional-scale morphological features would have been acquired during the Late Miocene-Early Pliocene orogenic pulse (Cembrano *et al*., 2002; Thomson, 2002) and farther developed during the Pliocene-Quaternary period. However, drainage anomalies or disequilibria along the river network should be younger (Late Quaternary at least, even Holocene in part), and subsequently the vertical displacements that cause them. Postglacial rebound and coseismic deformation are suitable triggering processes.

What is remarkable is that Holocene monogenetic cones sitting on top of the LOFZ does not show any surface disruption. In addition, transversal river channels do not show any kind of lateral displacement or head captures. Only few strike-slip focal mechanisms and the NE-striking flank cones and volcanic clusters along the arc are a clue for an active dextral transpressional regime during the Holocene. Submarine acoustic profiling near the Chile Triple Junction (Forsythe and Diemer, 2006) show Late Holocene normal and thrust faulting, which is compatible with the transpressional regime but evidenced at surface only as local vertical displacements. The close spatial and temporal relations between LOFZ-related volcanisms and major vertical separation along the master faults call for a causative connection between them.

Compression and transpression as competing regimes

The regional NE dextral transpressional regime described by Lavenu and Cembrano (1999) seems to alternate with local compressional conditions, as occurs in the Cordón Caulle-Puyehue area (40°S; Lara *et al*., 2006a). However, a NE-striking $\sigma 1$ appears constant along the entire intraarc zone. Compressional regimes (northeast $\sigma 1$ and

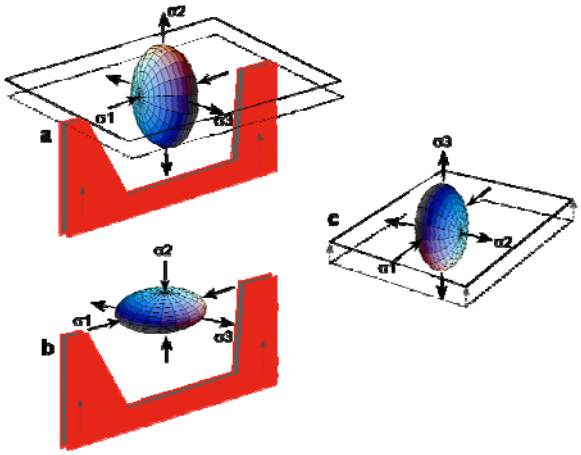

Fig. 8. Characteristic stress tensors found along the intraarc region and LOFZ in Southern Andes. Ινσταντανεουσ στραιν ελλιπσοιδσ αρε σηοων ϕ ορ ιλλυστρατινγ τηε ϕλυξ ματεριαλ. Μαγματιχ α σχεντ ισ ϕαϖουρεδ ωηεν σ3 is horizontal (figures a and b). Bedrock uplift is more efficient with transpression or pure compression (figures a and c). Transpression enhances both magma ascent and coeval orogenic growth.

vertical σ3) are especially clear where vertical separation occurs between blocks bounded by LOFZ master faults. In turn, transtension was documented mainly associated with large vertical offsets caused by normal faulting both at the northern and southern terminus of the LOFZ (Rosenau *et al*., in press; Forsythe and Diemer, 2006). Transpressional tensors occur frequently along the master faults either related to vertical separations or not. Thus, three types of stress tensors have been obtained (Fig. 8). When σ2 is vertical (transpression-transtension), magma ascent is favoured but bedrock uplift is only enhanced in the transpressional regime. In turn, compression inhibits magma ascent or arrests ascending dikes but promotes relief building. A plausible explanation for the shifting σ2 and σ3 stress axis and the absence of significant lateral displacement along the LOFZ can be found in the margin-scale strain field, which can be considered an analogue of the stress field in active tectonics (Teyssier *et al*., 1995). In fact, a small amount of partitioning for the strike-slip component can be deduced for a nearly orthogonal convergence, as occur in Southern Andes. In turn, highly oblique convergent margins (<20°) should produce wrench-dominated regimes with very active margin-parallel strike-slip faults (Withjack and Jamison, 1986; Richard and Cobbold, 1990) but this would be not the case of the LOFZ. Thus, the small component of lateral displacement could be absorbed either by only small-scale faults along the LOFZ, in the diffuse zone of deformation or as oblique tension cracks, represented at arc-scale by the NE-trending volcanic clusters

Monogenetic volcanism and tectonic regimes

LOFZ-related monogenetic cones are widely distributed along the entire system. Instead, NE-striking clusters are exclusively found in the northern segment between 38º-42ºS. NE-striking flank cones on stratovolcanoes are also widely recognised along the arc from Llaima (38.6ºS) to Maca (45.1º'S) volcanoes. Precise ^{14}C geochronology is scarce but some LOFZ-related cones seem to be early Holocene, as suggest their pyroclastic cover and dense forest on top as well. Ages from Villarrica volcano pyroclastic flows bracket the ages of Caburgua and Huelemolles cones between *ca*. 8000 and 6000 yBP (Clavero, 2004 *In* Lara and Clavero, 2004). In turn, Fui NE-striking cluster presents a multistage activity between *ca*. 9800 and 2400 yBP (Moreno and Lara, 2006) interbedded with Mocho-Choshuenco explosive volcanism. Carrán-Los Venados (40°S, 70 cones) erupted several times in the Holocene with 3 eruptions in the 20th century, including two phreatomagmatic cycles nested on Carrán maar (Moreno, 1977; Lara *et al*., 2006a). Cordón Cenizos cluster (41°S) is also a long-lived transversal chain that includes a Pleistocene stratocone and small cone built in the last centuries. Pyroclastic flows from Calbuco volcano bracket the age of a small cone of Cayutue-Ralún cluster between *ca*. 1730 and 1310 yBP (H.Moreno, written communication) but some of these cones could be older. Puyuhuapi cones remain undated.

Thus, LOFZ-related cones appear strictly monogenetic vents whereas NE transversal chains erupted frequently, formed long-lived transversal volcanic alignments and evacuated more evolved basalts and basaltic andesites.

Therefore, if LOFZ-related monogenetic volcanism is produced by decompression melting when sporadic major adjustments occur along the LOFZ, magmas from NE chains could be in turn explained as episodic ascent triggered by deep transpression expressed on the surface as vertical tension cracks following the S_{Hmax} trend. In that scenario, the LOFZ would provide a conduit to the surface for small magma batches that normally would be underplated in the MASH zone (Hildreth and Moorbath, 1988). However, the fault system would be sustained in the long-term mostly in response to the subduction-related mantle upwelling parallel to the trench

and hence a two-way coupling would be between transpression and volcanism. Instead, local and random vertical displacements along the LOFZ would trigger decompression melting and subsequent 'countercyclical' eruptions of monogenetic cones.

Isostatic rock uplift: slow climatically-driven erosion and fast postglacial rebound

Al-in-hornblende geobarometers and fission-track in Southern Andes show the widespread effect of climatically-driven erosion since the early Cenozoic (Rosenau, 2004). This slow process was enhanced by repeated Pliocene-Pleistocene glaciations that covered the entire Andean cordillera and even the forearc region south of 42°S (e.g., Denton et al., 1999). Up to 1 km thick glaciers coalesced and flowed to the western and eastern lowlands. Probably most of the cordilleran summits were totally ice-covered or cropped-out as 'nunatacks'. Glacial till and outwash sedimentary sequences, both piled at the forearc basins and the trench channel are evidence of the huge extended erosion (e.g., Bangs and Cande, 1997). For example, Quaternary infill of the Puerto Montt forearc basin reaches *ca*. 1336 meters as observed on deep wells made for oil exploration (Elgueta *et al*., 2000).

Paleogeographic evidence of fast ice-retreat during the Last Glacial Maxima (*e.g*., Lowel *et al*., 1995; Bentley, 1997; Denton *et al*., 1999) support the hypothesis of a significant postglacial rebound, which could have been induced vertical displacements of the LOFZ master faults followed by lateral spreading and erosion. At least *ca*. 100 meters would be the local effect of the Holocene isostatic rebound. At the northern North American cordillera this process was accompanied by increased seismicity (*e.g.,* Thorson, 1996; Grollimund and Zoback, 2001) but along a volcanic arc a seismic pumping (Sibson, 1985, 1987; Sibson *et al.*, 1988) could be the cause of the rapid magma ascent from a deep mantle source.

Coseismic deformation triggered by remote subduction earthquakes

In theory, static stresses transferred from large subduction earthquakes could trigger fault reshearing and strain changes by tens of kilometres inland. Barrientos (1994) estimated on *ca*. 200 km the far-reaching effect of the Mw: 9.5 1960 AD Chilean earthquake and Lara *et al*. (2004) proposed the reactivation of a blind basement fault as the cause of the Cordon Caulle fissure eruption that occurred 38 hours after the giant shaking. In 1960 AD the LOFZ, which main trace run few kilometres east of the site of Cordón Caulle eruption, no evidence of displacement was reported although massive landslides clustered along it (Weischet, 1960). Not enough transmitted forces to reshear the coupled LOFZ?; extreme misorientation or absence of fluids for reducing the shear strength?. From the updated recurrence of large (Mw > 8.5) earthquakes along the 40°-42°S segment (Cisternas *et al*., 2005), the best chance for this mechanism returns each *ca*. 300 years or more. So these well known processes seems to be not enough for resheraing the LOFZ.

9. Conclusions

Despite the spatial and temporal relations between volcanism and first-order structural system, a causative connection between them can be established. However, this relationship presents different behaviour that help to explain the contrasting geochemical signatures, morphology and eruptive styles found in monogenetic and polygenetic volcanoes. The main conclusions can be summarized as follows:

(1) Quaternary deformation along the intraarc zone is defined either by coeval transpression/transtension or compression, both with same NE-striking $\sigma 1$.
(2) Vertical displacement of the LOFZ can be inferred from the regional-scale relief and disruptions of the river network. At least part of this surface uplift could be Holocene and caused by either isostatic rebound after fast deglaciation, remote-triggered coseismic deformation or the ongoing bulk transpression.
(3) NE-striking volcanic chains, which are thought to be large tension cracks, are fed by slightly evolved basaltic magmas emplaced during the active transpression.
(4) LOFZ-related cones would be fed by mantle upwellings caused by decompression melting after transient vertical adjustment along the LOFZ.

Acknowledgements
This work is part of a collaborative effort between IRD (France) and SERNAGEOMIN (Chile), partially developed at the LMTG (Laboratoire des Mécanismes de Transferts en Géologie, Université Paul Sabatier, Toulouse). Farther support was provided J. Cembrano and L.E. Lara by the 1060187 Fondecyt grant. R. Forsythe and M. Rosenau kindly shared some ideas about the ongoing tectonics in Southern Andes. Guest editors T. Sempere and M. Gerbault are kindly acknowledged. This is also a contribution to the Volcanic Hazards Programme of SERNAGEOMIN.

References

Arancibia, G., Cembrano, J. & Lavenu, A. 1999. Transpresión dextral y partición de la deformación en la Zona de Falla Liquiñe-Ofqui, Aisén, Chile (44-45ºS). *Revista Geológica de Chile* 26 (1), 3-22.

Bangs, N. L., Cande, S. C. 1997. Episodic development of a convergent margin inferred from structures and processes along the southern Chile margin. Tectonics 16 (3), 489-503.

Barrientos, S. 1994. Large earthquakes and volcanic eruptions. Pageoph 42 (1), 225-237.

Barrientos, S., Acevedo, P. 1992. Seismological aspects of the 1988-1989 Lonqimay (Chile) volcanic eruption. J Volcanol Geotherm Res 53, 73-87.

Bentley, M.J. 1997. Relative and radiocarbon chronology of two former glaciers in the Chilean Lake District. J. Quaternary Science 12, 25-33.

Bohm, M., Lüth, S., Echtler, H., Asch, G., Bataille, K., Bruhn, C., Rietbrock, A., Wigger, P. 2002. The Southern Andes between 36º and 40ºS latitude: seismicity and average seismic velocities. Tectonophysics 356, 275-289.

Burbank, D. W., and Anderson, R. S. 2001. Tectonic Geomorphology. Blackwell Science, Berlin, 274 p.

Campos, A., Moreno, H., Muñoz, J., Antinao, J., Clayton, J. y Martin, M. 1998. Area de Futrono-Lago Ranco, Región de los Lagos. Servicio Nacional de Geología y Minería, Mapas Geológicos No. 8, 1 sheet, 1:100.000 scale. Santiago.

Carey, E., Mercier, J.L. 1987. A numerical method for determining the state of stress using focal mechanisms of earthquake populations: application to Tibetan teleseisms and microseismicity of Southern Peru. Earth and Planetary Science Letters 82, 165– 179.

Cembrano, J., Hervé, F., Lavenu, A. 1996. The Liquiñe-Ofqui fault zone: a long-lived intra-arc fault Zone in southern Chile. Tectonophysics 259, 55-66.

Cembrano, J., Shermer, E., Lavenu, A., Sanhueza, A. 2000. Contrasting nature of deformation along an intra-arc shear zone, the Liquiñe-Ofqui fault zone, southern Chilean Andes. Tectonophysics 319, 129-149.

Cembrano, J., Lavenu, A., Reynolds, P., Arancibia, G.; López, G., Sanhueza, A. 2002. Late Cenozoic transpressional ductile deformation north of the Nazca–South America–Antarctica triple junction. Tectonophysics 354, 289– 314.

Chinn, D.S. & Isacks, B.L. 1983. Accurate source depths and focal mechanisms of shallow earthquakes in western South America and in the News Hebrides islands arc. *Tectonics* 2, 529-563.

Chotin, P. 1975. Les Andes Méridionales et la termination du Bassin Andin. Le Lonquimay (Chili) et le Neuquén (Argentine) (lat.38º45'S). Université Pierre et Marie Curie, Ph.D. thesis (unpublished), 303 p. Paris.

Cifuentes, I.L. 1989. The 1960 Chilean earthquakes. J Geophys Res 94: 665-680.

Cisternas, M., Atwater, B., Torrejón, F., Sawai, Y., Machuca, G., Lagos, M., Eipert, A., Youlton, C., Salgado, I., Kamataki, T., Shishikura, M., Malik, J.K., Rizal, Y., Rajendran, C.P., Husni, M. 2005. Predecessors of the giant 1960 Chile earthquake. Nature, v. 437, doi:10.1038.

Clapperton, C. 1993. Quaternary geology and geomorphology of South America. Elsevier Science new York, 779 p.

DeMets, C., Gordon, R., Argus, D., Stein, S. 1994. Effect of recent revisions to the geomagnetic reversal time scale on estimates of current plate motions. Geophys Res Lett 21, 2191-2194.

Denton, G.H., Heusser, C.J., Lowell, T.V., Moreno, P.I., Andersen, B.G., Heusser, L.E., Schluchter, C., and Marchant, D.R. 1999. Interhemispheric linkage of paleoclimate during the last glaciation: Geografiska Annaler 81, 107-153.

Dhont, D.; Chorowicz, J.; Yürür, T.; Froger, J.L.; Köse, O.; Gündogdu, N. 1998. Emplacement of volcanic vents and geodynamics of Central Anatolia, Turkey. J Volcanol Geotherm Res 62, 207-224.

Echegaray, J. 2004. Evolución geológica y geoquímica del centro volcánico Mocho-Choshuenco, Andes del Sur, 40ºS. Thesis (unpublished), Universidad de Chile, 121 p.

Elgueta, S.; McDonough, M.; Le Roux, J.; Urqueta, E.; Duhart, P. 2000. Estratigrafía y Sedimentología de las Cuencas Terciarias de la Región de Los Lagos (39-41º30'S). Boletín No. 57, Servicio Nacional de Geología y Minería, 50 p.

Emerman, S.H., Marrett, R. 1990. Why dykes?. Geology 18, 231-233.

England, P., Molnar, P. 1990. Surface uplift, uplift of rocks, and exhumation of rocks. Geology 18 (12), 1173-1177.

Folguera, A., Ramos, V.A., Hermanns, R., Naranjo, J.A. 2004. Neotectonics in the foothills of the southernmost central Andes (37º–38ºS): Evidence of strike-slip displacement along the Antiñir-Copahue fault zone, Tectonics 23, TC 5008, 23 p.

Forsythe, R., Diemer, J. 2006. Late Cenozoic movement associated with the arc-parallel Liquiñe-Ofqui Fault Zone and the Chile Triple Junction documented by acoustic profiling of shallow marine and lacustrine deposits of Southern Chile. Backbone of the Americas GSA meeting, Abstracts, p. 48, Mendoza.

García, A.R., Beck, M., Burmester, R., Munizaga, F., Hervé, F. 1988. Paleomagnetic reconnaissance of the Region de Los Lagos, southern Chile, and its tectonic implications. Revista Geologica de Chile 15, 13-30.

Gerlach, D., Frey, F., Moreno, H., López-Escobar, L. 1988. Recent volcanism in the Puyehue-Cordón Caulle Region, Southern Andes, Chile (40.5ºS): petrogenesis of evolved lavas. J Petrol 29, 333-382.

González-Ferrán, O., Innocenti, F., Lahsen, A., Manetti, P., Mazzuolli. R., Omarini, R., Tamponi, M. 1996. Alkali basalt volcanism along a subduction related magmatic arc: the case of Puyuhuapi Quaternary volcanic line, Southern Andes (44º20'S). In XIII Congreso Geológico Argentino, Actas, p. 549-565. Buenos Aires.

Graefe, K., Glodny, J., Seifert, W., Rosenau, M., Echtler, H. 2002. Apatite fission track thermochronology of granitoids at the south Chilean active continental margin (37º-42ºS): implication for denudation, tectonics and mass transfer since the Cretaceous. 5th International Symposium of Andean Geodynamics, Abstracts, p. 275-278, Toulouse.

Grollimund, B., Zoback, M.D. 2001. Did deglaciation trigger intrapalte seismicity in the New Madrid seismic zone?. Geology 29 (2), 175-178.

Hack, J. T. 1973. Stream-profile analysis and stream-gradient index. J. Res. Geol. Survey, 1 (4), 421-429.

Hervé, F., Ota, Y. 1993. Fast Holocene uplift rates at the Andes of Chiloe, southern Chile. Revista Geológica de Chile v. 20 (1), 15-24.

Heusser, C.J. 1990. Chilotan piedmont glacier in the southern Andes during last glacial maximum, Revista Geológica de Chile 17 (1), 3-18,

Hickey-Vargas, R., Moreno, H., López Escobar, L.; Frey, F. 1989. Geochemical variations in Andean basaltic and silicic lavas from the Villarrica-Lanín volcanic chain (39.5°S): an evaluation of source heterogeneity, fractional crystallization and crustal assimilation. Contributions to Mineralogy and Petrology 103, 361-386.

Hickey-Vargas, R., Sun, M., López-Escobar, L., Moreno-Roa, H., Reagan, M., Morris, J. and Ryan, J. 2002. Multiple subduction components in the mantle wedge: Evidence from eruptive centers in the Central Southern Volcanic Zone, Chile, Geology 30, 199-202.

Hill, D. P. 1977. A model for earthquake swarms. J. Geophys. Res. 82, 1347-1352.

Hildreth, W., Moorbath, S. 1988. Crutal contributions to arc magmatism in the Andes of Central Chile. Contributions to Mineralogy and Petrology 98, 455-489.

Hulton, N., Sugden, D., Payne, A., Clapperton, Ch. 1994. Glacier modelling and the climate of Patagonia during the Last Glacial Maximum. Quaternary Research 42, 1-19.

Keskin, M. 2002. FC-Modeler: a Microsoft® Excel© spreadsheet program for modelling Rayleigh fractionation vectors in closed magmatic systems. Computers & Geoscience 28 (8), 919-928.

Lamy, F., Kaiser, J., Ninnemann, U.S., Hebbeln, D., Arz, H.W., Stoner, J.S. 2004. Antarctic timing of surface water changes off Chile and Patagonian Ice Sheet response. Science 304, 1959-1962.

Lara. L.E., Lavenu, A., Cembrano, J.; Rodríguez, C. 2006a. Structural controls of volcanism in transversal chains: resheared faults and neotectonics in the Cordón Caulle-Puyehue area (40.5ºS), Southern Andes. J Volcanol Geoth Res (in press).

Lara, L.E.; Moreno, H.; Naranjo, J.A.; Matthews, S.; Pérez de Arce, C. 2006b. Magmatic evolution of the Puyehue-Cordón Caulle Volcanic Complex (40º S), Southern Andean Volcanic Zone: from shield to unusual rhyolitic fissure volcanism. J Volcanol Geoth Res (in press).

Lara, L.E., Clavero, J. (editors). 2004. Villarrica volcano (39.5ºS), Southern Andes, Chile. Servicio Nacional de Geología y Minería, Boletín No. 61, 66 p.

Lara, L.E., Folguera, A. 2006. The Pliocene to Quaternary broading and narrowing of the Southern Andean volcanic arc between 371 and 41ºS latitude. In S.M. Kay and V.A. Ramos , eds., Late Cretaceous to Recent magmatism and tectonism of the Southern Andean margin at the latitude of the Neuquén Basin (36-39ºS), GSA Special Paper (in press).

Lara, L.E., Moreno, H., 2004, Geología del área Liquiñe-Neltume: Servicio Nacional de Geología y Minería Carta Geológica de Chile, Serie Geología Básica No. 83, scale 1:100,000, 1 sheet, 101 p. Santiago.

Lara, L.E., Naranjo, J.A., Moreno, H. 2004. Rhyodacitic fissure eruption in Southern Andes (Cordón Caulle; 40.5ºS) after the 1960 (Mw: 9.5) Chilean earthquake: a structural interpretation. Journal of Volcanology and Geothermal Research 138, 127-138.

Laugenie, C. 1982. La région des Lacs, Chili méridional. Recherche sur l'évolution géomorphologique d'un piémont glaciaire quaternaire andin. Université de Bordeaux III, PhD. Thesis (unpublished), 822 p. Bordeaux.

Lavenu, A., Cembrano, J. 1999. Compressional and traspressional-stress pattern for Pliocene and Quaternary brittle deformation in fore arc and intra-arc zones (Andes of Central and Southern Chile). J Struct Geol 21, 1669-1691.

Lister, J.R., Kerr, R.C. 1991. Fluid-mechanical models of crack-propagation and their application to magma transport in dykes. Journal of Geophysical Research 96, 10049-10077.

Lliboutry, L. 1999. Glaciers of the Wet Andes. In Williams, R.S., and Ferrigno, J.G. (eds.), Satellite image atlas of glaciers of the world: South America: U.S. Geological Survey Professional Paper 1386-I.

López-Escobar, L., Cembrano, J., Moreno, H. 1995. Geochemistry and tectonics of the Chilean Southern Andes basaltic quaternary volcanism (37-46ºS). Revista Geológica de Chile 22 (2), 219-234.

Lowell, T. V., C. J. Heusser, B. G. Andersen, P. I. Moreno, A. Hauser, L. E. Heusser, C. Schlüchter, D. R. Marchant, and G. H. Denton, 1995. Interhemispheric correlation of late Pleistocene glacial events. *Science* 269, 1541–1549.

McDonough, W.; Sun, S.; Ringwood, A.; Jagoutz, E.; Hofmann, A. 1991. K, Rb and Cs in the Earth and Moon evolution of the Earth's mantle. Geochemical and Cosmochemical Acta, Ross Taylor Symposium Volume.

Mercer, J. H. 1983. Cenozoic glaciation in the southern hemisphere. Annual Reviews in Earth and Planetary Science 11, 99–132.

Mercer, J.H. 1976. Glacial history of southernmost South America. Quaternary Research 6, 125-166.

Montgomery, D. R., Balco, G., and Willett, S. D. 2001. Climate, tectonics, and the morphology of the Andes. Geology 29 (7), 579-582.

Moreno, H. 1977. Geología del área volcánica Puyehue-Carrán en los Andes del sur de Chile. Universidad de Chile, thesis (unpublished). 181 p. Santiago.

Moreno, H., Clavero, J. 2006. Geología del Volcán Villarrica, IX Región de la Araucanía. Carta Geológica de Chile, Serie Geología Básica, 1 mapa escala 1:50.000. (in press).

Moreno, H., Lara, L.E. 2006. Geología del Complejo Volcánico Mocho-Choshuenco, X Región de los Lagos. Carta Geológica de Chile, Serie Geología Básica, 1 mapa escala 1:50.000. (in press).

Muir Wood, R., 1989, Recent normal faulting at Laguna de San Rafael, Aisen Province, southern Chile: Departamento de Geología, Universidad de Chile, Comunicaciones 40, 57-68.

Nakamura, K. 1977. Volcanoes as possible indicators of tectonic stress orientation: principle and proposal. J Volcanol Geotherm Res 2, 1-16.

Pearce, J. 1982. Trace elements characteristics of lavas from destructive plate boundaries. In Andesites (Torpe, R., editor). John Wiley & Sons.

Plafker, G.; Savage, J.C. 1970. Mechanism of chilean earthquakes of May 21 y May 22, 1960. Geol Soc Am Bull 81, 1001-1030.

Porter, S. 1981. Pleistocene glaciation in the Southern Lake District of Chile. Quaternary Research 16 (3), 263-292.

Potent, S., Reuther, C.D. 2001. Neogene Deformationsprozesse im aktiven magmatischen Bogen Südzentralchiles zwischen 37° und 39°S. Mitt. Geol. Pal. Inst. Univ. Hamburg 85, 1-22.

Ritz, J.F.; Taboada, A. 1993. Revolution stress ellipsoids in brittle tectonics resulting from an uncritical use of inverse methods. Bulletin de la Société Géologique de France, 164 (4), 519-531.

Rodríguez, C. 1999. Geoquímica del Grupo Carrán-Los Venados, Andes del Sur (40.3ºS). Universidad de Chile, thesis (unpublished). 133 p. Santiago.

Rosenau, M. R. 2004. Tectonics of the Southern Andean Intra-arc Zone (38°-42°S). Ph.D. thesis, Free University, Berlin, Germany, 154 pp. (available online: http://www.diss.fuberlin.de/2004/280/index.html)

Rosenau, M.R., Melnick, D., Echtler, H. 2006. Kinematic constraints on intra-arc shear and strain partitioning in the Southern Andes between 38°S and 42°S latitude. Tectonics (in press).

Seifert, W., Rosenau, M. R., Echtler, H. 2005. Crystallization depths of granitoids of South Central Chile estimated by Al-in-hornblende geobarometry: implications for mass transfer processes along the active continental margin. N. Jb. Geol. Paläont. Abh. 236 (1/2), 115-127.

Sepúlveda, F., Lahsen, A., Bonvalot, S., Cembrano, J., Alvarado, A., Letelier, P. 2005. Morpho-structural evolution of the Cordo´n Caulle geothermal region, Southern Volcanic Zone, Chile: Insights from gravity and $^{40}Ar/^{39}Ar$ dating. J Volcanol Geoth Res 148 (1-2), 165-189.

Shaw, H. R. 1980. The fracture mechanisms of magma transport from the mantle to the surface. In Hargraves, R. B. (editor), Physics of Magmatic Processes, 201–264. Princeton University Press, New Jersey.

Sibson, R. 1985. A note on fault reactivation. J Struct Geol 7, 751-754.

Sibson, R. 1987. Earthquake rupturing as a mineralizing agent in hydrothermal Zones. Geology 15, 701-704.

Sibson, R., Robert, F., Poulsen, K.H. 1988. High-angle reverse faults, fluid-pressure cycling, and mesothermal gold-quartz deposits. Geology 16: 551-555.

Singer, B.S., Ackert, R.P., Guillou, H. 2004. $^{40}Ar/^{39}Ar$ and K-Ar chronology of Pleistocene glaciations in Patagonia. GSA Bull 116, 434–450.

Teyssier, C., Tikoff, B., Markley, M. 1995. Oblique plate motion and continental tectonics. Geology 23 (5), 447-450.

Thomson, S. N. 2002. Late Cenozoic geomorphic and tectonic evolution of the Patagonian Andes between latitudes 42° and 46°S: An appraisal based on fission-track results from the transpressional intra-arc Liquiñe-Ofqui fault zone. Geol. Soc. Am. Bull., 114 (9), 1159-1173.

Thorson, R.M., 1996, Earthquake recurrence and glacial loading in western Washington: GSA Bull 108, 1182-1191.

Tibaldi, A. 1995. Morphology of pyroclastic cones and tectonics. J Geophys Res 100, 24,521-24,535.

Turcotte, D.; Schubert, G. 2002. Geodynamics (2nd. Edition). Cambridge University Press. 456 p. Cambridge.

Weischet, W. 1963. Farther observations of geologic and geomorphic changes resulting from the catastrophic earthquake of May 1960 in Chile. Seism. Soc. Am. Bull. 53, 1237-1257.

Withjack, M.O.; Jamison, W.R. 1986. Deformation produced by oblique rifting. Tectonophysics 13, 1061-1078.

Wood, D.; Joron, J.; Treuil, M.; Norry, M.; Tarney, J. 1979. Elemental and Sr isotope variations in basic lavas from Iceland and the surrounding ocean floor. Contributions to Mineralogy and Petrology 70, 319-339.

Chapitre 5
Discussion

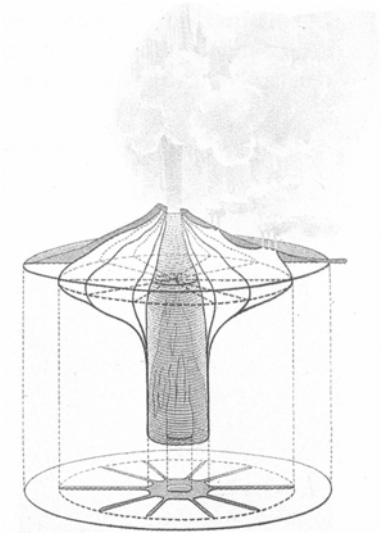

Chapitre 5. Discussion

5.1. Introduction

Comme il a été établi au début de cette étude, l'hypothèse de l'existence d'une relation causale entre néotectonique et volcanisme dans les Andes du Sud acquiert une validité en accord avec les résultats obtenus mais la nature de cette relation est complexe et variable. En effet, l'architecture de l'arc volcanique comme l'évolution magmatique et les styles éruptifs paraissent contrôlés par la tectonique de l'arc mais on démontre aussi que d'autres facteurs de premier ordre sont présents. Par exemple, à l'échelle de la marge des plaques, la géométrie de l'arc volcanique dépend des paramètres du système de subduction (angle de subduction, vitesse et direction de convergence). De même, la rhéologie de la lithosphère continentale détermine la manière dont le champ de contrainte s'exprime à l'intérieur de l'arc volcanique. Finalement, la nature fracturée de la croûte supérieure influence le champ de contrainte régional en induisant la réactivation de failles et une déviation des tenseurs de contrainte locaux, qui à leur tour contrôlent à plus petite échelle la présence du volcanisme d'arc.

5.2. Analyses des paléodéformations

Un aspect méthodologique qui mérite une révision est celui relatif à la validité de l'analyse des paléocontraintes. Une discussion de ces aspects a été récemment présentée dans le volume 28(6) (2006) du Journal of Structural Geology. Effectivement, des chercheurs préfèrent exprimer les données obtenues de l'analyse cinématique de populations de failles en termes de déformation (strain). À partir de cette prémisse, on peut seulement calculer des tenseurs de déformation finie qui représentent la déformation accumulée dans un volume de roche et on ne peut pas extrapoler à des interprétations dynamiques à l'échelle des plaques tectoniques. Par contre, l'analyse choisie dans cette étude assume qu'un champ de contraintes unique est le responsable du glissement sur un plan de faille et qu'il n'existe pas de rotations importantes

dans les blocs du substratum. Ces hypothèses sont raisonnables dans des études de néotectonique (Quaternaire) mais ne peuvent pas être extrapolées avec la même confiance à des déformations plus anciennes. Méthodologiquement, ces différentes méthodes d'analyse traitent les données avec des algorithmes différents. Tandis que l'analyse de déformation préfère, par exemple, la méthode des dièdres droits utilisée aussi en sismologie quand on ne connaît pas le plan de rupture mais seulement l'onde sismique propagée, l'analyse des contraintes se base sur des méthodes d'inversion qui calculent statistiquement le meilleur tenseur qui convient aux stries mesurées. Il existe plusieurs algorithmes d'inversion comme ceux de Carey et Brunier, (1974); Carey, (1979); Angelier (1984) et Etchecopar *et al*. (1981), la différence étant relativement petite dans l'analyse des nombreuses populations de failles. De même, il existe une importante discussion des termes de la validité statistique des analyses des paléocontraintes (*e.g.*, Orife et Lisle, 2006). On peut accepter comme seuil de validité que, en assumant les prémisses de l'analyse des contraintes, avec des populations d'au moins huit plans de failles appartenant à deux familles différentes mais compatibles, on peut obtenir des tenseurs stables pour l'analyse dynamique. D'autre part, les directions de contrainte maximale horizontale déduites des alignements volcaniques sont, par construction, une indication du champ de contraintes bien que sa validité requière d'assumer de possibles déviations dues à la fracturation préalable du substratum.

5.3 Age de la déformation

L'âge de la déformation traitée dans cette étude a été généralement un problème concret qui a été résolu au moyen de corrélations régionales. En effet, dû tant au faible taux de déplacement des failles d'intra-arc comme aux conditions climatiques qui compliquent la préservation des marqueurs de glissement ou des géoformes associées, les roches et les produits volcaniques quaternaires contiennent, de façon très exceptionnelle, des plans de failles. Par contre, les roches du substratum, principalement les granitoïdes du Batholite Nord Patagonien, montrent les meilleures expressions de la déformation. Toutefois, les âges K-Ar et $^{40}Ar/^{39}Ar$ de refroidissement des intrusifs qui

précèdent la déformation fragile atteignent des âges entre *ca*. 15 et 5 Ma. Dans quelques secteurs, les mylonites, associées à la déformation ductile contemporaine avec la mise en place des magmas, présentent des âges proches de 1.6 Ma (44ºS) qui limitent l'âge maximal de la déformation fragile superposée; ce critère a été extrapolé au segment d'étude (Lavenu et Cembrano, 1999). En effet, la déformation fragile compatible avec un tenseur de transpression dextre serait toujours postérieure à 1.6 Ma tandis que Lavenu et Cembrano (1999) reconnaissent un événement compressif préalable pliocène dont l'âge maximal dans le segment 38º-46ºS serait près de 3.6 Ma. La cohérence spatiale des tenseurs indique qu'ils représentent effectivement des phases tectoniques régionales et que, même s'ils étaient diachrones, ces âges, contenus dans ces limites bien définies, sont cohérents avec une déformation quaternaire dominée par la transpression dextre ou la compression avec σ_1 constant suivant la direction N-E comme l'indiquent les tenseurs calculés.

5.4 Architecture des arcs volcaniques

Les résultats obtenus montrent que l'architecture, c'est-à-dire, la distribution et la géométrie des centres volcaniques de l'arc, répond à des facteurs d'origine et d'échelle différentes. En premier lieu, la configuration de la zone de subduction (i.e. angle de subduction, déterminé à son tour par l'âge thermique de la plaque en subduction ; direction et vitesse de convergence) définit la position du front volcanique à *ca*. 112±19 km de profondeur au dessus de la surface de la plaque en subduction selon England *et al*. (2004) et la largeur de la région volcanique vers l'avant-pays (Shimozuru et Kubo, 1983). À l'échelle de chaque segment de marge, les structures d'intra-arc comme la ZFLO exercent un rôle déterminant dans la localisation des sites magmatiques en concentrant les centres émetteurs et en servant de canal d'ascension préférentielle. En même temps, la présence de la ZFLO est favorisée par la rhéologie de la lithosphère continentale dans laquelle elle se développe, laquelle est caractérisée par une composition basaltique, une faible épaisseur corticale et une importante épaisseur élastique (Tassara, 2005; Tassara *et al*., 2006) qui déterminent son comportement fragile. Finalement, à l'échelle de l'arc

volcanique, les structures préalables de la croûte supérieure continentale s'avèrent susceptibles à la réactivation ou appropriées comme canaux d'ascension passive en introduisant de nouvelles déviations de la géométrie attendue pour le champ de contrainte régional en vigueur. Cette somme de facteurs détermine la configuration finale de l'arc volcanique en montrant que dans des marges convergentes de long terme, il n'est pas possible que se développent des modèles géométriques simples du volcanisme.

5.5 Partition de la déformation

L'existence de tenseurs de contraintes compressifs et l'absence claire de marqueurs de déplacement dextre dans la ZFLO et, par contre, les réajustements verticaux du relief à travers cette structure, suggèrent une partition incomplète de la déformation dans la région d'arc et avant-arc. En effet, contrairement au modèle de partition complète proposé par Dewey et Lamb (1992) où l'arc absorberait totalement la composante latérale du vecteur de convergence, la partition serait partielle avec du raccourcissement et du transport vertical dans l'arc.

Mais ceci n'est pas rare dans une marge convergente avec une subduction presque orthogonale (*e.g.*, Teyssier *et al.*, 1995). Si les déplacements le long des plans de failles sont petits et la rotation des blocs n'est pas significative (García *et al.*, 1988; Cembrano *et al.*, 1992), les ellipsoïdes de la déformation finie et instantanée devraient être semblables et la contrainte horizontale maximum peut être interprétée comme l'axe du raccourcissement horizontal maximum (S_{Hmax}). Donc, selon Teyssier *et al.* (1995), le rapport entre S_{Hmax}, le vecteur de convergence et la limite de la frontière de marge de plaques, peut être appliqué pour estimer la partition. En effet, une faible quantité de partition (<5%) peut être déduite pour le segment de chaîne entre 37º et 42ºS. Cette condition aurait été le scénario depuis le Miocène, typique des régimes en 'cisaillement pur dominant' (Teyssier *et al.*, 1995) comme c'est le cas de l'île méridionale de la Nouvelle Zélande et d'une partie de l'arc japonais, parmi d'autres. Des degrés de partition plus élevés peuvent être atteints seulement avec une convergence plus oblique. Des modèles théoriques et empiriques (Withjack et Jamison, 1986; Richard et

Cobbold, 1990) proposent que les régimes 'wrench-dominated' avec des failles de glissement très actives peuvent être obtenus seulement avec des marges fortement obliques (α< 20º). Dans les Andes du Sud, la faible composante du déplacement latéral (<5%) devrait être absorbée dans la zone diffuse de la déformation ou en tant que fissures obliques de tension, représentées, par exemple, par les chaînons obliques des cônes monogéniques.

5.6 Tectonique et climat

Comme l'ont proposé Thomson (2002), Seifert *et al*. (2005) et Rosenau (2004), le climat du Cénozoïque exerce un important effet sur la tectonique des Andes du Sud. Et comme le montrent les données de traces de fission sur zircons et apatites, cet effet serait chaque fois plus important vers le sud. Pour cette raison, et considérant la grande extension des glaciers pendant la Grande Glaciation de la Patagonie durant le Pliocène ainsi que les glaciations du Pléistocène, il faut prendre en compte l'effet de chargement et de déchargement de la glace. Le rebond isostatique induit par érosion ou le retrait rapide des masses de glace induit d'importants taux de transport vertical à travers des failles dans l'arc. Cet ajustement vertical se superpose aux conséquences du régime transpressif et il pourrait, éventuellement, être un facteur dominant. L'ampleur du rebond isostatique induit par le climat et son effet spécifique sur le volcanisme est un aspect qui doit encore être élucidé.

5.7 Ascension magmatique, mis en place et temps de résidence dans la croûte

Les résultats obtenus montrent que, comme l'avaient indiqué antérieurement Cembrano et Moreno (1994), les domaines en compression de l'arc, en général, favorisent une plus grande résidence des magmas dans la croûte et une plus grande différenciation magmatique. Par contre, les domaines en extension favorisent l'ascension directe et l'éruption de magmas basaltiques bien que les domaines en compression soient aussi le lieu d'éruptions basaltiques, montrant ainsi la discontinuité temporaire du champ de contraintes. Toutefois, même si l'on peut établir des modèles pétrogénétiques de différenciation magmatique, les échelles de temps des processus sont encore

douteuses. Quelques tentatives basées sur des déséquilibres d'isotopes cosmogéniques (Sigmarsson *et al*., 1990; Tormey *et al*., 1991; Sigmarsson *et al*., 2002) montrent que les magmas basaltiques montent très rapidement depuis la source, de 10-100 mm/an à quelques heures à quelques jours à travers la croûte. Par contre, l'évolution des magmas silicatés est encore très difficile à quantifier.

Chapitre 6
Conclusions

Chapitre 6. Conclusions

6.1 Introduction

Comme résultat global de cette étude, on peut conclure qu'il existe effectivement une relation causale entre la néotectonique de l'arc volcanique quaternaire dans les Andes du Sud et le volcanisme dans le segment d'étude (37º-42ºS). Cependant, cette relation est encore complexe et polyvalente dans un milieu géodynamiquement simple (croûte continentale mince; subduction normale d'angle modéré). C'est pourquoi le volcanisme quaternaire (architecture de l'arc, évolution magmatique et pétrogenèse, styles éruptifs) est le résultat d'une intégration de facteurs parmi lesquels certains, externes, ont des influences comme le climat de la Patagonie. En effet, même s'il existe une importante continuité régionale du champ de contraintes (transpression dextre), on a reconnu des variations locales qui justifient des régimes compressifs et un transport vertical de masse. Le volcanisme, à son tour, est hétérogène comme l'expression des processus dans la région source du manteau asthénosphérique ou dans la croûte inférieure ainsi que de son transit et sa stagnation dans la croûte supérieure. Finalement, aussi bien le volcanisme que la tectonique du Quaternaire ont été fortement influencés par l'évolution préalable du segment et le résultat observé est la combinaison de ces facteurs.

6.2 Néotectonique

Malgré des hétérogénéités géologiques locales, le champ de contraintes quaternaire dans le segment 37º-42ºS de l'arc volcanique présente une grande régularité. Par exemple, la contrainte maximale horizontale déduite tant de l'analyse microtectonique de plans de failles que de l'orientation des centres volcaniques monogéniques ou des parasites, est toujours de direction NE (N50°-N60° E) et correspond à σ_1. La principale conséquence de ceci est que, en confirmant l'idée pionnière de Nakamura (1977), la disposition d'un important

ensemble de centres volcaniques de l'arc (interprétés comme l'expression en surface de ses dykes alimentés) est contrôlée par le champ de contraintes régional, idées développées dans les chapitres 3 et 4 au moyen des articles de Lara *et al*. (2006a) et Lara *et al*. (soumis). Évidemment, puisqu'il existe d'autres directions d'alignement volcanique, il existe aussi d'autres dispositions structurales.

Une autre conclusion importante découle de la découverte des tenseurs de contrainte avec σ_3 vertical (compression), occasionnels bien que non strictement associés à des caractéristiques morphologiques de premier ordre dans le relief, qui suggèrent un décalage apparent vertical. La conséquence de ce résultat est que le champ de contraintes serait aussi responsable de la croissance orogénique du segment de chaîne. Bien que le régime de transpression dextre contienne aussi une composante de raccourcissement, les régimes compressifs sont plus efficaces pour la construction du relief.

Un autre corollaire significatif est que les régimes compressifs inhibent l'ascension verticale des magmas en favorisant leur résidence dans l'écorce supérieure et la différenciation magmatique. Ainsi, pendant le Quaternaire, le champ de contraintes contrôlerait simultanément tant la distribution du volcanisme que la construction du relief, idées développées dans le chapitre 8 par l'article de Lara *et al*. (soumis).

Additionnellement, les variations spatiales et temporaires du champ de contraintes ont été examinées dans l'article de Lara *et al*. (2006a). Une partie du transport vertical, en tout cas, serait stimulée par des facteurs climatiques qui induiraient un ajustement isostatique suite à l'érosion glaciaire intense ou à une perte de charge rapide dans les cycles postglaciaires.

Finalement, une expression singulière de déformation dans la région de l'arc volcanique est celle associée à la propagation de la contrainte dynamique (déformation cosismique) lors des grands séismes de la zone de subduction. Dans le chapitre 3, l'article de Lara *et al*. (2004a) développe une analyse structurale de l'éruption fissurale du Cordón Caulle (40ºS) qui a suivi le séisme de Valdivia (Mw: 9.5). Vu la récurrence de ce type de séismes, les éruptions volcaniques dues à ce mécanisme pourraient être plus nombreuses que prévu et elles se superposeraient au régime de transpression/compression habituel dans la zone de l'arc volcanique.

6.3 Volcanisme et architecture de l'arc volcanique

L'architecture d'un arc volcanique, c'est-à-dire la géométrie du front volcanique, l'ampleur du volcanisme vers l'avant-pays, l'intensité exprimée en volume (ou surface) par unité de temps ou densité (linéaire ou par aire) des volcans dans chaque segment, entre autres caractéristiques, dépend d'abord de la configuration de premier ordre de la zone de subduction (principalement angle de subduction, vitesse et direction de convergence) et des caractéristiques géologiques et géophysiques de la lithosphère continentale (rhéologie, déformation préalable). Le chapitre 2 montre, au travers de l'article Lara et Folguera (2006) comment la vitesse de subduction a facilité le volcanisme durant le Quaternaire dans une région plus vaste que celle étudiée. Au début du Pléistocène, la ZFLO acquiert à nouveau la capacité de concentrer la déformation comme le volcanisme dans l'axe de la Cordillère Principale.

À son tour, le chapitre 4 montre au travers de l'article de Lara *et al*. (2006b) comment la nature des ruptures contrôle l'évolution morphostructurale du Complexe Volcanique Puyehue Cordón Caulle (40ºS). On peut observer dans ce cas d'étude comment la structure du substratum contrôle la distribution des centres émetteurs en facilitant même le volcanisme fissural dans des sites inattendus. A cette géométrie se superpose, à son tour, l'effet du champ de contraintes normal en produisant une configuration complexe en espace et en temps réduit.

6.4. Relations entre néotectonique et volcanisme

Les résultats obtenus et les conclusions que l'on en tire, suggèrent effectivement une relation causale entre la néotectonique de l'arc volcanique quaternaire dans les Andes du Sud et le volcanisme dans le segment d'étude (37º-42ºS). Loin des interprétations communes dans la littérature géologique sur le 'contrôle structural' du magmatisme, mentionnées principalement lors de l'association simplement spatiale entre les failles et les centres volcaniques ou les intrusions, la relation entre néotectonique et volcanisme est complexe

même dans un milieu géodynamiquement simple comme celui décrit pour le segment. Plusieurs facteurs interviennent dans les caractéristiques de l'arc volcanique, c'est-à-dire, l'architecture ou la distribution spatiale des centres émetteurs, l'évolution magmatique et la pétrogenèse ou les styles éruptifs. Parmi ces facteurs certains sont inhérents à la configuration de la marge convergente ou aux propriétés intrinsèques de la croûte continentale. Par conséquent, le champ de contraintes est installé dans un milieu hétérogène et opère sur lui en le modifiant ou en étant modifié par les caractéristiques locales. Cependant, il existe une importante continuité régionale du régime de déformation (transpression dextre ou compression) reflétée, par exemple, dans la cohérence de la contrainte maximale horizontale (équivalent à σ_1) d'orientation NE. De même, le champ de contraintes serait responsable, avec les facteurs climatiques externes, simultanément de la croissance orogénique et du volcanisme durant le Quaternaire. En dépit de la régularité régionale du champ de contraintes, on observe aussi d'importantes déviations locales qui expliquent mieux l'évolution des systèmes volcaniques. De même, cette évolution magmatique suggère aussi des variations temporaires du régime de déformation, probablement mises en rapport avec son intensité ou sa rotation selon les conditions locales.

Dans l'ensemble, on peut conclure que la relation entre volcanisme et tectonique est exprimée avec force dans la configuration spatiale de l'arc volcanique et dans l'évolution magmatique dans la croûte supérieure.

Dans le but de réaliser une synthèse et un modèle conceptuel, on peut établir que :

- Les domaines ou les chaînons volcaniques NW se situeraient sur les secteurs où les failles du socle, originellement senestres, seraient soumises à une contraction comme résultat d'un champ de contrainte régional de compression NE ou de transpression dextre NE. Dans ces secteurs, les magmas ont des compositions excessivement variées passant des basaltes aux rhyolites et le volcanisme présente des styles divers. Dans ces domaines de nombreux stratovolcans quaternaires se sont construits depuis *ca*. 600 ka, particulièrement ceux qui présentent un style éruptif complexe et où des phases de construction et de effondrement alternent avec des cycles éruptifs vigoureux. Dans ces

domaines, les magmas évolués auraient résidé plus longtemps dans la croûte en s'accumulant comme les complexes de filons, lesquels par la suite, par surpression magmatique, auraient modifier le champ de contrainte local pour monter finalement par de nouveaux conduits verticaux et pour générer à la surface, éventuellement, des contraintes locales extensives. Le cas typique le plus représentatif est le complexe Puyehue-Cordon volcanique Caulle (40°S).

- Les domaines ou les chaînons volcaniques NE seraient situés sur des secteurs sans structures reconnues dans le socle sous-jacent ni sur les flancs des stratovolcans. Ils correspondent à des zones de déformation en extension dans un champ de contrainte régional dominant transpressif dextre. Dans ces domaines se trouvent les cônes de flanc des stratovolcans et les chaînes transversales constituées de cônes monogéniques. Ils sont tous postglaciaires, c'est-à-dire plus jeunes que *ca*. 14 ka. Ces cônes sont essentiellement produits par des éruptions stromboliennes de basse énergie. Dans ces chaînons, les magmas couvrent un spectre de composition restreint qui va des basaltes aux andésites basaltiques et qui auraient résidé peu de temps dans la croûte. Un cas représentatif est le groupe volcanique Carran Los Venados (40°S)

- Les domaines NS se superposeraient à la Zone de Faille Liquine-Ofqui. Cette structure montrerait un déplacement dextre et/ou normal dans ses extrémités; mais dans le secteur central, son déplacement latéral n'est pas évident ou bien il présente des indices d'ajustement seulement verticaux à l'Holocène. Dans ce domaine se trouvent des cônes monogéniques postglaciaires, c'est-à-dire plus jeunes que *ca*. 14 ka. Les magmas émis depuis ces cônes sont principalement basaltiques et correspondent aux produits les moins évolués disponibles dans la ZVS. Les ajustements verticaux possibles répondraient aux processus externes qui se superposeraient au régime de transpression. On peut supposer que de tels ajustements auraient décomprimé le manteau asthénosphérique et ils auraient pompé des liquides primitifs directement

jusqu'à la surface. Un cas représentatif est celui-là du groupe de cônes Caburgua (39°S).

Les résultats obtenus pendant cette recherche sont un bon point de départ pour aborder ces nouveaux défis.

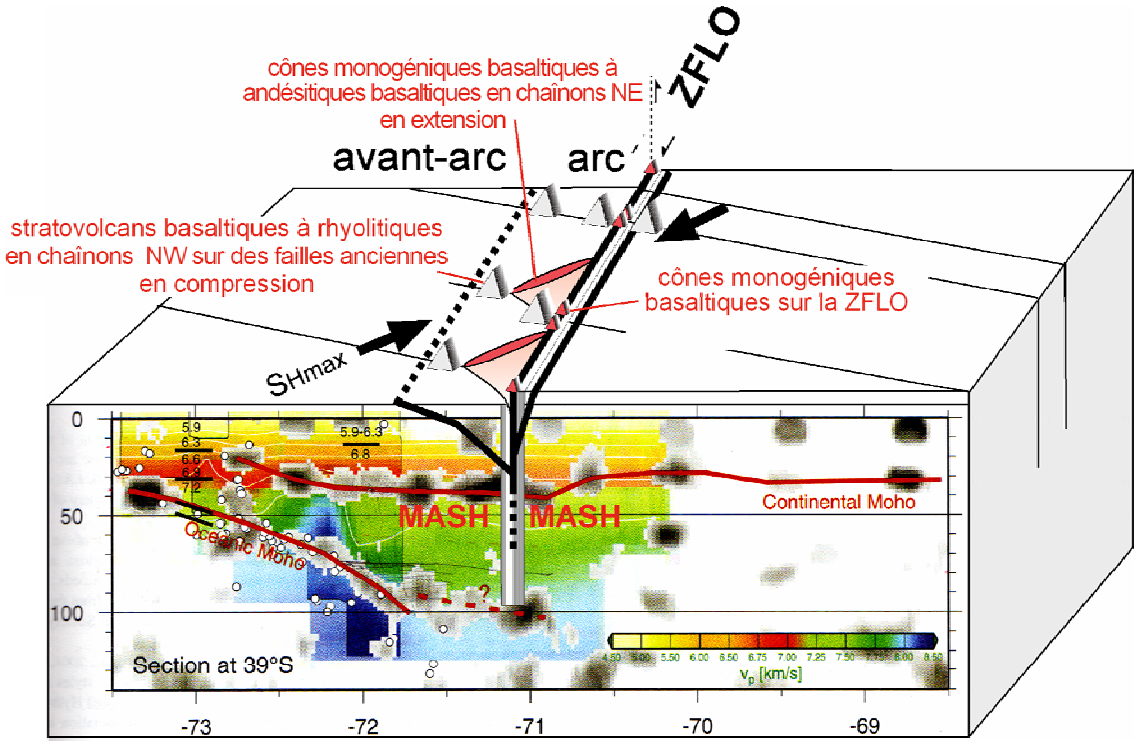

Fig. 6.1. Schèma interprétatif de la néotectonique et du volcanisme dans les Andes du Sud. Coupe sismique de Yuan *et al*., 2006. ZFLO : Zone de Faille Liquiñe-Ofqui ; MASH : Mixing, Assimilation, Storage, Homogenization (Hickey-Vargas *et al*., 1984)

6.5 Questions ouvertes et nouvelles approches

Quelques questions ouvertes dérivent de ce que l'on a examiné dans les paragraphes précédents. Par exemple, quel est l'effet spécifique de la charge exercée par la glace pendant une glaciation et son cycle postglaciaire et quel est son effet sur les systèmes volcaniques ? Les changements de pression pourraient particulièrement se refléter dans les systèmes magmatiques et dans la minéralogie des magmas. La géochimie de haute résolution pourrait éclairer l'évolution des cristaux individuels ou les inclusions fondues comme témoins du

déséquilibre. Comme certaines de ces réactions chimiques sont dépendantes de la pression, elles pourraient contribuer à comprendre l'ampleur des forces impliquées.

Un autre point important est lié à l'évolution temporaire du volcanisme associé à chaque domaine structural. En effet, l'âge précis des roches volcaniques quaternaires est un élément important pour restreindre les interprétations. Les roches volcaniques basaltiques et les roches silicatées, dans les Andes du Sud, sont pauvres en K et ne sont pas des transporteurs de minéraux appropriés pour les datations $^{40}Ar/^{39}Ar$. Toutefois, récemment, les techniques de laboratoire ont été améliorées considérablement en permettant de dater avec précision des roches du Pléistocène moyen à supérieur (500-50 ka) par laser de CO_2 dans le Laboratoire de Géochronologie du SERNAGEOMIN (*e.g.*, Lara *et al*., 2006b). Des résultats encore meilleurs ont été obtenus avec un appareillage de type 'four' (furnace) à l'Université de Wisconsin pour des roches du Pléistocène supérieur (100-13 ka; Lara *et al*. 2006b).

D'autre part, un défi fondamental est de lier l'information donnée par l'analyse microtectonique et la morphométrie volcanique avec la déformation à court terme donnée par les réseaux sismiques. Bien que les réseaux temporaires placés dans la région aient recueilli une faible sismicité corticale sous l'arc (*e.g.*, Bohm *et al*., 2002 ; Rietbrock *et al*., 2006), quelques domaines volcaniques, particulièrement ceux qui sont silicatés, montrent un signal riche en séismes de basse fréquence et occasionnellement en séismes volcano-tectoniques avec des phases P et S définies (Peña et Fuentealba, 2000) qui peuvent être interprétés comme représentatifs de l'ouverture de conduits d'ascension magmatique contrôlée par le champ de contraintes régional. Le meilleur exemple de ce processus est donné par l'éruption du volcan Lonquimay en 1989 (Barrientos et Acevedo, 1992) quand la fissure NE en surface à été accompagnée par un séisme de magnitude Mw: 5.3 avec un mécanisme au foyer décrochant compatible avec le régime de transpression dextre (Lavenu et Cembrano, 1999).

Chapitre 7
Références

Chapitre 7. Références

Acharya, H. 1982. Volcanic activity and large earthquakes. J. Volcanol. Geotherm. Res., 86, 335-344.

Adıyaman, O; Chorowicz, J.; Köse, O. 1998. Relationships between volcanic patterns and neotectonics in Eastern Anatolia from analysis of satellite images and DEM. Tectonophysics, 85, 17-32.

Adriasola, A., Thomson, S.N., Brix, M.R. & Stöckhert, B. 2005. Postmagmatic Cooling and Late Cenozoic Denudation of the North Patagonian Batholith in the Los Lagos Region of Chile, 41°-42°15'S. International Journal of Earth Sciences, 95, 504-528.

Alaniz-Alvarez, S., Nieto-Samaniego, A., Ferrari, L. 1998. Effect of strain rate in the distribution of monogenetic and polygenetic volcanism in the Transmexican volcanic belt. Geology, 26, 591-594.

Allmendinger, R.W.; Marrett, R.; Cladouhos, T. 1993. Software Fault kinematics v.3.8, Academic version.

Allmendinger, R.W.; Strecker, M.; Eremchuk, J.E.; Francis, P. 1989. Neotectonic deformation of the southern Puna Plateau northwestern Argentina. Journal of South American Earth Sciences, 2, 2, 111-130.

Anderson, E.M. 1936. The dynamics of the formation of cone sheets, ring dykes and cauldron subsidences. Proceedings of the Royal Society of Edimburgh, 56, 128-163.

Anderson, E.M. 1951. The dynamics of faulting and dyke formation with application to Britain. Oliver and Boyd, 206 p., Edinburgh.

Anderson, S.W., Fink, J.H. 1992. Crease structures: Indicators of emplacement rates and surface stress regimes of lava flows. Geological Society of America Bulletin 104, 615-625.

Angelier, J. 1994. Fault slip analysis and paleostress reconstruction. in Hancock P.L. (ed.), Continental deformation. 53-100, Pergamon Press, UK.

Angelier, J., Goguel J. 1979. Sur une méthode simple de détermination des axes principaux des contraintes pour une population de failles. Comptes Rendus de l'Académie des Sciences, Paris, 288, 3, D, 307-310.

Angelier, J., Mechler, P. 1977. Sur une méthode graphique de recherche des contraintes principales également utilisables en tectonique et en séismologie: la méthode des dièdres droits. Bulletin de la Société géologique de France, 19, 6, 1309-1318.

Angelier, J.; Tarantola, A.; Valette, B.; Manoussis, S. 1982. Inversion of field data in fault tectonics to obtain the regional stress 1: single phase fault populations: a new method of computing the stress tensor. Geophysical Journal of the Royal Astronomical Society, 69, 607-621.

Angermann, D.; Klotz, J.; Reigber, Ch. 1999. Space-geodetic estimation of the Nazca-South America Euler vector, Earth and Planetary Science Letters, 171, 3, 329-334.

Arancibia, G., Cembrano, J., Lavenu, A. 1999. Transpresión dextral y partición de la deformación en la Zona de Falla Liquiñe-Ofqui, Aisén, Chile (44°-45ºS). Revista Geológica de Chile 26, 1, 3-22.

Arancibia, G.; Matthews, S.; Pèrez de Arce, C. 2006. K-Ar and $^{40}Ar/^{39}Ar$ geochronology of supergene processes in the Atacama Desert, Northern Chile: tectonic and climatic relations. Journal of the Geological Society of London, 163, 107–118.

Armijo, R.; Carey, E.; Cisternas, A. 1982. The inverse problem in neotectonics and the separation of tectonic phases. Tectonophysics, 82, 145-160.

Armijo, R.; Cisternas, A. 1978. Un problème inverse en microtectonique cassante. Comptes Rendus de l'Académie des Sciences Paris, D, 287, 595-598.

Assumpçao, M., 1992. The regional intraplate stress field in South America. J. Geophys. Res., 97, 11,889–11,903.

Ayala, A. 1956. La erupción del Riñinahue. Revista Geográfica de Chile Terra Australis, 14, 52-64.

Bahar, I.; Girod, M. 1983. Controle structural du volcanisme indonesien (Sumatra, Java-Bali); application et critique de la methode de Nakamura. Bull. Soc. Geol. Fr., 7, 609-614.

Bangs, N. L., Cande, S. C. 1997. Episodic development of a convergent margin inferred from structures and processes along the southern Chile margin. Tectonics, 16, 3, 489-503.

Barreiro, B.A. 1984. Lead isotopes and Andean magmagenesis. In Andean magmatism: chemical and isotopic constraints (Harmon, R.S.; Barreiro, B.A.; editors). Shiva Geology Series, Shiva Publishing Limited, 21-30. Natwich, UK.

Barrientos, S. 1994. Large earthquakes and volcanic eruptions. Pageoph., 142, 1, 225-237.

Barrientos, S., Acevedo, P. 1992. Seismological aspects of the 1988-1989 Lonquimay (Chile) volcanic eruption. J. Volcanol. Geotherm. Res., 53, 73-87.

Barrientos, S.; Ward, S.N. 1990. The 1960 Chile earthquake: coseismic slip from surface deformation. J. Geophys. Int., 103, 589-598.

Bellier, O., Sébrier, M., 1994. Relationship between tectonism and volcanism along the Great Sumatran Fault deduced by SPOT image analyses. Tectonophysics, 233, 215–231.

Bengoa, J. 2003. Historia de los antiguos Mapuches del sur. Catalonia, Santiago.

Bentley, M.J. 1997. Relative and radiocarbon chronology of two former glaciers in the Chilean Lake District. J. Quaternary Science, 1, 25-33.

Berninghausen, W.H. 1962. Tsunamis reported from the west coast of South America. Seismol. Soc. Am. Bull., 52, 915-921.

Bertrand, S., Boës, X., Castiaux, J., Charlet, F., Urrutia, R., Espinoza, C., Lepoint, G., Charlier, B., Fagel, N., 2005. Temporal evolution of sediment supply in Lago Puyehue (Southern Chile) during the last 600 yr and its climatic significance. Quat. Res., 64, 163–175.

Best, J.L. 1992. Sedimentology and event timing of a catastrophic volcaniclastoic mass flow, Volcan Hudson, southern Chile. Bulletin of Volcanology, 54, 299-318.

Bird, P. 2003. An updated digital model of plate boundaries, Geochemistry Geophysics Geosystems, 4, (3), 1027, doi:10.1029/2001GC000252.

Blot, C. 1965. Relation entre les séismes profonds et les éruptions volcaniques au Japon. Bull. Volcanol., 28, 25-64.

Bohm, M., Lüth, S., Echtler, H., Asch, G., Bataille, K., Bruhn, C., Rietbrock, A., Wigger, P. 2002. The Southern Andes between 36º and 40ºS latitude: seismicity and average seismic velocities. Tectonophysics. 356, 275-289.

Bott, M.H.P. 1959. The mechanics of oblique slip faulting. Geological Magazine, 97, 2, 109-117.

Brasse, H., Soyer, W. 2001. A magnetotelluric study in the Southern Chilean Andes. Geophys. Res., Lett. 28, 3757-3760.

Brodsky, E.E.; Sturtevant, B.; Kanamori, H. 1998. Earthquakes, volcanoes, and rectified diffusion. J. Geophys. Res., 103, 23827- 23838.

Brüggen, J. 1950. Fundamentos de Geología de Chile. Instituto Geográfico Militar, Santiago.

Burbank, D. W., and Anderson, R. S. 2001. Tectonic Geomorphology. Blackwell Science, Berlin, 274 p.

Burns, W.M. 2002. Tectonics of the Southern Andes from stratigraphic, thermochronologic, and geochemical perspectives. Cornell University, thesis (unpublished), 204 pp.

Byerlee, J.D., 1978. Friction of rocks. Pure Appl. Geophys., 116, 615–626.

Cahill, T., Isacks, B. 1992. Seismicity and shape of the subducted Nazca plate. J. Geophys. Res., 97, 17503-17529.

Calder, E.; Harris, A.; Pea, P.; Pilger, E.; Flynn, L.; Fuentealba, G.; Moreno, H. 2004. Combined thermal and seismic analysis of the Villarrica volcano lava lake, Chile. Revista Geológica de Chile, 31, 2, 259-272.

Campos, A., Moreno, H., Muñoz, J., Antinao, J., Clayton, J., Martin, M. 1998. Area de Futrono-Lago Ranco, Región de los Lagos. Servicio Nacional de Geología y Minería, Mapas Geológicos No. 8, 1 mapa escala 1:100.000. Santiago.

Carey, E. 1979. Recherche des directions principales de contraintes associées au jeu d'une population de failles. Revue de Géographie physique et Géologie dynamique, 21,1, 57-66.

Carey, E., Brunier, B. 1974. Analyse théorique et numérique d'un modèle élémentaire appliqué à l'étude d'une population de failles. Comptes Rendus de l'Académie des Sciences, Paris, D, 269, 891-894.

Carey, E., Mercier, J.L. 1987. A numerical method for determining the state of stress using focal mechanisms of earthquake populations: application to Tibetan teleseisms and microseismicity of Southern Peru. Earth and Planetary Science Letters, 82, 165– 179.

Carey, E.; Mercier, J.L. 1989. Software E.C.G.-GEOLDYNSOFT-5.0.

Casertano, L. 1960. Relación entre vulcanismo y sismicidad. Universidad de Chile, Boletín, 12, 23-27.

Casertano, L. 1962. Sui fenomeni sismo-vulcanici del Sud del Chile. Annali Osservatorio Vesubiano 4 (serie 6), Naples.

Cembrano, J., Beck, M.E.; Burmester, R.F.; Rojas, C.; García, A.; Hervé, F. 1992. Paleomagnetism of Lower Cretaceous rocks from east of the Liquiñe-Ofqui Fault zone, southern Chile: evidence of smali in-situ clockwise rotations. Earth and Planetary Science Letters, 113, 539-551.

Cembrano, J., Hervé, F., Lavenu, A. 1996. The Liquiñe-Ofqui fault zone: a long-lived intra-arc fault Zone in southern Chile. Tectonophysics, 259, 55-66.

Cembrano, J., Lavenu, A., Reynolds, P., Arancibia, G.; López, G., Sanhueza, A. 2002. Late Cenozoic transpressional ductile deformation north of the Nazca-South America-Antarctica triple junction. Tectonophysics, 354, 289-314.

Cembrano, J., Moreno, H. 1994. Geometría y naturaleza contrastante del volcanismo cuaternario entre los 38ºS y 46ºS: ¿Dominios compresionales y tensionales en un régimen transcurrente?. Congreso Geológico Chileno No. 7, Actas 1, 240-244.

Cembrano, J., Shermer, E., Lavenu, A., Sanhueza, A. 2000. Contrasting nature of deformation along an intra-arc shear zone, the Liquiñe-Ofqui fault zone, southern Chilean Andes. Tectonophysics, 319, 129-149.

Chadwick, W.W. ; Dietrich, J.H. 1995. Mechanical modeling of circumferential and radial dike intrusion on Galapagos volcanoes. Journal of Volcanology and Geothermal Research, 66, 37-52.

Charrier, R.; Baeza, O.; Elgueta, S.; Flynn, J.J.; Gans P.; Kay S.M.; Munoz N.; Wyss A.R.; Zurita E. 2002. Evidence for Cenozoic extensional basin development and tectonic inversion south of the flat-slab segment, southern Central Andes, Chile (33º-36ºS.L.). Journal of South American Earth Sciences, 15, 1, 117-139.

Chinn, D.S.; Isacks, B.L. 1983. Accurate source depths and focal mechanisms of shallow earthquakes in western south America and in the New Hebrides island arc. Tectonics, 2, 6, 529-563.

Chotin, P. 1975. Les Andes Méridionales et la termination du Bassin Andin. Le Lonquimay (Chili) et le Neuquén (Argentine) (lat.38º45'S), Université Pierre et Marie Curie, (Ph.D. Thesis), 303 p. Paris.

Cifuentes, I.L. 1989. The 1960 Chilean earthquakes. J Geophys Res 94: 665-680.

Cisternas, M., Atwater, B., Torrejón, F., Sawai, Y., Machuca, G., Lagos, M., Eipert, A., Youlton, C., Salgado, I., Kamataki, T., Shishikura, M., Malik, J.K., Rizal, Y., Rajendran, C.P., Husni, M. 2005. Predecessors of the giant 1960 Chile earthquake. Nature, v. 437, doi:10.1038.

Clapperton, C. 1993. Quaternary geology and geomorphology of South America. Elsevier Science Publishers, 779 p. Amsterdam.

Clavero R., 1996. Ignimbritas andesítico-basálticas postglaciales del volcán Villarrica, Andes del Sur (39º25'S). Universidad de Chile, (thèse), 126 p., Santiago.

Cobbold, P. R.; Rossello, E. A. 2003. Aptian to recent compressional deformation of the Neuquén Basin, Argentina. Marine and Petroleum Geology, 20, 5, 429-443.

Coira, B., Nullo, F., Proserpio, C.; Ramos, V. 1975. Tectónica de basamento de la región occidental del Macizo Nordpatagónico (provincias de Río Negro y Chubut) República Argentina. Revista de la Asociación Geológica Argentina, 30, 361-383.

Corbella, H. ; Lara, L.E. (sous-presse). Late Cenozoic Quaternary volcanism in Patagonia and Tierra del Fuego. In Quaternary of Patagonia (J. Rabassa, Ed.) Elsevier.

Davidson, J. P.; Harmon, R.S.; Wörner, G. 1991. The source of central Andean magmas: some considerations. In Andean Magmatism and Its tectonic Setting (Harmon, R.S.; Rapela, C.W.; editors). Geological Society of America, Special Publication, 265, 233-243.

Deino, A., and Potts, R., 1990, Single-crystal $^{40}Ar/^{39}Ar$ dating of the Olorgesailie Formation, southern Kenya Rift: Journal of Geophysical Research, 95, 8453-8470.

Delaney, P.T; Pollard, D.D.; Ziony, J.I.; Mckee, E.H. 1986. Field relations between dykes and joints: emplacement processes and paleostress analysis. J. Geophys. Res., 91, 4920-4938.

Delpino, D.: Deza, M. 1995. Mapa geológico y de recursos minerales de la provincia del Neuquén, República Argentina. Secretaría de Minería y Ministerio de Producción y Turismo, escala 1:500,000, 1 hoja. Buenos Aires.

DeMets, C., Gordon, R., Argus, D., Stein, S. 1994. Effect of recent revisions to the geomagnetic reversal time scale on estimates of current plate motions. Geophys. Res. Lett. 21, 2191-2194.

Denton, G.H., Heusser, C.J., Lowell, T.V., Moreno, P.I., Andersen, B.G., Heusser, L.E., Schluchter, C., and Marchant, D.R. 1999. Interhemispheric linkage of paleoclimate during the last glaciation. Geografiska Annaler, 81, 107-153.

Dewey, J.F.; Lamb, S.H. 1992. Active tectonics of the Andes. Tectonophysics, 205, 79-95.

Dhont, D.; Chorowicz, J.; Yürür, T.; Froger, J.L.; Köse, O.; Gündogdu, N. 1998. Emplacement of volcanic vents and geodynamics of Central Anatolia, Turkey. J Volcanol. Geotherm. Res., 62, 207-224.

Dixon, H.J.; Murphy, M.D.; Sparks, S.J.; Chávez, R.; Naranjo, J.A.; Dunkley, P.N.; Simon, Young, S.Y.; Gilbert, J.S.; Pringle, M.R. 1999. The geology of Nevados de Chillán volcano, Chile. Revista Geológica de Chile, 26, 2, 227-253.

D'Orazio, M.; Innocenti, F.; Manetti, P.; Tamponi, M.; Tonarini, S.; González-Ferrán, O.; Lahsen, A.; Omarini, R. 2003. The Quaternary calc-alkaline volcanism of the Patagonian Andes close to the Chile triple junction: geochemistry and petrogenesis of volcanic rocks from the Cay and Maca volcanoes (~45°S, Chile). Journal of South American Earth Sciences, 16, 4, 219-242.

Drake, E.R., Curtis, G., Vergara, M. 1976 Potassium-argon dating of igneous activity in the central Chilean Andes. Journal of Volcanology and Geothermal Research, 1 : 285-295, doi: 10.1016/0377-0273(76)90012-3.

Duda, S.J. 1963. Strain release in the circum-Pacific belt, Chile, 1960. J Geophys Res 68, 5 531-5 544.

Duhart, P., McDonough, M.; Muñoz, J., Martin, M., Villeneuve, M. 2001. El Complejo Metamórfico Bahía Mansa en la cordillera de la Costa del centro-sur de Chile (39º30'-42º00'S): geocronología K-Ar, $^{40}Ar/^{39}Ar$ y U-Pb e implicancias en la

evolución del margen sur-occidental de Gondwana. Revista Geológica de Chile, 28, 179-208.

Dungan, M.A., Wulff, A., Thompson, R. 2001. Eruptive stratigraphy of Tatara-San Pedro complex, 36ºS, Southern Volcanic Zone, Chilean Andes: reconstruction meted and implications for magma evolution at long-lived arc volcanic centres. J. Petrol., 42, 555-626.

Eaton, J.P.; Richter, D.H.; Ault, W.U. 1961. The tsunami of May 23, 1960, on the island of Hawaii. Seism. Soc. Am. Bull., 51, 135-157.

Echegaray, J. 2004. Evolución geológica y geoquímica del centro volcánico Mocho-Choshuenco, Andes del Sur, 40ºS. Universidad de Chile, (thesis),121 p. Santiago.

Elgueta, S.; McDonough, M.; Le Roux, J.; Urqueta, E.; Duhart, P. 2000. Estratigrafía y Sedimentología de las Cuencas Terciarias de la Región de Los Lagos (39-41º30'S). Boletín No. 57, Servicio Nacional de Geología y Minería, 50 p.

Emmerman, S.H., Marrett, R. 1990. Why dykes? Geology, 18, 231-233.

Engebretson, D.C., Cox, A., Gordon, R.G. 1986. Relative motions between oceanic and continental plates in Pacific Basin: Geological Society of America Special Paper, 206, 59 p.

England, P. ; Engdahl, R. ; Thatcher, W. 2004. Systematic variation in depthts of slab beneath arc volcanos. Geophys. J. Int., 156, 377-408.

England, P., Molnar, P. 1990. Surface uplift, uplift of rocks, and exhumation of rocks. Geology, 18 (12), 1173-1177.

Etchecopar, A.; Vasseur, G.; Daignières, M. 1981. An inverse problem in microtectonics for the determination of stress tensors from fault striation analysis. Journal of Structural Geology, 3, 51-65.

Féraud, G., Giannerini, G., and Campredon, R. 1987. Dyke swarms as paleostress indicators in areas adjacent to continental collision zones: examples from the European and Northwest Arabian Plates. In Halls, H.C., and Fahrig, W.F. (eds.), Mafic Dyke Swarms, Geological Society of Canada Special Paper, 34, p. 273-278.

Fleck, R.J., Sutter, J.F., Elliot, D.H. 1977. Interpretation of discordant $^{40}Ar/^{39}Ar$ age-spectra of Mesozoic tholeiites from Antarctica. Geochim. Cosmochim. Acta, 41, 15-32.

Folguera, A., Ramos, V.A. 2000. Control estructural del volcán Copahue (38°S-71°W): implicancias tectónicas para el arco volcánico cuaternario (36°S-39°S). Revista de la Asociación Geológica Argentina, 55, 3, 229-244.

Folguera, A., Ramos, V.A., Hermanns, R., Naranjo, J.A. 2004. Neotectonics in the foothills of the southernmost central Andes (37º-38ºS): Evidence of strike-slip displacement along the Antiñir-Copahue fault zone, Tectonics, 23, TC 5008.

Folguera, A., Ramos, V.A., Melnick, D., 2002. Partición de la deformación en la zona del arco volcánico de la cordillera Neuquina en los últimos 30 millones de años (36°–39°S): Revista Geológica de Chile, 29, 2, 227–240.

Folguera, A., Ramos, V.A., Melnick, D., 2003. Recurrencia en el desarrollo de cuencas de intraarco: Colapso de estructuras orogénicas, Cordillera Neuquina (37°30′S). Revista de la Asociación Geológica Argentina, 58, 3-19.

Folguera, A., Zapata, T., Ramos, V.A. 2006. Late Cenozoic extensión and the evolution of the Neuquén Andes. in Kay, S.M. and Ramos V.A., eds., Evolution of an Andean margin: A tectonic and magmatic view from the Andes to the Neuquén Basin (35°-39°S lat). Geological Society of America Special Paper, 407, doi: 10.1130/2006.2407(12).

Forsythe, R., Diemer, J. 2006. Late Cenozoic movement associated with the arc-parallel Liquiñe-Ofqui Fault Zone and the Chile Triple Junction documented by acoustic profiling of shallo w marine and lacustrine deposits of Southern Chile. Backbone of the Americas GSA meeting, Abstracts, p.48, Mendoza.

Forsythe, R.D.; Nelson, E.P. 1985. Geological manifestations of ridge collision: Evidence from the Golfo de Penas-Taitao basin, Southern Chile. Tectonics, 4, 477-495.

Franzese, J., 1995. El Complejo Piedra Santa (Neuquén, Argentina): parte de un cinturón metamórfico neopaleozoico del Gondwana suroccidental. Revista Geológica de Chile, 22, 2, 193–202.

Frey, F.A.; Gerlach, D.C.; Hickey, R.L.; López-Escobar, L.; Munizaga, F. 1984. Petrogenesis of the Laguna del Maule volcanic complex, Chile (36°S). Contributions to Mineralogy and Petrology, 88, 133-149.

Futa, K.; Stern, C.R. 1988. Sr and Nd isotopic and trace element compositions of Quaternary volcanic centers of the Southern Andes. Earth and Planetary Sciences Letters, 88, 253-262.

Galland, O. 2004. Interactions mécaniques entre la tectonique compressive et le magmatisme: expériences analogiques et exemple naturel. Université de Rennes I, (thèse), 423 p.

García, A.R., Beck, M., Burmester, R., Munizaga, F., Hervé, F. 1988. Paleomagnetic reconnaissance of the Region de Los Lagos, southern Chile, and its tectonic implications. Revista Geológica de Chile, 15, 13-30.

Gephart, J.W. 1988. On the use of stress invedrsion of fault-slip data to infer the frictional strenght of rocks. Abstract, EOS Transactions, American Geophysical Union, 69, 1462.

Gerlach, D., Frey, F., Moreno, H., López-Escobar, L. 1988. Recent volcanism in the Puyehue-Cordón Caulle Region, Southern Andes, Chile (40.5ºS): petrogenesis of evolved lavas. J .Petrol., 29, 333-382.

Gilbert, J.S.; Stasiuk, M.V.; Lane, S.J.; Adam, C.R.; Murphy, M.D.; Sparks, R.S.J.; Naranjo, J.A. 1996. Non-explosive, constructional evolution of the ice-filled caldera at Volcán Sollipulli. Bulletin of Volcanology, 58, 67-83.

Glazner, A.; Bartley, J.; Carl, B. 1999. Oblique opening and non-coaxial emplacement of the Jurassic Independence dike swarms. J. Struct. Geol., 21, 1275-1283.

Godoy, E.; Yañez, G ; Vera, E. 1999. Inversion of an Oligocene volcano-tectonic basin and uplifting of its superimposed Miocene magmatic arc in the Chilean Central Andes: first seismic and gravity evidences. Tectonophysics, 306, 2, 217-236.

González, O., Vergara, M. 1962. Reconocimiento geológico de la Cordillera de los Andes entre los paralelos 35º y 38º latitud sur: Universidad de Chile, Publicaciones, 24, 119 p.

González-Ferrán, O., Innocenti, F., Lahsen, A., Manetti, P., Mazzuolli. R., Omarini, R., Tamponi, M. 1996. Alkali basalt volcanism along a subduction related magmatic arc: the case of Puyuhuapi Quaternary volcanic line, Southern Andes (44º20'S). In XIII Congreso Geológico Argentino, Actas vol. 3, 549-565. Buenos Aires.

Gorring, M.L.; Kay, S.M.; Zeitler, P.K.; Ramos, V.A.; Rubiolo, D.; Fernández, M.I.; Panza, J.L. 1997. Neogene Patagonian plateau lavas. Tectonics, 16, 1-17.

Graefe, K., Glodny, J., Seifert, W., Rosenau, M., Echtler, H. 2002. Apatite fission track thermochronology of granitoids at the south Chilean active continental margin (37º-42ºS): implication for denudation, tectonics and mass transfer since the Cretaceous. 5th International Symposium of Andean Geodynamics, Abstracts, 275-278, Toulouse.

Grifith, A.A. 1921. The phenomena of rupture and flow in solids. Philosophical Transactions of the Royal Society of London, Series A, 221, 163-198.

Grifith, A.A. 1924. The theory of rupture. In C.B. Biezeno and J.M Burgers (eds). Proceedings of the First International Congress on Applied Mechanics, J. Waltman Delft, 55-63.

Grollimund, B., Zoback, M.D. 2001. Did deglaciation trigger intrapalte seismicity in the New Madrid seismic zone? Geology 29 (2), 175-178.

Gutenberg, B. 1956. The energy of the earthquakes. Quart. J. Geol. Soc. London, 112, 1-14.

Hack, J. T. 1973. Stream-profile analysis and stream-gradient index. J. Res. Geol. Survey, 1 (4), 421-429.

Hantke, G. 1940. Das Vulkangebeit zwischen den Seen Ranco und Puyehue in Süd Chile. Annali Osservatorio Vesubiano 7 (serie 2), Naples.

Hantke, G. 1961. Der Vulkanismus in Chile. Smithsonian Institution, Washington.

Harper, M.A. 2003. $^{40}Ar/^{39}Ar$ Constraints on the Evolution of the Puyehue-Cordon Caulle Volcanic Complex, Andean Southern Volcanic Zone, Chile. University of Wisconsin-Madison (thesis). Wisconsin.

Harper, M.A., Singer, B.S., Moreno-Roa, H., Lara, L.E., Naranjo, J.A. 2004. $^{40}Ar/^{39}Ar$ Constraints on the Evolution of the Puyehue-Cordon Caulle Volcanic Complex, Andean Southern Volcanic Zone, Chile, IAVCEI General Assembly, Abstracts, Pucón.

Harris, R., 1998. Introduction to special section: stress triggers, stress shadows, and implications for seismic hazard. J. Geophys. Res., 103, 24,347–24,358.

Harris, R.; Simpson, R. 1998. Supression of large earthquakes by stress shadows: A comparison of Coulomb and rate-and-state failure. J. Geophys. Res., 103, 24 439-24 451.

Hervé, F. 1994. The southern Andes between 39° and 44°S latitude: the geological signature of a transpressive tectonic regime related to a magmatic arc. In: Reutter, K.-J., Scheuber, E., Wigger, P.J. (Eds.), Tectonics of the Southern Andes, 243–248.

Hervé, F., Fuenzalida, I.; Araya, E.; Solano, A. 1979. Edades radiometricas y tectónicas neógenas en el sector costero de Chiloé, X Región. In Congreso Geológico Chileno, No. 2, Actas 1, Fl-F18. Arica.

Hervé, F., Ota, Y. 1993. Fast Holocene uplift rates at the Andes of Chiloe, southern Chile. Revista Geológica de Chile, 20, 1, 15-24.

Heusser, C.J. 1990. Chilotan piedmont glacier in the southern Andes during last glacial maximum. Revista Geológica de Chile, 17, 1, 3-18.

Hickey-Vargas, R., Abdollahi, M.J.; Parada, M.A.; López-Escobar, L.; Frey, F.A. 1995. Crustal xenoliths from Calbuco Volcano, Andean Southern Volcanic Zone: implications for crustal composition and magma-crust interaction. Contributions to Mineralogy and Petrology, 119, 331-344.

Hickey-Vargas, R., Frey, F.A.; Gerlach, D.C.; López-Escobar, L. 1986. Multiple sources for basaltic arc rocks from the Southern Volcanic Zone of the Andes (34°-41°S): Trace element and isotopic evidence for contributions from subducted oceanic crust, mantle and continental crust. Journal Geophysical Research, 91, 6, 5963-5983.

Hickey-Vargas, R., Gerlach, D.; Frey, F. 1984. Geochemical variations in volcanic rocks from central-south Chile (33°-42°S): implications for their petrogenesis. In Andean magmatism: chemical and isotopic constraints (Harmon R.; Barreiro, B.; editors). Shiva Publishing Limited: 72-95. Nantwich, U.K.

Hickey-Vargas, R., Moreno, H., López Escobar, L.; Frey, F. 1989. Geochemical variations in Andean basaltic and silicic lavas from the Villarrica-Lanín volcanic chain (39.5°S): an evaluation of source heterogeneity, fractional crystallization and crustal assimilation. Contributions to Mineralogy and Petrology, 103, 361-386.

Hickey-Vargas, R., Sun, M., López-Escobar, L., Moreno-Roa, H., Reagan, M., Morris, J. and Ryan, J. 2002. Multiple subduction components in the mantle wedge: Evidence from eruptive centers in the Central Southern Volcanic Zone, Chile, Geology, 30, 199-202.

Hildreth, W.; Drake, R.E. 1992. Volcán Quizapu, Chilean Andes. Bulletin of Volcanology, 54, 93-125.

Hildreth, W.; Grunder, A.L.; Drake, R.E. 1984. The Loma Seca Tuff and the Calabozos caldera: A major ash-flow and caldera complex in the southern Andes of central Chile. Geological Society of America Bulletin, 95, 45-54.

Hildreth, W.; Moorbath, S. 1988. Crutal contributions to arc magmatism in the Andes of Central Chile. Contributions to Mineralogy and Petrology, 98, 455-489.

Hildreth, W.; Singer, B.; Godoy, E.; Munizaga, F. 1998. The age and constitution of Cerro Campanario, a mafic stratovolcano in the Andes of Central Chile. Revista Geológica de Chile, 25, 1, 17-28.

Hill, D. P. 1977. A model for earthquake swarms. J. Geophys. Res., 82, 1347-1352.

Hoek, J.D., Seitz, HM. 1995. Continental mafic dyke swarms as tectonic indicators: An example from the Vestfold Hills, East Antarctica. Precambrian Research, 75, 121-139.

Hubbert, M.K., Rubey, W.W. 1959. Role of fluid pressure in the mechanics of overthrust faulting. Geol. Soc. Am. Bull., 70, 115-205.

Hubbert, M.K., Willis, D.G. 1957. Mechanics of hydraulic fracturing: Journal of Petroleum Technology, 9, 6,153-168.

Hulton, N., Sugden, D., Payne, A., Clapperton, Ch. 1994. Glacier modelling and the climate of Patagonia during the Last Glacial Maximum. Quaternary Research, 42, 1-19.

Huyghe, P.; Mugnier, J.L. 1992. The influence of the depth on reactivation in normal faulting. J. Struct. Geol. 14, 991-998.

Illies, H. 1959. Die entstehungsgeschichte eines Maars in Süd Chile. Geol. Rundschau, 28, 232-247.

Inglis, C.E. 1913. Stresses in a plate due to the presence of cracks and sharp corners. Transactions of the Institute of Naval Architecture, 55, 219-230.

Ivins, E.R.; Dixon, T.H.; Golombek, M.P. 1990. Extensional reactivation of an abandoned thrust: a bound on shallowing in the brittle regime. J. Struct. Geol., 12, 303-314.

James, D.E. 1984. Quantitative models for crustal contamination in the central and northern Andes. In Andean Magmatism: chemical and isotopic constraints. (Harmon, R.S.; Barreiro B.A., eds.). Shiva Geology Series, Shiva Publishing Limited:124-138. Natwich, UK.

Jarrard, R.D. 1986. Relation among subduction parameters. Reviews of Geophysics, 24, 2, 217-284.

Jordan, T.E., Burns, W.M., Veiga, R., Pángaro, F., Copeland, P.I., Kelley, S., Mpodozis, C., 2001. Extension and basin formation in the southern Andes caused by increased convergence rate: a mid-Cenozoic trigger for the Andes. Tectonics, 20, 308–324.

Kanamori, H. 1977. The energy release in great earthquakes. J. Geophys. Res., 82, 2981-2987.

Kanamori, H., Cipar, J.J. 1974. Focal process of the great Chilean earthquake, May 22, 1960. Phys. Earth. Planet. Inter., 9, 128–136.

Katsui, J; Katz, H. 1967. Lateral fissure eruptions in the Southern Andes of Chile. Faculty of Science Series, 4, 433-448, Hokkaido.

Kay, S.M., Godoy, E., Kurtz, A. 2005. Episodic arc migration, crustal thickening, subduction erosion, and magmatism in the south-central Andes. Geological Society of America Bulletin, 117, 67-88, doi: 10.1130/B25431.1.

Kay, S.M., Ramos, V.; Marquez, M., 1993. Evidence in Cerro Pampa volcanic rocks for slab-melting prior to ridge-trench collision in southern South America. Journal of Geology 101: 703-714.

Keskin, M. 2002. FC-Modeler: a Microsoft® Excel© spreadsheet program for modelling Rayleigh fractionation vectors in closed magmatic systems. Computers & Geoscience, 28, 8, 919-928.

Klohn, C. 1955. Informe geológico sobre el volcán Pillanilahue. CORFO, 61 p. Santiago.

Klotz, J.; Khazaradze, G.; Angermann, D.; Reigber, Ch.; Perdomo, R.; Cifuentes, O. 2001. Earthquake cycle dominates contemporary crustal deformation in Central and Southern Andes, Earth and Planetary Science Letters, 193, 3-4, 437-446.

Kozlowski, E., Cruz, C., Sylwan, C. 1996. Geología estructural de la zona de Chos Malal, Cuenca Neuquina, Argentina, in Proceedings, 13th Congreso Geológico Argentino and Congreso de Exploración de Hidrocarburos, Buenos Aires, Actas, 1, 15-26.

Krumm, F. 1923. Topographische und geologische Nachrichten über die Gegend östlich des Ranco Sees in Süd Chile, im Besonderen über den jüngsten Vulkanausbruch 'Los Azufres' (Dezember 1921). Geol. Rundschau, 14, 146-150.

Lamy, F., Kaiser, J., Ninnemann, U.S., Hebbeln, D., Arz, H.W., Stoner, J.S. 2004. Antarctic timing of surface water changes off Chile and Patagonian Ice Sheet response. Science, 304, 1959-1962.

Lanphere, M. 2000, Comparison of conventional K-Ar and $^{40}Ar/^{39}Ar$ dating of young mafic volcanic rocks. Quaternary Research, 53, 294-301, doi: 10.1006/qres.1999.2122.

Lara, L. E. 2004. Geología del volcán Lanín, IX Región de la Araucanía y X Región de Los Lagos, Chile. Servicio Nacional de Geología y Minería, Carta Geológica de Chile, Serie Geología Básica, No. 86, 1 mapa escala 1:50.000 y texto.

Lara, L. E., Cembrano, J., Lavenu, A., Darrozes, J. 2005. Holocene volcanism and vertical displacements along a major intra-arc transpressional system in the southern Andes. 6th Internacional Symposium on Andean Geodynamics, Extended Abstracts, Barcelona, 438-441.

Lara, L. E., Clavero, J. (editors). 2004. Villarrica volcano (39.5ºS), Southern Andes, Chile. Servicio Nacional de Geología y Minería, Boletín No. 61, 66 p.

Lara, L. E., Folguera, A. 2006. The Pliocene to Quaternary broading and narrowing of the Southern Andean volcanic arc between 37° and 41ºS latitude. In S.M. Kay and V.A. Ramos , eds., Late Cretaceous to Recent magmatism and tectonism of the Southern Andean margin at the latitude of the Neuquén Basin (36-39ºS), GSA Special Paper 407, 299-315.

Lara, L. E., Lavenu, A., Cembrano, J. Darrozes, J. (sousmis). Quaternary vertical displacement along the Liquiñe-Ofqui Fault Zone: bedrock uplift and coeval volcanism in Southern Andes. Tectonophysics.

Lara, L. E., Lavenu, A., Cembrano, J.; Rodríguez, C. 2006a. Structural controls of volcanism in transversal chains: resheared faults and neotectonics in the Cordón Caulle-Puyehue area (40.5ºS), Southern Andes. J. Volcanol. Geoth. Res.: doi:10.1016/j.jvolgeores.2006.04.017.

Lara, L. E., Mathews, S., Pérez, C., Moreno, H. 2002. Evolución morfoestructural del Complejo Volcánico Cordón Caulle (40°S): evidencias geocronológicas 40Ar-

39Ar. Proceedings, 10° Congreso Geológico Chileno, Concepción, Electronic File.

Lara, L. E., Moreno, H. 2004. Geología del área Liquiñe-Neltume, X Región de Los Lagos, Chile. Servicio Nacional de Geología y Minería, Carta Geológica de Chile, Serie Geología Básica, No. 83, 1 mapa escala 1:100.000 y texto, 101 p.

Lara, L. E., Moreno, H. 2006. Geología del Complejo Volcánico Puyehue-Cordón Caulle, X Región de Los Lagos, Chile. Servicio Nacional de Geología y Minería, Carta Geológica de Chile, Serie Geología Básica, 1 mapa escala 1:50.000 y texto (in press).

Lara, L. E., Moreno, H.; Naranjo, J.A.; Matthews, S.; Pérez de Arce, C. 2006b. Magmatic evolution of the Puyehue-Cordón Caulle Volcanic Complex (40º S), Southern Andean Volcanic Zone: from shield to unusual rhyolitic fissure volcanism. J. Volcanol. Geoth. Res.: doi:10.1016/j.jvolgeores.2006.04.010.

Lara, L. E., Naranjo, J.A., Moreno, H. 2004a. Rhyodacitic fissure eruption in Southern Andes (Cordón Caulle; 40.5ºS) after the 1960 (Mw: 9.5) Chilean earthquake: a structural interpretation. Journal of Volcanology and Geothermal Research, 138, 127-138.

Lara, L. E., Naranjo, J.A.; Moreno, H. 2004b. Lanín volcano (39.5ºS), Southern Andes: Geology and morphostructural evolution. Revista Geológica de Chile, 31, 2, 241-257.

Lara, L. E., Rodríguez, C.; Moreno, H.; Pérez de Arce, C. 2001. Geocronología K-Ar y geoquímica del volcanismo plioceno superior-pleistoceno de los Andes del Sur (39º-42ºS). Revista Geológica de Chile, 28, 67-90.

Laugenie, C. 1982. La région des Lacs, Chili méridional. Recherche sur l'évolution géomorphologique d'un piémont glaciaire quaternaire andin. Thèse de Doctorat, Université de Bordeaux III, 822 p.

Lavenu, A. 2006. Fallas Cuaternarias de Chile. Servicio Nacional de Geología y Minería, Boletín No. 62, Santiago.

Lavenu, A., Cembrano, J. 1999. Compressional and traspressional-stress pattern for Pliocene and Quaternary brittle deformation in fore arc and intra-arc zones (Andes of Central and Southern Chile). J. Struct. Geol., 21, 1669-1691.

Lavenu, A., Cembrano, J. 1999b. Estados de esfuerzo compresivo plioceno y compresivo-transpresivo pleistoceno, Andes del sur, Chile (38 y 42°30' S). Revista Geológica de Chile, 26, 1, 67-87.

Leanza, H., Hugo, C., Repol, D., González, R., and Danieli, J., 2001, Hoja geológica Zapala: Instituto de Geología y Recursos Hoja 3969-I, Boletin no. 275, scale 1:250,000, 1 sheet, 128

Legrand, D., Calahorrano, A., Guillier, B., Rivera, L., Ruiz, M., Villagómez, D., Yepes, H., 2002. Stress tensor analysis of the volcanic swarm of Guagua Pichincha volcano, Ecuador. Tectonophysics, 344, 15–36.

León, L., Polle, E. 1956. Las capas volcánicas de Carrán y la erupción del Nilahue. Comunicaciones, 7, 24.

Lescinsky, D., Fink, J. 2000. Lava and ice interaction at stratovolcanoes: use of characteristic features to determine past glacial events and future volcanic hazards. J. Geophys. Res., 105, 23,711-23,726.

Linares, E., Gonzalez, R.R. 1990. Catálogo de edades radimétricas de la República Argentina 1957-1987. Asociación Geológica Argentina, Publicaciones especiales Serie B, Didáctica y Complementaria, 19, 1-628.

Linares, E., Ostera, H.A., Cagnoni, M.C., 2001. Sr isotopes at Copahue volcanic center, Neuquén, Argentina: Preliminary report. III Simposio Sudamericano de Geología Isotópica, Pucón-Chile, Electronic files, 4p.

Linares, E., Ostera, H.A., Mas, L., 1999. Cronología Potasio-Argón del complejo efusivo Copahue–Caviahue, Provincia de Neuquén. Asociación Geológica Argentina Revista, 54, 240-247.

Linde, A.T.; Sacks, I.S. 1998. Triggering of volcanic eruptions. Nature, 395, 888-890.

Lister, J.R., Kerr, R.C. 1991. Fluid-mechanical models of crack-propagation and their application to magma transport in dykes. Journal of Geophysical Research, 96, 10049-10077.

Llambías, E.J., Palacios, M., and Danderfer, J.C., 1982, Las erupciones Holocenas del Volcán Tromen (Provincia del Neuquén) y su significado en un perfil transversal E-O a la latitud de 37ºS, in 5th Proceedings, Congreso Latinoamericano de Geología (Buenos Aires), Actas 3, 537-545.

Lliboutry, L. 1999. Glaciers of the Wet Andes. In Williams, R.S., and Ferrigno, J.G. (eds.), Satellite image atlas of glaciers of the world: South America: U.S. Geological Survey Professional Paper, 1386-I.

Lohmar, S. 2000. Estratigrafía, petrografía y geoquímica del volcán Antuco y sus depósitos (Andes del Sur, 37,25ºS). Universidad de Concepción, thesis (unpublished), 185 p. Concepción.

López-Escobar, L.; Cembrano, J.; Moreno, H. 1995a. Geochemistry and tectonics of the Chilean Southern Andes basaltic Quaternary volcanism (37°-46°S). Revista Geológica de Chile, 22, 219-234.

López-Escobar, L.; Kempton, P.D.; Moreno, H.; Parada, M.A.; Hickey-Vargas, R.; Frey, F.A. 1995b. Calbuco volcano and minor eruptive centers distributed along the Liquiñe-Ofqui fault zone, Chile (41°-42°S): contrasting origin of andesitic and

basaltic magma in the Southern Volcanic Zone of the Andes. Contributions to Mineralogy and Petrology, 119, 345-361.

López-Escobar, L.; Parada, M.A.; Moreno, H.; Frey, F.A.; Hickey-Vargas, R.L. 1992. A contribution to the petrogenesis of Osorno and Calbuco volcanoes, Southern Andes (41°00'-41°30'S): comparative study. Revista Geológica de Chile, 19, 2: 211-226.

López-Escobar, L.; Moreno, H.; Tagiri, M.; Notsy, K.; Onuma, N.; 1985. Geochemistry of lavas from San José volcano, southern Andes (33°45'S). Geochemical Journal, 19, 209-222.

López-Escobar, L.; Vergara, M.; Frey, F.A. 1981. Petrology and geochemistry of lavas from Antuco volcano, a basaltic volcano of the Southern Andes (37°25'S). Journal of Volcanology and Geothermal Research, 11, 329-352.

Lowell, T.V., Heusser, C.J., Andersen, B.G., Moreno, P.I., Hauser, A., Heusser, L.E., Schluchter, C., Marchant, D.R., and Denton, G.H. 1995. Interhemispheric correlation of late Pleistocene glacial events. Science, 269, 1541–1549.

Marrett, R.; Allmendinger, R.W. 1990. Kinematic analysis oif fault-slip data. Journal of Structural Geology, 12, 8, 973-986.

Marsh, B.D. 1979. Island arc development: Some observations, experiments, and speculations: The Journal of Geology, 87, 687-713.

Martin, M.W., Kato, T., Rodríguez, C., Godoy, E., Duhart, P., McDonough, M., Campos, A., 1999. Evolution of the Palaeozoic accretionary complex and overlying forearc–magmatic arc, south central Chile (38°–41° S): constraints for the tectonic setting along the southwestern margin of Gondwana. Tectonics, 18, 4, 582–605.

McCormac, F. G., Hogg, A. G., Blackwell, P. G., Buck, C. E., Higham, T. F. G., and Reimer, P. J. 2004. SHCal04 Southern Hemisphere Calibration 0 - 1000 cal BP. Radiocarbon, 46, 1087-1092.

McDonough, W.; Sun, S.; Ringwood, A.; Jagoutz, E.; Hofmann, A. 1991. K, Rb and Cs in the Earth and Moon evolution of the Earth's mantle. Geochemical and Cosmochemical Acta, Ross Taylor Symposium Volume.

McFarlane, A.W., 1999. Isotopic studies of northern Andean crustal evolution and ore metal sources, In Geology and Ore Deposits of the Central Andes (Skinner, B.J. editor). Society of Economic Geologists, Special Publication, 7, 195-217.

McMillan, N.J., Harmon, R.S., Moorbath, S., López-Escobar, L.; Strong, D. 1989. Crustal sources involved in continental arc magmatism: A case study of Volcan Mocho-Choshuenco, southern Chile. Geology, 17, 1152-1156.

Mella, M., Muñoz, J., Vergara, M., Klohn, E., Farmer, G.L., Stern, C.R. 2005. Petrogenesis of the Tronador Volcanic Group (41°10'S), Andean Southern Volcanic Zone: evolution from volcanic arc front to behind the front type volcanism. Revista Geológica de Chile, 32, 1, 131-154.

Mercer, J. H. 1976. Glacial history of southernmost South America. Quaternary Research, 6, 125-166.

Mercer, J. H. 1983. Cenozoic glaciation in the southern hemisphere. Annual Reviews in Earth and Planetary Science, 11, 99-132.

Meyer Rusca, W. 1955. Diccionario geográfico-etimológico indígena de las provincias de Valdivia, Osorno y Llanquihue. Editorial Universitaria, 2° ed., 299 p. Temuco.

Michael, A.J. 1984. determination of stress from slip data, faults and folds. Journal of Geophysical Research, B 89, 13, 11517-11526.

Michael, A.J. 1987. Use of focal mechanisms to determine stress: a control study. Journal of Geophysical Research, 92, 357-368.

Molnar, P., Freedman, D., Shih, J.S.F. 1979. Lengths of intermediate and deep seismic zones and temperatures in downgoing slabs of lithosphere. Geophysics Journal of the Royal Astronomical Society, 56, 41-54.

Montgomery, D.R., Balco, G., Willet, S.D. 2001. Climate, tectonics, and the morphology of the Andes. Geology, 29, 7, 579-582.

Moreno, H. 1977. Geología del área volcánica Puyehue-Carrán en los Andes del sur de Chile. Universidad de Chile, (thèse). 181 p.

Moreno, H. 1980. La erupción del volcán Mirador en abril-mayo de 1979, Lago Ranco-Riñinahue, Andes del Sur. Comunicaciones, 28, 1-23.

Moreno, H., 2000. Mapa de peligros geológicos del volcán Villarrica, regiones de la Araucanía y de los Lagos. Servicio Nacional de Geología y Minería, 1 mapa escala 1:75.000. Santiago.

Moreno, H., Clavero, J. 2006. Geología del Volcán Villarrica, IX Región de la Araucanía. Carta Geológica de Chile, Serie Geología Básica, 1 mapa escala 1:50.000. (in press).

Moreno, H., Gardeweg, M.C. 1989. La erupción en el complejo volcánico Lonquimay (Diciembre 1988-), Andes del Sur. Revista Geológica de Chile, 16, 93-117.

Moreno, H., Lahsen, A., Thiele, R., Varela, J., López, L. 1986. Edades K-Ar de rocas volcánicas en el área del volcán Callaqui, Andes del sur (38ºS). Comunicaciones, 36, 27-32.

Moreno, H., Lara, L.E. 2006. Geología del Complejo Volcánico Mocho-Choshuenco, X Región de los Lagos. Carta Geológica de Chile, Serie Geología Básica, 1 mapa escala 1:50.000. (in press).

Moreno, H., Naranjo, J.A. 2003. Servicio Nacional de Geología y Minería, Carta Geológica de Chile, Serie Geología Ambiental, No. 7, 1 mapa escala 1: 75.000. Santiago.

Moreno, H., Petit-Breuilh, M.E. 1999. El volcán fisural Cordón Caulle, Andes del Sur (40.5ºS): Geología general y comportamiento eruptivo histórico. 14th Congreso Geológico Argentino, Actas Vol. 2, 258-260. Salta.

Moreno, H., Varela, J., López, L., Munizaga, F., Lahsen, A. 1985. Geología y riesgo volcánico del volcán Osorno y centros eruptivos menores: Unpublished report No. OICB-06C to ENDESA-CORFO, 212 p.

Morris, A., Ferril, D. A., Henderson, D. B., 1996. Slip-tendency analysis and fault. reactivation. Geology, 24, 275-275.

Morris, J.D.; Leeman, W.P.; Tera, F. 1990. The subducted component in island arc lavas constraints from Be isotopes and B-Be systematics. Nature, 344, 31-36.

Muir-Wood, R.M. 1989. Fallamiento normal reciente en la Laguna de San Rafael, Provincia de Aysen, Chile Austral. Comunicaciones, Depto. de Geología, Univ. de Chile, 40, 57-68.

Müller, G.; Veyl, G. 1957. The birth of Nilahue, a new maar type volcano at Riñinahue, Chile. 20th International Geological Congress, Proceedings, 1-II, 375-396, Ciudad de México.

Muller, O.H., Pollard, D.D. 1977. The state of stress near Spanish Peaks, Colorado, determined from a dike pattern. Pure Appl. Geophys. 115, 69-86.

Muñoz, J.; Stern, C.R. 1985. El complejo volcánico Pino Hachado en el sector nor-occidental de la Patagonia (38°-39°S): volcanismo plio-cuaternario trasarco en Sudamérica. *in* Proceedings, 4th Congreso Geológico Chileno, Antofagasta, Universidad Católica del Norte, 3, 381-412.

Muñoz, J.; Stern, C.R. 1988. The Quaternary volcanic belt of the southern continental margin of South America: transverse structural and petrochemical variations across the segment between 38°S and 39°S. Journal of South American Earth Sciences, 1, 147-161.

Muñoz, J.; Stern, C.R. 1989. Alkaline magmatism within the segment 38°-39° S of the Plio-Quaternary volcanic belt of the southern South American margin. Journal of Geophysical Research, 794, B4, 4545-4560.

Murdie, R.E.; Prior, D.J.; Styles, P.; Flint, S.S.; Pearce, R.G.; Agar, S.M. 1993. Seismic responses to ridge-transform subduction: Chile triple junction. Geology, 21, 1095-1098.

Nakamura, K. 1977. Volcanoes as possible indicators of tectonic stress orientation: principle and proposal. J. Volcanol. Geotherm. Res., 2, 1-16.

Nakamura, K., Uyeda, S., 1980. Stress gradient in arc–back arc regions and plate subduction. J. Geophys. Res., 85, 6419–6428.

Naranjo, J.A., Haller, M.J. 2002. Erupciones holocenas principalmente explosivas del volcán Planchón, Andes del sur (35°15'S). Revista Geológica de Chile, 29, 1, 93-113.

Naranjo, J.A., Lara, L.E. 2004. August-September 2003 eruption in the Nevados de Chillán volcanic complex (36°50'S), southern Andes. Revista Geológica de Chile, 31, 2, 359-366.

Naranjo, J.A., Moreno, H. 1991. Actividad explosive postglacial en el Volcán Llaima, Andes del Sur (38°45'S). Revista Geológica de Chile, 18, 1, 69-80.

Naranjo, J.A., Moreno, H., 2005. Geología del volcán Villarica, región de la Araucanía. Servicio Nacional de Geología y Minería, 1 mapa escala 1:50.000. Santiago.

Naranjo, J.A., Moreno, H., Banks, N.G. 1993b. La erupción del volcán Hudson 1991 (46°S), Región de Aisén, Chile. Servicio Nacional de Geología y Minería, Boletín, No. 44, 50 p.

Naranjo, J.A., Moreno, H., Emparan, C.; Murphy, M. 1993a. Volcanismo explosive reciente en la caldera del volcán Sollipulli, Andes del sur (39°S). Revista Geológica de Chile, 20, 167-192.

Naranjo, J.A., Moreno, H., Polanco, E., Young, S. 2000. Mapa de Peligros de los volcanes del Alto Biobío. Servicio Nacional de Geología y Minería, Documentos de Trabajo N° 15.

Naranjo, J.A., Polanco, E. 2004. The 2000 AD eruption of Copahue volcano, southern Andes. Revista Geológica de Chile, 31, 2, 279-292.

Naranjo, J.A., Sparks, R.S.J.; Stasiuk, M.V.; Moreno, H.; Ablay, G.J. 1992. Morphological, structural and textural variations in the 1988-1990 andesite lava of Lonquimay Volcano, Chile. Geological Magazine, 129, 657-678.

Naranjo, J.A., Stern, C.R. 2004. Holocene tephrochronology of the southernmost part (42°30'-45°S) of the Andean Southern Volcanic Zone. Revista Geológica de Chile, 31, 2, 225-240.

Newhall, C.G., Self, S. 1982. The volcanic explosivity index (VEI): An estimate of explosive magnitude for historical volcanism. J. Geophys. Res., 87, 1231-1238.

Nishenko, S., 1985. Seismic potential for large and great interplate earthquakes along the Chilean and Southern Peruvian margins of South America: a quantitative reappraisal. J. Geophys. Res., 90, B5, 3589–3615.

Nostro, C.; Ross, S.; Cocco, M.; Belardinelli, M.E.; Marzochi, W. 1998. Two-way coupling between Vesuvius eruptions and southern Apennine earthquakes, Italy, by elastic stress transfer. J. Geophys. Res. 103, 24,439-24,451.

Nyström, J.O.; Vergara, M.; Morata, D.; Levi, B. 2003. Tertiary volcanism during extension in the Andean foothills of central Chile (33°15'-33°45'S). Geological Society of America Bulletin, 115, 1523-1537.

Orife, T., Lisle, R. 2006. Assessing the statistical significance of palaeostress estimates: simulations using random fault-slips. Journal of Structural Geology, 28, 952-956.

Pankhurst, R.J.; Hervé, F.; Rojas, L.; Cembrano, J. 1992. Magmatism and tectonics in continental Chiloé, Chile (42°-42°30' S). Tectonophysics, 205, 283-294.

Pankhurst, R.J.; Weaver,S.; Hervé, F.; Larrondo, P. 1999. Mesozoic-Cenozoic evolution of the North Patagonian batholith in Aysen, southern Chile. Journal of the Geological Society of London, 156, 673-694.

Parada, M.A.; Lahsen, A.; Palacios, C. 2000. The Miocene plutonic event of the Patagonian Batholith at 44º30': thermochronological and geobarometric evidence for melting of rapidily exhumed lower crust. Transactions of the Royal Society of Edimburg, Earth Sciences, 91, 169-179.

Pavez, A. 1997. Geología e historia evolutiva del Complejo Volcánico Quetrupillán, Andes del Sur, 39.5ºS. *in* 8° Congreso Geológico, Actas 2, 1443-1447. Antofagasta.

Pearce, J. 1982. Trace elements characteristics of lavas from destructive plate boundaries. In Andesites (Torpe, R., editor). John Wiley & Sons.

Peña, P., Fuentealba, G. 2000. Antecedentes preliminares de sismicidad asociada al complejo volcánico activo Cordón Caulle, Andes del Sur (40,5ºS). 9th Congreso Geológico Chileno, Actas 2, 52– 53. Puerto Varas.

Pérez de Arce, C., Becker, T., Roeschmann, C. 2000. El nuevo sistema de datación ^{40}Ar-^{39}Ar equipado con láser de CO_2 en el SERNAGEOMIN. 9th Congreso Geológico Chileno, Actas Vol.1, p. 675. Puerto Varas.

Pérez, Y. 1999. Fuentes de aguas termales de la Cordillera Andina del Centro-Sur de Chile (39º-42ºS). Servicio Nacional de Geología y Minería, Boletín No.54, 65 p., 2 anexos, 1 mapa escala 1:500.000.

Pérez de Arce, C., Matthews, S., Klein, J. 2003. Geochronology by the $^{40}Ar/^{39}Ar$ method at the SERNAGEOMIN Laboratory, Santiago, Chile. International Conference on Research Reactor, Utilization, Safety, Decommissioning, Fuel and Waste Management, Actas, Santiago.

Pesce, A., 1989. Evolución volcano-tectónica del complejo efusivo Copahue-Caviahue y su modelo geotérmico preliminar. Asociación Geológica Argentina, Revista XLIV(1/4): 307-327, Buenos Aires.

Petford, N., Kerr, R.C., Lister, J.R. 1993. Dike transport of granitoid magmas. Geology, 21, 845-848.

Petit-Breuilh, M.E. 1999. Cronología eruptiva histórica de los volcanes Osorno y Calbuco, Andes del Sur (41º-40º30'S). Servicio Nacional de Geología y Minería, Boletin No. 53, 46 p. Santiago.

Pfiffner, D.A.; Burkhard, M. 1987. Determination of paleo-stress axes orientations from faults, twin and earthquake data. Annale Tectonicae, 1, 48-57.

Pierson, T.; Janda, R. 1994. Volcanic mixed avalanches: a distinct eruption-triggered mass-flow process at snow-clad volcanoes. Geol. Soc. Am. Bull., 106, 1351-1358.

Plafker, G.; Savage, J.C. 1970. Mechanism of Chilean earthquakes of May 21 y May 22, 1960. Geol. Soc. Am. Bull., 81, 1001-1030.

Porter, S. 1981. Pleistocene glaciation in the Southern Lake District of Chile. Quaternary Research, 16, 3, 263-292.

Potent, S., Reuther, C.D. 2001. Neogene Deformationsprozesse im aktiven magmatischen Bogen Südzentralchiles zwischen 37° und 39°S. Mitt. Geol. Pal. Inst. Univ. Hamburg, 85, 1-22.

Price, N.J. 1966. Fault and joint development in brittle and semi-brittle rock. Pergamon Press. 176 p. Oxford.

Pritchard, M.E., Simons, M., 2004. An InSAR-based survey of volcanic deformation in the southern Andes. Geophysical Research Letters, 31, doi:10.1029/2004GL020545.

Ramos, V.A. 1977. Estructura de la Provincia de Neuquén. in Rolleri, E.O., ed., Geología y recursos naturales de la Provincia de Neuquén, *in* Proceedings, 7th Congreso Geológico Argentino, Buenos Aires, Asociación Geológica Argentina, 9-14.

Ramos, V.A. 1998. Estructura del sector occidental de la faja plegada y corrida del Agrio, cuenca neuquina, Argentina. *in* Proceedings, 10th Congreso Latinoamericano de Geología, Buenos Aires, Asociación Geológica Argentina, 2, 105-110.

Ramos, V.A.; Kay, S.M. 1992. Southern Patagonian plateau basalts and deformation: Backarc testimony of ridge collision. Tectonophysics, 205, 261-282.

Ramsay, J., Huber, M., 1987. The techniques of modern structural geology. Folds and Fractures, vol. 2. Academic Press, 462 p., London.

Rapela, C., Pankhurst, R. 1992. The granites of northern Patagonia and the Gastre Fault System in relation to the break-up of Gondwana. *in* Magmatism and

causes of continental break-up, Storey, B., (Alabaster, T. y Pankhurst, R. eds.). Geological Society, Special Publication 68, 209-220.

Rebaï, S., Phillip, H., Dorbath, L., Borissoff, B., Haessler, H., Cisternas, A., 1993. Active tectonics in the lesser Caucasus: coexistence of compressive and extensional structures. Teconics, 12, 1089–1114.

Reches, Z.E. 1987. Determination of the tectonic stress tensor from slip along fault that obey the Coulomb yield condition. Tectonics, 6, 6, 845-861.

Reches, Z.E.; Baer, G.; Hatzor, Y. 1992. contraints on the strenght of the upper crust from stress inversion of fault slip data. Journal of Geophysical Research, 97, B89, 12481-12493.

Renne, P.R., Deino, A.L., Walter, R.C., Turrin, B.D., Swisher, C.C., Becker,T.A., Curtis, G.H., Sharp, W.D., Jaouni,A.R. 1994. Intercalibration of astronomic and radioisotopic time. Geology, 22, 783-786.

Renne, P.R., Swisher, C.C., Deino, A.L., Karner, D.B., Owens, T.L., DePaolo, D.J. 1998. Intercalibration of standards, absolute ages, and uncertainties in 40Ar/39Ar dating. Chem. Geol., 145, 117-152.

Richard, P., Cobbold, P., 1990. Experimental insights into partitioning of fault motions in continental convergent wrench zones. Ann. Tecton. IV, 35–44.

Rietbrock, A., Haberland, Ch., Dahm, T., Bataille, K., Tilmann, F., Flüh, E., Lange, D., Hofmann, S., TIPTEQ Research Group. 2006. The TIPTEQ seismological network in Southern Chile: a deep insight into the seismogenic coupling zone. *in* Congreso Geológico Chileno No. 11, Actas 1, 451-452.

Rimbach, C. 1930. Kurze Mitteilungen Über einige Chilenische vulkane Mit 9 Textfigure, Zeitschrift für Vulkanologie, Band XVVV, 105-108.

Ritz, J.F.; Taboada, A. 1993. Revolution stress ellipsoids in brittle tectonics resulting from an uncritical use of inverse methods. Bulletin de la Société Géologique de France, 164, 4, 519-531.

Rodríguez, C., Pérez, Y., Moreno, H., Clayton, J., Antinao, J., Duhart, P., Martin, M. 1999. Area de Panguipulli-Riñihue, región de los Lagos. Santiago, Servicio Nacional de Geología y Minería, Mapas Geológicos, No. 10, escala 1:100.000, 1 hoja.

Rodríguez, C. 1999. Geoquímica del Grupo Carrán-Los Venados, Andes del Sur (40.3ºS). Universidad de Chile, thesis (unpublished). 133 p. Santiago.

Rogers, G.; Hawkesworth, C.J. 1989. A geochemical transverse across the North Chilean Andes: evidence of crust generation from the mantle wedge. Earth and Planetary Science Letters, 91, 271-285.

Roman, D., Moran, S.C., Power, J.A., Cashman, K.V., 2004. Temporal and Spatial Variation of Local Stress Fields before and after the 1992 Eruptions of Crater Peak Vent, Mount Spurr Volcano, Alaska. Bull. Seismol. Soc. Am., 94, 6,

Rosenau, M. R. 2004. Tectonics of the Southern Andean Intra-arc Zone (38°-42°S). Ph.D. thesis, Free University, Berlin, Germany, 154 pp. (available online: http://www.diss.fuberlin.de/2004/280/index.html)

Rosenau, M.R., Melnick, D., Echtler, H. 2006. Kinematic constraints on intra-arc shear and strain partitioning in the Southern Andes between 38°S and 42°S latitude. Tectonics, doi:10.1029/2005TC001943.

Rossello, E.A., Cobbold, P.R., Diraison, M., Arnaud, N. 2002. Auca Mahuida (Neuquén Basin, Argentina): A Quaternary shield volcano on a hydrocarbon-producing substrate. *in* Proceeding, 5th International Symposium on Andean Geodynamics, Toulouse, IRD Editions, 549-552.

Rubin, A.M. 1993. Dikes vs. diapirs in viscoelastic rock. Earth and Planetary Science Letters, 117, 653-670.

Ryan, M.P. 1988. The mechanics and three-dimensional internal structure of active magmatic systems: Kilauea volcano, Hawaii. J. Geophys. Res., 93, B5, 4213-4248.

Saint Amand, P. 1961. Observaciones e interpretación de los terremotos chilenos de 1960. Comunicaciones, 2, 1-54.

Salmi, M. 1941. Die postglacialen Eruptansschichten Patagoniens und Feuerlands. Ann Acad Scient Fenn (Serie A), Helsinski.

Sanderson, D.J.; Marchini, W.R.D. 1984. Transpression. Journal of Structural Geology, 6, 449-458.

Sapper, K. 1927. Vulkankunde. J Engelhorn Nachf, 424 p. Stuttgart.

Sébrier, M.; Mercier, J.L.; Mégard, F.; Laubacher, G.; Carey-Gailhardis, E. 1985. Quaternary normal and reverse faulting and the state of stress in the central Andes of southern Peru. Tectonics, 4, 7, 739-780.

Seifert, W., Rosenau, M. R., Echtler, H. 2005. Crystallization depths of granitoids of South Central Chile estimated by Al-in-hornblende geobarometry: implications for mass transfer processes along the active continental margin. N. Jb. Geol. Paläont. Abh., 236 (1/2), 115-127.

Sellés, D.; Rodríguez, C.; Dungan, M.A.; Naranjo, J.A.; Gardeweg, M. 2004. Nevado de Longaví volcano (36.2°S): geology and geochemistry of a compositionally atypical arc volcano in the Southern Volcanic Zone of the Andes. Revista Geológica de Chile, 31, 2, 293-315.

Sepúlveda, F. 2006. El sistema geotérmico de Cordón Caulle, sur de Chile. Caracterización geológica y geoquímica. Universidad de Chile, (thèse). Santiago.

Sepúlveda, F., Dorsch, K., Lahsen, A., Bender, S., Palacios, C., 2004. Chemical and isotopic composition of geothermal discharges from the Puyehue–Cordón Caulle area (40.5°S), Southern Chile. Geothermics, 33, 655–673.

Sepúlveda, F., Lahsen, A., Bonvalot, S., Cembrano, J., Alvarado, A., Letelier, P. 2005. Morphostructural evolution of the Cordón Caulle geothermal region, Southern Volcanic Zone, Chile: Insights from gravity and $^{40}Ar/^{39}Ar$ dating. J. Volcanol. Geotherm. Res., 148, 165-189.

SERNAGEOMIN, 1998. Estudio geológico-económico de la Xa región norte, Chile. Servicio Nacional de Geología y Minería, Informe Registrado IR-9815, 6 Vols., 13 sheets 1:100,000 scale. Santiago.

SERNAGEOMIN. 2002. Mapa Geológico de Chile, Servicio Nacional de Geología y Minería, Carta Geológica de Chile, Serie Geología Básica No. 75, 1 mapa en 3 hojas, escala 1:1.000.000. Santiago.

SERNAGEOMIN-BGRM, 1995, Carta metalogénica X región sur: Servicio Nacional de Geología y Minería (SERNAGEOMIN), Bureau de Recherches Géologiques et Minières (BGRM) Informe Registrado IR-95-05, v. 4, 10 hojas.

Shaw, H. R. 1980. The fracture mechanisms of magma transport from the mantle to the surface. *in* Hargraves, R. B. (editor), Physics of Magmatic Processes: Princeton, New Jersey, Princeton University Press, 201–264.

Shimozuru, D., Kubo, N., 1983, Volcano spacing and subduction, In Shimozuru, D., *et al*., (eds.), Arc volcanism: Physics and tectonics. Tokyo, Terra Publishers, 141-151.

Sibson, R. 1985. A note on fault reactivation. J. Struct. Geol., 7, 751-754.

Sibson, R. 1987. Earthquake rupturing as a mineralizing agent in hydrothermal Zones. Geology, 15, 701-704.

Sibson, R. 1996. Structural permeability of fluid-driven fault-fracture meshes. J. Struct. Geol., 18, 1031-1042.

Sibson, R. 2000. A brittle failure mode plot defining conditions for high-flux flow. Econom. Geol., 95, 41-48.

Sibson, R. 2003. Brittle-failure controls on maximum sustanaible overpressure in different tectonic regimes. AAPG Bulletin, 87, 6, 901-908.

Sibson, R., Robert, F., Poulsen, K.H. 1988. High-angle reverse faults, fluid-pressure cycling, and mesothermal gold-quartz deposits. Geology, 16, 551-555.

Sievers, H.; Villegas, G.; Barros, G. 1963. The seismic sea wave of 22 May 1960 along Chilean Coast. Seism. Soc. Am. Bull., 1125-1190.

Sigmarsson, O.; Chmeleff, J.; Morris, J.; López-Escobar, L. 2002. Origin of ^{226}Ra-^{230}Th disequilibria in arc lavas from southern Chile and implications for magma transfer time. Earth and Planetary Science Letters, 196, 189-196.

Sigmarsson, O.; Condomines, M.; Morris, J.D.; Harmon, R.S. 1990. Uranium and ^{10}Be enrichments by fluids in Andean arc magmas. Nature, 346, 163-165.

Simkin, T., y Siebert, L. 1994. Volcanoes of the World. Geoscience Press, Tucson, Arizona, 349 p.

Singer, B.S., Ackert, R.P., Guillou, H. 2004. ^{40}Ar/^{39}Ar and K-Ar chronology of Pleistocene glaciations in Patagonia. Geological Society of America Bulletin, 116, 434-450.

Singer, B.S., Jicha, B.R., Harper, M.A., Moreno, H., Naranjo, J.A.; Lara, L.E. 2004. Genesis of basalt and rhyolite erupted in the last 35 ka at Volcán Puyehue Chilean SVZ: Initiation of a U-Th Isotope study. IAVCEI General Assembly, Abstracts, Pucón.

Singer, B.S., Relle, M.R., Hoffman,K.A., Battle, A., Guillou, H, Laj, C., Carracedo, J.C. 2002. ^{40}Ar/^{39}Ar ages of transitionally magnetized lavas on La Palma, Canary Islands, and the geomagnetic instability timescale. J. Geophys. Res., 107, B11, doi:10.1029/2001JB001613.

Singer, B.S., Thompson, R.A., Dungan, M.A., Feeley, T.C., Nelson, S.T., Pickens, J.C., Brown, L.L., Wulff, A.W., Davidson, J.P., and Metzger, J. 1997. Volcanism and erosion during the past 930 ka at the Tatara-San Pedro complex, Chilean Andes. Geol. Soc. Am. Bull., 109, 127-142.

Skewes, M.A.; Stern, C.R. 1979. Petrology and geochemistry of alkali basalts and ultramafic inclusions from the Pali-Aike volcanic fields in southern Chile and the origin of the Patagonian plateau lavas. Journal of Volcanology and Geothermal Research, 6, 3-25.

Smylie, D.E.; Mansinha, L. 1968. Earthquakes and the observed motion of rotation pole. J. Geophys. Res. 73, 7661-7663.

Soon, W., Baliunas, S. 2003. Proxy climatic and environmental changes of the past 1000 years. Clim. Res., 23, 89-110.

Spalletti, L.A., Dalla Salda, L.H., 1996. A pull-apart volcanic related Tertiary basin, an example from the Patagonian Andes. J. South Am. Earth Sci., 9, 3-4, 197-206.

Steffen, H. 1922. Nachrichten aus den vulkangebieten der Kordilleren von Mittel-Chile. Z. Ges. Erdkunde, 273-277.

Stern, C.R., Frey, F.A., Futa, K., Zartman, R.E., Peng, Z., Kyser, T.K. 1990. Trace-element and Sr, Nd, Pb, and O isotopic composition of Pliocene and Quaternary alkali basalts of the Patagonian Plateau lavas of southernmost South America. Contribution to Mineralogy and Petrology, 104, 294-308, doi: 10.1007/BF00321486.

Stern, C.R. 1989. Pliocene to present migration of the volcanic front, Andean Southern Volcanic Front. Revista Geológica de Chile, 16, 2, 145-162.

Stern, C.R. 1991. Role of subduction erosion in the generation of the Andean magmas. Geology, 19, 78-81.

Stern, C.R. 2004. Active Andean volcanism: its geologic and tectonic setting. Revista Geológica de Chile, 31, 2, 161-206.

Stern, C.R., Futa, K.; and Muehelnbachs, K.; Dobbs, F.M.; Muñoz, J.; Godoy, E.; and Charrier, R. 1984. Sr, Nd, Pb and O isotope composition of Late Cenozoic volcanics, northernmost SVZ (33-34°S). *in* Andean Magmatism: Chemical and Isotopic Constraints (Harmon, R.S.; Barriero, B.A., editors). Shiva Geology Series, Shiva Publishing, 96-105. Cheshire, UK.

Stern, C.R., Kilian, R. 1996. Role of the subducted slab, mantle wedge and continental crust in the generation of adakites from the Andean Austral Volcanic Zone. Contributions to Mineralogy and Petrology, 123, 263-281.

Stern, C.R., Moreno, H.; López-Escobar, L.; Clavero, J.; Lara, L.E.; Naranjo, J.A.; Skewes, M.A.. Chilean Volcanoes. *in* Geology of Chile (T. Moreno, Ed.). Geological Society of London. (sous presse)

Stern, C.R., Skewes, M.A. 1995. Miocene to Present magmatic evolution at the northern end of the Andean Southern Volcanic Zone, Central Chile. Revista Geológica de Chile, 22, 2, 261-272.

Stevens, B. 1911. The laws of intrusion. Bulletin of the American Institute of Mining Engineers, 1-23.

Stone, J. 1935. The volcanoes of Southern Chile. Zeitschrift für Vulkanologie, 16, 81-97

Stone, J., Ingerson, E. 1934. Algunos volcanes del sur de Chile. Boletín de Minas y Petróleo., 5, 40.

Stuiver, M., Reimer, P.J. 1993. Extended ^{14}C database and revised CALIB radiocarbon calibration program. Radiocarbon. 35, 215-230.

Suárez, M., Emparán, C. 1997. Hoja Curacautín. Regiones de la Araucanía y del Bío Bío: Santiago, Servicio Nacional de Geología y Minería de Chile, Carta Geológica de Chile, No. 71, escala 1:250,000, 1 hoja, 105 p.

Sun, S.S., McDonough, W.F. 1989. Chemical and isotopic systematics of oceanic basalts: implications for mantle composition and processes. In Magmatism in

the Ocean Basins, Saunders, A.D. and Norry, M.J. (eds.). Geological Society Special Publications, 42, 313-345.

Tagiri, M., Moreno, H., López, L., Notsu, K. 1993. Two magma types of high-alumina basalt series of Osorno volcano, Southern Andes (41º06′S). Plagioclase dilution effect. Journal Mineral and Petrology Economic Geology, 88, 7.

Takada, A. 1994. The influence of regional stress and magmatic input on styles of monogenetic and polygenetic volcanism. J. Geophys. Res., 99, 13,563-13,573.

Tamaki, K. 2000. Nuvel 1-A calculation results. Ocean Research Institute, University of Tokio. http://ofgs.ori.u-tokyo.ac.jp/~okino//rate_calc_new.cgi

Tassara, A. 2005. Interaction between the Nazca and South American plates and formation of the Altiplano–Puna plateau: Review of a flexural analysis along the Andean margin (15°-34°S). Tectonophysics, 399, 39-57.

Tassara, A., Götze, H-J, Schmidt, S., and Hackney, R. 2006. Three-dimensional density model of the Nazca plate and the Andean continental margin. J. Geopphys. Res., (in press).

Tassara, A., Yáñez, G. 2003. Relación entre el espesor elástico de la litósfera y la segmentación tectónica del margen andino (15-47ºS). Revista Geológica de Chile, 30, 159-186.

Tatsumi, Y., and Eggins, S., 1995, Subduction zone magmatism; frontiers in earth sciences: Cambridge, Blackwell Science, 211 p.

Teyssier, C., Tikoff, B., Markley, M. 1995. Oblique plate motion and continental tectonics. Geology, 23, 5, 447-450.

Thiele, R., Moreno, H., Elgueta, S., Lahsen, A., Rebolledo, S. 1998. Evolución geológico-geomorfológica cuaternaria del tramo superior del valle del río Laja. Revista Geológica de Chile, 25, 2, 229-253.

Thomson, S. N. 2002. Late Cenozoic geomorphic and tectonic evolution of the Patagonian Andes between latitudes 42° and 46°S: An appraisal based on fission-track results from the transpressional intra-arc Liquiñe-Ofqui fault zone. Geol. Soc. Am. Bull., 114 (9), 1159-1173.

Thornburg, T.M., Kulm, L.D., Hussong, D.M. 1990. Submarine-fan development in the southern Chile Trench: A dynamic interplay of tectonics and sedimentation.: Geological Society of America Bulletin 102 : 1658–1680.

Thorson, R.M., 1996, Earthquake recurrence and glacial loading in western Washington: Geological Society of America Bulletin, 108, 1182-1191.

Tibaldi, A. 1995. Morphology of pyroclastic cones and tectonics. J. Geophys. Res. 100, 24521-24535.

Toda, S., Stein, R., Reasenberg, P., Dietrich, J., Yoshida, A. 1998. Stress transferred by 1995 Mw=6.9 Kobe, Japan shock: effect on the aftershocks and future earthquake probabilities. J. Geophys. Res., 103, 24543-24565.

Toda, S., Stein, R.S., Sagiya, T., 2002. Evidence from the AD 2000 Izu islands earthquake swarm that stressing rate governs seismicity. Nature, 419, 58-61.

Tolson, G.; Alaniz-Alvarez, S.A.; Nieto-Samaniego, A. 2001. ReActiva, a plotting program to calculate the potential of reactivation of preexisting planes of weakness. Instituto de Geología, Universidad Autónoma de México. http://geologia.igeolcu.unam.mx/Tolson/Software/ReActivaV24En.exe

Tormey, D., Frey, F.A.; López-Escobar, L. 1995. Geochemistry of the active Azufre-Planchón-Peteroa volcanic complex, Chile (35°15'S): evidence for multiple sources and processes in a cordilleran arc magmatic system. Journal of Petrology, 36, 2, 265-298.

Tormey, D., Schuller, P., López, L., Frey, F. 1991. Uranium-Thorium activities and disequilibria in volcanic rocks from the Andes (33º-46S): petrogenetic constraints and environmental consequences. Revista Geológica de Chile, 18, 165-175.

Turcotte, D.; Schubert, G. 2002. Geodynamics (2nd. Edition). Cambridge University Press. 456 p.

Varekamp, J.C. Ouimette, A.P.; Herman, S.W.; Bermúdez, A.; Delpino, D. 2001. Hydrothemal element fluxes from Copahue, Argentina; a 'beehive' volcano in turmoil. Geology, 29, 11, 1059-1062.

Vergani, G., Tankard, A.J., Belotti, H.J., Welsnik, H.J. 1995. Tectonic evolution and paleogeography of the Neuquén Basin. *in* Suárez, A.J., *et al*., eds., Petroleum basins of South America: Tulsa, American Association of Petroleum Geologists (AAPG) Memoir 62, 383-402.

Veyl, C. 1960. Los fenómenos volcánicos y sísmicos de fines de Mayo de 1960 en el sur de Chile. Universidad de Concepción, 42 p. Concepción.

Vogel, M. 1934. Caulle (Chile). Zeitschrift für Vulkanologie 16, 128.

von Wolff, F. 1929. Der Vulkanismus. Stuttgart.

Wallace, R.E. 1951. Geometry of shearing stress and relation to faulting. Journal of Geology, 59, 118-130.

Ward, S.N. 1984. A note on lithospheric bending calculations. Geophys. J. R. Astr. Soc., 78, 241-253.

Weischet, W. 1963. Further observations of geologic and geomorphic changes resulting from the catastrophic earthquake of May 1960, in Chile. Seism. Soc. Am. Bull., 53, 1237-1257.

Wetzel, W. 1959. Informe sobre investigaciones efectuadas durante el segundo semestre de 1958. Universidad Austral, 11 p. Valdivia.

Withjack, M.O.; Jamison, W.R. 1986. Deformation produced by oblique rifting. Tectonophysics, 13, 1061-1078.

Witter, J.B.; Delmelle, P. 2004. Acid gas hazards in the crater of Villarrica volcano (Chile). Revista Geológica de Chile, 31, 2, 273-278.

Wittgenstein, L. 1958. Philosophical Investigations. Trads. Rush Rhees and G.H. von Wright (eds.). G.E.M. Anscombe. 3th edition, New York: Macmillan, 1958 (Investigaciones Filosóficas (Barcelona: Crítica, 1988), U. García Suárez (trad.)

Wittgenstein, L. 1969. Tractatus Logico-Philosophicus. Trads. D.F. and B.F. McGuinnes. London: Routeledge and Kegan Paul, 1969 (Tractatus Logico-Philosophicus (Barcelona: Atalaya, 1994), I. Requenq (trad.).

Wood, D.; Joron, J.; Treuil, M.; Norry, M.; Tarney, J. 1979. Elemental and Sr isotope variations in basic lavas from Iceland and the surrounding ocean floor. Contributions to Mineralogy and Petrology, 70, 319-339.

Yañez, G., Cembrano, J., Pardo, M., Ranero, C., and Sellés, D. 2002. The Challenger-Juan Fernández-Maipo major transition of the Nazca-Andean subduction system at 33-34S: geodynamic evidence and implications. Journal of South American Earth Sciences, 15, 23-38.

Yin, Z.M. 1996. An improved method for the determination of the tectonic stress field from focal mechanism data. Geophysical Journal International, B 98, 7: 12165-12176.

Yin, Z.M.; Ranalli, G. 1993. determination of tectonic stress field from fault slip data; toward a probabilistic model. Journal of Geophysical Research, 97, B8: 11945-11982.

Zapata, T., Brissón, I., Dzelajica, F., Zamora, G. 1999. The role of the basement in the Andean fold and thrust belt of the Neuquén Basin, Argentina. Thrust Tectonics "99 Conference", Abstracts with Programs, 122-124.

Zapata, T., Córsico, S., Dzelajica, F., Zamora, G. 2002. La faja plegada y corrida del Agrio: Análissi structural y su relación con los estratos terciarios de la cuenca neuquina argentina. *in* Proceedings, 5th Congreso de Exploración y Desarrollo de Hidrocarburos, Mar del Plata, CD ROM.

Zoback, M.L., Zoback, M., 1980. State of stress in the conterminous United States. J. Geophys. Res., 85, 6113-6156.

Annexes

Table 1. Selected stress tensors along the volcanic arc(37º-42ºS)

Site	Locality	Lat°S/Long°W	N	σ1			σ2			σ3			R	Tectonic regime	Age	References
				strike	dip	eigenvalue	strike	dip	eigenvalue	strike	dip	eigenvalue				
Lonqui	Bíobío river	38.0º/71.5º	16	106	8	-0,80	196	5	0,25	15	85	0,54	0,778	transtension	Quaternary	unpublished
Lolco	Lolco river	38.1º/71.4	10	52	49	-0.92	313	8	-0.10	216	40	1.03	0.419	transtension	Quaternary	Lara *et al*. (submitted)
Cabur121	Caburgua lake	39.2º/71.8º	34	228	14	-1.01	137	2	0.41	41	76	0.60	0.881	uniaxial compression	Quaternary	Lavenu and Cembrano (1999)
quine1	Curarrehue	39.2º/71.4º	8	304	2	-0.92	211	55	0.39	35	35	0.53	0.907	transpression	Miocene-Pliocene	unpublished
curamod1	Trancura river	39.4º/71.7º	11	239	7	-1.07	115	78	0.30	331	10	0.77	0.770	transpression	Quaternary	Lara *et al*. (submitted)
curamod2	Trancura river	39.4º/71.7º	5	49	5	-0.64	306	70	-0.46	140	20	1.1	0.106	transtension	Quaternary	Lara *et al*. (submitted)
lagopal1	Pucón	39.3º/71.8º	16	250	6	-0.81	350	57	-0.21	157	32	1.03	0.328	transtension	Quaternary	unpublished
x1	Pucón	39.6º/71.8º	21	88	5	-0.65	339	74	-0.17	180	15	0.82	0.33	compression	Miocene-Pliocene	Lavenu and Cembrano (1999)
Aninor13	Liquiñe river	39.6º/71.9º	28	238	12	-1.05	34	76	0.12	147	5	0.93	0.593	transpression	Quaternary	Lavenu and Cembrano (1999)
momo13	Momolluco river	39.5º/71.5º	25	83	16	-0.91	260	74	0.35	353	1	0.56	0.859	transpression	Miocene-Pliocene	unpublished
Maihue1	Maihue lake	40.1º/72.0º	14	260	3	-0.43	350	3	-0.39	130	86	0.82	0.029	uniaxial compression	Miocene-Pliocene	Lara *et al*. (submitted)
cauna1	Ranco lake	40.1º/72.3º	14	95	24	-0.9	286	65	0.36	187	4	0.54	0.87	uniaxial compression	Quaternary	Lavenu and Cembrano (1999)
rupum1	Maihue lake	40.3º/72.0º	10	51	1	-0.94	141	19	0.29	317	71	0.65	0.773	compression	Quaternary	Lara *et al*. (2006a)
rupum2	Maihue lake	40.3º/72.0º	5	278	12	-0.84	182	25	0.29	32	62	0.55	0.809	uniaxial compression	Miocene-Pliocene	unpublished
melli	Ranco lake	40.3º/72.2º	13	87	11	-0.87	332	64	0.38	181	23	0.49	0.916	transpression	Miocene-Pliocene	Lavenu and Cembrano (1999)
trahu	Ranco lake	40.3º/72.3º	18	102	16		195	11		319	70		0.560	compression	Miocene-Pliocene	Lavenu and Cembrano (1999)
trahu1	Ranco lake	40.3º/72.3º	12	110	17	-0.79	204	11	0.03	326	69	0.76	0.528	compression	Miocene-Pliocene	unpublished
eplaza1	Maihue lake	40.4º/72.1º	13	262	12	-0.90	357	23	0.44	146	64	0.46	0.988	uniaxial compression	Miocene-Pliocene	Lara *et al*. (2006a)
eplaza2	Maihue lake	40.4º/72.1º	6	219	41	-1.02	123	7	0.05	25	48	0.97	0.536	compression	Quaternary	Lara *et al*. (2006a)
rblanco2	Blanco river	41.1º/72.1º	4	27	18	-0.92	240	69	0.32	120	11	0.60	0.814	transpression	Quaternary	unpublished
rblanco1	Blanco river	41.1º/72.1º	7	309	21	-1.02	205	32	0.46	66	50	0.56	0.939	compression	Miocene-Pliocene	unpublished
rel1	Reloncaví estuary	41.4º/71.3º	38	261	5	-0.85	171	7	0.27	28	82	0.58	0.783	compression	Miocene-Pliocene	Lavenu and Cembrano (1999)
rel2	Reloncaví estuary	41.3º/71.3º	20	261	7	-0.85	170	11	0.27	25	77	0.59	0.778	compression	Miocene-Pliocene	Lavenu and Cembrano (1999)
reloq2	Reloncaví estuary	41.5º/72.3º	42	229	9	-1.04	56	80	0.16	319	1	0.88	0.626	transtension	Quaternary	Lavenu and Cembrano (1999)
reloq1	Reloncaví estuary	41.6º/72.2º	29	219	2	-0.94	122	71	0.13	310	19	0.81	0.610	transtension	Quaternary	Lavenu and Cembrano (1999)
Yate1	Yate volcano	41.7º/72.5º	12	225	6	-1.01	134	12	0.50	341	77	0.51	0.995	uniaxial compression	Quaternary	Lara *et al*. (submitted)
Puelo1	Puelo river	41.6º/72.3º	14	100	4	-0.78	210	79	0.17	370	11	0.61	0.686	transpression	Miocene-Pliocene	Lara *et al*. (submitted)
Puelo2	Puelo river	41.6º/72.3º	20	48	3	-0.70	162	84	-0.36	318	6	1.06	0.192	transtension	Quaternary	Lara *et al*. (submitted)
Apagado	Apagado volcano	41.9º/72.7º	24	210	2	-0.66	300	9	-0.11	105	81	0.78	0.381	radial compression	Quaternary	Lavenu and Cembrano (1999)
Horn4	Hornopirén	42.0º/72.5º	51	234	8	-0.89	31	81	-0.17	143	3	1.06	0.372	transtension	Quaternary	Lavenu and Cembrano (1999)

N: number of fault measurements with reliable slip markers
R: ellipsoid shape ratio (R=σ2- σ1/ σ3- σ1)

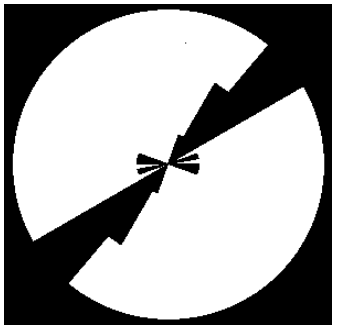

σ1=SHmax

Table 2. Volcanoes and Maximum Horizontal Stress from volcanic morphometry along the volcanic arc (37º-42ºS)

Volcano	Lat (º)	Long (ºW)	Basement structure strike	SHmax strike	Compositional range % SiO2	Age	References (only neotectonics and volcanology)
Antuco	37,4	71.4	.	40	51-66	Quaternary	Lohmar (2000)
Copahue	37,85	71.2	60	.	54-73	Quaternary	Melnick *et al*. (2005)
Callaqui	37,93333	71.4	.	55	53-61	Holocene	Rosenau (2005)
Laguna Mariñaqui	38.3	71.1	.	40		Holocene	Rosenau (2005)
Tolhuaca	38,3	71.7	.	140		Pleistocene	Rosenau (2005)
Lonquimay	38,36667	71.6	.	50	49-64	Holocene	
Llaima	38,7	71.7	.	55-70	51-65	Quaternary	
Sollipulli	38,96667	71.5	.	.	53-73	Quaternary	
Caburgua cluster	39,2	71.8	10	.	51	Holocene	Lara *et al*. (submitted)
Huelemolles cluster	39,32	71.8	10	.	52	Holocene	Lara *et al*. (submitted)
Villarrica	39,41667	71.9	.	40-55	51-70	Quaternary	
Quetrupillán	39,5	71.8	10	45	52-65	Quaternary	(Pavez, 1997)
Llizàn cluster	39,62	71.8	10	.	53-58	Holocene	
Lanín	39,63333	71.5	.	.	49-61	Quaternary	Lara *et al*. (2004)
Fui cluster	39,86667	71.9	.	45	54-58	Holocene	Lara *et al*. (submitted)
Mocho-Choshuenco	39,93333	72.0	.	45-55	52-68	Quaternary	
Carrán-Los Venados cluster	40,37083	72.1	.	45	49-57	Holocene	Lara et al. (2006a); (2006b)
Cordillera Nevada caldera	40,45833	72.3	135	.	52-63	Pleistocene	Lara et al. (2006a); (2006b)
Puyehue	40,6	72.1	135	.	48-71	Pleistocene	Lara et al. (2006a); (2006b)
Cordón Caulle	40.6	72.2	135	.	51-71	Quaternary	Lara et al. (2006a); (2006b)
Golgol cluster	40,6	72.0	.	45		Holocene	Lara et al. (2006a); (2006b)
Los Ñirres cluster	40,6	72,0	.	42		Holocene	Lara et al. (2006a); (2006b)
Anticura cluster	40,7	72.1	5	.	51-57	Holocene	Lara et al. (2006a); (2006b)
Casablanca	40,75	72.1	.	10-55	54-65	Quaternary	
Puntiagudo-Cordón Cenizos clu	40,98333	72.3	.	50	46-51	Quaternary	
Osorno	41,1	72.5	.	55-80	50-57	Quaternary	
Tronador	41.2	71.9	.	.	49-61	Pleistocene	Mella *et al*. (2005)
Cayutue cluster	41,3	72.3	5	.	51-52	Holocene	Lara *et al*. (submitted)
Calbuco	41,33333	72.6	.	.	55-60	Quaternary	
Yate	41,7	72.4	10	.	-60	Quaternary	
Cordón Cabrera	41,8	72,4	.	55		Holocene	
Hornopirén	41,86667	72.4	.	40	53	Quaternary	Rosenau (2005)
Apagado	41,88333	72.6	.	.	51	Quaternary	

Shmax

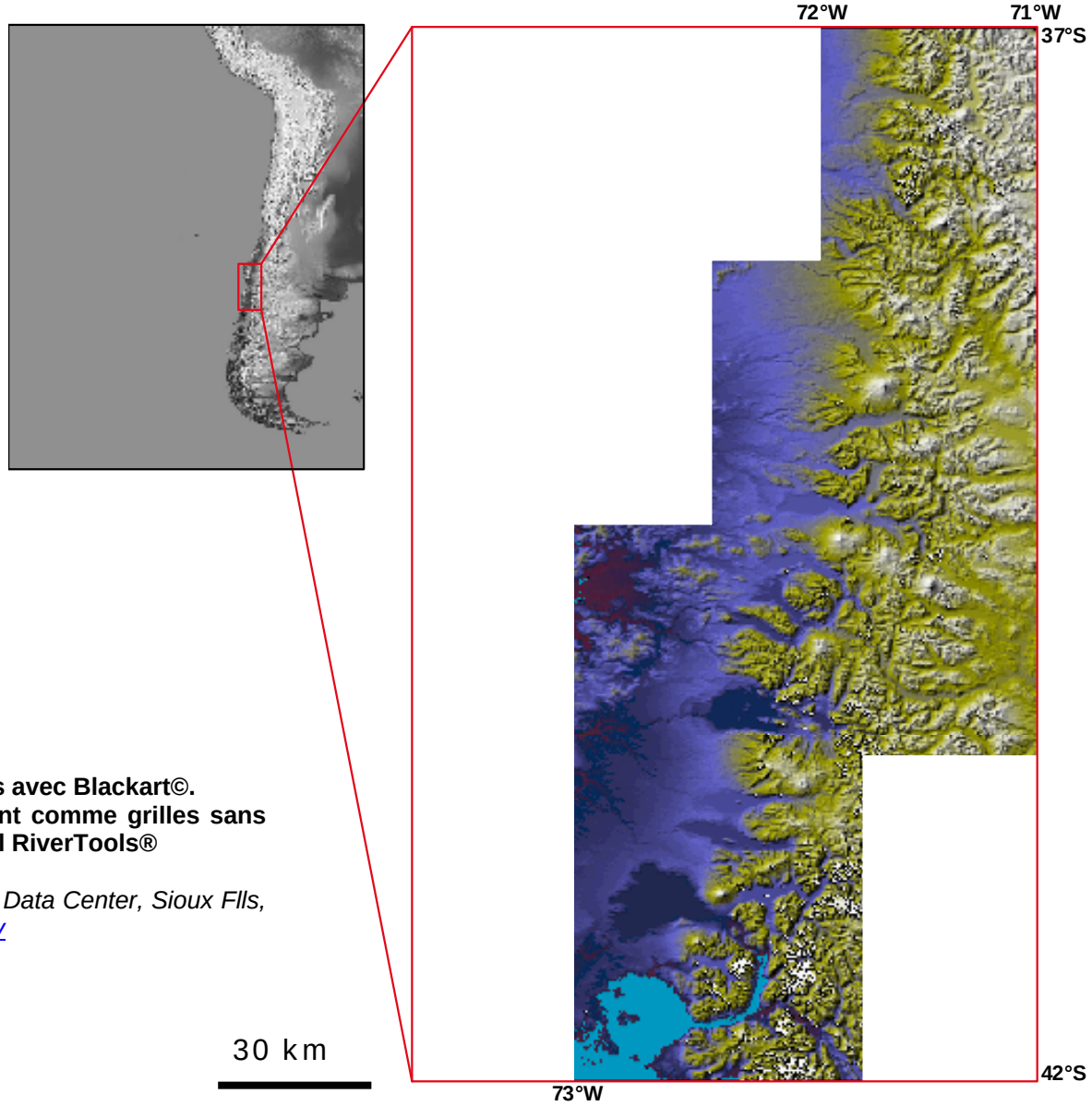

Modéles numériques de terrain SRTM 90 corrigés avec Blackart©. Ils ont eté reconvertis et attachés postérieurment comme grilles sans dépressions (Depressionles DEM) avec le logiciel RiverTools®

Data avalilable from U.S. Geological Survey, EROS Data Center, Sioux Flls, SD. http://seamless.usgs.gov; http://gisdata.usgs.gov

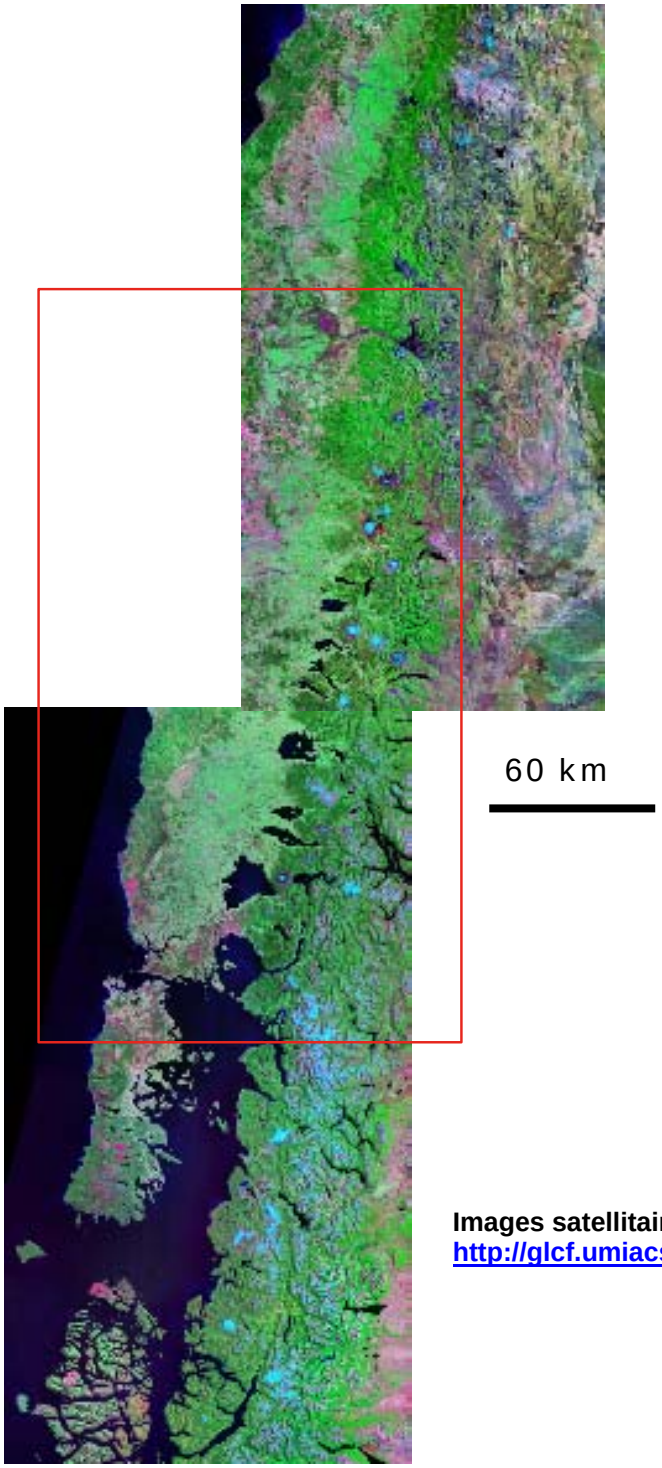

Images satellitaires Landsat 7 (ETM+) S-18-40 et S-19-35 (15-30 m)
http://glcf.umiacs.umd.edu

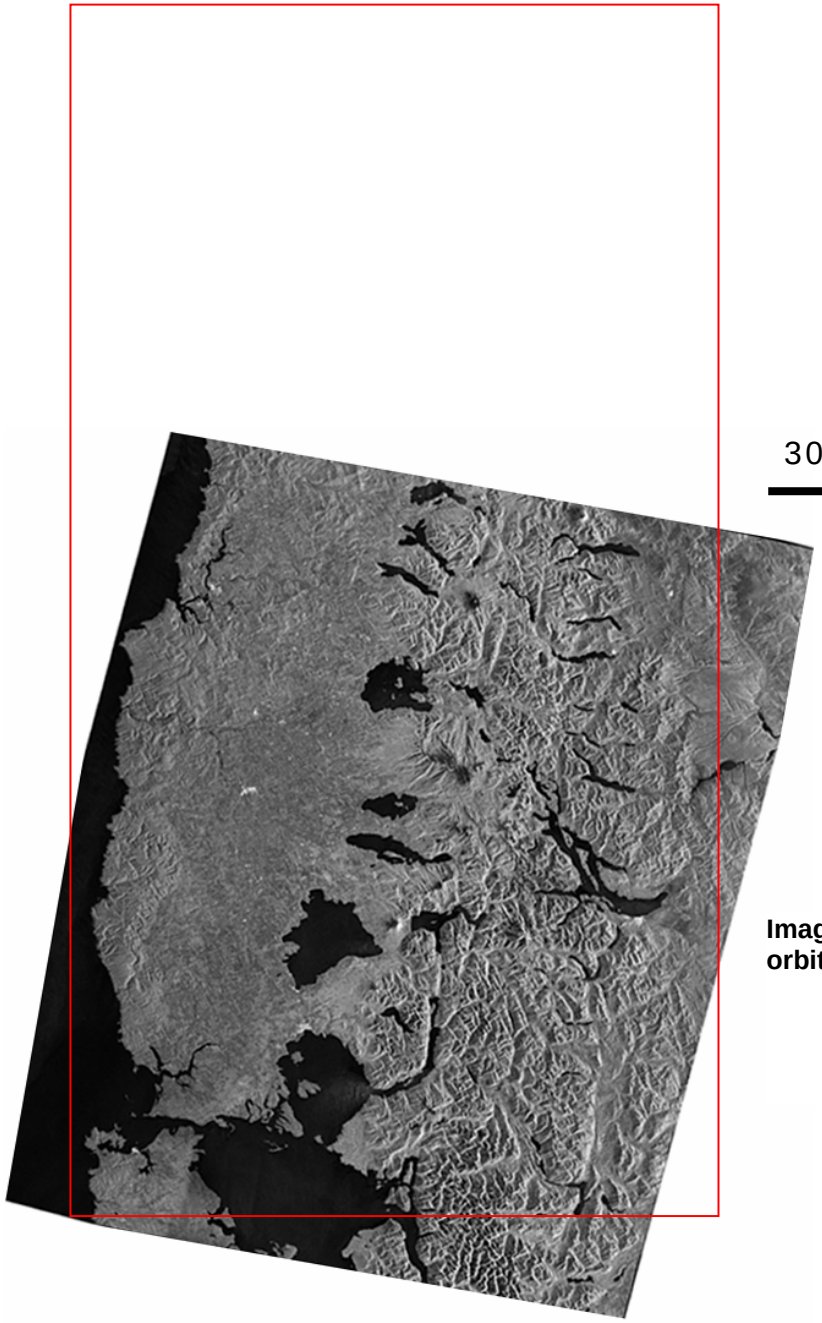

Image Radarsat 1 Scan SAR Narrow (August 6, 1996/3942, descending orbit, positive view)

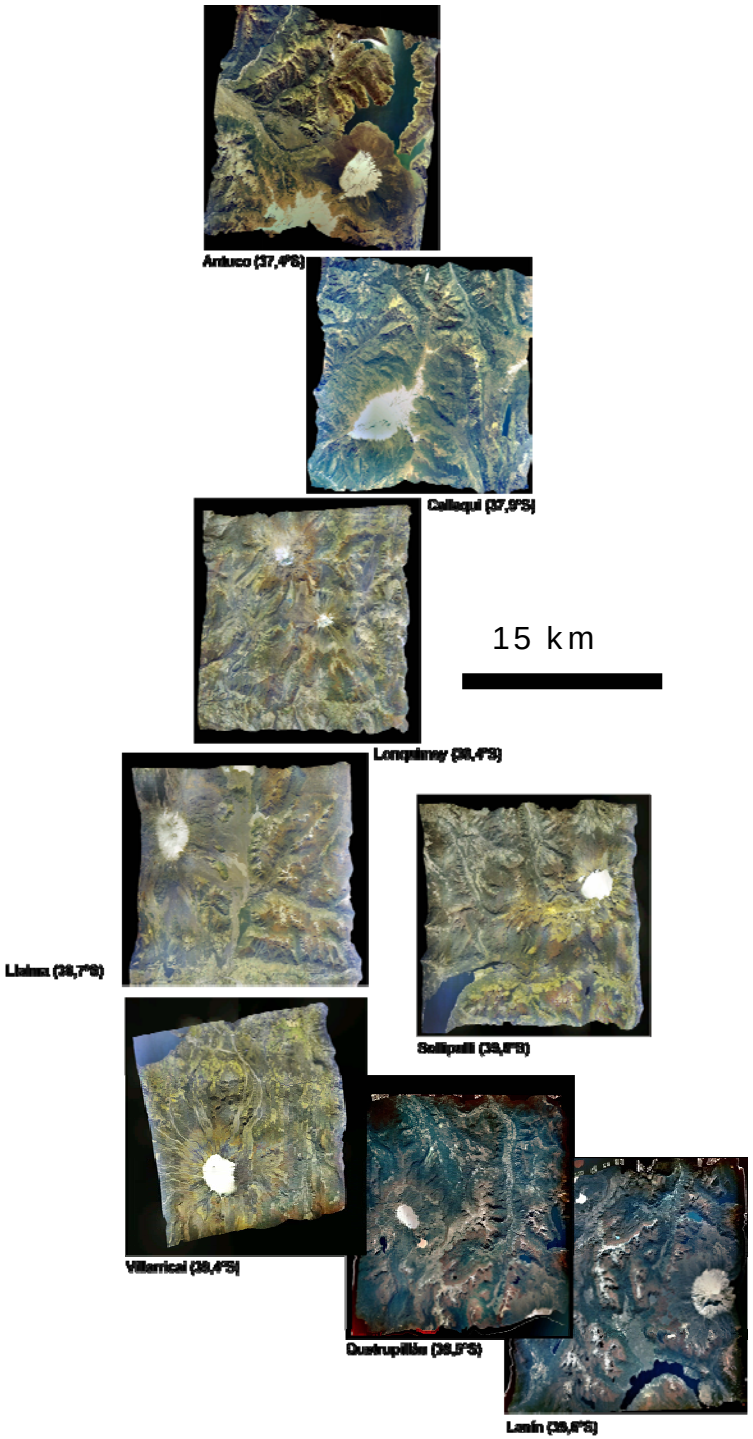

Photographies aériennes des volcans quaternaires dans le secteur d'étude. http://www.sinia.cl

Neotectonics of the Quaternary volcanic arc of Southern Andes, Chile, between 37° and 42°S

Abstract

Neotectonics of the volcanic arc between 37°-42°S and the main features of volcanism in the region suggest a complex interaction, beside the close spatial relationship between volcanoes and faults. The influence of the prefractured crust that underlies the arc should be remarked. Quaternary stress regime, characterised by a dextral transpression with a NE-SW-striking maximum horizontal stress (σ_1=S_{Hmax}) controls the distribution of both the Holocene oblique chains and the flank cones of stratovolcanoes. Local compressive regimes along the Liquiñe-Ofqui Fault System can partially explain local uplift which in turn could be related to discrete volcanic events However, both transpressional and compressive tensors have a constant σ_1, which support the regional influence of crustal tectonics on magma ascent and volcanism. The regional-scale study of the stress regimes and volcanic features of arc segments allow understanding how the complex arc architecture is configured and how the mass transfer occurs through the crust.